Université catholique de Louvain
Louvain Institute of Biomolecular Science and Technology

EXPLORATION AND CHARACTERIZATION OF A SUPERFAMILY OF NICKEL-DEPENDENT HYDROXY ACID RACEMASES AND EPIMERASES

Julian Urdiain-Arraiza

Supervisor

Pr. Benoît Desguin (UCLouvain, Belgium)

Thesis Committee

Pr. Bernard Hallet, Chair (UCLouvain, Belgium)
Pr. Patrice Soumillion (UCLouvain, Belgium)
Pr. Pierre Morsomme (UCLouvain, Belgium)
Pr. Tom Desmet (UGent, Belgium)
Pr. Filip Meysman (UAntwerpen, Belgium)

Thesis submitted to obtain the degree of Doctor of Sciences

October 2024

"Science is more than a body of knowledge. It is a way of thinking; a way of skeptically interrogating the universe with a fine understanding of human fallibility. If we are not able to ask skeptical questions, to interrogate those who tell us that something is true, to be skeptical of those in authority, then we're up for grabs for the next charlatan, political or religious, who comes ambling along."

- Carl Sagan

ACKNOLEDGMENTS

The thesis presented in this manuscript has been a challenging yet rewarding journey, made possible thanks to the support, guidance, and encouragement of many people. I would like to express my deepest gratitude to everyone who contributed to this work, both professionally and personally.

First, I sincerely thank my thesis supervisor, Professor Benoît Desguin, for his invaluable guidance and support throughout my PhD. His expertise and insightful feedback greatly enhanced the quality and depth of this work, while his patience and willingness to challenge my thinking were crucial to my growth as a researcher. For all of this, I am profoundly grateful.

I extend my appreciation to all the jury members for their valuable feedback and enriching discussions during my defense. Special thanks to Patrice Soumillion and Pierre Morsomme, not only for serving as members of my research committee but also for being part of my thesis jury. It was your courses, along with those of Bernard Hallet, that ignited my passion for biochemistry during my university studies. I am also deeply grateful to Tom Desmet and Filip Meysman for agreeing to serve on my thesis jury and for sharing their esteemed expertise during the private defense. Additionally, I would like to thank Bernard Hallet for his role as jury chairman.

My heartfelt thanks go to Damien and Brigitte, the two incredible technicians of our lab, whose unwavering support and dedication have been indispensable throughout my research. Their constant availability, patience, and willingness to assist, even when lab members like myself occasionally made a mess, have been truly remarkable and have kept the lab running smoothly. Their kindness, expertise, and commitment have created an environment where everyone feels supported and capable, and for that, I am deeply grateful. Damien, thank you also for the many discussions and laughs we've shared in the office. To Cyril, thank you for the many years we've spent together in the same office, for your constant good mood, and for your essential contributions to the laboratory. I am also grateful to Véronique, who manages the lab's finances, administration, and orders with a masterful hand – the lab is truly fortunate to have you.

I would like to extend my sincere thanks to Amandine Vanderberghe, Florine Croquet, and Gergana Dimitrova, the master's students I had the pleasure of

supervising during my PhD. Their enthusiasm, hard work, and fresh perspectives were a source of motivation for me, and they contributed in many ways to the progress of my research.

Thanks to the FNRS for funding me for four years. Another important thank you goes to all our scientific collaborators at Michigan State University, especially Prof. Hausinger's team.

I am also deeply grateful to all the members of the BGM lab. Thank you for creating an incredible working atmosphere, for the Friday afternoon beer hours, the wild Christmas parties, the LIBST days, the barbecue afternoons, and all the other moments we shared together. Julien, Fref, Denis, Nicolas, Martin – you are not only great scientists but also wonderful people. Thank you for the lunches spent chatting about everything and nothing in the sunshine, the climbing sessions, the congresses abroad, and all the fun we've had. Julien, it's been 10 years since we started our biology studies together, and I wish you all the best for the future.

To my friends, thank you for your time, love, and energy throughout this long journey. Our many evenings, sometimes quiet over a drink, sometimes not so quiet on the dance floor, helped me think about something other than science and prevented me from getting lost in the depths of my thoughts.

I would like to express my deepest gratitude to my family, especially my mother and father, whose unconditional love, encouragement, and belief in me have been the foundation of everything I have achieved. Their constant support and guidance throughout my studies have been a source of strength and motivation, and I owe much of who I am today to their unwavering faith in my abilities. For their endless sacrifices and encouragement, I am profoundly grateful.

Finally, I want to thank you, Judith. You have been my main pillar over these past five years. The woman you are is a true source of inspiration to me, helping me grow in countless ways. Your patience, gentleness, empathy, and understanding have been essential in keeping me afloat during difficult moments. I can never thank you enough for the unwavering support you have given and continue to give me every day.

SUMMARY

Hydroxy acids (HAs) are organic carboxylic acids found throughout the living world and serve as essential building blocks for various industries, including food, cosmetics, and pharmaceuticals. Recently, a superfamily of nickel-dependent HA racemases and epimerases using the nickel-pincer nucleotide (NPN) cofactor was discovered: the LarA superfamily. This enzyme superfamily is present in all domains of life and holds potential for use in the stereoselective conversion of chiral HAs. However, the study of the LarA superfamily is still in its infancy, and much remains to be understood about the full range of reactions catalyzed by these enzymes, the LarA homologs (LarAHs).

In this thesis, we delve into the exploration and biotechnological potential of the LarA superfamily through a comprehensive approach involving biochemical characterization, taxonomic analysis, and structural modeling. For the biochemical approach, we developed a robust and versatile capillary electrophoresis (CE) method enabling highly efficient chiral analysis of a wide range of underivatized α-hydroxy acids (AHAs), β-hydroxy acids (BHAs) and polyhydroxy acids (PHAs) of biological and industrial importance. Using this novel CE method, we further explored and expanded five different families within the LarA superfamily: the lactate racemase (LAR) family, the short-chain aliphatic HA racemase (SAR) family, the malate racemase (MAR) family, the α-hydroxyglutarate racemase (HGR) family, and the D-gluconate 2-epimerase (GntE) family. We also identified two novel families of LarAHs: the hydrophobic HA racemase (HHR) family, and the broad-spectrum HA isomerase (BSHI) family. In total, we overexpressed, purified, and characterized 13 LarAHs for their biochemical properties and substrate specificities, uncovering 11 novel AHA racemization reactions and 23 novel PHA/sugar acid C2-epimerization reactions.

Altogether, these findings widely expand the scope of substrates isomerized by NPN-dependent enzymes from the LarA superfamily. The broad-spectrum activity of many LarAHs offers new possibilities for the production of valuable stereoisomers of HAs, paving the way for future biotechnological applications of LarAHs.

CONTENTS

LIST OF ABBREVIATIONS

AHAE(s)	2-hydroxy acid epimerase(s)
AHAR(s)	2-hydroxy acid racemase(s)
AHA(s)	2-hydroxy acid(s)
HGR(s)	2-hydroxyglutarate racemase(s)
DHB	2,4-dihydroxybutyric acid
BHA(s)	3-hydroxy acid(s)
ABC	ATP binding cassette
AMP	Adenosine monophosphate
ACEI	Angiotensin-converting enzyme inhibitors
BGE	Background electrolyte
CCDC	Cambridge Crystallographic Data Centre
CE	Capillary electrophoresis
CDM	Chemically defined medium
COG(s)	Clusters of Orthologous Gene(s)
Dha	Dehydroalanine
GntE(s)	D-gluconate epimerase(s)
HGDH	D-hydroxyglutarate dehydrogenase
DKR	Dynamic kinetic resolution
EPG	Electropherogram
EC	Enzyme Commission
EOF	Electroosmotic flow
HA(s)	Hydroxy acid(s)
HHR(s)	Hydrophobic hydroxy acid racemase(s)
IDH	Isocitrate dehydrogenase
ITC	Isothermal titration calorimetry
K_{eq}	Equilibrium constant
KIE	Kinetic isotope effect
Ldh	Lactate dehydrogenase
LarAH(s)	Lactate racemase homolog(s)
LAR(s)	Lactate racemase(s)
LarA1	*Lactiplantibacillus plantarum* lactate racemase

LarA2	*T. thermosaccharolyticum* lactate racemase
LAB	Lactic acid bacteria
LAAD	L-amino acid deaminase
LOD	Limit of detection
MA	Macrocyclic glycopeptide antibiotic
Mar(s)	Malate racemase(s)
MR	Mandelate racemase
MS	Mass spectrometry
MSU	Michigan State University
MW	Molecular weight
NCBI	National Center for Biotechnology Information
NaAD	Nicotinic acid adenine dinucleotide
NPN	Nickel-Pincer Nucleotide
Plr(s)	Phenyllactate racemase(s)
PHAs	Polyhydroxy acid(s)
PCHT	Proton-coupled hydride transfer
P2CMN	Pyridinium 3,5-biscarboxylic acid mononucleotide
P2TMN	Pyridinium-3,5-bisthiocarboxylic acid mononucleotide
R.S.D.	Relative standard deviation
Rs	Resolution
RM	Restriction-modification
α	Separation factor
SAR(s)	Short-chain aliphatic 2-hydroxy acid racemase(s)
SPR	Surface plasmon resonance
UxaE	Tagaturonate epimerase
TBI	Toulouse Biotechnology Institute
TCA	Tricarboxylic acid
XRD	X-ray diffraction
μ_{app}	Apparent electrophoretic mobility
μ_{eff}	Effective electrophoretic mobility
μ_{EOF}	Electroosmotic mobility

I. INTRODUCTION

I.1 α-Hydroxy acids and polyhydroxy acids

Hydroxy acids (HAs), which are carboxylic acids containing at least one hydroxyl group, are widespread compounds in nature and serve as essential biological building blocks in industry [1]. The HAs are subdivided into three main categories: (i) α-hydroxy acids (AHAs) with the hydroxyl group attached to the second carbon; (ii) β-hydroxy acids (BHAs), with the hydroxyl group attached to the third carbon; (iii) polyhydroxy acids (PHAs) with multiple hydroxyl groups in their structure [2]. The substrates of interest in this thesis are AHAs and PHAs, the two categories of HAs the most prevalent in nature and in industry.

I.1.1 Classification

AHAs can be further subdivided into three main categories according to their chemical structure: (i) aliphatic AHAs, with straight or branched non-aromatic side chain; (ii) aromatic AHAs, with an aromatic ring-bearing side chain; (iii) polycarboxylic AHAs, with more than one carboxyl group (Fig. 1) [1,2]. Among PHAs, sugar acids are derived from saccharides through oxidation. The oxidation can occur at different positions on the sugar molecule, leading to 3 main categories of sugar acids with distinct properties and functions: (i) Aldonic acids, formed by oxidizing the aldehyde group of an aldose to a carboxylic acid; (ii) Uronic acids, formed by oxidizing the terminal hydroxyl group of an aldose or ketose to a carboxylic acid; (iii) Aldaric acids, formed by oxidizing both the aldehyde and the terminal hydroxyl groups of an aldose, generating a dicarboxylic acid [3,4]. For example, oxidation of D-glucose at C1 yields D-gluconic acid, at C6 yields D-glucuronic acid, both at C1 and C6 yields D-glucaric acid (Fig. 1).

I.1.2 Metabolic roles

Hydroxy acids play crucial roles in a diverse range of metabolic processes across plants, animals, and microorganisms. They function as both metabolic intermediates and signaling molecules, essential for primary metabolism, energy production, and regulatory functions [1].

In mammals, specific AHAs, such as 2-hydroxyisocaproate, 2-hydroxy-3-methylvalerate, and 2-hydroxyisovalerate, serve as biomarkers for metabolic and liver health, with lower levels associated with obesity [5]. During physical exertion, L-lactate accumulates in muscles, contributing to fatigue in humans [6]. In contrast, D-lactic acid, which the body less efficiently clears, can lead to D-lactic acidosis, characterized by severe symptoms [7,8]. Moreover, both L- and D-2-hydroxyglutarate, often produced due to enzyme irregularities, are oncometabolites associated with cancer and neurological disorders known as 2-hydroxyglutaric aciduria [9–14]. In eukaryotes, AHAs such as malate, lactate, and 2-hydroxyglutarate are indispensable for various metabolic pathways, including photorespiration, the tricarboxylic acid (TCA) cycle, the glyoxylate cycle, the methylglyoxal pathway, and lysine catabolism [15]. In prokaryotes, these AHAs play significant roles in similar metabolic processes. For instance, lactate play a crucial role in the growth and metabolism of many archaea [16–18] and bacteria [19], serving as a source of carbon and energy. Like certain bacteria, some archaea also produce lactate [18,20,21]. Malate is essential in archaeal metabolism, particularly in the glyoxylate cycle and the TCA cycle [22–25], and many bacterial species use malate as a carbon source [26–29]. Finally, D-2-hydroxyglutarate is involved in L-serine biosynthesis, while L-2-hydroxyglutarate is an intermediate in the lysine degradation pathway of many bacteria [30–32]. Overall, AHAs and PHAs are key metabolites involved in numerous metabolic pathways, such as amino acid degradation [30,33], cellular component biosynthesis [34], and sugar metabolism [15,35].

The examples mentioned above represent only a partial list of the metabolic roles of AHAs and PHAs in nature. The racemization and C2-epimerization of these compounds, catalyzed by AHA racemases and PHA C2-epimerases, respectively, are vital for maintaining stereoisomeric equilibrium within cells. Besides their roles in cellular homeostasis, AHARs and AHAEs may also have implications for the synthesis of a broad range of biologically active compounds, including pharmaceuticals and agrochemicals [1,2].

I.1.3 Industrial applications

In addition to being key metabolites of most metabolic pathways, AHAs and PHAs have considerable market potential and find extensive applications in a wide range of industries. (i) In cosmetics and skincare, these compounds are valued for their cleansing, conditioning, humectant and moisturing properties. For instance, lactic acid and gluconic acid are known to exfoliate the skin and offer anti-aging benefits [2,36,37]. (ii) In medicine, they can serve as drug precursors for synthesizing various significant chiral compounds, including antimicrobial agents [38,39], antibiotics [40,41], and angiotensin-converting inhibitors [42,43]. Notably, compounds like 2-hydroxyisocaproic acid and 3-phenyllactic acid exhibit antibacterial and antifungal activity [44,45]. (iii) In the food industry, they can function as food components and additives [46–48]. Lactic acid, for instance, is commonly used in processed foods as a pH regulator, preservative, and flavoring agent [49]. (iv) In chemical synthesis, they can serve as versatile building blocks. For example, 2,4-hydroxybutyrate can be used as a versatile chemical synthon [50]. (v) In polymer synthesis, they can act as monomers for producing diverse biopolymers [39,51,52]. Polylactic acid, derived from lactic acid, is notable for its application as a biodegradable plastic [53]. The significant growth in both quantity and variety of AHAs has driven the global market size to exceed USD$ 1.2 billion in 2021, projected to reach USD$ 2.3 billion by 2028 [54]. Similarly, the market for gluconic acid, a prominent PHA, is expected to grow from USD$ 0.18 billion in 2023 to USD$ 0.24 billion by 2032 [55]. Consequently, research focusing on the production, analysis, and enzymatic interconversion of AHAs and PHAs has garnered considerable attention from researchers [1,56–59].

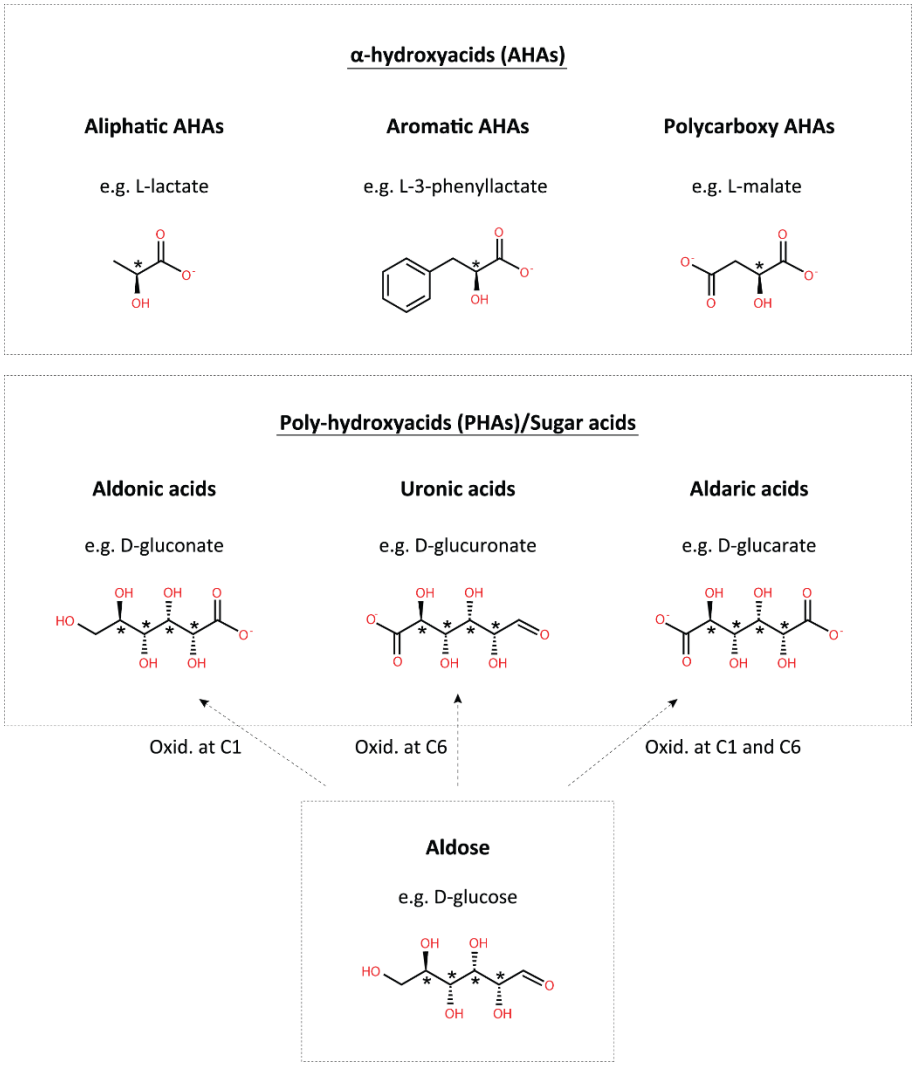

Figure 1 | **Main categories of AHAs and PHAs.** Each category is illustrated by an example compound. AHAs are subdivided into aliphatic, aromatic and polycarboxy AHAs. Sugar acids are subdivided into aldonic, uronic and aldaric acids. Oxidation of D-glucose at C1 yields D-gluconic acid, at C6 yields D-glucuronic acid, both at C1 and C6 yields D-glucaric acid. Asterisks indicate chiral centers.

I.2 LarA1 and LarAHs among the diversity of enzymes

This section serves as a foundational introduction to the complex roles and classifications of the lactate racemase (LarA) and its homologs (LarAHs). By situating LarA and LarAHs within the diversity of enzymes, this section lays the groundwork for comprehending their unique roles in catalyzing isomerization reactions—a process crucial in numerous biological and industrial contexts. This understanding is essential for grasping intricate details discussed in the subsequent sections.

I.2.1 Enzymes

Enzymes are essential proteins present in every living organism and play a crucial role in catalyzing biochemical reactions necessary for life [60]. These proteins not only accelerate the majority of biochemical processes but do so more efficiently than synthetic catalysts. This high efficiency is due to their ability to operate under mild conditions, exhibit high reaction rates, and maintain excellent specificity towards substrates and products, minimizing unwanted by-products. This specificity includes both geometric and stereospecific interactions, allowing precise interactions with the chemical groups of substrates and products [61,62]. Despite this high degree of specificity, enzymes can exhibit promiscuity, where they catalyze reactions with substrates other than their primary ones [63].

The realization of the pivotal role of enzymes in biology emerged prominently in the 20th century, marking a significant advancement in both medicine and technology. This led to the development of enzymology as a distinct scientific field focused on understanding the molecular functions of these proteins [64]. The unique properties of enzymes make them invaluable in various industries, including pharmaceuticals, food and beverage, detergents, and biofuels, for numerous reasons due to their lower toxicity and environmental impact [65–68]. However, some enzymes require the presence of cofactors to activate and function effectively. An enzyme without its cofactor, known as an apoenzyme, becomes a holoenzyme upon cofactor association. This activation is essential for the enzyme to catalyze specific types of chemical reactions, such as oxidation-reduction and group transfers [61]. Overall, the study of enzymes not only deepens our

understanding of biological processes but also drives significant technological and industrial advancements, making it a cornerstone of modern biochemical research.

Enzymes are categorized into seven major classes by the Enzyme Commission (EC) of the Nomenclature Committee of the International Union of Biochemistry and Molecular Biology (NC-IUBMB). These classes include oxidoreductases (EC 1), transferases (EC 2), hydrolases (EC 3), lyases (EC 4), isomerases (EC 5), ligases (EC 6), and translocases (EC 7) each defined by the nature of the chemical reaction they catalyze (Fig. 2A) [69,70]. This thesis focuses on a superfamily of isomerases.

I.2.2 Isomerases (EC 5)

Isomerases, categorized under the enzyme class EC 5, catalyze the interconversion between isomers. Isomers have identical chemical formulas but differ in their three-dimensional structures [71,72]. Chemical isomers exhibit subtle changes in their structures, yet can show different pharmacological, toxicological, pharmacokinetic, pharmacodynamic or metabolic effects [73,74]. Therefore, interconversions of isomers by isomerases are crucial in the metabolism of living organisms and have many applications in biocatalysis, biotechnology, and drug discovery [75]. The classification of isomerases encompasses three hierarchical levels: 6 subclasses (EC 5.b), 17 sub-subclasses (EC 5.b.c), and a total of 254 EC numbers (5.b.c.d). The primary subclasses include racemases and epimerases (EC 5.1), cis-trans isomerases (EC 5.2), intramolecular oxidoreductases (EC 5.3), intramolecular transferases (EC 5.4), intramolecular lyases (EC 5.5), isomerases altering macromolecular conformation (EC 5.6) and a diverse group referred to as other isomerases (EC 5.99) (Fig. 2A). These subclasses reflect differences based on the type of isomerism between substrate and product, distinguishing two primary groups of reactions: stereoisomerism and structural isomerism. Stereoisomerism involves the interconversion between stereoisomers differing by the orientation of bonds between atoms (EC 5.1 and EC 5.2). On the other hand, structural isomerism entails the interconversion between structural isomers differing by the nature of bonds between atoms (EC 5.3, EC 5.4, EC 5.5, and EC 5.6). The other isomerases (EC 5.99) comprise both stereoisomers and structural isomers (Fig. 2A) [75,76].

Isomers typically differ in their biological role, and nature has a general tendency to use only one isomer of a molecule in essential biochemical pathways (e.g. L-amino acids and D-sugars). However, organisms also use amino acids and sugars with unusual stereochemistry as biosynthetic building blocks or metabolic precursors. Isomerases facilitate the production of these compounds, making them central to the metabolism of most living organisms. For instance, genes coding for isomerase activity comprise approximately 2.6% of all enzyme-encoding genes in humans and 6.2% in *Escherichia coli* [76].

In synthetic organic chemistry, isomerases are pivotal for catalyzing "chemically impossible" isomerization reactions, such as stereochemical inversions that involve breaking and reforming bonds in a non-specific manner. Most isomerases operate at a chiral center adjacent to a carboxyl group, where they reversibly cleave a C-H bond [77]. Therefore, the discovery and application of new isomerases are rapidly expanding in organic synthesis, biotechnology, and drug discovery, driven by the unique properties of the isomers they produce [78,79]. The most striking example is the use of glucose isomerase for the production of 14 million tons per annum of high fructose corn syrup from glucose [80].

I.2.3 Racemases and epimerases (EC 5.1)

LarAHs explored in this thesis exhibit both racemase and epimerase activities and are categorized within the EC 5.1 subclass of enzymes known as racemases and epimerases. A racemase catalyzes the inversion of a stereocenter in a molecule with only one stereocenter leading to the formation of two enantiomers, which are molecules having non-superimposable mirror images of each other [61]. An epimerase catalyzes the same reaction in a molecule with multiple stereocenters, thereby resulting in more than 2 possible diastereomers. Unlike enantiomeric pairs, diastereomers of a molecule have distinguishable physico-chemical properties (melting points, spectra, chemical reactivity) [61,81].

Racemization and epimerization reactions require the non-stereospecific breakage and reformation of a bond which can be between a carbon and a hydrogen, a heteroatom (oxygen or nitrogen), or another carbon. For C-H bonds, the mechanism is a deprotonation followed by a reprotonation in the

case of an activated hydrogen (pKa < 30). In the case of a non-activated hydrogen (pKa > 30), the hydrogen transfer is done under the form of a hydride [77]. Due to the fact that biochemical processes are predominantly stereospecific, Nature has faced little need for racemization and epimerization and, as a consequence, racemases and epimerases are a small group of enzymes. This small and largely overlooked group of enzymes is increasingly being used for dynamic kinetic resolution or in auxiliary biocatalytic recycling processes, allowing the production of a single stereoisomeric product from racemic starting materials [82]. Racemases and epimerases are classified according to their substrate type, which can be amino acids and their derivatives (EC 5.1.1), hydroxy acids and their derivatives (EC 5.1.2), carbohydrates and their derivatives (EC 5.1.3) or other substrates (5.1.99) (Fig. 2A) [75].

I.2.4 Racemases and epimerases acting on hydroxy acids and derivatives (EC 5.1.2)

LarAHs are racemases and epimerases acting on hydroxy acids and their derivatives (EC 5.1.2) (Fig. 2B). Specifically, LarAHs act on α-hydroxy acids (AHAs) and polyhydroxyacids (PHAs). The EC 5.1.2 sub-subclass currently comprises seven enzymes [83,84], yet only three have been purified and characterized: lactate racemase (LarA1, EC 5.1.2.1), mandelate racemase (MR, EC 5.1.2.2) [85,86] and tagaturonate epimerase (UxaE, EC 5.1.2.7) [87]. The remaining four enzymes, including 3-hydroxybutyryl-CoA epimerase (EC 5.1.2.3) [88], acetoin racemase (EC 5.1.2.4) [89], tartrate epimerase (EC 5.1.2.5) [90], and isocitrate epimerase (EC 5.1.2.6) [91], have solely been detected in organisms and have not been purified due to the lack of knowledge regarding their respective genes (Fig. 2A).

Among the characterized enzymes, LarA, MR, and UxaE exhibit a reliance on divalent metal ions for their catalytic activities, classifying them as metalloenzymes. Specifically, the catalytic mechanism of MR involves the deprotonation of the α-carbon of mandelic acid to form a carbanion intermediate, which is then reprotonated, leading to the racemization of mandelate [92,93]. This mechanism requires divalent metal ions, with magnesium (Mg^{2+}) being the preferred ion, although cobalt (Co^{2+}), nickel (Ni^{2+}), manganese (Mn^{2+}), and iron (Fe^{2+}) can also function in this capacity [94]. In the case of UxaE, the enzyme catalyzes the epimerization of D-

tagaturonate and D-fructuronate via carbon–carbon bond cleavage with zinc (Zn^{2+}) serving as the necessary divalent metal ion. LarA, however, employs a distinctive mechanism among racemases and epimerases. Instead of relying on proton transfer, LarA uses a hydride transfer, facilitated by a Ni^{2+}-containing organometallic cofactor. The details of this unique cofactor and its catalytic mechanism will be developed later in this thesis (see Section 1.2.4).

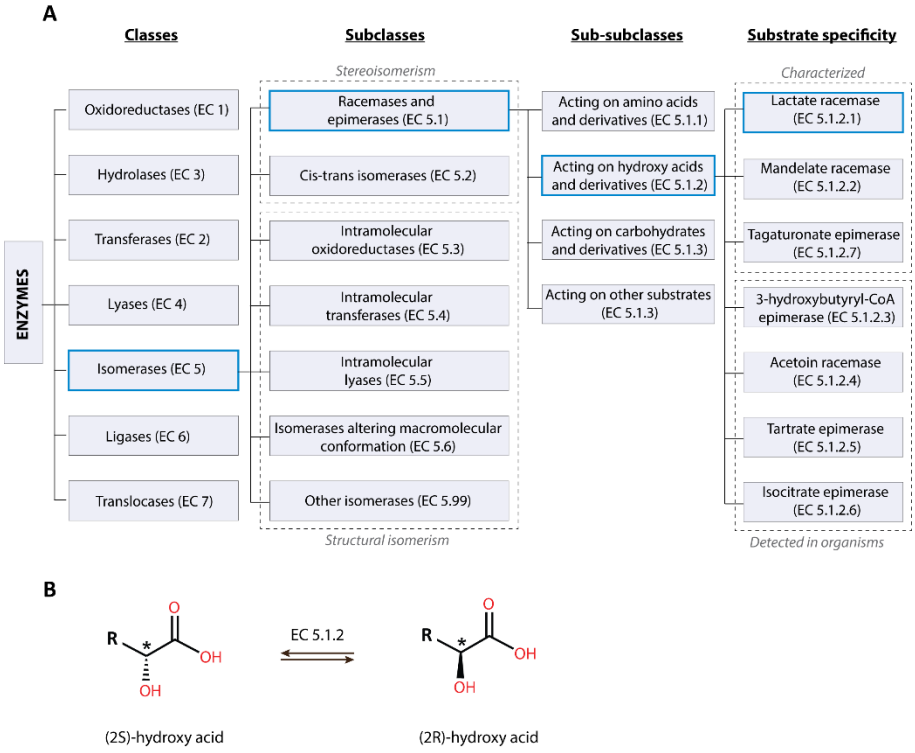

Figure 2 | Enzymes and reactions of interest in this thesis. (A) Enzyme classification by the enzyme commission. Enzymes are classified according to the type of reaction that they catalyze. Isomerases are classified according to the type of isomerization that they catalyze. Racemases and epimerases are divided according to their substrate type. Racemases and epimerases acting on hydroxy acids consist of 7 EC numbers to this day. **(B)** Racemization and C2-epimerization of 2-hydroxy acids. If the R group has no chiral center, the enzyme is a racemase. If the R group has one or more than one chiral center, the enzyme is an epimerase. Chiral centers are indicated by an asterisk.

I.3 LarA1 and the NPN cofactor

Cofactors, derived from vitamins, are essential tools enabling enzymes to catalyze reactions in living organisms. In the context of this thesis, the focus will be on lactate racemase of *Lactiplantibacillus plantarum* (EC 5.1.2.1, LarA1), which catalyze the interconversion between L- and D-isomers of lactic acid, aided by its nickel-containing cofactor, termed the Nickel-Pincer Nucleotide (NPN) cofactor, making it the ninth nickel-dependent enzyme discovered [95][96]. This section aims to present a state-of-the-art overview encompassing the research developments on LarA1 and the NPN cofactor.

I.3.1 Lactic acid bacteria (LAB) and the lactate racemase activity

LAB constitute a group of Gram-positive, non-motile, non-spore forming and rod- and coccus-shaped bacteria. Metabolically, LAB share the ability to produce lactate as primary fermentation product of hexoses [21,97]. This metabolic trait and the rapid growth of LABs have led to a wide variety of applications in food fermentation, probiotics, biopreservation, healthcare, agriculture and biotechnology, and *L. plantarum* is no exception [49,98–101].

The enzymatic racemization of D- and L-lactate, known as lactate racemase (Lar) activity, was initially observed in 1936 in *Clostridium acetobutylicum* and *Clostridium beijerinckii* (formerly *C. butylicum*) [102]. Subsequently, this activity was identified in *Staphylococcus aureus* (formerly *S. ureae*) and *Lactobacillus sakei* (formerly *L. sake*) in 1937 [103]. In 1938, LAR activity was detected for the first time in *L. plantarum* [104]. Studies suggested that LAR activity in *L. plantarum* was not a single enzyme but a system composed of 2 enzymes: L- and D-lactate dehydrogenases, namely LdhL and LdhD, which will be described further (Fig. 3) [105–108]. In 1961, a “racemiase” from *C. acetobutylicum* was purified and its characterization suggested a cofactor requirement, though pyruvate was excluded as an intermediate for its activity [109]. In 1965, the mechanism of lactic acid racemisation in *Clostridium butylicum* was proposed to involve a direct internal hydride shift [110]. The lactate racemase of *L. sakei* was characterised in 1968, suggesting no additional cofactor required for its activity [111]. Numerous other studies attempted to elucidate the lactate racemase mechanism, mainly in LAB belonging to the genus *Lactobacillus* [112,113]. However, since its discovery in 1936, most studies on LAR activity in various microorganisms provide contradictory evidence that depends to some extent on the source of the enzyme. It wasn’t until 2014, with a detailed investigation of LarA1, that a clearer understanding began to emerge [95].

In LAB such as *L. plantarum*, both L-lactate and D-lactate are produced through the reduction of pyruvate by two stereospecific NAD-dependent enzymes: LdhL and LdhD, respectively (Fig. 3) [113,114]. The production of D-lactate is particularly important as *L. plantarum* incorporates it as the final residue of the peptidoglycan precursor during cell wall biosynthesis [34]. This mechanism provides vancomycin resistance to *L. plantarum* and other LABs [113]. Typically, in most bacteria, the peptidoglycan precursor ends with a D-alanyl residue: UDP–N-acetylmuramyl–L-Ala–γ-D-Glu–L-Lys–D-Ala–D-Ala. In contrast, in *L. plantarum* and related LABs, this precursor ends with a D-lactate residue instead of D-alanine [115]. Vancomycin, a glycopeptide antibiotic, disrupts cell wall synthesis by bonding with the D-Ala-D-Ala end of peptidoglycan precursors, thus hindering polymerization and subsequent cross-linking reactions [116]. Substituting the terminal D-alanine residue with D-lactate consequently reduces the affinity of the antibiotic for its target [115].

I.3.2 In vivo role of LarA1

However, the reduction of pyruvate by LdhD is not the only pathway for D-lactate production in *L. plantarum*. Indeed, a *ldhD* knockout mutant in *L. plantarum* still resulted in the production of a racemic mixture of lactate, indicating a lactate racemase activity [95,115]. LarA1 could therefore act as a rescue pathway for D-lactate production for cell wall biosynthesis in the absence or inhibition of the LdhD enzyme [34]. Consequently, *L. plantarum* has two main pathways for D-lactate production from pyruvate: (1) the LdhD enzyme and (2) the LdhL enzyme coupled with lactate racemase. Additionally, a third pathway exists where lactate production is independent of both LdhD and LdhL. This pathway is malolactic fermentation, where the malolactic enzyme directly converts L-malate to L-lactate, which can then be converted to D-lactate [117,118]. D-Lactate is likely necessary for cell wall biosynthesis in many other LABs as well; thus, LarA1 can serve as an alternative pathway for D-lactate synthesis in LAB lacking LdhD activity or performing malolactic fermentation [113]. In *L. plantarum*, the pathway for D-lactate production is induced by L-lactate. The activity was attributed to an operon, known as the *lar* operon, which consists of five genes: *larA*, *larB*, *larC*, *larD*, *larE*. Its involvement in lactate racemization was supported by observing a complete absence of D-lactate production in a *ldhD* mutant when the *lar* operon was also deleted [34].

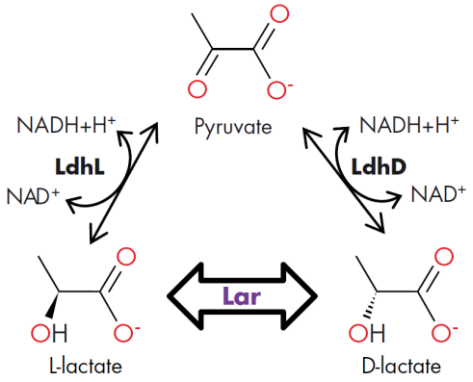

Figure 3 | The lactate racemase activity. L- and D-lactate dehydrogenases (LdhL and LdhD respectively) produce L- and D-lactate from pyruvate during the EMP glycolysis pathway. Lactate racemase (Lar) can serve as a rescue pathway for D-lactate production in case of LdhD inactivity. Taken from [113].

I.3.3 The Lar system in *L. plantarum*

Genetic and biochemical studies of the Lar system in *L. plantarum* have revealed its intricate complexity. Transcriptomic analyses have demonstrated the involvement of another operon, adjacent to the previously identified one and transcribed in opposite directions, in lactate racemization. Both operons, namely *larR(MN)QO* and *larABCDE*, are induced by L-lactate (Fig. 4) [95,113].

Within the *larABCDE* operon, *larA* encodes the LarA apoenzyme [95]. LarB, LarC and LarE, encoded by their 3 respective genes, are essential for the biosynthesis of the NPN cofactor (see next Section) [95,96,119]. LarC is formed by the fusion of proteins encoded by the *larC1* and *larC2* ORFs, likely due to a programmed ribosomal frameshift [95,120]. Furthermore, *larD* gene encodes for the LarD aquaglyceroporin, also known as glpF1, which transports both lactic acid enantiomers and is not required for lactate racemization activity [95,121].

The *larR(MN)QO* operon encodes LarR, a key transcriptional regulator, and a three-component ATP binding cassette (ABC) high affinity nickel transporter [122]. Lar(MN), with fused M and N components, functions as the substrate binding protein. LarQ acts as a permease, while LarO serves as the ATP binding protein [95].

In the regulation of the *lar* genes, LarR plays a crucial role as a positive transcriptional regulator. It functions by binding to the *Lar* box, a 16-bp palindromic sequence located in the *larR-larA* intergenic region. LarR not only multimerizes on the *Lar* box but also on adjacent half-*Lar* boxes, thereby promoting gene activation. The presence of L-lactate enhances LarR binding to the Lar box and multimerization on the half-boxes, whereas D-lactate antagonizes this effect. Consequently, the expression of both *lar* operons is transcriptionally controlled by the L-lactate/D-lactate ratio [122,123].

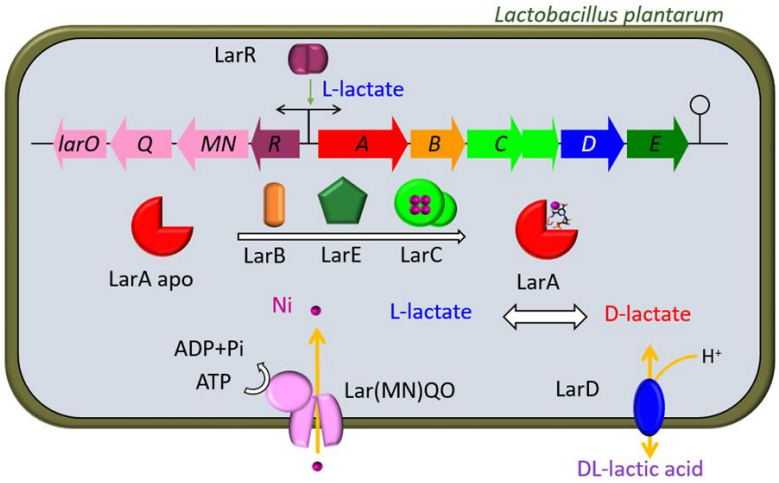

Figure 4 | **The Lar system in *L. plantarum***. *larMNQO* encode an ATP-binding cassette nickel importer; *larR* codes for a transcriptional regulator that is induced by L-lactate; *larA* encodes the LarA1 apoprotein; *larB*, *larC*, and *larE* code for the NPN cofactor biosynthetic enzymes; and *larD* encodes an aquaglyceroporin. Adapted from [123].

I.3.4 Structure of LarA1 and the NPN cofactor

The crystal structure of LarA1 revealed a homodimeric structure comprising two monomers, each with a molecular weight of 46.2 kDa [113]. Lactic acid likely binds at a position occupied by sulfate in the crystal structure (above the pyridinium ring, Fig. 5). Through site-directed mutagenesis experiments, crucial residues within LarA1 were identified, revealing their significance in enzyme activity. Substituting His108, His174, His200, and Lys298 with alanine resulted in complete loss of LAR activity *in vivo*, while substitutions at Asp72, Arg75, Lys184, and Gln295 led to enzymes with residual activity. Notably, the K184A variant exhibited no *in vitro* activity and lacked nickel, suggesting its

role in NPN cofactor binding. Furthermore, the H200A mutant also displayed decreased nickel content. This comprehensive analysis, complemented by structural analyses and subsequent investigations, allowed the attribution of specific functions to essential residues within the LarA1 catalytic site, as summarized in Table 1 [96,124].

It is the structure of LarA1, solved in 2015, that revealed the presence of the NPN cofactor (Fig. 5) [96]. The pincer part of the name derives from planar tri-coordinating ligands of metal ions that are well known in the field of organometallic chemistry [125–127]. In biology, however, pincer-like compounds are limited to the NPN cofactor and pyrroloquinoline quinone metal complexes [128]. The NPN cofactor consists of a nicotinic acid mononucleotide derivative wherein a nickel ion is coordinated by two sulphur atoms and the C4 carbon of the pyridinium ring, forming a pincer complex. A bond between a nickel atom and a carbon is particularly unusual. Additionally, His200 of LarA1 completes the coordination geometry of the nickel ion, resulting in a four-coordinate square planar arrangement. In LarA1, the cofactor is covalently bound by a thioamide linkage between one thiocarboxylate and Lys184, thus forming the LarA1 holoenzyme [96,129]. Overall, the NPN cofactor provides a stable coordination environment for the nickel ion within the enzyme's active site. Furthermore, it plays a crucial role in the catalytic function of LarA1, which will be detailed in Section 1.2.6.

Table 1 | **Essential residues of LarA1 and their functions.**

LarA1 residue	**Function**
H108 and H174	Acid/base catalysis (see Section 1.2.7)
K174	Covalent bond with the NPN cofactor
H200	Fourth ligand for Ni^{2+} coordination of the NPN
R75	Hydrogen bonding with the NPN cofactor
F175, F176, Y294, Q295, V297, T353, P355, D356, W358, T359, I362	Substrate recognition and binding

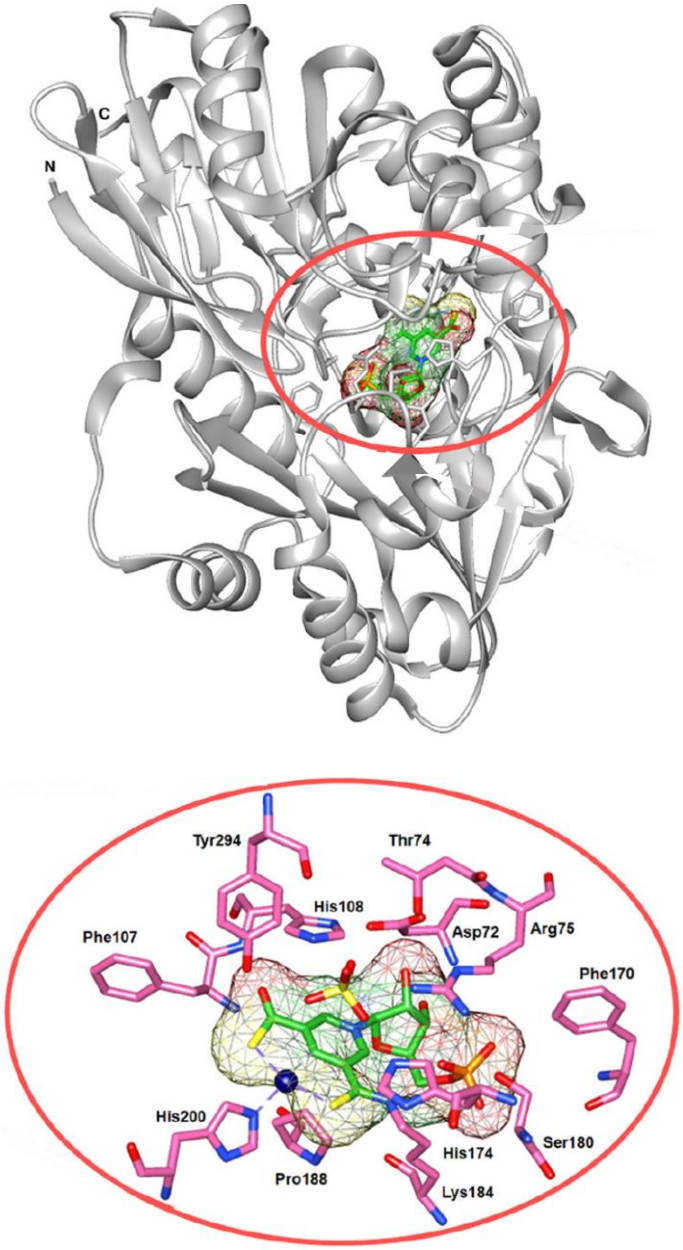

Figure 5 | **Structure of LarA1, highlighting its NPN cofactor.** The protein (PDB: 5HUQ) is shown as a cartoon ribbon with sticks representing both selected side chains (gray) and the cofactor (C atoms in green, O in red, N in blue, S in dark yellow, and P in orange), with nickel shown as a blue sphere, and with mesh depicting the surface of the cofactor (except nickel). The expanded view of the catalytic site also shows, as sticks, sulphite and residues within 4 Å of the cofactor (pink C atoms). Adapted from [130].

I.3.5 The NPN cofactor biosynthetic pathway

The NPN cofactor is synthesized from the precursor nicotinic acid adenine dinucleotide (NaAD) through the action of three NPN biosynthetic enzymes: LarB, LarC and LarE (Fig. 6) [95,96,130]. The first step in NPN biosynthesis involves LarB, which functions as a NaAD carboxylase/hydrolase. LarB catalyzes the carboxylation of the pyridinium ring of NaAD in the presence of CO_2 and Mg^{2+}, and the hydrolysis of the phosphoanhydride bond. This reaction generates adenosine monophosphate (AMP) and pyridinium 3,5-biscarboxylic acid mononucleotide (P2CMN) [119,131].

Following this, the conversion of P2CMN into pyridinium-3,5-bisthiocarboxylic acid mononucleotide (P2TMN) is catalyzed by LarE, an ATP-dependent sacrificial sulfur insertase. Two LarE enzymes are catalyzing two single-turnover sacrificial sulphurization reactions for the synthesis of one NPN. Specifically, Cys176 residues in both LarE enzymes are converted to dehydroalanine (Dha), and the carboxylates of P2CMN are sulphurized into thiocarboxylates by incorporating the two sulphur atoms [119,132].

The last enzyme of the NPN biosynthesis pathway, LarC, inserts nickel into P2TMN to yield the mature cofactor. This reaction introduces nickel-carbon and nickel-sulphur sigma bonds, forming a ring structure, a process termed cyclometalation in organometallic chemistry [133]. Notably, LarC is the first biological example of a cyclometallase. This protein also is unusual in that it is a single-turnover CTP-dependent enzyme *in vitro* [120].

NPN can subsequently react with Lys184 of LarA1, forming a covalent bond that activates LarA1. In NPNylated LarA1, the nickel coordinates with the sulfur atoms from thioamide and thioacid groups of NPN, the C4 of the pyridinium, and His200 of LarA1. The overall process of NPN biosynthesis is depicted in Fig. 6.

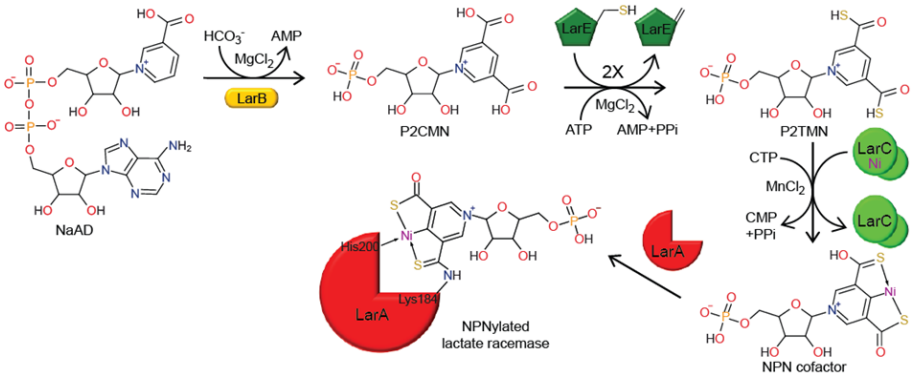

Figure 6 | **The NPN cofactor and its biosynthesis.** Starting from nicotinic acid adenine dinucleotide (NaAD), LarB produces pyridinium 3,5-biscarboxylic acid mononucleotide (P2CMN). From this, two LarE molecules produce pyridinium-3,5-bisthiocarboxylic acid mononucleotide (P2TMN), into which LarC inserts nickel to produce NPN. Adapted from [123].

I.3.6 Mechanism of LarA1

Biochemical studies, along with the analysis of the LarA1 structure, suggested that the NPN cofactor racemize lactate via a proton-coupled hydride transfer (PCHT) mechanism (Fig. 7A). One study synthesized NPN-like complexes and used alcohol dehydrogenation reactions as a model for hydride transfer [134]. Consistent with this, three other computational studies also proposed hydride transfer to C4 of the NPN pyridinium ring [135–138]. In 2018, Rankin *et al.* presented direct evidence supporting the PCHT mechanism through various methods such as electron paramagnetic resonance spectroscopy, detection of pyruvate as a reaction intermediate, kinetic isotope effect (KIE) studies, UV-visible spectroscopy, crystallography, and computational analysis [124].

The PCHT mechanism of LarA1 start by either His108 or His174 (depending on the isomer of lactate) abstracting the proton from the C2-hydroxyl group of lactate. Concomitantly, the C2-hydrogen atom transfers as a hydride onto C4 of the pyridinium ring of the NPN cofactor, forming the intermediate pyruvate and a reduced NPN cofactor. The hydride then rapidly attacks the intermediate held at the active site, and either His108 or His174 (depending on the isomer of lactate) reprotonates the intermediate, resulting in lactate racemization (Fig. 7A). As a result, NPN is only transiently reduced with a probably very short lifetime [124,139].

An alternative PCHT mechanism have been proposed where the hydride transfer occurs either onto C4 of the pyridinium ring or onto the Ni atom if dissociated from His200. The hydride then reduces the intermediate by attacking on either face (Fig. 7B). The proposed capacity for NPN to accept a hydride at 2 different positions may explain the loss of stereospecificity when the hydride returns onto the pyruvate intermediate. A different enantiomer is formed when the hydride is transferred from the C4 of the pyridinium ring to the Ni atom, resulting in its placement on the opposite side of the pyruvate intermediate. This hypothesis could explain the presence of both a highly modified pyridinium ring and Ni in the cofactor and would imply a more essential catalytic role for Ni [140]. However, a recent study consistently supported hydride transfer to C4 of the NPN cofactor through biochemical, spectroscopic, and MS analysis of LarA1 inactivation by $NaBH_4$ [139].

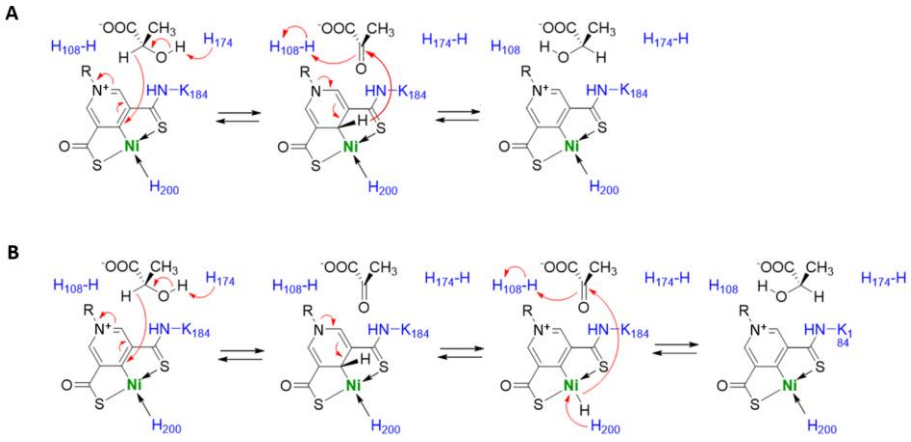

Figure 7 | **Mechanism of LarA1 and the NPN cofactor. (A)** Racemization of D-/L-lactate by LarA1 via a proton-coupled hydride-transfer (PCHT) mechanism. **(B)** Alternative PCHT reaction mechanism for LarA1 with two sites for hydride binding to NPN. LarA1 residues are indicated in blue, nickel is indicated in green. Adapted from [139,141].

I.4 The LarA superfamily

The study of LarA1 and the NPN cofactor led to the discovery of LarAHs, collectively forming the LarA superfamily, which includes mostly 2-hydroxy acid racemases and epimerases. This section outlines the path leading to these discoveries and offers insights into the initial understanding of the LarA superfamily at the start of this thesis, presenting preliminary data collected before this thesis. Here, we gain a preliminary understanding of the functional diversity of the LarAHs, highlighting their significance and widespread occurrence in the microbial world. Overall, this section provides a comprehensive context for fully appreciating the outcomes of this thesis, laying the groundwork for a deeper exploration of the enzymatic landscape and biotechnological prospects offered by the LarA superfamily.

I.4.1 Occurrence of Lar genes in microorganisms

To gain insight into the role of Lar proteins in the microbial world, the distribution of *lar* genes from the *larABCDE* operon in prokaryotic genomes was estimated. Homologous sequences of the *lar* genes of *L. plantarum* WCFS1 were searched using BlastP on a collection of complete prokaryotic genomes (1,087 bacterial and archaeal genomes) from the NCBI database. At least one homolog of *larA*, *larB*, *larC*, *larD* and *larE* was found in 111, 260, 263, 9 and 259 genomes, respectively (Fig. 8A), showing a wide distribution of *lar*-like genes and their potential importance in prokaryotes [95]. Specifically, 1% of the genomes analyzed contain *larABCE*, as well as the *larR* and *larD* genes, suggesting that the *larAH* genes present in 1% of these genomes probably code for a lactate racemase. Furthermore, 11% of the organisms whose genomes were analyzed possess the *larABCE* genes but not the *larR* and *larD* genes, which are generally linked to the lactate racemization system. These species may therefore be able to synthesize NPN and produce LarAHs which are probably not lactate racemases. Finally, 15% of the genomes analyzed possess *larBCE* genes but no *larA* homologous gene (Fig. 8B), suggesting the existence of one or more superfamilies of NPN-dependent enzymes that are not LarAHs, not necessarily involving an epimerization or racemization reaction and not necessarily involving a hydride transfer mechanism [95,123,142].

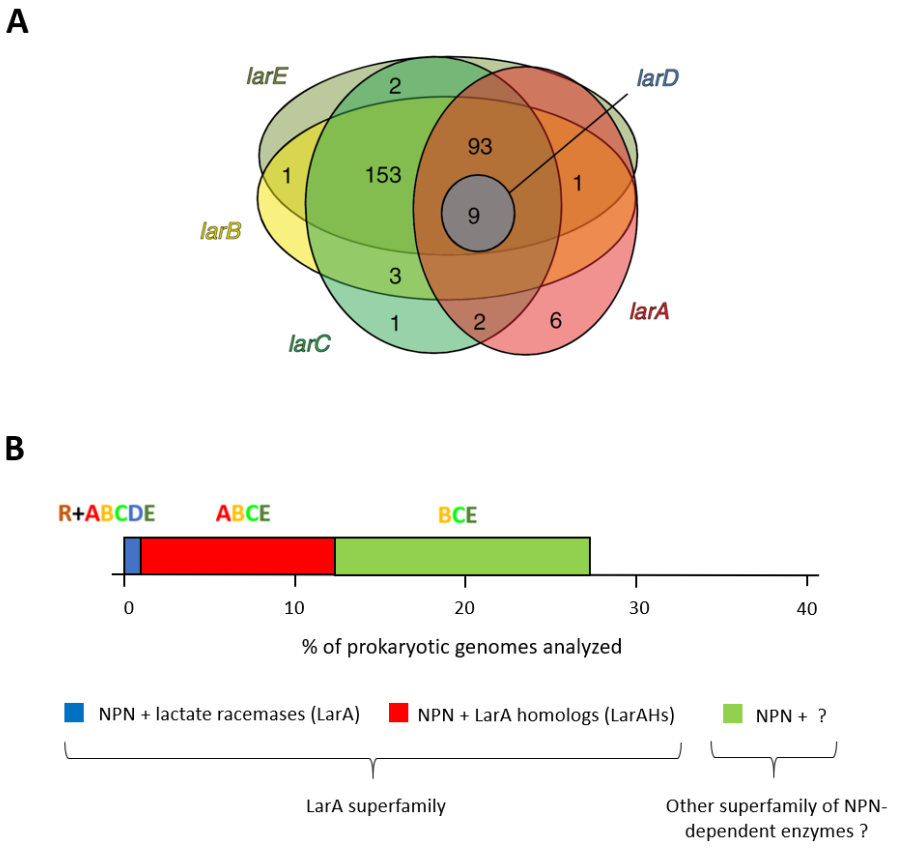

Figure 8 | Occurrence of *Lar* genes in 1,087 sequenced bacterial and archaeal genomes. (A) Venn diagram illustrating the occurrence and overlap of *larA* (red), larB (yellow), *larC* (green), *larD* (blue) and *larE* genes (olive green). **(B)** Distribution of *lar* genes in prokaryotic genomes. In blue, genomes containing the entire lactate racemase system (*larR+ABCDE*); in red, genomes containing a *larA* homologous gene and *larBCE* genes; in green, genomes possessing *larBCE*. Panel A adapted from [95].

I.4.2 Beyond lactate racemization: LarA homologs (LarAHs)

The LarA superfamily, also referred to as the DUF2088 superfamily (PF09861) due to its previously unknown function, represents a highly diverse group of enzymes. In addition to being widespread in bacteria and archaea, the genes encoding for the NPN-biosynthetic enzymes and LarAHs are even found in unicellular eukaryotes [123]. Among bacteria, LarAHs are predominantly found in *Clostridia* and *δ-Proteobacteria*, which utilize lactate as a carbon and electron source, unlike lactate-producing lactic acid bacteria such as *L. plantarum*. This shows that LarAHs are not restricted to lactate-producing bacteria but are also present in various species with different metabolic profiles [95,113]. In *L. plantarum*, the genes encoding LarA1 and NPN biosynthetic enzymes are present in a single copy and organized within an operon. However, other microorganisms may possess a distinct *lar* gene order, only cluster a subset or none of the genes, duplicate one or more of these genes, or possess an incomplete gene set [95,142]. Notably, certain species, e.g. *Enterocloster asparagiformis* and *Thermosinus carboxydivorans*, have multiple *larA* paralogs, with up to eight copies [95], suggesting potential for these LarAHs to catalyze distinct isomerization reactions. The high sequence diversity and genomic contexts of LarAHs within the LarA superfamily also indicated their potential to catalyze a broad range of isomerization reactions. These collective data suggested that LarAHs not only catalyze lactate racemization but may also catalyze the racemization or epimerization of various α-hydroxy acids [113,123].

I.4.3 LarAHs characterized so far

To hypothesize the potential reactions catalyzed by LarAHs, it is useful to examine their genomic context. Bacterial and archaeal genes are often clustered into functional units as part of operons [143] or transcription units [144], enabling the inference of the function of an unknown gene within a cluster [145]. This inference can be facilitated by bioinformatic tools such as GeConT 2 [146]. However, this method is not always informative [147].

In 2020, through biochemical studies guided by genomic context analysis, we identified six new NPN-dependent racemase and epimerase activities shared among seven LarAHs: two malate racemases (LarAH5/MAR1 and LarAH6/MAR2), one phenyllactate racemase (LarAH10/PLR), one 2-hydroxyglutarate racemase (LarAH7/HGR), two D-gluconate 2-epimerases (LarAH19/GntE1 and LarAH20/GntE2), and one short-chain aliphatic 2-hydroxy acid racemase (LarAH2/SAR) (Fig. 9, Fig. 10 & Table 2). These enzymes catalyze previously unidentified 2-hydroxyacid racemization or C2-epimerization reactions. Thus, LarA1 and the LarAHs constitute a superfamily of 2-hydroxy acid racemases and epimerases [147]. A summary of these enzymes is provided below, with detailed characterization results outlined in Table 2.

LarAH2 from *Isosphaera pallida*: SAR
LarAH2 is found in *Isosphaera pallida*, an aerobic, mesophilic, Gram-negative bacterium isolated from freshwater hot springs. *I. pallida* belongs to the *Planctomycetota* phylum and grows at temperatures up to 55°C, utilizing lactate as a carbon source [148,149]. LarAH2 exhibits short-chain aliphatic 2-hydroxy acid racemase activity (SAR) towards lactate, 2-hydroxyisovalerate, 2-hydroxyisocaproate, and likely similar substrates (Fig. 9, Fig. 10 & Table 2).

LarAH5 from *Desulfitobacterium hafniense*: MAR1
LarAH5 is found in *Desulfitobacterium hafniense*, an anaerobic, mesophilic, spore-forming, Gram-positive bacterium capable of reductive dichlorination [150]. *D. hafniense* belongs to the *Bacillota* phylum [151]. LarAH5 exhibits malate racemase (MAR) activity, hence designated as MAR1 (Fig. 9, Fig. 10 & Table 2). Interestingly, malate may not be its native substrate, indicated by the high K_M for L-malate. Instead, tartrate or 2-hydroxysuccinamate might be preferred substrates [147].

LarAH6 from *Thermoanaerobacterium thermosaccharolyticum*: MAR2

LarAH6 is found in *Thermoanaerobacterium thermosaccharolyticum*, an anaerobic, thermophilic, Gram-positive bacterium hosting another LarA paralog, the lactate racemase LarA2. *T. thermosaccharolyticum* belongs to the *Bacillota* phylum [95,152]. Similarly to LarAH5/MAR1, LarAH6 exhibits MAR activity, hence named MAR2 [147]. We recently expanded its substrate scope to include tartrate [153] (Fig. 9, Fig. 10 & Table 2). Moreover, a higher resolution crystal structure than that shown previously was obtained (2.25 Å, PDB: 7S91). Site-directed mutagenesis allowed for better characterization of MAR2's active site and confirmed that the racemization mechanism of MAR2 is similar to that of LarA1. Additionally, mutagenesis was performed on two residues of MAR2, changing the substrate recognition residues to match the corresponding residues in LarA1. This allowed for modulation of MAR2's activity as it acquired low levels of LAR activity [153].

LarAH7 from *Deferribacter desulfuricans*: HGR

LarAH7 is found in *Deferribacter desulfuricans*, an anaerobic, mesophilic, sulphur-reducing, Gram-negative bacterium isolated from deep-sea hydrothermal vents. *D. desulfuricans* belongs to the *Deferribacteres* phylum [154]. LarAH7 displays 2-hydroxyglutarate racemization (HGR) activity, thus named HGR. Its instability made k_{cat} measurements imprecise (Fig. 9, Fig. 10 & Table 2) [147].

LarAH10 from *Megasphaera elsdenii*: PLR

LarAH10 is found in *Megasphaera elsdenii*, an anaerobic, mesophilic, Gram-negative bacterium found in the rumen of sheep and cattle [155], as well as the human gut [156]. *M. elsdenii* belongs to the *Bacillota* phylum. LarAH10 catalyzes phenyllactate racemization (PLR) and was named PLR (Fig. 9, Fig. 10 & Table 2) [147].

LarAH19 from *Corynebacterium glutamicum*: GntE1

LarAH19 is found in *Corynebacterium glutamicum*, a facultative anaerobic, mesophilic, Gram-positive bacterium commonly used in industrial biotechnology for amino acid synthesis, among other applications [157]. *C. glutamicum* belongs to the *Actinomycetota* phylum. LarAH19 catalyzes D-gluconate C2-epimerization, and was named GntE1. When assayed with D-mannonate, the enzyme exhibited a high K_M, suggesting that this might not be its native substrate (Fig. 9, Fig. 10 & Table 2) [147].

LarAH20 from Thermotoga maritima: GntE2

LarAH20 is present in *T. maritima*, an anaerobic, hyperthermophilic, Gram-negative bacterium growing between 55 and 90°C. It was isolated from geothermal areas on the sea floor and it produces L-lactate as a product of carbohydrate fermentation. *T. maritima* belongs to the *Thermotogae* phylum [158,159]. Similarly to LarAH19/GntE1, LarAH20 catalyzes D-gluconate C2-epimerization and was therefore named GntE2 [147]. Prior to its characterization, the activity of GntE2 was inferred based on the analysis of its genomic context, which showed its association with genes of the hexuronate catabolic pathway [87,160]. Consistent with the extremely thermophilic nature of its source organism, LarAH20 exhibited the highest optimal temperature, around 80-90°C (Fig. 9, Fig. 10 & Table 2) [147]. Analysis of its structure, which had been solved prior to our 2020 study, suggests that LarAH20 uses the same mechanism as LarA1 [124,147].

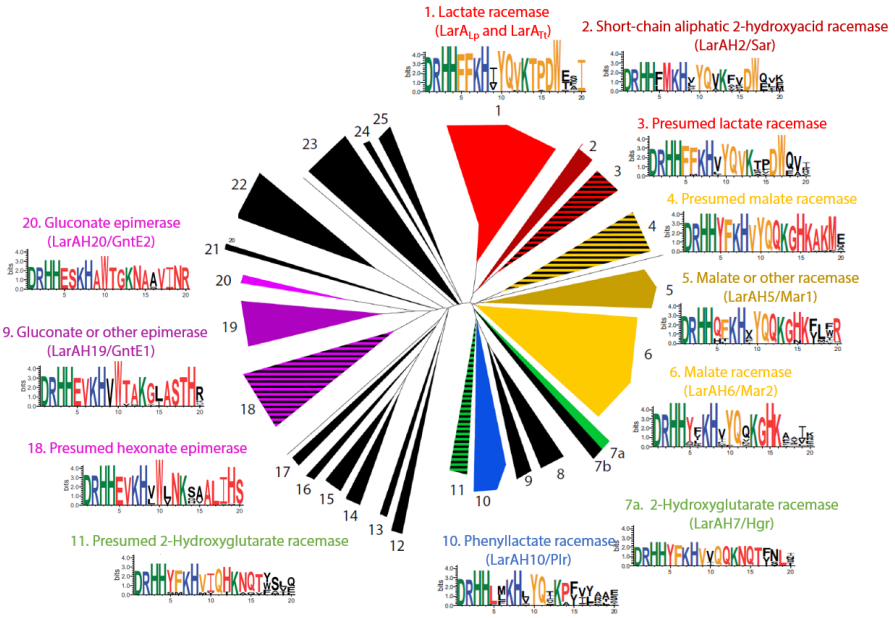

Figure 9 | Phylogenetic tree of the LarAH groups. For each group whose activity is suspected the sequence logo is shown, with residues equivalent to D72, R75, H108, H174, F175, F176, K184, H200, I220, Y294, Q295, V297, K298, T353, P355, D356, W358, T359, A360, I362 of LarA1. Inside each logo, residues involved in catalytic activity are green, those involved in NPN binding are blue, those probably involved in substrate recognition are yellow, conserved residues differing from LarA1 are red, and those not conserved within the group are black. The logos were generated using Weblogo [161]. The groups for which at least one member have shown enzymatic activity are colored plain, the groups whose activity is suspected are striped black. The groups for which no activity was shown or suspected are colored black.

Table 2 | Kinetic parameters of LarA superfamily members characterized so far. Adapted from [147,153].

	Substrate	pH opt[a]	Temp opt[a] (°C)	K_M (mM)[b]	k_{cat} (s-1)[b]	k_{cat}/K_M (mM^{-1} s^{-1})
LarA1	D-lactate	6	35-40	11 ± 4	1,300 ± 130	103 ± 50
	L-lactate			46 ± 20	4,750 ± 500	121 ± 56
LarA2	D-lactate	NI	NI	3 ± 2	551 ± 102	184 ± 127
	L-lactate			8 ± 3	986 ± 76	123 ± 47
LarAH2/SAR	D-lactate	7.5	45-50	0.15 ± 0.04	4.7 ± 0.3	31 ± 10
	L-lactate			0.56 ± 0.10	8.1 ± 0.5	14 ± 4
LarAH5/MAR1	L-malate	9	45-50	55 ± 6	140 ± 9	0.39 ± 0.07
LarAH6/MAR2	L-malate	6	35-45	0.4 ± 0.04	66 ± 10	185 ± 49
	L-tartrate			19.9 ± 0.3	14.7 ± 0.0	0.74 ± 0.02
	D-tartrate			47.8 ± 0.8	20 ± 0.1	0.42 ± 0.01
LarAH7/HGR	L-2-hydroxyglutarate	7-8	NI	0.32 ± 0.06	> 1.5	> 4.7 ± 1
LarAH10/PLR	L-3-phenyllactate	NI	NI	0.4 ± 0.3	0.16 ± 0.03	0.28 ± 0.21
LarAH19/GntE1	D-mannonate	5.5-8	30-55	120 ± 23	59 ± 12	0.48 ± 0.15
LarAH20/GntE2	D-mannonate	6	80-90	17 ± 6	197 ± 20	11 ± 5

[a]: optimal pH range or temperature (temp), where activity was > 90% of the maximum activity.
[b]: ± 95% confidence interval based on non-linear regression using the Michaelis–Menten equation.
NI: not investigated.

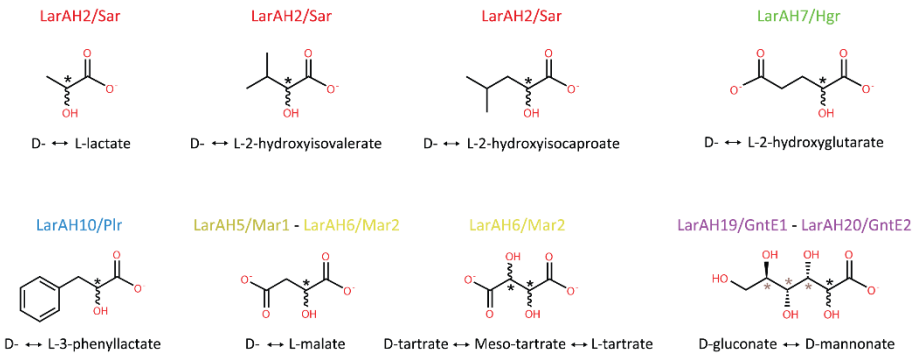

Figure 10 | Reactions catalyzed by the LarAHs characterized so far. The colors of the LarAHs correspond to the groups in the LarA superfamily phylogenetic tree (Fig. 9). The alpha chiral carbons of substrates are depicted achiral for simplification. Black asterisks indicate stereoinversion sites, grey asterisks indicate other stereocenters in the molecule.

II. OBJECTIVES

HAs have been shown to play crucial roles in a diverse range of metabolic processes across all domains of life. Additionally, these carboxylic acids possess considerable market potential and are extensively used in numerous industries. Consequently, research on developing analysis methods and stereoselective production of HAs has garnered substantial attention. However, the class of HA racemases and epimerases (EC 5.1.2) remains poorly understood and studied as only a few of these enzymes have been characterized.

The study of the LarA superfamily is therefore of great interest, as it can expand our scientific knowledge of hydroxy acid metabolism while potentially leading to novel biotechnological applications. However, research on the LarA superfamily is still in its early stages, and much remains to be discovered about the full range of NPN-dependent racemization and C2-epimerization reactions catalyzed by LarAHs. Moreover, investigating racemization and epimerization reactions still represent a significant challenge in today's biochemistry due to the subtle structural changes between substrates and products. Therefore, the 2 main questions that led to this research project were "What is the best tool to develop in order to deepen the exploration of the LarA superfamily ?" and "What is the full scope of reactions catalyzed by members of the LarA superfamily ?". The broad aim of this thesis was therefore the discovery and *in vitro* characterization of novel HA racemases and C2-epimerases in the LarA superfamily.

The first objective of this thesis was to develop an efficient method for the chiral analysis and quantification of HA stereoisomers, particularly AHA enantiomers and PHA stereoisomers, which are the substrates of interest of LarAHs. Existing analytical methods for the chiral analysis of HAs are either labor-intensive or costly, and none provide a universal procedure for various types of HAs. Additionally, robust analytical methods for chiral analysis of PHA stereoisomers are nearly nonexistent. The objective of this section was to fill this major gap in the field of chiral analysis while providing an efficient tool for investigating the LarA superfamily.

The second objective of this thesis was to explore the diversity of reactions catalyzed by LarA superfamily members. Our recent discoveries (see Section I.3.3) likely represent just a fraction of the scope of racemization and C2-epimerization reactions catalyzed by LarAHs. The specific enzymatic

functions within most phylogenetic families in the LarA superfamily remain largely unexplored and require further investigation. The objective of this section was to purify LarAHs primarily from unexplored phylogenetic clusters of the LarA superfamily and to determine their range of activity combining phylogenetic, structural, enzymatic, and capillary electrophoresis analysis.

The final objective of this thesis was to biochemically characterize each purified LarAH to identify candidates for the production of valuable AHAs or PHAs, potentially leading to industrial or biotechnological applications in the long term. This involved a comprehensive biochemical characterization of the purified LarAHs by experimentally determining their optimal pH and temperature conditions, as well as their kinetic parameters for one representative substrate (k_{cat}, K_M and k_{cat}/K_M). Additionally, we aimed to identify the preferred substrates of the purified LarAHs by determining the k_{cat}/K_M values for all their active substrates using the developed CE method.

III. RESULTS

CHAPTER 1

Versatile capillary electrophoresis method for the direct chiral separation of aliphatic and aromatic α-hydroxy acids, β-hydroxy acids and polyhydroxy acids using vancomycin as chiral selector

Julian Urdiain-Arraiza and Benoît Desguin

Published in Journal of Chromatography A

Submitted 6 October 2023
Submitted in revised form 19 December 2023
Accepted 26 December 2023
Published online 27 December 2023

Author's contributions

The study was conceived and designed by JUA and BD.
The laboratory work was performed by JUA (all Figures and Tables).
The data were analyzed and interpreted by JUA (all Figures and Tables).
The manuscript was written by JUA.
The manuscript was revised by JUA and BD.

In this chapter, we aimed to establish a robust methodology for a comprehensive exploration and characterization of the LarA superfamily. However, elucidating the reactions catalyzed by LarA superfamily members presents significant challenges, primarily due to the need for the separation of AHA enantiomers and PHA C2-epimers. Moreover, the majority of existing analytical approaches for AHA chiral analysis are often labor-intensive, expensive, and lack the versatility required for simultaneous chiral analysis of both AHAs and PHAs.

To address this gap, we opted for chiral separation by CE as existing literature indicates it as a rapid and efficient technique for resolving AHA enantiomers. CE is an analytical technique that separates ionic species based on their electrophoretic mobility in an electric field applied across a capillary containing a buffer solution. The main components of a CE system include a capillary tube, a high-voltage power supply, an injection system to introduce the sample, and a detection system to monitor separated ions. The application of high voltage across the electrodes initiates an electric field, facilitating the migration of analytes from the anode to the cathode within the capillary. Each end of the capillary is immersed in a vial containing an electrode and an electrolyte solution, into which a chiral selector (e.g. vancomycin) can be added for chiral analysis. During the process, a small amount of sample is injected into the capillary, and the electric field causes ions to migrate at different speeds depending on their charge and size, resulting in their separation. In the case of chiral analysis, given that the stereoisomers of the same molecule have the same charge and the same size, the chiral selector is used to separate them depending to their stereochemistry. Detection occurs as ions reach the detector, producing an electropherogram (EPG) that represents signal intensity (commonly absorbance or fluorescence) over time (Fig. 15).

To develop a protocol tailored to our objectives, we combined elements from previously published methodologies for the chiral separation of amino and hydroxy acids. The optimized protocol employed a partial filling-counter current method with indirect UV detection, utilizing vancomycin as the chiral selector in a background electrolyte comprising 10 mM benzoic acid/L-histidine at pH 5, and a polyacrylamide-coated capillary.

This protocol proved to be a versatile and highly efficient CE method, enabling the direct chiral analysis and quantification of a wide range of HA stereoisomers, including both aliphatic and aromatic AHA enantiomers, aliphatic BHA enantiomers, and aliphatic PHA stereoisomers. This versatility represents a substantial improvement over prior methods, which were often limited to narrower analyte ranges or necessitated different separation conditions for distinct compound classes. Consequently, this protocol simplifies analytical workflows and obviates the requirement for multiple chiral separation strategies. Additionally, the ability to perform direct chiral separation without derivatization streamlines sample preparation, reduces analysis time, and preserves the native structures and properties the analytes.

In order to optimize the utilization of the developed method, we also determined the variation of chiral resolution, analysis time, signal intensity and limit of detection as a function of vancomycin concentration and capillary length. Collectively, this chapter addresses a critical gap in the field of chiral analysis while providing a highly efficient and adaptable tool for the investigation of the LarA superfamily.

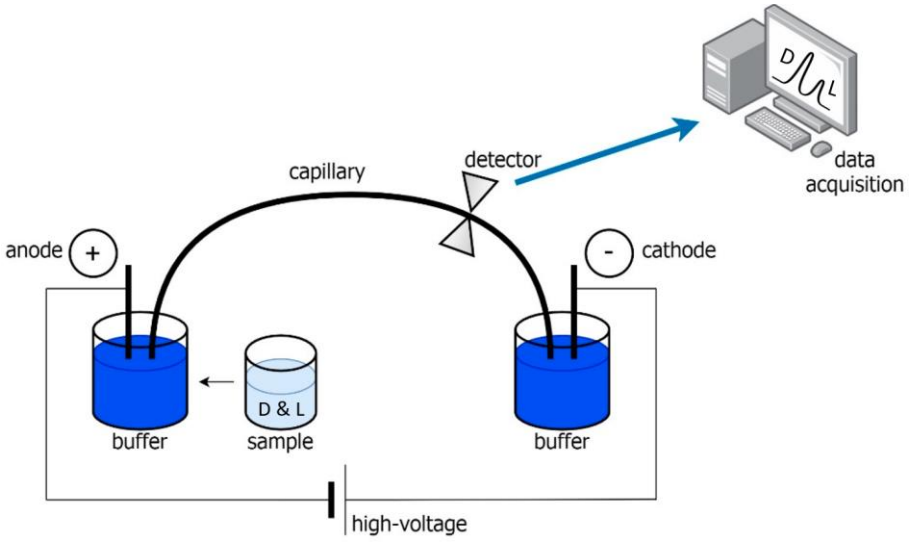

Figure 15. Capillary electrophoresis system. Adapter from [162]

III.1.1 Manuscript

Versatile capillary electrophoresis method for the direct chiral separation of aliphatic and aromatic α-hydroxy acids, β-hydroxy acids and polyhydroxy acids using vancomycin as chiral selector

Julian Urdiain-Arraiza[1] and Benoît Desguin[1]

[1] Louvain Institute of Biomolecular Science and Technology (LIBST), UCLouvain, 1348 Louvain-La-Neuve, Belgium.

Abstract

Hydroxy acids (HAs) are ubiquitous in nature and play significant roles in various industrial and biological processes. Most HAs harbor at least one chiral center, therefore the development of efficient chiral analysis techniques for HA stereoisomers is of crucial importance across a wide range of fields. A capillary electrophoresis (CE) method was developed for the chiral analysis and quantification of aliphatic and aromatic α-hydroxy acid (AHA) enantiomers, aliphatic β-hydroxy acid (BHA) enantiomers and aliphatic polyhydroxy acid (PHA) stereoisomers. Using a modified partial filling-counter current method with indirect UV detection, high resolution (Rs) was achieved with vancomycin as a chiral selector added to the background electrolyte composed of 10 mM of benzoic acid/L-histidine at pH 5 using a polyacrylamide-coated capillary. This method could be readily applied to the determination of the enantiomers of 12 aliphatic AHAs, 4 aromatic AHAs, 3 aliphatic BHAs, as well as to the determination of the stereoisomers of tartaric acid, 2,3-dihydroxybutanoic acid, 2,3,4,5-tetrahydroxypentanoic acid, and 2,3,4,5,6-pentahydroxyhexanoic acid without the need for sample derivatization. Finally, our study provides a robust and versatile strategy for the chiral and stereoselective analysis of a broad range of hydroxy acid compounds.

Keywords

Capillary electrophoresis, enantiomer separation, hydroxy acids, enantioselective analysis, chiral analysis, vancomycin

INTRODUCTION

Hydroxy acids (HAs), which are carboxylic acids containing at least one hydroxyl group, are widespread chiral compounds in nature and serve as essential biological building blocks [163]. Among HAs, α-hydroxy acids (AHAs) have their hydroxyl group attached to the second carbon, β-hydroxy acids (BHAs) have their hydroxyl group attached to the third carbon, and polyhydroxy acids (PHAs) possess multiple hydroxyl groups in their structure [2]. In addition to being key metabolites of most metabolic pathways, these acids have considerable market potential and find extensive applications as cosmetics [36,37], drug precursors [164], food components and additives [46,47], building blocks in chemical synthesis [164], monomers for diverse biopolymers [51], and in the production of various basic chemicals [1].

Over the last decades, the chiral analysis of HA stereoisomers, which include enantiomers and diastereomers, has become of major interest. Different stereoisomers exhibit distinct chemical and biochemical properties, emphasizing the need to accurately determine and utilize the appropriate stereoisomer for specific applications. Consequently, efficient chiral analysis methods of HA stereoisomers play a crucial role in a wide range of fields. (i) In pharmacology and cosmetics: HAs have significant clinical and pharmacological activity on the skin [2,36]. However, the stereochemistry of compounds is crucial for their therapeutic efficacy and safety [165]. Enantiomeric analysis is essential to ensure the production of stereochemically pure chiral compounds, particularly in pharmaceutical drug research, production, and monitoring processes. (ii) In microbiology: Some HAs are produced by microorganisms and are involved in biodegradation processes. In some cases, the degradation or synthesis rate of a compound may depend on its stereochemistry [166]. Analysis of enantiomers can help researchers investigate the degradation pathways involved. (iii) In food industry: HAs can be important components of food and flavor additives [46,47]. Quality control based on enantioselective analysis of specific enantiomers of HAs can help improve the quality and safety of food products by ensuring that only the desired enantiomer is present. (iv) In industrial chemistry: HA diastereomers may have different physical or chemical properties that affect their performance in industrial processes. Analysis of diastereomers can help optimize industrial production and improve the yield and quality of the final product. (v) In clinical analysis: Alterations in the expected levels of many AHAs have been associated to specific diseases or

health benefits [5]. Their enantioselective analysis is consequently a major concern in biomarker studies and clinical analysis [167,168]. Overall, the chiral analysis of HA stereoisomers is important to ensure the safety, efficacy, and environmental impact of drugs, food additives, and industrial products.

Direct chiral analysis of HAs involves the formation of transient diastereomeric complexes and does not require derivatization. In contrast, indirect chiral analysis of HAs involves the formation of stable diastereomers and requires derivatization [169]. A variety of different analytical methods have been employed to separate underivatized HAs. Aliphatic AHA enantiomers have been separated by CE [170,171], HPLC [167,172,173], HPLC-MS [174], LC-MS/MS [175], and ligand exchange CE (LE-CE) [176]. The separation of aromatic AHA enantiomers has been accomplished using techniques such as CE [177,178], LE-CE [179], ligand-exchange capillary electrochromatography (LE-CEC) [180], ligand exchange high-speed countercurrent chromatography (LE-HSCCC) [181], and HPLC [182,183]. Similarly, aliphatic BHA enantiomers have been separated by HPLC [167,184], HPLC-ESI-MS/MS [185], and UHPLC-MS/MS [186]. To date, no CE method has been described for the chiral analysis of underivatized BHAs or PHAs, except for DL-tartaric acid using CE [187,188] or HPLC [167], to the best of our knowledge.

Among these methods, CE has proven to be a cheap, simple and highly effective technique for the analysis of enantiomers without the need for derivatization or polar solvents, and it offers versatile capabilities due to the availability of numerous chiral selectors [189,190]. In particular, CE excels in the analysis of charged solutes and constitutes a powerful tool for the analysis of carboxylic acids in general [191]. Moreover, of all the analytical methods available, none yet offers a general procedure for the chiral analysis of different types of HAs. The lack of a chiral analysis method for PHAs and of a versatile procedure for chiral analysis of different types of HAs leaves a major gap in the field of chiral analysis of these valuable compounds.

This study addresses this gap in the field of chiral analysis of HA stereoisomers. We have developed a versatile and highly efficient CE method that allows the direct chiral analysis and quantification of a broad spectrum of HA stereoisomers, including aliphatic and aromatic AHA enantiomers, aliphatic BHA enantiomers, and aliphatic PHA stereoisomers. The chemical structures of the chiral HAs investigated are shown in Fig. 1.1.

RESULTS & DISCUSSION

Method development and robustness

For our method, we used a background electrolyte (BGE) consisting of an aqueous buffer of 10 mM benzoic acid/L-histidine at pH 5. Vancomycin was chosen as a chiral selector because it is a macrocyclic glycopeptide antibiotic (MA) commonly used in capillary electrophoresis for the enantioseparation of chiral compounds with carboxylic groups [192–194]. We opted for a hydrodynamic partial-filling countercurrent separation method with indirect UV detection in a polyacrylamide-coated capillary, as this method provides several advantages. First, indirect UV detection enables the analysis of non-UV-absorbing compounds such as aliphatic HAs, thus broadening the range of detectable analytes. Second, the polyacrylamide coating reduces the adsorption of analytes and chiral selectors on the capillary wall, resulting in improved separation efficiency and reduced EOF [195]. Third, the partial filling technique allows for improved analyte detectability by eliminating vancomycin from the detection cell, thereby minimizing its interference. This is particularly important since vancomycin absorbs strongly in the UV region [196,197]. Lastly, the countercurrent separation method enhances the separation of enantiomers due to the opposite migration directions of the HAs and the vancomycin cations [195,198].

Fig. 1.2 shows an electropherogram (EPG) obtained with our method displaying the simultaneous enantioseparation of the enantiomers of an AHA (DL-2-hydroxybutyric acid), a BHA (DL-3-hydroxybutyric acid), and a PHA (DL-gluconic acid). A large absorbing zone was observed at the beginning of each run. This was previously shown by Bednar P. *et al.* that it is due to the presence of chloride anions associated with the vancomycin cations [199]. By using a partial-filling countercurrent separation method, the vancomycin cations migrate away from the detection window, while the chloride anions and hydroxy acid anions migrate towards the detection window. The chloride anions are detected first due to their higher mobility within the system. The area of the peak corresponding to chloride anions is directly proportional to both the concentration of vancomycin and the effective length of the capillary used for chiral separation. In general, when using 25 mM vancomycin, the chloride anion peak ends at 31 minutes using a capillary with an effective length of 112 cm, and at 8 minutes using a capillary with an effective length of 46 cm.

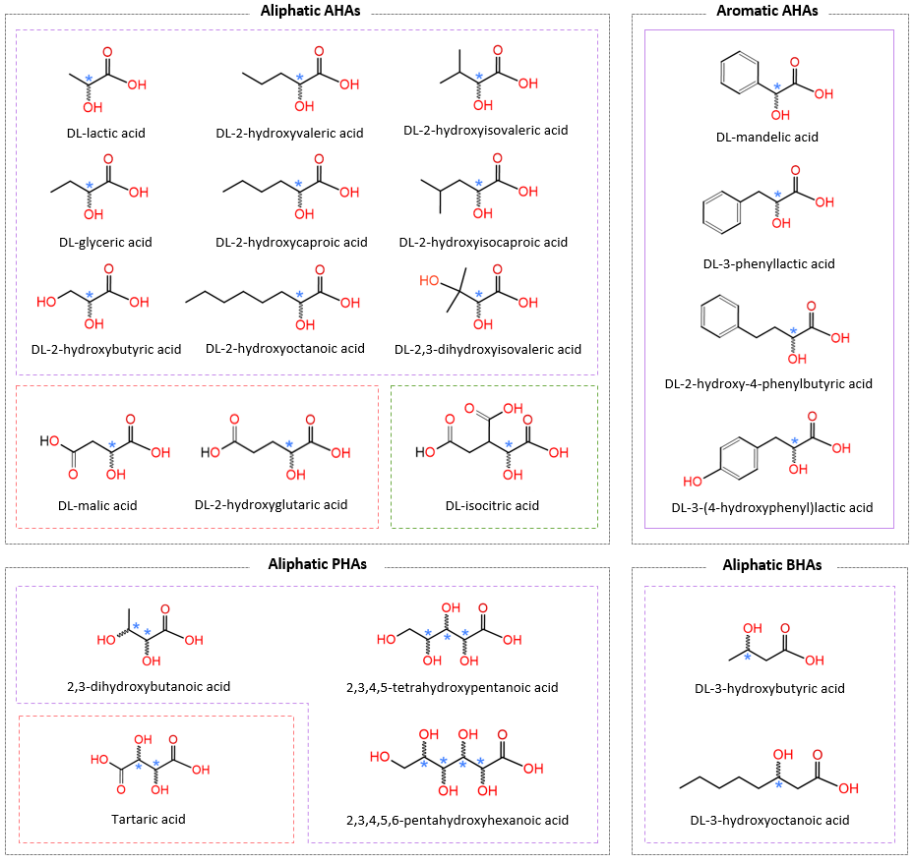

Figure 1.1 | **Chemical structures of the HAs investigated.** Monocarboxylic acids are boxed in violet, dicarboxylic are boxed in salmon pink, tricarboxylic acids are boxed in green. Non-UV-absorbing compounds are boxed by a dashed line, while UV-absorbing compounds are boxed by a solid line. The chiral carbons are indicated by blue asterisk and are left achiral for simplification.

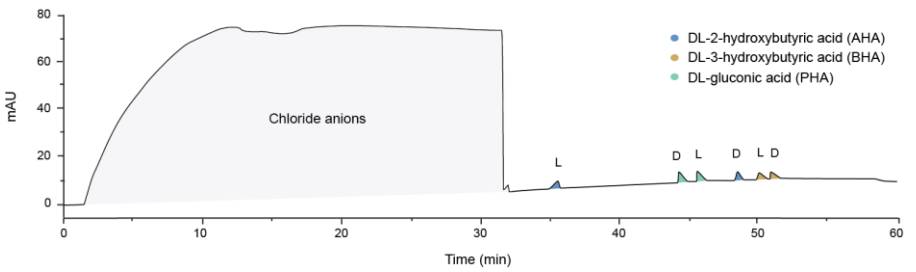

Figure 1.2 | **EPG of the simultaneous enantioseparation of the enantiomers of an AHA, a BHA and a PHA.** All enantiomers are at a concentration of 8 mM. Electrophoretic conditions: polyacrylamide-coated capillary, 122 (112) cm x 50 µm; BGE, 10 mM benzoic acid/L-histidine, pH 5, and 25 mM vancomycin; partial filling, 145 s at 1000 mbar; injection, 5 s at 30 mbar; voltage, –25 kV; temperature, 20°C; indirect detection at 230 nm.

For the separation of DL-2-hydroxybutyric acid, DL-3-hydroxybutyric acid and DL-gluconic acid, we calculated the intra-day and inter-day relative standard deviation (R.S.D.) for various parameters. Inter-day R.S.D. values are between 0.5% and 3.9% for peak areas, 0.1% and 1.1% for migration times, 2.8% and 4.9% for resolutions and 0.2% and 0.7% for separation factors. Intra-day R.S.D. values are between 1.1% and 4.9% for peak areas, 1.8% and 3.5% for migration times, 3.5% and 6.9% for resolutions and 0.3% and 1.3% for separation factors. These low inter- and intra-day variabilities demonstrate the robustness of our method for the chiral separation of AHAs, BHAs and PHAs (Table 1.S1).

Chiral separation of AHA enantiomers

Chiral separation of aliphatic AHA enantiomers

Our method allowed the highly efficient chiral analysis of 12 different aliphatic AHAs which are non-UV-absorbing: DL-lactic acid, DL-glyceric acid, DL-2-hydroxybutyric acid, DL-2-hydroxycaproic acid, DL-2-hydroxyisocaproic acid, DL-malic acid, DL-2-hydroxyvaleric acid, DL-2-hydroxyisovaleric acid, DL-2-hydroxyoctanoic acid, DL-2,3-dihydroxyisovaleric acid, DL-2-hydroxyglutaric acid, and DL-isocitric acid (Figs. 1.3A and 1.3B). Baseline resolution ($Rs \geq 1.5$) was obtained for all aliphatic AHA enantiomers (Table 1.1). This demonstrates that our protocol allows the chiral separation of monocarboxylic (e.g. lactic acid), dicarboxylic (e.g. 2-hydroxyglutaric acid) and tricarboxylic (e.g. isocitric acid) AHA enantiomers. The migration times of the AHA anions positively correlate with their molecular weight and negatively correlate with the number of negative charges (Table 1.1 and Fig. 1.3). Lactic acid is one of the AHAs whose chiral separation has been most widely reported in the literature, with Rs values ranging from 1.25 to 3.8 [170,171,173,174,200–203]. In comparison, our method allows the chiral separation of DL-lactic acid with a Rs of 28.3 (Table 1.1).

Chiral separation of aromatic AHA enantiomers

Aromatic AHAs have wide-ranging applications for the production of biocompatible and biodegradable polymers, as antimicrobial compounds, for biomarker usage, and as versatile chiral building blocks for the large-scale production of active pharmaceutical compounds including antibiotics, antitumor, and antiobesity agents [164,182]. Fig. 1.4 shows an efficient

chiral separation of four different aromatic AHAs which are UV-absorbing due to their aromatic ring acting as a chromophore: DL-mandelic acid, DL-3-phenyllactic acid, DL-3-(4-hydroxyphenyl)lactic acid, and DL-2-hydroxy-4-phenylbutyric acid. Baseline resolution was obtained for all aromatic AHA enantiomers (Table 1.1).

Chiral separation of aliphatic BHA enantiomers

Aliphatic BHAs have multifaceted applications, serving as starting materials for chemical synthesis and biochemical transformations for the production of optically active bioactive compounds such as vitamins, antibiotics, antifungals, pheromones and flavors [204,205]. For example, 3-hydroxybutyrate has gained significant interest in medicine, dietetics, and for the biodegradable plastics industry [206]. In addition, many aliphatic BHAs are important chiral building blocks for lipopeptide synthesis and as disease-related biomarkers [207,208]. As such, enantioselective analysis of aliphatic BHAs is crucial for an unbiased biological or clinical interpretation.

However, in spite of the advanced state of enantiomer separation methods, the direct or indirect chiral separation of aliphatic BHAs remains a challenge in comparison to the chiral separation of AHAs. Currently, no CE method has been published for the enantioseparation of BHAs. Using our method, both D- and L- enantiomers of 3-hydroxybutyric acid and of 3-hydroxyoctanoic acid were separated (Fig. 1.5). Baseline resolution was obtained for all aliphatic BHA enantiomers (Table 1.1). Enantioselectivity may also be expected for aliphatic BHA with carbon chain lengths between four and eight carbons, as resolution improved with carbon chain length from four to eight.

When comparing the chiral separation of AHA and BHA enantiomers, we observed that the resolution was 8 to 12 times lower for BHA enantiomers, thus requiring a higher concentration of vancomycin for their efficient separation (Fig. 1.6). Vancomycin probably interacts less specifically with the molecules when the hydroxyl group is located on C3 rather than on C2, as the distance and flexibility between the carboxyl group and both the hydroxyl and carbon side chain increase.

Table 1.1 | **Separation data of AHA and BHA enantiomers.** All separations were performed with 0.5 mM of each enantiomer. Rs = resolution; α = separation factor; MW = molecular weight (g/mol); MO = migration order. Vancomycin concentrations as indicated, other electrophoretic conditions as in Fig. 1.2.

	DL-enantiomers	MW	Vancomycin	MO	α	Rs
Aliphatic AHAs	DL-isocitric acid	192.1	12	D < L	1.06	4.3
	DL-malic acid	134.1			1.03	1.5
	DL-lactic acid	90.1	15		1.43	28.3
	DL-glyceric acid	106.1			1.11	6.3
	DL-2-hydroxyglutaric acid	148.1			1.07	4.8
	DL-2-hydroxybutyric acid	104.1			1.29	20.4
	DL-2-hydroxyvaleric acid	118.1			1.32	26.1
	DL-2-hydroxyisovaleric acid	118.1			1.16	11.3
	DL-2-hydroxycaproic acid	132.2			1.26	21.8
	DL-2-hydroxyisocaproic acid	132.2		L < D	1.28	23.2
	DL-2,3-dihydroxyisovaleric acid	134.1			1.11	8.3
	DL-2-hydroxyoctanoic acid	160.2	25		1.22	18.3
Aromatic AHAs	DL-mandelic acid	152.2			1.02	1.7
	DL-3-phenyllactic acid	166.2			1.38	29.4
	DL-3-(4-hydroxyphenyl)lactic acid	182.2			1.47	43.2
	DL-2-hydroxy-4-phenylbutyric acid	180.2			1.16	15.3
Aliphatic BHAs	DL-3-hydroxybutyric acid	104.1			1.02	1.8
	DL-3-hydroxyoctanoic acid	160.2			1.03	2.7

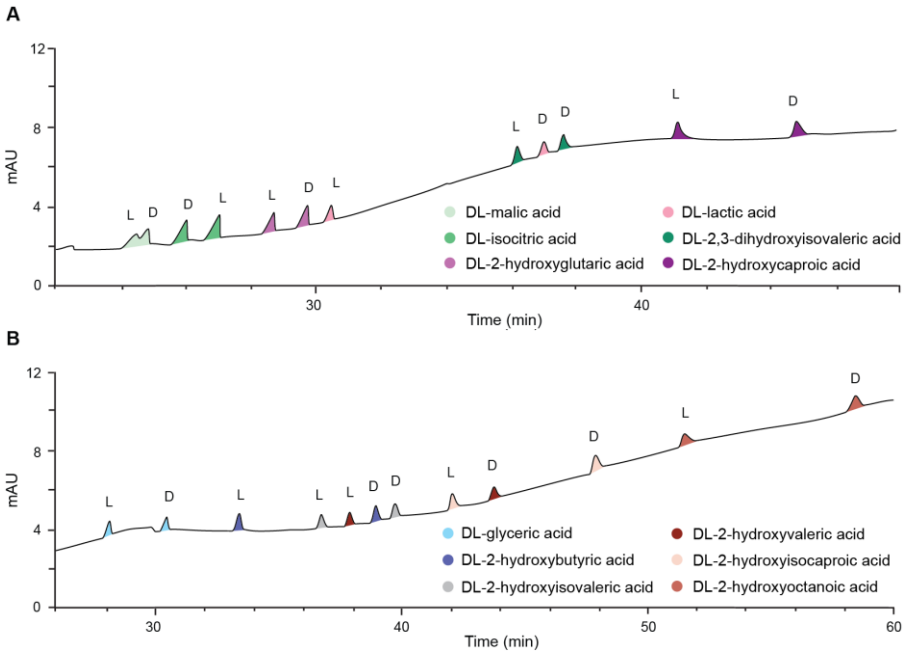

Figure 1.3 | **Simultaneous enantioseparation of aliphatic AHA enantiomers.** All enantiomers are at a concentration of 1 mM. (**A**) Vancomycin concentration 10 mM, other electrophoretic conditions as in Fig. 1.2. (**B**) Vancomycin concentration 15 mM, other electrophoretic conditions as in Fig. 1.2.

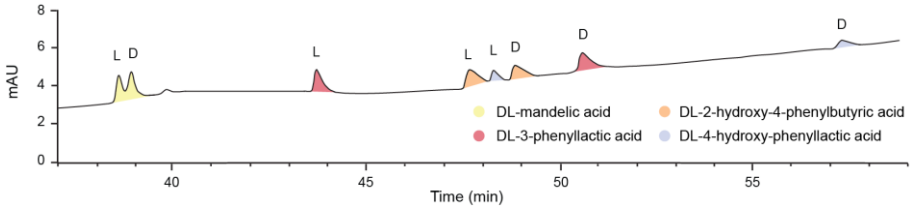

Figure 1.4 | Simultaneous enantioseparation of aromatic AHA enantiomers. All enantiomers are at a concentration of 2 mM. Vancomycin concentration 10 mM, other electrophoretic conditions as in Fig. 1.2.

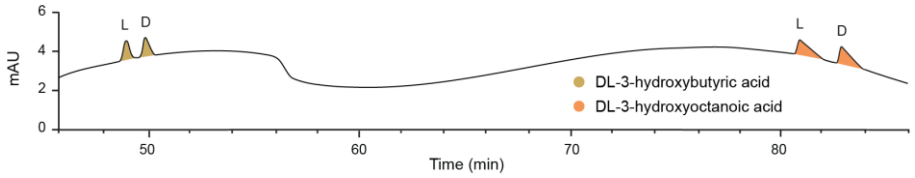

Figure 1.5 | Simultaneous enantioseparation of BHA enantiomers. All enantiomers are at a concentration of 2 mM. Electrophoretic conditions as in Fig. 1.2.

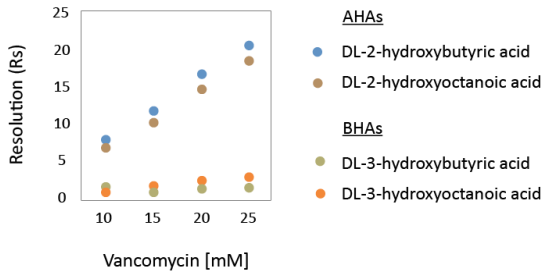

Figure 1.6 | Chiral separation of AHA enantiomers compared to the chiral separation of BHA enantiomers. Vancomycin concentrations as indicated, other electrophoretic conditions as in Fig. 1.2.

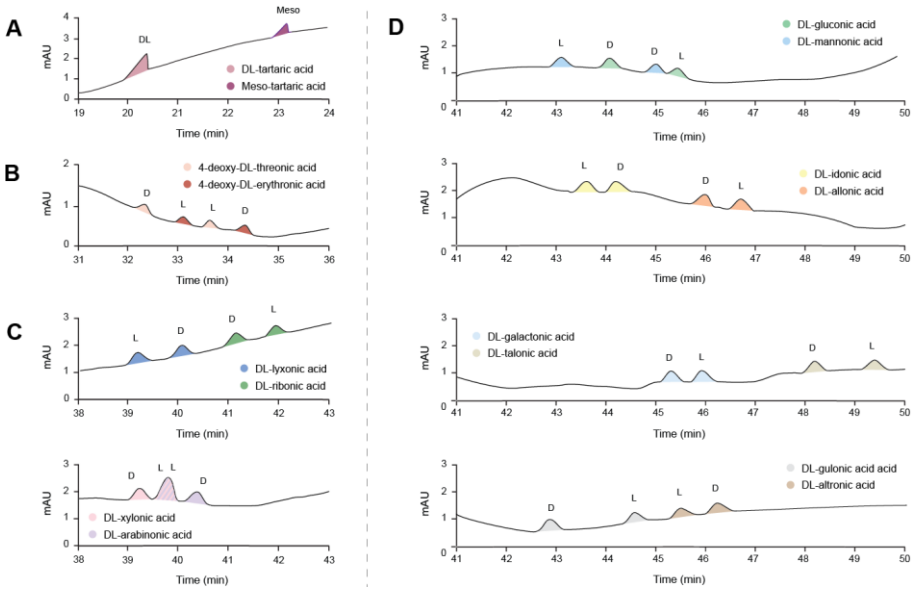

Figure 1.7 | **Chiral separation of PHAs stereoisomers.** All enantiomers are at a concentration of 0.5 mM. (**A**) Chiral separations of tartaric acid stereoisomers. Electrophoretic conditions: vancomycin 5 mM. (**B**) Chiral separations of 2,3-dihydroxybutanoic acid stereoisomers. Electrophoretic conditions: vancomycin 20 mM. (**C**) Chiral separations of 2,3,4,5-tetrahydroxypentanoic acid stereoisomers. (**D**) Chiral separations of 2,3,4,5,6-pentahydroxyhexanoic acid stereoisomers. Other electrophoretic conditions as in Fig. 1.2 for **A**, **B**, **C** and **D**.

Chiral separation of aliphatic PHA stereoisomers

While underivatized AHAs and BHAs have been previously enantioseparated using various chiral methods, analogous applications for underivatized PHAs are absent in the scientific literature, except for tartaric acid. In this study, we analyzed the enantiomers and diastereomers of tartaric acid (DL- and meso-tartaric acid) (Fig. 1.7A), 2,3-dihydroxybutanoic acid (4-deoxy-DL-erythronic acid and 4-deoxy-DL-threonic acid) (Fig. 1.7B), 2,3,4,5-tetrahydroxypentanoic acid (DL-ribonic acid, DL-arabinonic acid, DL-xylonic acid, and DL-lyxonic acid) (Fig; 1.7C) and 2,3,4,5,6-pentahydroxyhexanoic acid (DL-gluconic acid, DL-allonic acid, DL-gulonic acid, DL-altronic acid, DL-talonic acid, DL-galactonic acid, DL-idonic acid, and DL-mannonic acid) (Fig. 1.7D). All of these compounds are aldonic sugar acids, except tartaric acid which is an aldaric sugar acid. The chiral separation of sugar acids could become of utmost interest since these acids are widely distributed in nature and are used for numerous applications, such as detergent components, pH regulators, corrosion inhibitors, additives in the food industry, monomers for polymeric materials, and biodegradable chelators for pharmaceuticals [59].

Most reports on the chiral separation of tartaric acid only mention the separation of its enantiomers, D- and L-tartaric acid. In our case, the separation of tartaric acid enantiomers was not successful, but we could achieve the separation of its diastereomers, D- from meso- and L- from meso (Table 1.2). Additionally, with our method, we were able to differentiate all six possible stereoisomer combinations of 2,3-dihydroxybutanoic acid (Table 1.3), 24 out of the 28 possible stereoisomer combinations of 2,3,4,5-tetrahydroxypentanoic acid (Table 1.4), and 101 out of the 120 possible stereoisomer combinations of 2,3,4,5,6-pentahydroxyhexanoic acid (Table 1.5). When a Rs cut-off of 1.5 is applied, which corresponds to the baseline separation of two different peaks, we were still able to differentiate five out of six possible stereoisomer combinations of 2,3-dihydroxybutanoic acid, 15 out of 28 possible stereoisomer combinations of 2,3,4,5-tetrahydroxypentanoic acid, and 89 out of 120 possible stereoisomer combinations of 2,3,4,5,6-pentahydroxyhexanoic acid (Table 1.6). This demonstrates that our method is capable of differentiating the vast majority of PHA stereoisomers.

Table 1.2 | **Chiral separation of tartaric acid stereoisomers.** Enantiomers (yellow boxes), C-2 and C-3 epimers (red boxes). NS = not separated. The resolution is underlined and the separation factor is italicized. Vancomycin concentration 5 mM, other electrophoretic conditions as in Fig. 1.2.

	Resolution (Rs) and separation factor (α)			
	D-tartaric acid (2S,3S)		L-tartaric acid (2R,3R)	
L-tartaric acid (2R,3R)	NS			
Meso-tartaric acid (2R,3S) or (2S,3R)	5.7	*1.12*	5.7	*1.12*

Table 1.3 | **Chiral separation of 2,3-dihydroxybutanoic acid stereoisomers.** Enantiomers (yellow boxes), C-2 epimers (purple boxes), C-3 epimers (blue boxes)**.** D-4DE = 4-deoxy-D-erythronic acid (2R,3R), L-4DE = 4-deoxy-L-erythronic acid (2S,3S), D-4DT = 4-deoxy-D-threonic acid (2S,3R), L-4DT = 4-deoxy-L-threonic acid (2R,3S), NS = not separated. The resolution is underlined and the separation factor is italicized. Vancomycin concentration 20 mM, other electrophoretic conditions as in Fig. 1.2.

	Resolution (Rs) and separation factor (α)					
	D-4DE (2R,3R)		L-4DE (2S,3S)		D-4DT (2S,3R)	
L-4DE (2S,3S)	2.8	*1.04*				
D-4DT (2S,3R)	4.3	*1.07*	1.9	*1.03*		
L-4DT (2R,3S)	1.5	*1.02*	1.3	*1.02*	3.1	*1.05*

Table 1.4 | **Chiral separation of 2,3,4,5-tetrahydroxypentanoic acid stereoisomers.** Enantiomers (yellow boxes), C-2 epimers (purple boxes), C-3 epimers (blue boxes), C-4 epimers (grey boxes). D-xylo = D-xylonic acid (2R,3S,4R), L-xylo = L-xylonic acid (2S,3R,4S), D-lyxo = D-lyxonic acid (2S,3S,4R), L-lyxo = L-lyxonic acid (2R,3R,4S), D-ribo = D-ribonic acid (2R,3R,4R), L-ribo = L-ribonic acid (2S,3S,4S), D-ara = D-arabinonic acid (2S,3R,4R), L-ara = L-arabinonic acid (2R,3S,4S), NS = not separated. The resolution is underlined and the separation factor is italicized. Electrophoretic conditions as in Fig. 1.2.

	Resolution (Rs) and separation factor (α)													
	D-xylo		L-xylo		D-lyxo		L-lyxo		D-ribo		L-ribo		D-ara	
L-xylo	1.1	*1.02*												
D-lyxo	1.6	*1.02*	0.6	*1.01*										
L-lyxo	NS		1.1	*1.02*	1.6	1.02								
D-ribo	3.4	*1.05*	2.2	*1.03*	1.8	*1.03*	3.4	1.05						
L-ribo	4.9	*1.07*	3.5	*1.05*	3.1	*1.04*	4.9	1.07	1.4	1.02				
D-ara	2.4	*1.03*	1.4	*1.02*	1.1	*1.02*	2.4	1.03	1.2	1.02	2.6	1.03		
L-ara	1.1	*1.02*	NS		0.6	*1.01*	1.1	1.02	2.2	1.03	3.5	1.05	1.4	1.02

	Resolution (Rs) and separation factor (α)														
	D-glu	L-glu	D-gal	L-gal	D-aln	L-aln	D-ma	L-ma	D-ido	L-ido	D-alt	L-alt	D-tal	L-tal	D-gul
L-glu	1.8 *1.02*														
D-gal	1.7 *1.02*	0.5 *1.01*													
L-gal	2.8 *1.03*	0.8 *1.01*	1.1 *1.01*												
D-aln	2.8 *1.03*	0.8 *1.01*	1.1 *1.01*	NS											
L-aln	3.9 *1.05*	2.2 *1.02*	2.4 *1.03*	1.2 *1.01*	1.2 *1.01*										
D-ma	1.3 *1.02*	0.7 *1.01*	0.8 *1.01*	1.7 *1.02*	1.7 *1.02*	2.5 *1.03*									
L-ma	2.2 *1.03*	3.8 *1.05*	3.5 *1.04*	4.7 *1.06*	4.7 *1.06*	5.5 *1.07*	2.9 *1.03*								
D-ido	NS	1.8 *1.02*	1.7 *1.01*	2.8 *1.03*	2.8 *1.03*	3.9 *1.05*	1.3 *1.01*	2.2 *1.02*							
L-ido	1.1 *1.01*	2.6 *1.03*	2.4 *1.03*	3.8 *1.05*	3.8 *1.05*	4.8 *1.06*	2 *1.02*	1.2 *1.01*	1.1 *1.01*						
D-alt	3.3 *1.04*	1.6 *1.02*	1.8 *1.02*	0.8 *1.01*	0.8 *1.01*	0.4 *1.01*	2.3 *1.03*	5.4 *1.07*	3.3 *1.04*	4.4 *1.05*					
L-alt	1.8 *1.02*	NS	0.5 *1.01*	0.8 *1.01*	0.8 *1.01*	2.2 *1.02*	0.7 *1.01*	3.8 *1.05*	1.8 *1.02*	2.6 *1.03*	1.6 *1.02*				
D-tal	7.7 *1.1*	5.4 *1.07*	5.7 *1.07*	4.7 *1.06*	4.7 *1.06*	3.6 *1.05*	6.2 *1.08*	9.6 *1.12*	7.7 *1.1*	8.6 *1.11*	4.1 *1.05*	5.4 *1.07*			
L-tal	10.8 *1.13*	8.2 *1.11*	8.4 *1.11*	7.6 *1.1*	7.6 *1.1*	6.4 *1.08*	9.1 *1.11*	12.4 *1.16*	10.8 *1.13*	11.6 *1.14*	6.9 *1.09*	8.2 *1.11*	2.7 *1.03*		
D-gul	2.6 *1.03*	4.7 *1.06*	4.4 *1.05*	5.3 *1.07*	5.3 *1.07*	6.5 *1.08*	3.8 *1.05*	0.8 *1.01*	2.6 *1.03*	1.9 *1.02*	6 *1.08*	4.7 *1.06*	10.4 *1.13*	13.1 *1.17*	
L-gul	0.6 *1.01*	1.3 *1.02*	1.1 *1.01*	2.3 *1.03*	2.3 *1.03*	3.3 *1.04*	0.5 *1.01*	2.4 *1.03*	0.6 *1.01*	1.5 *1.02*	2.8 *1.03*	1.3 *1.02*	6.8 *1.09*	10.1 *1.13*	3.2 *1.04*

Table 1.5 | Chiral separation of 2,3,4,5,6-pentahydroxyhexanoic acid stereoisomers. Enantiomers (yellow boxes), C-2 epimers (purple boxes), C-3 epimers (blue boxes), C-4 epimers (grey boxes), C-5 epimers (green boxes). D-glu = D-gluconic acid (2R,3S,4R,5R), L-glu = L-gluconic acid (2S,3R,4S,5S), D-gal = D-galactonic acid (2R,3S,4S,5R), L-gal = L-galactonic acid (2S,3R,4R,5S), D-aln = D-allonic acid (2R,3R,4R,5R) , L-aln = L-allonic acid (2S,3S,4S,5S), D-ma = D-mannonic acid (2S,3S,4R,5R), L-ma = L-mannonic acid (2R,3R,4S,5S), D-ido = D-idonic acid (2S,3R,4S,5R) , L-ido = L-idonic acid (2R,3S,4R,5S), D-alt = D-altronic acid (2S,3R,4R,5R), L-alt = L-altronic acid (2R,3S,4S,5S), D-tal = D-talonic acid (2S,3S,4S,5R), L-tal = L-talonic acid (2R,3R,4R,5S), D-gul = D-gulonic acid (2R,3R,4S,5R); L-gul = L-gulonic acid (2S,3S,4R,5S); NS = not separated. The resolution is underlined and the separation factor is italicized. Electrophoretic conditions as in Fig. 1.2.

Table 1.6 | **Efficiency of the chiral separation of PHA stereoisomers.** Electrophoretic conditions as in Fig. 1.7.

Stereoisomers of	MW (g/mol)	# of Rs ≥ 1	# of Rs ≥ 1.5
Tartaric acid	150.1	2/3	2/3
2,3-dihydroxybutanoic acid	120.1	6/6	5/6
2,3,4,5-tetrahydroxypentanoic acid	166.1	24/28	15/28
2,3,4,5,6-pentahydroxyhexanoic acid	196.2	101/120	89/120

Migration order and electrophoretic mobilities

When analyzing a mixture of unknown enantiomeric ratio, the knowledge of the migration order allows direct identification of the L- and D-enantiomers. For all AHAs and BHAs, except for isocitric acid, the L-enantiomer with 2S stereochemistry migrated faster than the D-enantiomer with 2R stereochemistry (Fig. 1.3, Fig. 1.4, Fig. 1.5 and Table 1.1). For tartaric acids, L- and D-tartaric acid migrated faster than meso-tartaric acid (Fig. 1.8A). For enantiomeric pairs or C2 epimeric pairs of 2,3-dihydroxybutanoic acids, the enantiomer or C2 epimers with a 2S stereochemistry migrated faster than the enantiomer or C2 epimers with a 2R stereochemistry. Conversely, for enantiomeric pairs or C2 epimeric pairs of 2,3,4,5-tetrahydroxypentanoic acids and 2,3,4,5,6-pentahydroxyhexanoic acids, the enantiomer or C2 epimers with a 2R stereochemistry migrated faster than the enantiomer or C2 epimers with a 2S stereochemistry, except for the D-arabinonic acid/D-ribonic acid C2 epimeric pair and the D-talonic acid/L-talonic acid enantiomeric pair (Fig. 1.8A and 1.8B). For C3, C4 and C5 epimeric pairs of PHAs, the epimers with different stereochemistry between the last two carbons migrated faster than the epimers with the same stereochemistry between the last two carbons. In other words, the epimers with different stereochemistry between CX and CX-1 migrated faster than the epimers with the same stereochemistry between CX and CX-1, where X is the total number of carbons of the PHA (Fig. 1.8A and 1.8B). The effective electrophoretic mobilities (μ_{eff}) of the HAs and the chiral selector (μ_{eff} vancomycin = 12.26 x 10^{-9}.m^2.V^{-1}.s^{-1}) were determined based on their respective migration times and the electroosmotic mobility of the EOF (μ_{EOF} = -2.94 x 10^{-9}. m^2.V^{-1}.s^{-1}) (Table 1.S2).

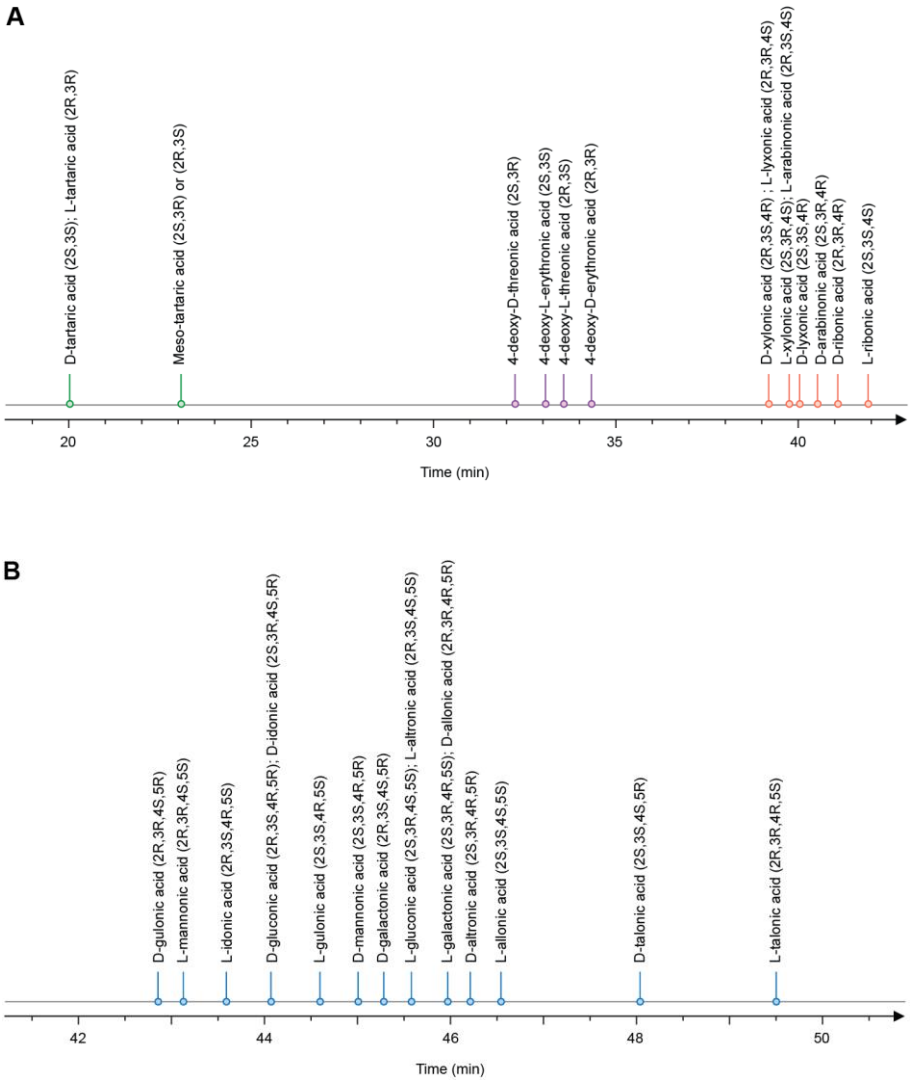

Figure 1.8 | **Schematic representation of the chiral separation and migration times of PHAs stereoisomers.** (**A**) Schematic representation of the chiral separations and migration times of the stereoisomers of tartaric acid (green), 2,3-dihydroxybutanoic acid (purple) and 2,3,4,5-tetrahydroxypentanoic acid (orange). (**B**) Schematic representation of the chiral separations and migration times of (2,3,4,5,6)-pentahydroxyhexanoic acid stereoisomers (blue). Electrophoretic conditions as in Fig. 1.7 for **A** and **B**.

Variation of resolution, analysis time, signal intensity and limit of detection

Effect of vancomycin concentration

We determined the variation of chiral resolution as a function of vancomycin concentration for a representative AHA (DL-2-hydroxybutyric acid), BHA (DL-3-hydroxyoctanoic acid) and PHA (DL-gluconic acid). Increasing the concentration of vancomycin resulted in enhanced chiral separation for all HAs investigated by increasing the resolution and migration time for AHAs, BHAs, and PHAs (Fig. 1.9A and 1.9B). This means that a high concentration of vancomycin would always be recommended for the initial chiral analysis of an unknown HA, the vancomycin concentration may later be decreased for faster migration time, if the resolution allows it.

However, increasing the vancomycin concentration also results in a lower signal intensity and higher limit of detection (LOD; signal-to-noise ratio = 3). Fig. 1.9C shows that the signals corresponding to 1 mM of DL-2-hydroxybutyric acid, DL-3-hydroxyoctanoic acid and DL-gluconic acid decrease with an increase in vancomycin concentration. And Fig. 1.9D shows that the LOD of D-2-hydroxybutyric acid, D-3-hydroxybutyric acid and DL-gluconic acid increases with higher vancomycin concentrations. Therefore, if large resolution is not required, a low concentration of vancomycin is recommended. At a fixed concentration of vancomycin, we observed that the signal of aliphatic HAs is directly proportional to their molecular weight. However, this correlation does not hold for aromatic AHAs, which are UV-absorbing, as their signal varies depending on their chromophore (Fig 1.10)

Effect of capillary length

We also determined the influence of capillary length on the resolution, analysis time, signal intensity and LOD for a representative AHA (DL-2-hydroxybutyric acid), BHA (DL-3-hydroxyoctanoic acid) and PHA (DL-gluconic acid) (Fig. 1.11). We observed an enhancement of chiral resolution and a prolonged analysis time as capillary length increased (Fig. 1.11A and 1.11B), highlighting a trade-off between enhanced resolution and analysis time. The signal intensity remained constant but the LOD increased with the length of the capillary (Fig. 1.11C and 1.11D), due to the widening of the peak. Using

electrophoretic conditions for optimal resolution, LOD values were in the range of 39–152 µM for aliphatic HAs and 194-447 µM for aromatic HAs (Table 1.S2). However, it is possible to significantly reduce the LOD at the expense of resolution by lowering the vancomycin concentration as shown in Fig. 1.9D or by using a shorter capillary as shown in Fig. 1.11D. Overall, these results underscore the importance of capillary length optimization in electrophoretic separations, considering the trade-offs between resolution, analysis time, and LOD, for achieving specific analytical goals.

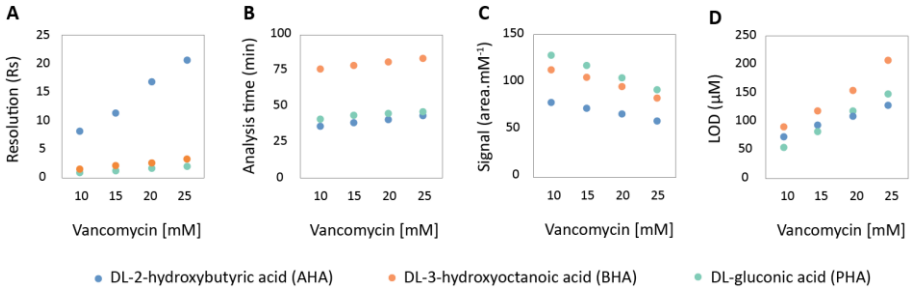

Figure 1.9 | Resolution, analysis time, signal intensity and limit of detection as a function of vancomycin concentration. (**A**) Chiral resolution as a function of vancomycin concentration. Separations were conducted with 0.5 mM of each enantiomer. (**B**) Analysis time as a function of vancomycin concentration. The indicated analysis time for each enantiomeric pair corresponds to the migration time of the slowest enantiomer. (**C**) Signal intensity as a function of vancomycin concentration. **(D)** LOD as a function of vancomycin concentration. The indicated LOD for each enantiomeric pair refers to the D-enantiomer. Vancomycin concentrations as indicated, other electrophoretic conditions as in Fig. 1.2 for **A**, **B**, **C** and **D**.

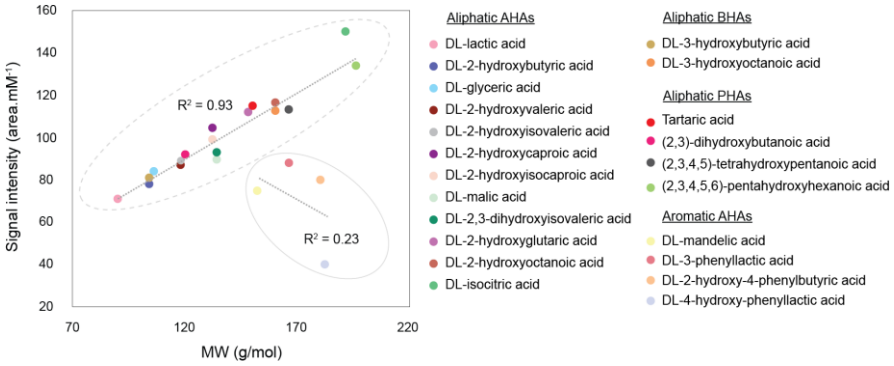

Figure 1.10 | **Signal intensity variation as a function of HAs molecular weight.** For AHAs and BHAs, we used the area corresponding to 1 mM of the enantiomeric mixture. For PHAs, we used the mean of the areas corresponding to 1 mM of each stereoisomers. Aliphatic HAs are encircled by a dashed grey line, while aromatic HAs are encircled by a solid grey line. Pearson correlation: r(18) = 0.96, $p < 0.001$ and r(4) = -0.48, $p > 0.5$. Vancomycin concentration 10 mM, other electrophoretic conditions as in Fig. 1.2.

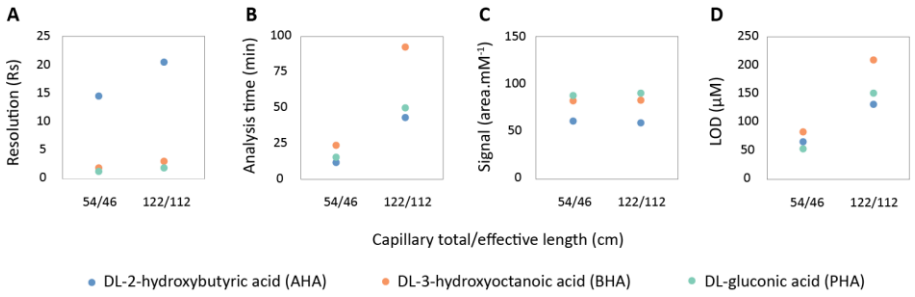

Figure 1.11 | **Resolution, analysis time, signal intensity and LOD as a function of capillary length. (A)** Chiral resolution as a function of capillary length. Separations were conducted with 0.5 mM of each enantiomer. **(B)** Analysis time as a function of capillary length. The indicated analysis time for each enantiomeric pair corresponds to the migration time of the slowest enantiomer. (**C**) Signal intensity as a function of capillary length. (**D**) LOD as a function of capillary length. The indicated LOD for each enantiomeric pair refers to the D-enantiomer. Electrophoretic conditions as in Fig. 1.2 for **A**, **B**, **C**, and **D**.

Analysis of complex matrices

In this section, we demonstrate the versatility of our method for analyzing complex matrices, such as in vitro enzymatic reactions and real-world samples. Utilizing GntE1, a D-gluconate C-2 epimerase from the LarA superfamily [59], we showcased the analysis of the epimerization of D-gluconate into D-mannonate over time (Fig. 1.S1). This shows the applicability of the method in studying isomerization reactions such as racemization or epimerization of HAs, and its possible use for the determination of the stereochemical specificity and kinetic parameters of HA isomerases. Previously, we successfully applied this method to determine the kinetic parameters of tartrate epimerization by MAR2, a malate racemase and tartrate epimerase from the LarA superfamily [209]. In addition, we utilized isocitrate dehydrogenase (IDH) to monitor the decarboxylation of D-isocitrate into 2-ketoglutarate and CO_2 over time (Fig. 1.S2). This demonstrates the efficacy of the method in studying dehydrogenation reactions involving HAs and its potential for determining the stereochemical specificity and kinetic parameters of HA dehydrogenases.

We also analyzed a zinc gluconate dietary supplement containing 353 mg of gluconate per 530 mg tablet. Employing our method, we estimated the concentration of D-gluconate, which corresponded to 95 ± 4 % of its theoretical concentration. No traces of L-gluconate were detected (Fig. 1.S3). This validation confirms the ability of our method to identify and quantify a HA within a complex matrix.

CONCLUSION

This work presents for the first time a robust and versatile method allowing a highly efficient chiral analysis of a wide range of underivatized HAs of biological and industrial importance by CE. The significance of this method lies in its broad applicability across various fields, e.g. in pharmaceutical, biomarkers, and biochemistry research. Notably, it plays a pivotal role in the study of the LarA superfamily, a recently discovered superfamily of AHA racemases and epimerases [209,210]. Similarly, chiral analysis of BHAs is indispensable in chemical synthesis and medicinal chemistry, as BHAs serve as essential building blocks for bioactive compounds. Furthermore, the chiral analysis of underivatized PHAs, an area previously undocumented in the literature, opens new avenues for the study of aldonic sugar acids with implications across various research areas and in industry. Overall, the effectiveness of the protocol in the stereoisomeric separation of AHAs, BHAs, and PHAs underscores its suitability for the analysis of a wide range of samples containing carboxyl and hydroxyl groups. This versatility not only supports stereochemical investigations but also offers the potential to improve our understanding of complex biological and chemical systems. In conclusion, the interest of the developed method extends to diverse applications, from exploring enzymatic mechanisms and metabolic pathways to practical uses in pharmaceutical and industrial chemistry. It provides a means to understand intricate stereochemical relationships and offers an effective tool for chiral analysis of HAs.

MATERIAL & METHODS

Chemicals and reagents

All chemicals were either of analytical grade or reagent grade. D-lactic acid (sodium salt), L-lactic acid (sodium salt), D-glyceric acid (sodium salt), L-glyceric acid (sodium salt), D-malic acid, L-malic acid, D-2-hydroxybutyric acid, L-2-hydroxybutyric acid, DL-2-hydroxycaproic acid, DL-2-hydroxyisocaproic acid, L-2-hydroxyisocaproic acid, D-2-hydroxyisovaleric acid, L-2-hydroxyisovaleric acid, DL-2-hydroxyoctanoic acid, D-2,3-dihydroxyisovaleric acid (sodium salt), L-2,3-dihydroxyisovaleric acid (sodium salt), D-2-hydroxyglutaric acid (disodium salt), L-2-hydroxyglutaric acid (disodium salt), D-3-phenyllactic acid, L-3-phenyllactic acid, D-2-hydroxy-4-phenylbutyric acid, DL-mandelic acid, D-mandelic acid, D-ribonic acid (lithium salt), L-ribonic acid (lithium salt), D-arabinonic acid (sodium salt), D-lyxonic acid (potassium salt), L-lyxonic acid (potassium salt), D-gluconic acid (sodium salt), D-altronic acid (lithium salt), L-gulonic acid (lactone), D-gulonic acid (lithium salt), benzoic acid and L-histidine were purchased from Sigma-Aldrich. L-2-hydroxyvaleric acid, L-2-hydroxycaproic acid, L-2-hydroxy-4-phenylbutyric acid, DL-3-hydroxyoctanoic acid, L-arabinonic acid (lithium salt), D-xylonic acid (lithium salt), L-xylonic acid (lithium salt), L-gluconic acid (lactone), D-galactonic acid (lactone), L-galactonic acid (lactone), D-allonic acid (lactone), L-allonic acid (lactone), D-mannonic acid (lactone), L-mannonic acid (lactone), D-idonic acid (lactone), L-idonic acid (lactone), D-talonic acid (lactone) were purchased from Biosynth. L-talonic acid (potassium salt) was purchased from Omicro Biochemicals Inc. L-altronic acid was produced in our lab by the C2-epimerization of L-allonic acid (data not published). DL-2-hydroxyvaleric acid was purchased from Acros Organics. D-2-hydroxyoctanoic acid was purchased from BLDpharm. 4-Deoxy-D-erythronic acid (sodium salt hydrate), 4-Deoxy-L-erythronic acid (sodium salt hydrate), 4-Deoxy-D-threonic acid (sodium salt hydrate), 4-Deoxy-L-threonic acid (sodium salt hydrate), DL-3-hydroxybutyric acid, L-3-hydroxybutyric acid were purchased from Supelco. Vancomycin was purchased from Thermo Fisher Scientific.

Apparatus and separation procedure

All electrophoretic runs were performed on the CE system Capel 105 M from Lumex Instrument in a polyacrylamide-coated capillary with 50 µm i.d. x 122/112.5 cm total/effective length. Prior to the first experiment of the day, the coated capillary was rinsed daily for 10 minutes with the BGE consisting of 10 mM benzoic acid/L-histidine at pH 5.0. To control the partial filling process and to prevent the presence of vancomycin in the detector window, the BGE supplemented with vancomycin was introduced into the capillary at a pressure of 1000 mbar for 145 seconds. The positioning of vancomycin just before the detection window was fine-tuned based on absorbance measurements during capillary filling. Samples were injected at a pressure of 30 mbar for 5 s. A counter current method was employed throughout the analysis with an applied voltage of -25 kV. Detection was performed in the indirect UV photometric detection mode at 230 nm. The capillary temperature was maintained at 20°C during all steps. Between runs, the capillary was rinsed with BGE at 1000 mbar for 5 minutes. At the end of the day, the capillary was rinsed with distilled water for 10 minutes and both ends of the capillary were kept in water.

Capillary-coating procedure

The coating process of the capillary inner surface by polyacryamide was based on previously published procedures [211,212]. The fused-silica capillary was rinsed with 0.5 M HCl for 30 min and then with deionized water for 30 min. After rinsing, the capillary was silylated by flushing with a 3% v/v solution of 3-(trimethoxysilyl)propylmethacrylate in 50% aqueous acetone for 1 h. After the silylation process, the capillary was rinsed with deionized water for 25 min. The final polymerization step was performed by flushing of 3% w/v solution of acrylamide in deionized water with additions of 0.05% w/v ammonium persulfate and 0.04% v/V tetramethylethylenediamine for 45 min for the capillary with 50 µm i.d. x 122/112 cm total/effective length and 1h for the capillary with 50 µm i.d. x 54/46 cm total/effective length. After the coating procedure, the capillary was rinsed with deionized water at 2000 mbar for 2 hours.

Effective electrophoretic mobility calculation

The effective electrophoretic mobilities were calculated using Eq. (1), with water as neutral marker to determine the electroosmotic flow (EOF) [213]:

$$\mu_{eff} = \mu_{app} - \mu_{EOF} = \frac{L_e.L_t}{U} \cdot \left(\frac{1}{t_m} - \frac{1}{t_{EOF}}\right) \quad (1)$$

where μ_{eff} is the effective electrophoretic mobility of the analyte ($m^2.V^{-1}.s^{-1}$), μ_{app} is the apparent electrophoretic mobility of the analyte ($m^2.V^{-1}.s^{-1}$), μ_{EOF} is the electroosmotic mobility ($m^2.V^{-1}.s^{-1}$), t_m is the migration time of the analyte (s), t_{EOF} is the migration time of the neutral marker (s), L_t is the total length of the capillary (m), L_e is the effective length of the capillary (m), and U is the applied voltage (V).

Complex matrices preparation

GntE1-catalyzed epimerization reactions of D-gluconate to D-mannonate were made in a 200 µl final volume containing 10 mM of D-gluconate, 5 µM of in vitro synthesized NPN, 1 µM of purified GntE1 and 0.1 M Tris-HCL buffer, pH 8, incubated for 0, 1, 2 or 3 hours. IDH-catalyzed dehydrogenation reactions of D-isocitrate to 2-ketoglutarate and CO_2 were made using the D-isocitric Acid Assay Kit from Megazyme in a 200 µl final volume containing 2 mM of D-isocitrate, 5 mM of $NADP^+$, 50 nM of IDH and the kit buffer, pH 7.8, incubated for 0, 5, 10 or 15 minutes. Reactions were stopped by heat inactivation at 90 °C for 10 minutes.

A 530 mg zinc-gluconate dietary supplement tablet (Now Foods) contained 50 mg of Zinc, 353 mf of D-gluconate, microcrystalline cellulose, vegetarian coating, magnesium stearate and silicon dioxide. Matrices of 0.5 mg/ml zinc-gluconate dietary supplement were prepared by grinding tablets and resolubilizing them in boiling water (n=3).

III.1.2 Supplementary data

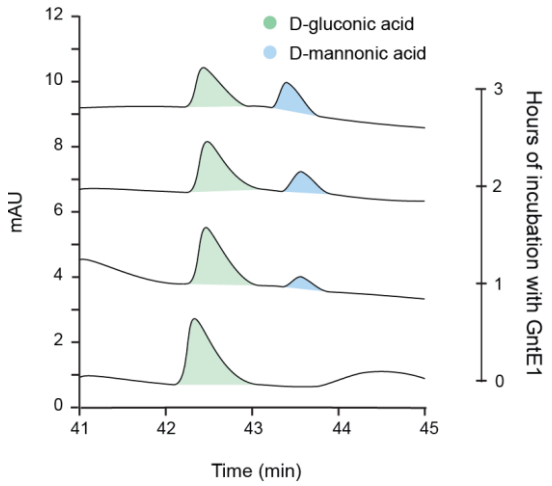

Figure 1.S1 | Analysis of the GntE1-catalyzed epimerization of D-gluconate to D-mannonate over time. Electrophoretic conditions as in Fig. 1.2.

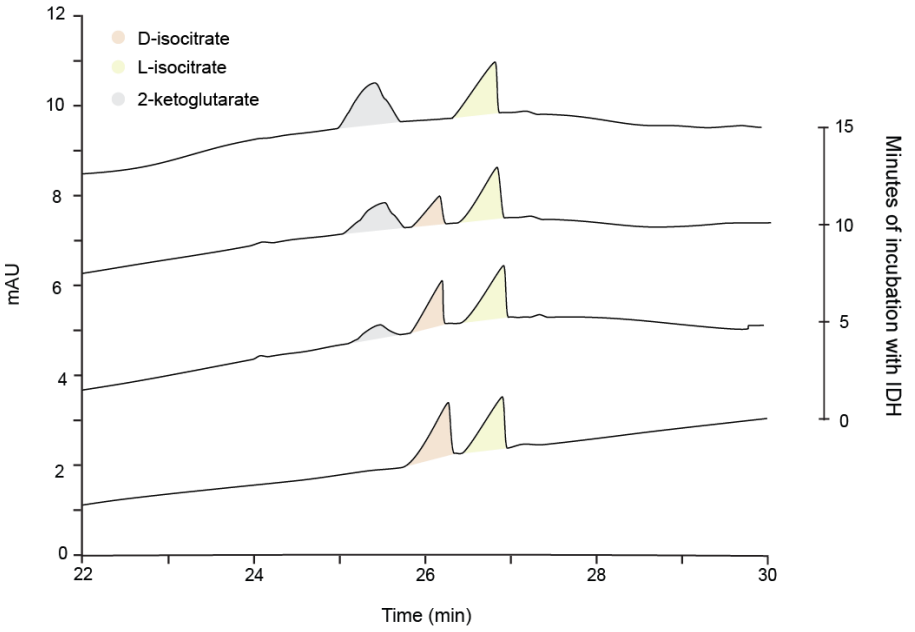

Figure 1.S2 | Analysis of the IDH-catalyzed decarboxylation of D-isocitrate to 2-ketoglutarate and CO_2 over time. Vancomycin concentration 7 mM, other electrophoretic conditions as in Fig. 1.2.

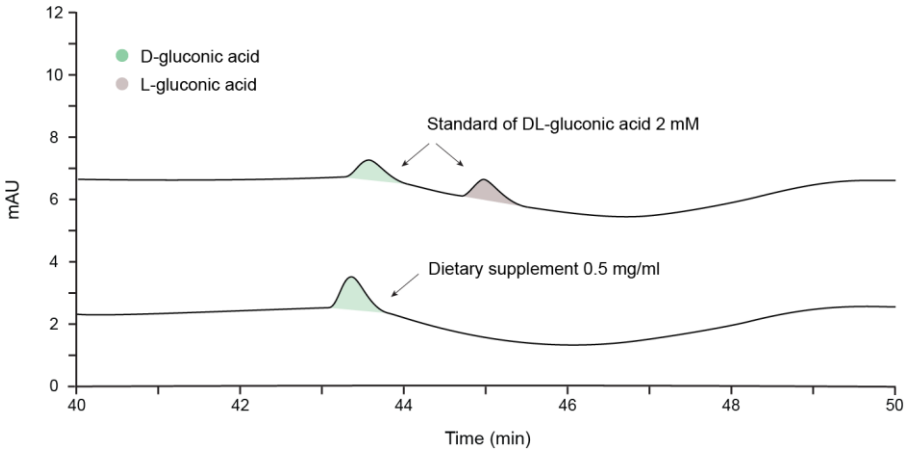

Figure 1.S3 | **Analysis of a dietary supplement containing gluconate.** Electrophoretic conditions as in Fig. 1.2.

Table 1.S1 | **Intra- and inter-day variabilities of peak areas, migration times, resolutions and separation factors for a representative AHA, BHA and PHA.** Separations were performed with a standard mixture containing 0.5 mM of each enantiomer. Electrophoretic conditions as in Fig. 1.2.

	Intra-day R.S.D. (%, n=3)						Inter-day R.S.D. (%, n=3)					
	Peak area		Migration time		Rs	α	Peak area		Migration time		Rs	α
	D-	L-	D-	L-			D-	L-	D-	L-		
DL-2-hydroxybutyric acid (AHA)	1.9	1.3	0.7	1.1	3.9	0.7	1.3	1.2	1.8	1.4	6.9	1.2
DL-3-hydroxybutyric acid (BHA)	0.5	1.1	0.2	0.1	4.9	0.2	4.9	4.4	2.7	2	6.6	0.3
DL-2-gluconic acid (PHA)	3.8	1.2	0.2	0.3	2.8	0.2	3.4	1.1	3.5	2.8	3.5	0.3

Table 1.S2 | LOD and electrophoretic mobilities of the investigated HAs. Effective electrophoretic mobility was calculated according to the Eq. 1. L_t = 1.22 m; L_e = 1.12 m; t_{EOF} = 18615 s; μ_{EOF} = -2.94x10^{-9}.m^2.V^{-1}.s^{-1}. For AHA and BHA enantiomers: electrophoretic conditions as in Table 1.1, and the indicated LOD for each enantiomeric pair refers to the D-enantiomer. For PHA stereoisomers, electrophoretic conditions as in Fig. 1.7, and the indicated LOD refers to the D-enantiomer of the enantiomeric pair indicated with an asterisk

	HAs	D-		L-		LOD (µM)
		t_m (s)	µeff (10^{-9}.m^2.V^{-1}.s^{-1})	t_m (s)	µeff (10^{-9}.m^2.V^{-1}.s^{-1})	
AHAs	DL-isocitric acid	1590	-31.41	1674	-29.68	39
	DL-malic acid	1524	-32.90	1470	-34.21	59
	DL-lactic acid	2532	-18.62	1776	-27.81	81
	DL-glyceric acid	1830	-26.90	1662	-29.92	75
	DL-2-hydroxyglutaric acid	1902	-25.77	1782	-27.70	63
	DL-2-hydroxybutyric acid	2574	-18.27	1986	-24.55	116
	DL-2-hydroxyvaleric acid	3222	-14.00	2436	-19.47	114
	DL-2-hydroxyisovaleric acid	2694	-17.32	2328	-20.51	117
	DL-2-hydroxycaproic acid	3438	-12.93	2712	-17.19	106
	DL-2-hydroxyisocaproic acid	3588	-12.27	2790	-16.62	109
	DL-2,3-dihydroxyisovaleric acid	2538	-18.57	2274	-21.07	129
	DL-2-hydroxyoctanoic acid	4122	-10.29	3408	-13.07	147
	DL-mandelic acid	2772	-16.75	2688	-17.37	194
	DL-3-phenyllactic acid	4272	-9.83	3090	-14.72	238
	DL-3-(4-hydroxyphenyl)lactic acid	5103	-7.74	3546	-12.45	293
	DL-2-hydroxy-4-phenylbutyric acid	4068	-10.47	3498	-12.66	447
BHAs	DL-3-hydroxybutyric acid	2988	-15.32	2916	-15.78	116
	DL-3-hydroxyoctanoic acid	4998	-7.97	4866	-8.27	152
PHAs	DL-tartaric acid*	1218	-41.91	1218	-41.91	88
	Meso-tartaric acid	1392	-36.30	1392	-36.30	
	4-deoxy-DL-erythronic acid*	2064	-23.51	1986	-24.55	135
	4-deoxy-DL-threonic acid	1938	-25.24	2022	-24.06	
	DL-ribonic acid*	2472	-19.14	2520	-18.72	122
	DL-lyxonic acid	2406	-19.75	2346	-20.33	
	DL-xylonic acid	2346	-20.33	2388	-19.92	
	DL-arabinonic acid	2430	-19.52	2388	-19.92	
	DL-gluconic acid*	2646	-17.69	2736	-17.01	131
	DL-allonic acid	2760	-16.84	2793	-16.60	
	DL-gulonic acid	2571	-18.29	2676	-17.46	
	DL-altronic acid	2775	-16.73	2736	-17.01	
	DL-talonic acid	2880	-16.01	2970	-15.44	
	DL-galactonic acid	2718	-17.14	2760	-16.84	
	DL-idonic acid	2646	-17.69	2616	-17.93	
	DL-mannonic acid	2700	-17.28	2589	-18.14	

CHAPTER 2

Unveiling 14 novel 2-hydroxy acid racemization and epimerization reactions in the lactate racemase superfamily

Julian Urdiain-Arraiza, Amandine Vandenberghe, Gergana Dimitrova and Benoît Desguin

Journal of Biological Chemistry (In revision)

Submitted 25 June 2024
Invitation for revision 15 July 2024

Author's contributions

The study was conceived and designed by JUA and BD.
The laboratory work was performed by JUA (Figures 2.5, 2.S2, 2.S3, 2.S4, 2.S5 and Tables 2.1, 2.2, 2.S4, 2.S5.
The data were analyzed and interpreted by JUA (Figures 2.1, 2.2, 2.3, 2.4, 2.S1 and Table 2.S1) and BD (Figures. 2.6, 2.S6).
The manuscript was written by JUA.
The manuscript was revised by JUA and BD.

As outlined in the introduction, the LarA superfamily remains largely unexplored, with the enzymatic functions of the majority of phylogenetic families still requiring further investigation. To address this gap, we sought to investigate the scope of AHA racemization and PHA C2-epimerization reactions catalyzed by members of the LarA superfamily using the CE method developed in Chapter 1.

We began by analyzing the genetic diversity of the LarA superfamily, filtering over 14,000 LarAH sequences from the InterPro database and selecting around 1,000 representative sequences to construct a phylogenetic tree of the LarA superfamily. Furthermore, a taxonomic analysis conducted using the InterPro and Clusters of Orthologous Genes (COGs) databases revealed the distribution and prevalence of LarAH sequences across bacteria, archaea, and eukaryotes.

Subsequently, we purified and biochemically characterized nine novel LarAHs predominantly belonging to unexplored phylogenetic clusters. These enzymes were analyzed for substrate specificity, kinetic parameters, optimal temperature, and optimal pH. As a result, we were able to expand the characterization of four families within the LarA superfamily: the lactate racemase (LAR) family, the malate racemase (MAR) family, the 2-hydroxyglutarate racemase (HGR) family, and the D-gluconate 2-epimerase (GntE) family. It is noteworthy that the first eukaryotic enzyme with GntE activity was discovered, which suggests a pivotal role in eukaryotic metabolism. Additionally, we identified a novel family of LarAHs: the hydrophobic HA racemase (HHR) family. HHRs were found to act on a wide range of hydrophobic HAs, with some HHRs able to isomerize up to 16 different substrates. In total, we identified 14 previously unreported 2-HA racemization and C2-epimerization reactions.

Lastly, comparative analysis of AlphaFold structural predictions allowed us to identify key residues involved in substrate specificity, enabling the functional prediction of half of the LarAHs within the LarA superfamily. Our comprehensive study, integrating phylogenetic, structural, enzymatic, and CE analyses, significantly expanded the known substrate scope of NPN-dependent enzymes and highlighted the evolutionary diversity and metabolic significance of LarAHs across all domains of life.

III.2.1 Manuscript

Unveiling 14 novel 2-hydroxy acid racemization and C2-epimerization reactions in the lactate racemase superfamily

Julian Urdiain-Arraiza[1], Amandine Vandenberghe[1], Gergana Dimitrova[1] and Benoît Desguin[1]

[1]Louvain Institute of Biomolecular Science and Technology (LIBST), UCLouvain, 1348 Louvain-La-Neuve, Belgium.

Abstract

2-Hydroxy acids are organic carboxylic acids ubiquitous in the living world and are important building blocks in organic synthesis. Recently, the lactate racemase (LarA) superfamily, a diverse superfamily of 2-hydroxy acid racemases and epimerases using the nickel-pincer nucleotide (NPN) cofactor, has been uncovered. In this study, we performed a taxonomic analysis of the LarA superfamily, showing the distribution of LarAHs sequences across the three domains of life. Subsequently, we overexpressed and purified 9 lactate racemase homologs (LarAHs) and investigated their biochemical properties and substrate specificities. We show that LarAHs from the lactate racemases group are more promiscuous than previously thought, with some members showing high specificity towards glycerate or 2-hydroxybutyrate. In other phylogenetic groups, we identified a new malate racemase and 2-hydroxyglutarate racemase, as well as a new 2-gluconate epimerase from an eukaryotic organism. We show that some LarAHs are able to isomerize up to 16 different substrates, mostly 2-hydroxy acids with hydrophobic side chains, thereby identifying 14 novel 2-hydroxy acid racemization and C2-epimerization reactions catalyzed by LarAHs. These include the racemization of glycerate, 2-hydroxybutyrate, 2,4-dihydroxybutyrate, 2-hydroxyvalerate, 2-hydroxycaproate, 2,3-dihydroxyisovalérate, 2-hydroxy-3,3-dimethylbutyrate, 3-(4-hydroxyphenyl)lactate, 2-hydroxy-4-phenylbutyrate, and 2-hydroxy-4-oxo-4-phenylbutyrate. Additionally, we observed the C2-epimerization of all 2,3-dihydroxybutyrate stereoisomers (4-deoxy-DL-threonate and 4-deoxy-DL-erythronate) and the C2-epimerization of D-

arabinarate epimers. Finally, through comparative analysis of Alphafold structural predictions, we identified key residues likely involved in substrate specificity and predicted the function of half of the LarAHs from the LarA superfamily. In conclusion, this study widely expands the scope of substrates isomerized by NPN-dependent enzymes.

Keywords

NPN cofactor, hydroxy acids, racemase, epimerase, capillary electrophoresis

INTRODUCTION

2-Hydroxy acid racemases (2-HARs) and epimerases (2-HAEs) are enzymes that play a crucial role in biochemical systems across a multitude of organisms by catalyzing the stereochemical inversion of the α-carbon of 2-hydroxy acids (2-HAs), a type of organic carboxylic acid ubiquitous in the living world.

2-HARs converts the two enantiomeric forms of 2-HAs with one chiral center (e.g. lactate racemase) whereas 2-HAEs act on 2-HAs with more than one chiral center by converting a stereoisomer into its epimer, which differs in the configuration of only one chiral center (e.g. D-gluconate epimerase). In both cases, the product of the reaction retains the same functional groups and connectivity than the substrate but shows different biological properties.

Moreover, 2-HAs are key metabolites and involved in most metabolic pathways, including, but not limited to, the degradation of amino acids [30,33,214], the biosynthesis of cellular components [34], and the metabolism of sugars [15,35]. The racemization and C2-epimerization of these compounds, catalyzed by 2-HARs and 2-HAEs, respectively, are critical for maintaining the equilibrium between different stereoisomers within the cell. 2-HARs and 2-HAEs are not only fundamental to cellular homeostasis but may also have implications for the synthesis of a broad range of biologically active molecules, including pharmaceuticals and agrochemicals [1,2].

Recent discoveries have shed light on a superfamily of nickel-dependent 2-HARs and 2-HAEs, the LarA superfamily [210]. The founding member of the

LarA superfamily is *Lactiplantibacillus plantarum* lactate racemase (LarA1) which catalyzes the racemization of D- and L-lactate by using the Nickel-Pincer Nucleotide (NPN) cofactor [95,96]. LarA and the NPN cofactor operate by a proton-coupled hydride-transfer (PCHT) mechanism during which the NPN transiently accepts the substrate-derived hydride (Fig. 2.1) [124,210]. The NPN cofactor, a substituted pyridinium mononucleotide that tricoordinates nickel, is sequentially synthesized by the LarB, LarE, and LarC biosynthetic enzymes from the precursor nicotinic acid adenine dinucleotide through consecutive carboxylation/hydrolysis, sulfur insertion, and nickel insertion reactions, respectively [113,119,120,132,160,215].

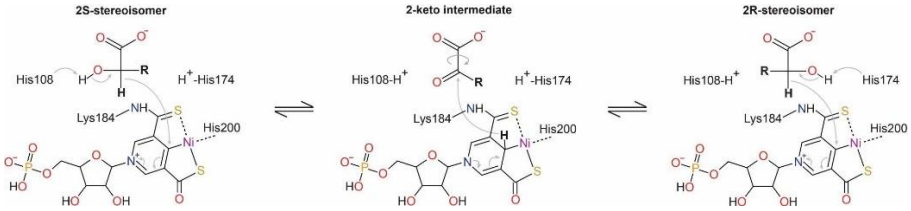

Figure 2.1 | **NPN cofactor and proton-coupled hydride transfer reaction of LarAHs.** The residues numbers correspond to the residues of *L. plantarum* LarA1 (PDB code 5HUQ or 6C1W).

Interestingly, the genes encoding for the NPN-biosynthetic enzymes and LarA homologs (LarAHs) are widespread within eubacteria and archaea, and some are even found in unicellular eukaryotes [95]. The high sequence diversity and genomic contexts of LarAHs within the LarA superfamily suggested that they may catalyze a wide range of enzymatic reactions. To date, several LarAHs have been shown to use the NPN cofactor and catalyze racemization or C2-epimerization activities of the α-carbon of 2-HAs other than lactate. Two malate racemases (LarAH5/MAR1 and LarAH6/MAR2), a 2-hydroxyglutarate racemase (LarAH7/HGR), two D-gluconate 2-epimerases (LarAH19/GntE1 and LarAH20/GntE2), a short-chain aliphatic 2-hydroxyacid racemase (LarAH2/SAR), and a phenyllactate racemase (LarAH10/PLR) were identified among these LarAHs [210]. LarA and the LarAHs likely share the same reaction mechanism in which the α chiral carbon of a 2-HA is transiently oxidized generating an α-keto acid intermediate (Fig. 2.1), while the active site residues unique to each family in the LarA superfamily allow the determination of the substrate specificity [209,210]. These latest discoveries likely represent just a fraction of the scope of racemization or C2-

epimerization reactions catalyzed by LarAHs. The specific enzymatic functions within the majority of phylogenetic families in the LarA superfamily remain largely unexplored and require further investigation.

In this study, we undertook a phylogenetic analysis and exploration of the LarA superfamily in order to uncover the scope of reactions catalyzed by different LarAHs. We have thoroughly characterized 9 new LarAHs, predominantly from unexplored phylogenetic clusters. Among these enzymes, we have identified 14 previously unreported 2-HA racemization and C2-epimerization reactions. Remarkably, certain LarAHs exhibit catalytic activity on over 16 distinct 2-HAs. These findings demonstrate the potential of the LarA superfamily for biotechnological and pharmaceutical applications in the synthesis of valuable 2-HA stereoisomers.

RESULTS

Taxonomic analysis of the LarA superfamily

The LarA superfamily, also referred to as the DUF2088 superfamily due to its previously unknown enzyme functions, represents a highly diverse group of enzymes [216]. This superfamily includes LarA-like domains, corresponding to the Interpro entry IPR048068 [217], which encompasses currently a total of 12,441 LarAHs found across 3,804 species, mostly bacteria (Fig. 2.S1A). Among bacteria, the majority of LarAHs are currently observed in taxa such as *Bacillota* (*Firmicutes*), *Actinomycetota*, *Pseudomonadota* (*Proteobacteria*) and *Planctomycetota* (Fig. 2.S1B). The phylogenetic tree built from the alignment of 1212 representative LarAHs sequences shows the diversity of sequences in the LarA superfamily (Fig. 2.2), suggesting that many racemization or C2-epimerization reactions of 2-HAs are still to be discovered.

Using the Clusters of Orthologous Genes (COGs) entry COG3875, the prevalence of the *larAH* sequence across archaea and bacteria was analyzed, revealing distinct distribution patterns. In archaea, 29.5% of species contain at least one *larAH* sequence, with the highest prevalence observed in *Asgardarchaeota* (87.5%, Table 2.S1). In bacteria, 16.4% of species harbor at least one *larAH* sequence, with *Deferribacterota*, Myxococcota, *Planctomycetota*, and *Negativicutes* showing the highest abundance (80% to 100%, Fig. 2.3A & Table 2.S1). Most species possess a single *larAH* sequence,

although species from several bacterial taxa, such as *Negativicutes, Synergistota, Clostridia*, *Planctomycetota* and *Spirochaetota*, possess an average of two or more *larAHs* per genome (Fig. 2.3B & Table 2.S1). Notably, taxa with the highest prevalence of LarAHs are predominantly anaerobic, although a few, including *Actinomycetota* (e.g., *Corynebacterium glutamicum*), *Planctomycetota* (e.g., *Planctomyces limnophilus*), and *Acidobacteriota* (e.g., *Luteitalea pratensis*), contain aerobic species with LarAHs (Fig. 2.3). These findings highlight the diverse distribution of *larAH* sequences among bacterial and archaeal taxa, suggesting a high ecological significance.

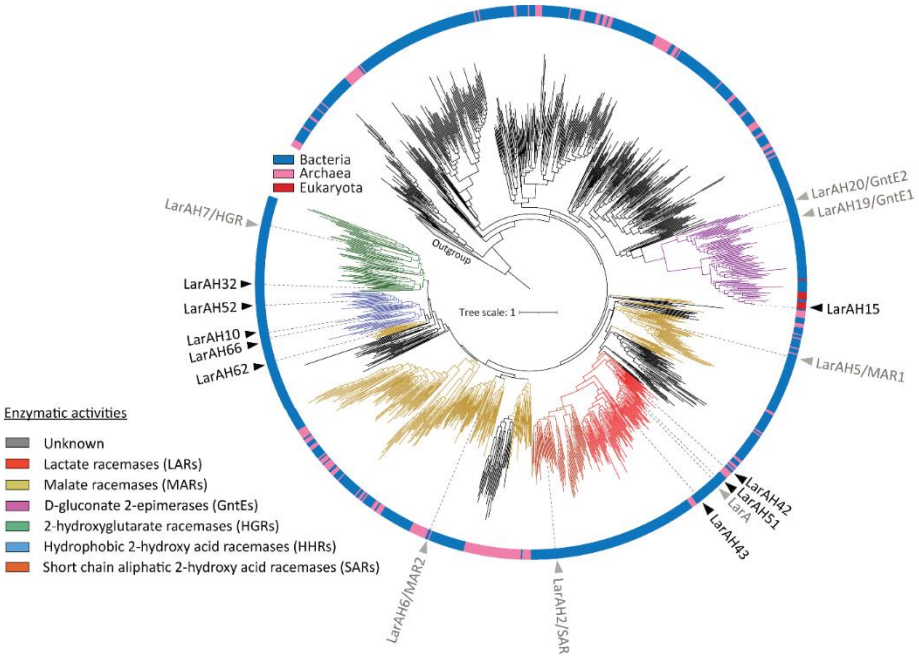

Figure 2.2 | **Representative phylogenetic tree of the LarA superfamily**. The tree includes 1212 representative LarAHs sequences from DUF2088 and 10 sequences from DUF362 used as an outgroup. All LarAHs mentioned in this report are indicated as "LarAHX" at their respective phylogenetic position. LarAHs characterized in this work are shown in black, previously characterized LarAHs are shown in gray. The colors of the phylogenetic groups correspond to the different reactions identified in these groups. The taxonomic group each sequence belongs to is labeled by a color strip at the circumference and the color code can be cross-referenced with Fig. 2.S1. LarA1 is from *Lactiplantibacillus plantarum;* LarAH2/SAR is from *Isosphaera pallida*; LarAH5/MAR1 is from *Desulfitobacterium hafniense*; LarAH6/MAR2 is from *Thermoanaerobacterium thermosaccharolyticum*; LarAH7/HGR is from *Deferribacter desulfuricans*; LarAH19/GntE1 is from *Corynebacterium glutamicum*; LarAH20/GntE2 is from *Thermotoga maritima*; LarAH10 is from *Megasphaera Elsdenii*; LarAH15 is from *Phytophthora nicotianae*; LarAH32 is from *Geobacter metallireducens*; LarAH42 and LarAH43 are from *Enterocloster asparagiformis*; LarAH51 and LarAH52 are from *Clostridium pasteurianum*; LarAH62 and LarAH66 are from *Sporomusa termitida*.

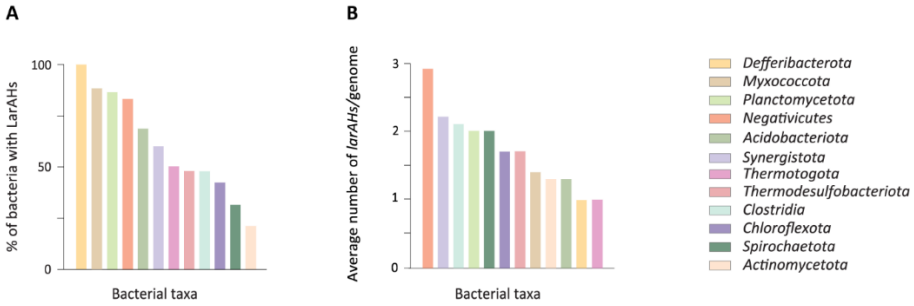

Figure 2.3 | **Bacterial taxa with the highest prevalence of LarAHs.** (**A**) Bacterial taxa with the highest percentage of bacteria with LarAHs. (**B**) Bacterial taxa with the highest mean of *larAHs* per genome. All bacterial taxa represented are phyla, except for the *Clostridia* and *Negativicutes* which are a class of bacteria within the phylum *Bacillota* (*Firmicutes*) and for *Deltaproteobacteria* which are a class of bacteria within the phylum *Pseudomonadota* (*Proteobacteria*). Data assembled from the database of Clusters of Orthologous Genes (COGs) entry COG3875 on the National Center for Biotechnology Information (NCBI) obtained on February 22, 2024.

Biochemical characterization of 9 selected LarAHs.

To gain further insight into the LarA superfamily, we selected nine *larAH* genes from five distinct bacteria and one eukaryote (Fig. 2.2). Subsequently, we engineered vectors to generate the respective C-terminal Strep-Tag fusion proteins for overexpression and purification in *Escherichia coli* cells. After purification, the nine LarAHs were obtained in soluble form and their identity was confirmed by electrospray ionization quadrupole time-of-flight mass spectrometry (ESI-Q-TOF-MS) analysis (Fig. 2.S2, Tables 2.S2 & 2.S3). Each purified LarAH was then supplemented with *in vitro* synthesized NPN and subjected to activity assays in the presence of all substrates showed in Fig. 2.4. These assays were conducted through either coupling to another enzymatic reaction for spectrophotometric measurement or via chiral capillary electrophoresis (CE) [218].

For a comprehensive biochemical characterization of each LarAH, we experimentally determined their optimal pH and temperature conditions, as well as their kinetic parameters for one representative substrate (k_{cat}, K_M and k_{cat}/K_M). Kinetic parameters of the NPN-supplemented enzymes were determined by assuming 100% loading, given that an excess of NPN was added to the apoprotein; however, the extent of NPN loading could not be established. As a result, the values of k_{cat} and k_{cat}/K_M are probably underestimated. Temperature and pH profiles of the nine investigated

LarAHs showed that the majority of LarAHs exhibited a pH optimum around pH 7 and a temperature optimum around 40°C, which is expected for enzymes from mesophilic organisms (Table 2.1 & Figs. 2.S3 and 2.S4). Kinetic studies showed that their affinity for their substrate was generally higher than the affinity of LarA1 for lactate, yet their k_{cat} was generally lower, resulting in similar catalytic efficiencies for most LarAHs. However, some LarAHs showed significantly lower catalytic efficiencies (Table 2.1 & Fig. 2.S5). Overall, the k_{cat} and k_{cat}/K_M values obtained for most of the LarAHs investigated are close to the kinetic parameters of the 'average enzyme' corresponding to a k_{cat} of ~10 s^{-1} and k_{cat}/K_M of ~10^5 $s^{-1}.M^{-1}$ [219]. We then determined the relative catalytic efficiencies for all substrates identified for each LarAH (Fig. 2.5). This analysis allowed us to identify the preferred substrates of each LarAH and evaluate their specificity for each other substrate. The k_{cat}/K_M values of all substrates of each LarAH were calculated using the experimentally determined k_{cat}/K_M for one substrate and the relative catalytic efficiencies for all substrates (Table 2.2).

This study revealed that lactate racemases (LARs) exhibit a greater degree of promiscuity than previously assumed. All LARs were found to be capable of catalyzing the racemization of several other small 2-HAs, including glycerate and hydroxybutyrate. In some instances, their catalytic efficiency was even higher than that of lactate, which is traditionally regarded as the major substrate of LARs (Fig. 2.5 & Table 2.2). We also identified an additional MAR, an additional HGR and an additional GntE, which all showed a very narrow substrate spectrum (Fig. 2.5 & Table 2.2). Finally, we discovered a new family of LarAHs, comprising LarAH10, LarAH52 and LarAH66 which were found to act on up to 16 different substrates, predominantly 2-HAs with hydrophobic side chains (Fig. 2.5 & Table 2.2). One member of this group had already been identified previously, but only one substrate had been identified at the time: phenyllactate [210]. Given that these LarAHs are capable of racemizing a diverse range of 2-HAs, we have chosen to refer to these new LarAHs as hydrophobic 2-HA racemases (HHRs) rather than phenyllactate racemases. Most of the discovered reactions have not been previously reported, resulting in the identification of 14 new 2-HA racemization and C2-epimerization reactions (Fig. 2.5 & Table 2.2).

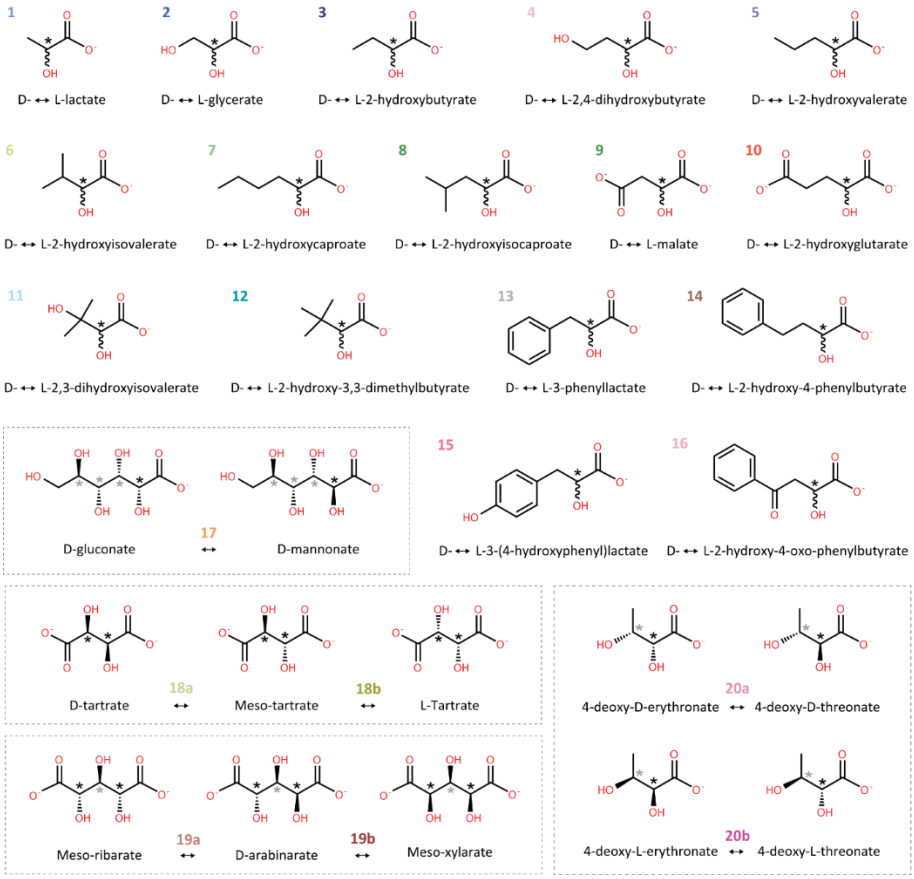

Figure 2.4 | **Chemical structure of substrates racemized and C2-epimerized by LarAHs**. For racemization reactions, the chiral carbons of enantiomers are depicted achiral for simplification. For C2-epimerization reactions, both epimers are depicted, with diastereomers of the same molecule boxed together. Black asterisks indicate stereoinversion sites, grey asterisks indicate other stereocenters in the molecule.

Table 2.1 | Kinetic parameters of LarA1 and of the 9 investigated LarAHs.

	Substrate	pH opt[a]	Temp opt[a] (°C)	K_M (mM)[b]	k_{cat} (s^{-1})[b]	k_{cat}/K_M (M^{-1} s^{-1})
LarA1	D-lactate	6	35-40	11 ± 4	1,300 ± 150	(12 ± 6) x 10^4
	L-lactate			46 ± 20	4,750 ± 500	(10 ± 5) x 10^4
LarAH42	D-lactate	7	35-40	4.4 ± 0.5	1.1 ± 0.2	(22 ± 5) x 10^1
	L-lactate			6.9 ± 1.2	1.4 ± 0.3	(20 ± 5) x 10^1
LarAH43	D-lactate	7-7.5	40-50	0.45 ± 0.04	30 ± 3	(66 ± 7) x 10^3
	L-lactate			0.51 ± 0.08	42 ± 5	(83 ± 9) x 10^3
LarAH51	D-lactate	6	40-45	0.33 ± 0.02	40 ± 6	(118 ± 18) x 10^3
	L-lactate			0.49 ± 0.02	48 ± 4	(98 ± 9) x 10^3
LarAH32	L-2-hydroxyglutarate	7-8	40-45	0.27 ± 0.05	4.1 ± 0.8	(15 ± 4) x 10^3
LarAH10	D-mannonate	7.5-8	30-35	3.8 ± 0.8	0.7 ± 0.5	(17 ± 4) x 10^1
LarAH52	D-2-hydroxy-4-oxo-phenylbutyrate	5.5-6.5	30-35	44 ± 8	510 ± 60	(12 ± 2) x 10^3
LarAH15	D-mannonate	6.5-7	40-50	9.4 ± 1.5	111 ± 12	(12 ± 3) x 10^3
LarAH62	D-malate	6-6.5	40	0.21 ± 0.02	138 ± 8	(63 ± 7) x 10^4
LarAH66	D-2-hydroxybutyrate	8	40	25 ± 4	0.92 ± 0.11	36 ± 5

[a] opt: optimal pH range or temperature (temp), where activity was > 90% of the maximum activity.
[b]: ± 95% confidence interval based on non-linear regression using the Michaelis–Menten equation.

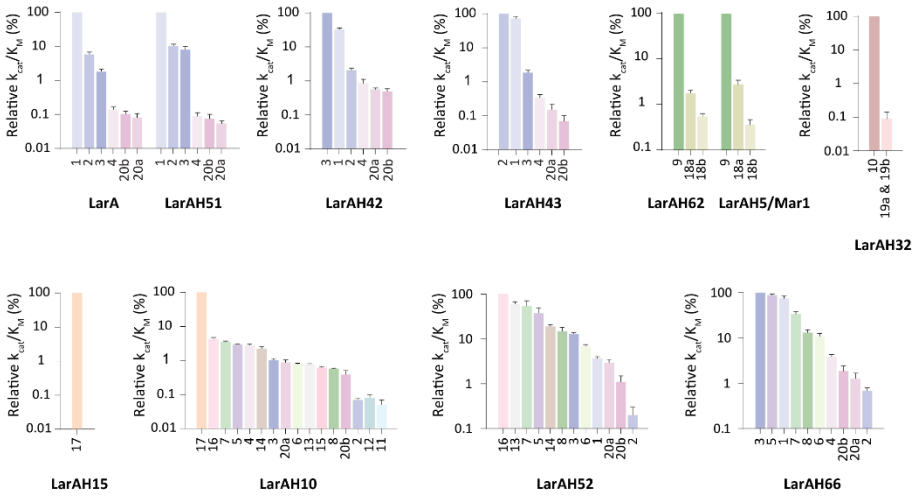

Figure 2.5 | Relative catalytic efficiencies of LarA1 and of the 9 investigated LarAHs.
The catalytic efficiency for the preferred substrate was set to 100%. The error bars represent the standard error (n=3).

Table 2.2 | **Catalytic efficiencies of LarA1 and of the 9 investigated LarAHs.** For each LarAH, the k_{cat}/K_M value of the substrate for which the kinetic parameters were obtained experimentally is italicized (Fig. 2.S5 & Table 2.1). Additional k_{cat}/K_M values were calculated using the experimentally determined k_{cat}/K_M and the relative k_{cat}/K_M values. "-": no activity.

Reactions		**k_{cat}/K_M (M^{-1} s^{-1})**			
		LarA1	LarAH51	LarAH43	LarAH42
1	L- ↔ D-lactate	*(10 ± 5) x 10^4*	*(98 ± 9) x 10^3*	*(83 ± 9) x 10^3*	*(20 ± 5) x 10^1*
2	L- ↔ D-glycerate	(6 ± 3) x 10^3	(102 ± 12) x 10^2	(114 ± 20) x 10^3	12 ± 3
3	L- ↔ D-2-hydroxybutyrate	(2 ± 1) x 10^3	(80 ± 8) x 10^2	(21 ± 5) x 10^2	(61 ± 15) x 10^1
4	L- ↔ D-2,4-dihydroxybutyrate	(14 ± 7) x 10^1	(9 ± 3) x 10^1	(4 ± 1) x 10^2	5 ± 2
20a	4-deoxy-D-threonate ↔ 4-deoxy-D-erythronate	(8 ± 4) x 10^1	(5 ± 2) x 10^1	(17 ± 8) x 10^1	3 ± 1
20b	4-deoxy-L-threonate ↔ 4-deoxy-L-erythronate	(10 ± 5) x 10^1	(7 ± 2) x 10^1	(8 ± 3) x 10^1	3 ± 1
		LarAH10	LarAH52	LarAH66	LarAH15
1	L- ↔ D-lactate	-	(34 ± 7) x 10^1	28 ± 6	-
2	L- ↔ D-glycerate	0.12 ± 0.03	18 ± 9	0.25 ± 0.06	-
3	L- ↔ D-2-hydroxybutyrate	1.7 ± 0.5	(12 ± 3) x 10^2	*37 ± 7*	-
4	L- ↔ D-2,4-dihydroxybutyrate	5.3 ± 1.6	-	1.40 ± 0.32	-
5	L- ↔ D-2-hydroxyvalérate	5.1 ± 1.2	(34 ± 12) x 10^2	33.0 ± 6.5	-
6	L- ↔ D-2-hydroxyisovalérate	1.4 ± 0.3	(62 ± 14) x 10^1	4.0 ± 1.1	-
7	L- ↔ D-2-hydroxycaproate	6.1 ± 1.4	(49 ± 17) x 10^2	12.0 ± 2.9	-
8	L- ↔ D-2-hydroxyisocaproate	1 ± 0.3	(14 ± 4) x 10^2	4.8 ± 1.2	-
11	L- ↔ D-2,3-dihydroxyisovalérate	0.10 ± 0.04	-	-	-
12	L- ↔ D-2-hydroxy-3,3-dimethylbutyrate	0.13 ± 0.05	-	-	-
13	L- ↔ D-3-phenyllactate	1.3 ± 0.3	(55 ± 13) x 10^2	-	-
14	L- ↔ D-2-hydroxy-4-phenylbutyric acid	3.9 ± 1.1	(17 ± 4) x 10^2	-	-
15	L- ↔ D-4-hydroxyphenyllactate	1.0 ± 0.3	-	-	-
16	L- ↔ D-2-hydroxy-4-oxo-4-phenylbutyrate	7.5 ± 1.9	*(92 ± 18) x 10^2*	-	-
17	D-gluconate ↔ D-mannonate	*(17 ± 4) x 10^1*	-	-	*(12 ± 3) x 10^3*
20a	4-deoxy-D-threonate ↔ 4-deoxy-D-erythronate	1.2 ± 0.3	(10 ± 4) x 10^1	0.69 ± 0.19	-
20b	4-deoxy-L-threonate ↔ 4-deoxy-L-erythronate	1.1 ± 0.3	(27 ± 8) x 10^1	0.25 ± 0.06	-
		LarAH27 [210]	LarAH62	LarAH32	
9	L- ↔ D-malate	*(39 ± 7) x 10^1*	*(63 ± 7) x 10^4*	-	
18b	L- ↔ Meso-tartrate	2 ± 1	(35 ± 8) x 10^2	-	
18a	D- ↔ Meso-tartrate	14 ± 4	(11 ± 2) x 10^3	-	
10	L- ↔ D-2-hydroxyglutarate	-	-	*(15 ± 4) x 10^3*	
19a-b	Meso-ribarate ↔ D-arabinarate ↔ Meso-xylarate	-	-	13 ± 6	

Structural model analysis of 9 selected LarAHs and exploration of the phylogenetic tree

The structural models of the nine LarAHs were retrieved from the AlphaFold database [220,221]. These models were aligned with the LarA1 structure using Pymol in order to deduce the position of the NPN cofactor (Fig. 2.6 & 2.S6).

With regard to the group comprising LARs, very few differences are observed in the catalytic site (Fig. 2.S6). The most significant difference, which may account for the observed differences in substrate specificities, is the residue

corresponding to T359 in LarA1, which is equivalent to E357 in LarAH51, Q359 in LarAH43, and C357 in LarAH42. As the glutamine residue is more hydrophilic than threonine residues and is a good hydrogen bond acceptor, this could explain the high specificity of LarAH43 for glycerate (Fig. 2.S6). The catalytic pocket of LarAH15 and of LarAH62 is similar to that of previously identified GntEs and MARs, respectively (Fig. 2.6) [210].

The HGR LarAH32 showed a catalytic site comprising several hydrophilic residues, including a glutamine at position 352 and a threonine at position 353 (Fig. 2.6), which were also present in the sequence of the previously identified HGR [210]. The newly identified group of HHRs, comprising LarAH10, LarAH52 and LarAH66, exhibit a high prevalence of hydrophobic residues within their catalytic site. LarAH10 exhibits three methionine residues in its catalytic site (Fig. 2.6), which are flexible and can likely adopt different conformations depending on the substrate. This explains the wide range of possible substrates on which LarAH10 can act (Fig. 2.5 & Table 2.2). In contrast, LarAH52, is more specific for 2-HAs with bulky side chains, whereas LarAH66 acts preferentially on 2-HAs with small side chains (Fig. 2.5 & Table 2.2). Nevertheless, this difference in specificity is not readily apparent from the structural models of the catalytic sites of LarAH52 and LarAH66 (Fig. 2.6).

Based on the results obtained for the new LarAHs (Fig. 2.5 & Table 2.2) and on their structural models (Fig. 2.6), we assigned probable functions to as many unknown LarAHs as possible on the phylogenetic tree of the LarA superfamily (Fig. 2.2). The residues equivalent to F175, F176, W358, and T359 in LarA1 were previously identified as important for substrate selectivity [209,210], so we focused on these four residues. LARs usually exhibit F, F, W, and E/Q at these positions. GntEs usually exhibit E, V, A, and H at these positions. HGRs usually exhibit Y, F, H/Q and T at these positions. MARs usually exhibit H/Q and K at the positions corresponding to W358 and T359 in LarA1, with the first two positions being more variable. In contrast, HHRs appear to exhibit a markedly lower degree of residue conservation at these positions. However, a general observation can be made regarding HHRs: the presence of a F/Y at the position corresponding to W358 in LarA1 (Fig. 2.6 and 2.S6). Based on these observations, we have predicted the function of more than half the LarAHs of the LarA superfamily (Fig. 2.3).

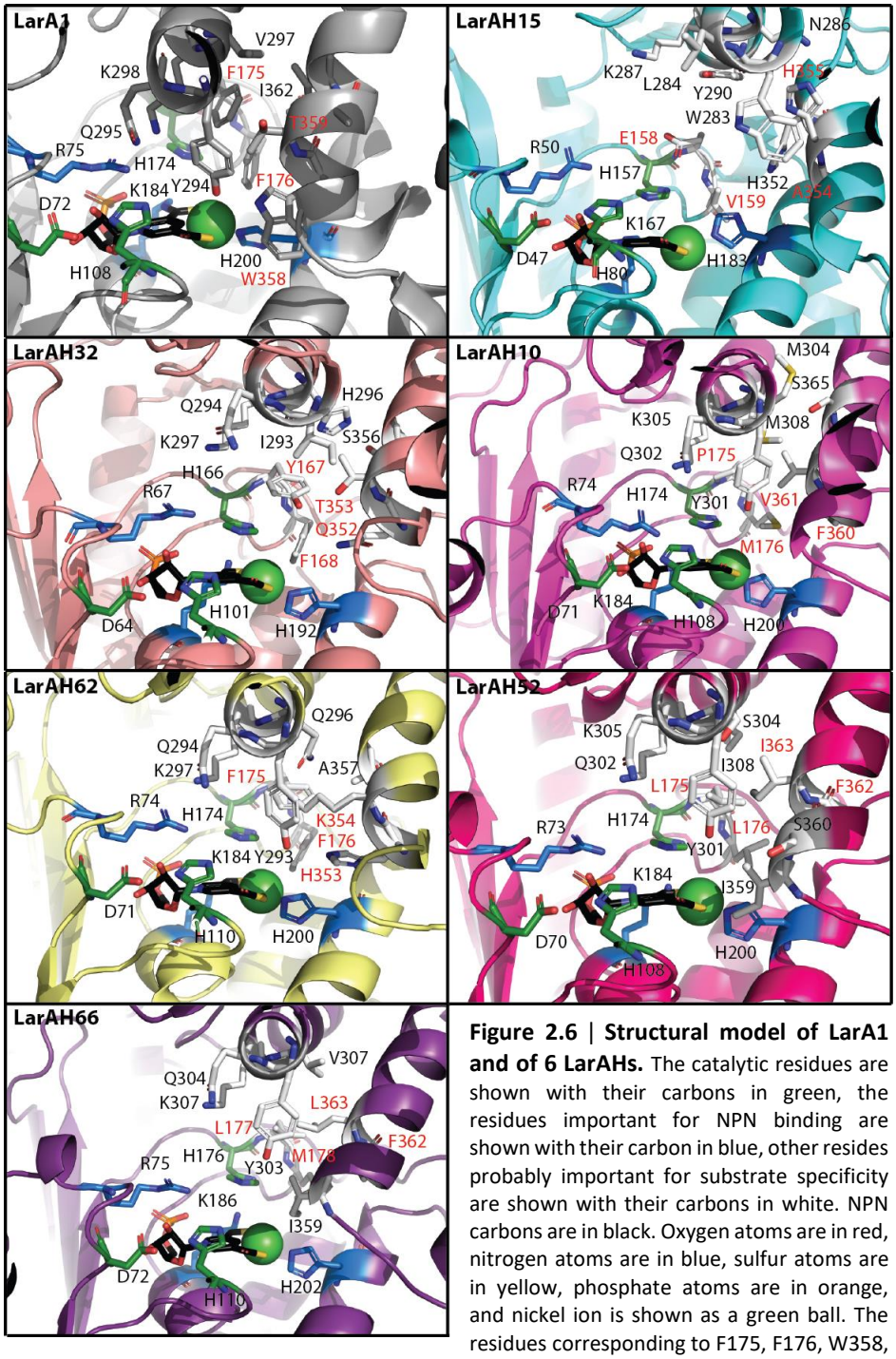

Figure 2.6 | Structural model of LarA1 and of 6 LarAHs. The catalytic residues are shown with their carbons in green, the residues important for NPN binding are shown with their carbon in blue, other resides probably important for substrate specificity are shown with their carbons in white. NPN carbons are in black. Oxygen atoms are in red, nitrogen atoms are in blue, sulfur atoms are in yellow, phosphate atoms are in orange, and nickel ion is shown as a green ball. The residues corresponding to F175, F176, W358, and T359 of LarA1 are labelled in red.

DISCUSSION

Lactate racemases (LARs)

Our exploration of the LarA superfamily started with an investigation of the phylogenetic subgroups surrounding LarA1, aiming to deepen our understanding of this phylogenetic branch and explore the potential catalytic versatility beyond lactate racemization. We characterized the substrate specificity of three novel LARs belonging to distinct subgroups of the branch: LarAH42 and LarAH43 from *Enterocloster asparagiformis*, and LarAH51 from *Clostridium pasteurianum* (Fig. 2.5 & Table 2.2). Our findings highlight the broader catalytic potential of LARs, demonstrating their ability to accommodate a diverse range of very short-chain 2-HAs, in addition to lactate. Notably, despite originating from the same organism, LarAH42 and LarAH43 exhibit distinct catalytic efficiencies, suggesting specialized *in vivo* roles: LarAH42 appears to be more specialized in the racemization of 2-hydroxybutyrate, while LarAH43 is more active on lactate and glycerate (Fig. 2.5 & Table 2.2). The physiological significance of these activities remains to be determined through *in vivo* investigations.

Hydrophobic 2-hydroxyacid racemases (HHRs)

Our findings also revealed that LarAHs from various phylogenetic groups within the LarA superfamily phylogenetic tree catalyze the racemization of a wide range of 2-HAs with hydrophobic side chains. For instance, LarAH52 from *C. pasteurianum* catalyzes the isomerization of 12 compounds, with a preference for 2-HAs with a side chain containing an aromatic ring, notably 2-hydroxy-4-oxo-4-phenylbutyrate and 3-phenyllactate (Fig. 2.5 & Table 2.2). However, its low affinity for these substrates suggests that the preferred substrate we identified may not be the native substrate of the enzyme (Table 2.1). One hypothesis is that this enzyme may racemize indole-3-lactic acid, a product of tryptophan metabolism that regulates intestinal homeostasis through epithelium–macrophage interactions [222], which unfortunately is not readily available in its pure enantiomeric form. Similarly, LarAH10 from *Megasphaera Elsdenii* exhibits isomerization activity on 16 different HAs, mostly 2-HAs with hydrophobic side chains. To our surprise, LarAH10 also showed the ability to catalyze the C2-epimerization of D-gluconate/D-mannonate, which had not been detected previously [210], probably due to the low k_{cat} of this enzyme (Table 2.1). Like LarAH52, LarAH10 displays a higher k_{cat}/K_M for bulky 2-HAs. LarAH66, on the other hand, shows specific

activity towards small 2-HAs, such as 2-hydroxybutyrate and 2-hydroxyvalerate, indicating a smaller catalytic site (Fig. 2.5 & Table 2.2). These differences cannot be inferred form the observation of the structural models, which shows the limits of these models (Fig. 2.6). Furthermore, LarAH10, LarAH52 and LarAH66 prefer substrates with linear side chains, compared to branched side chains. For example, these three LarAHs display a higher k_{cat}/K_M for 2-hydroxyvalerate compared to 2-hydroxyisovalerate, and for 2-hydroxycaproate compared to 2-hydroxyisocaproate (Fig. 2.5 & Table 2.2).

Malate racemases (MARs)

In addition to the two enzymes which have been previously identified as MARs [210], we identified LarAH62 from *Sporomusa termitida*, which exhibits a main racemization activity on malate enantiomers and promiscuous C2-epimerization activities on tartrate stereoisomers, similar to what was observed for LarAH6/MAR2 [209] and for LarAH5/MAR1 (Fig. 2.5 & Table 2.2). Both malate and tartrate share a similar 4-carbon backbone with 2 carboxylates, explaining the entry of tartrate in the catalytic site. MARs form the largest group of LarAHs within the LarA superfamily, and are observed in different phylogenetic groups (Fig. 2.2), emphasizing the importance of MAR activity in bacteria and archaea.

D-gluconate 2-epimerases (GntEs)

In addition to the two previously identified GntEs [210], we identified LarAH15 as a GntE. Notably, LarAH15 is from *Phytophthora nicotianae*, a model soilborne oomycete pathogen known to infect a broad spectrum of host plants [223], making it the first eukaryotic LarAH enzyme with confirmed activity. Interestingly, all LarAHs from eukaryotic organisms are part of the GntE phylogenetic branch, indicating a likely significant role for D-gluconate C2-epimerization in some unicellular eukaryotes.

2-hydroxyglutarate racemases (HGRs)

In addition to the previously identified HGR [210], we identified LarAH32 from *Geobacter metallireducens*, which exhibits a main racemization activity on 2-hydroxyglutarate and a promiscuous C2-epimerization activity on D-arabinarate. Both substrates share a similar 5-carbon backbone with 2 carboxylates.

CONCLUSION

In conclusion, we significantly expanded the scope of NPN-dependent reactions catalyzed by members of the LarA superfamily. Through a comprehensive approach involving taxonomic analysis, biochemical characterization, and structural modeling, we have identified and characterized the substrate specificities of 8 novel LarAHs. We identified three additional LARs, one additional MAR, one additional HGR, one additional GntE, and two additional HHRs. We showed that HHRs exhibit broad activity on a wide range of 2-HAs, with some capable of catalyzing up to 16 distinct isomerization reactions. Furthermore, the prevalence of LARs, MARs, GntEs, HHRs and HGRs within the LarA superfamily suggests the metabolic importance of these enzymes across diverse organisms. Taken together, our findings demonstrate the remarkable adaptability and importance of NPN-dependent enzymes for the catalysis of isomerization reactions in bacteria and archaea. The study of LarAHs is a completely new field of research that could have many implications in bacterial and archaeal physiology and lead to potential medical or industrial applications, e.g. for the optimization of probiotics, for the production of rare isomers of 2-HAs, or as fungicide targets in oomycete pathogens. Looking ahead, further exploration of LarAHs promises to uncover additional enzymatic functions and metabolic pathways, facilitating the development of novel biocatalysts and potential biotechnological applications.

MATERIAL & METHODS

Biological materials and growth conditions

Bacterial strains and plasmids used in the present study are listed in Table 2.S4. All plasmid constructions were performed in *E. coli* DH10B. E. coli DH10B cells were grown with agitation at 37 °C in lysogeny broth with ampicillin (200 mg·L−1) or erythromycin (200 mg·L−1), when required. When expressing pBADHisA derivatives, induction was initiated by addition of L-arabinose (0.1%) and cells were grown at 30 °C for 4 h with agitation.

DNA techniques

DNA was introduced into *E. coli* cells by electrotransformation [224]. PCR amplifications used Q5 high-fidelity DNA polymerase (New England Biolabs). The primers used in this study were purchased from Eurogentec (Seraing, Belgium) and are listed in Table 2.S5. Synthetic genes for LarAH15, LarAH10 and LarAH32 sequences were purchased from Biomatik, digested with NcoI and NheI, and cloned into a similarly digested pGIR076 [132]. Genes encoding LarAH42 and LarAH43 were amplified from the genomic DNA of *E. asparagiformis*, digested (PciI and NheI), and cloned into digested (NcoI and NheI) pGIR076. Genes encoding LarAH51 and LarAH52 were amplified from the genomic DNA of *C. pasteurianum*, digested (PciI and NheI), and cloned into digested (NcoI and NheI) pGIR076. Genes encoding LarAH62 and LarAH66 were amplified from the genomic DNA of *S. termitida*, digested (PciI and NheI for LaraH62, NcoI and NheI for LarAH66) and cloned into digested (NcoI and NheI) pGIR076. *E. asparagiformis* (DSM 15981), *C. pasteurianum* (DSM 525) and *S. termitida* (DSM 4440) genomes were purchased from DSMZ-German Collection of Microorganisms and Cell Cultures. In all cases, the sequence of the expression cassettes was verified by sequencing. Strains and primers used are listed in Tables 2.S4 & 2.S5, respectively.

Protein purification and in vitro NPN biosynthesis

In vitro biosynthesis of NPN was performed with purified LarB, LarE, and LarC as previously described [120,141]. *E. coli* cells were induced to express LarAHs when the OD600 reached 0.4 with 0.1% L-arabinose. After 4 h, the culture was cooled to 4 °C and the cells were harvested by centrifugation at 6000×g for 10 min. The pellet was stored at −80 °C until further use. The cell

pellet was thawed and resuspended in 20 ml of lysis buffer containing 100 mM Tris-HCl (pH 7.5), 300 mM NaCl and 1 mg/ml lysozyme. The cell suspension was incubated at 4°C for 30 min and sonicated 4 times for 1 min with one 2-minute rest on ice between each sonication. The supernatant was separated by centrifuging the lysate at 20000×g for 30 min at 4°C. Clarified supernatant was loaded onto 2 ml of Strep-Tactin XT Superflow (IBA) resin equilibrated with 10 ml of wash buffer (W) composed of 100 mM Tris-HCl (pH 7.5), 300 mM NaCl. After loading, the resin was washed with 20 ml of W followed by elution with 15 ml of W containing 50 mM D-biotin (Sigma-Aldrich). The eluted proteins were ultracentrifuged using Amicon Ultra—15 mL MWCO 10 kDa filter units to increase purified protein concentration. The identities of each purified LarAH protein were confirmed by electrospray ionization–time-of-flight mass spectrometry analysis. The protein concentrations were estimated with the Bradford assay.

Chemicals and reagents

All chemicals were either of analytical grade or reagent grade. D-lactic acid (sodium salt), L-lactic acid (sodium salt), D-glyceric acid (sodium salt), L-glyceric acid (sodium salt), D-malic acid, L-malic acid, D-2-hydroxybutyric acid, L-2-hydroxybutyric acid, DL-2-hydroxycaproic acid, DL-2-hydroxyisocaproic acid, L-2-hydroxyisocaproic acid, D-2-hydroxyisovaleric acid, L-2-hydroxyisovaleric acid, D-2,3-dihydroxyisovaleric acid (sodium salt), L-2,3-dihydroxyisovaleric acid (sodium salt), D-2-hydroxyglutaric acid (disodium salt), L-2-hydroxyglutaric acid (disodium salt), D-3-phenyllactic acid, L-3-phenyllactic acid, D-2-hydroxy-4-phenylbutyric acid, DL-mandelic acid, D-mandelic acid, D-gluconic acid (sodium salt), benzoic acid and L-histidine were purchased from Sigma-Aldrich. L-2-hydroxyvaleric acid, L-2-hydroxycaproic acid, L-2-hydroxy-4-phenylbutyric acid, were purchased from Biosynth. DL-2-hydroxyvaleric acid was purchased from Acros Organics. 4-Deoxy-D-erythronic acid (sodium salt hydrate), 4-Deoxy-L-erythronic acid (sodium salt hydrate), 4-Deoxy-D-threonic acid (sodium salt hydrate), 4-Deoxy-L-threonic acid (sodium salt hydrate) were purchased from Supelco. Vancomycin was purchased from Thermo Fisher Scientific.

Enzymatic assays

The general protocol for assaying LarAHs was as follows if not stated otherwise: 1 µM of in vitro synthesized NPN, 30 mM substrate, 0.2 µM of purified LarAH, 100 mM Tris–HCl buffer pH 8, in 50 µl final volume for 20 min at 30°C.

For the discovery of LarAH activities, reactions were performed with 5 µM of in vitro synthesized NPN and 2 µM of purified LarAH for 12 h.

For the determination of temperature profiles, LarAHs were incubated at the indicated temperatures.

For the determination of pH profiles, LarAHs were incubated with acetic acid buffer (pH 4 to pH 5), potassium phosphate buffer (pH 6 to pH 8) or borate buffer (pH 9 to pH 10).

For K_M measurements, reactions were performed with variable concentrations of substrate, 1 µM of *in vitro* synthesized NPN, 0.1 µM of purified LarAH, 100 mM Tris–HCl buffer pH 8, in 50 µl final volume for 20 min at 30°C.

For k_{cat} measurements, reactions were performed with the substrate concentration corresponding to the V_{max} of LarAHs for 5 min at the optimal pH and temperature of LarAHs.

All reactions were then stopped by incubation at 90 °C for 10 min and the products were assayed spectrophotometrically or by capillary electrophoresis. D-lactate, L-lactate, D-malate, D-2-hydroxyglutarate racemization reactions and D-mannonate C2-epimerization reactions were assayed spectrophotometrically at 340 nm with an Infinite 200 PRO plate reader (Tecan) using Megazyme kits. D-Lactate and L-lactate racemization reactions were assayed using the D-/L-Lactic Acid Assay Kit from Megazyme. D-malate racemization reactions were assayed using the L-Malic Acid Assay Kit from Megazyme. D-gluconate/D-mannonate C2-epimerization reactions were assayed using the D-Gluconic Acid Assay Kit from Megazyme. L-2-hydroxyglutarate racemization reactions were assayed using Acidaminococcus fermentans D-hydroxyglutarate dehydrogenase (HGDH) [225], as previously described [210]. All other racemization and C2-epimerization reactions shown in Fig. 2.4 were assayed by capillary electrophoresis [218].

Capillary electrophoresis

Enantiomers and epimers of HAs have been separated and detected using a versatile capillary electrophoresis method allowing the direct chiral separation of aliphatic and aromatic 2-HAs and polyHAs [218]. Reaction mixtures were loaded onto a polyacrylamide-coated capillary of 54/46 cm total/effective length with an internal diameter of 50 µm from Agilent, and run on a Capel 105 M from Lumex Instrument at 20 °C using -25 kV. Using a modified partial filling-counter current method with indirect UV detection, high resolution was achieved with vancomycin as a chiral selector added to the background electrolyte composed of 10 mM of benzoic acid/L-histidine at pH 5. Products were detected at 230 nm.

Peptide separation using nanoUPLC

Proteolysis was performed with 1 µg of sequencing grade trypsin (Promega, USA) and allowed to continue overnight at 37°C. Each sample was dried under vacuum with Savant Speed Vac Concentrator. Digested proteins were dissolved in 20 µl of 0.1 % (v/v) formic acid and 2% (v/v) acetonitrile (ACN). Peptide mixture was separated by reverse phase chromatography on a NanoACQUITY UPLC MClass system (Waters) working with MassLynx V4.1 (Waters) software. 200ng of digested proteins were injected on a trap C18, 100Å 5 µm, 180 µm x 20 mm column (Waters) and desalted using isocratic conditions with at a flow rate of 15 µL/min using a 99% formic acid and 1% (v/v) ACN buffer for 3 min. Peptide mixture was subjected to reverse phase chromatography on a C18, 100Å 1.8 µm, 75 µm x 150 mm column (Waters) PepMap for 130 min at 35°C at a flow rate of 300 nL/min using a two part linear gradient from 1% (v/v) ACN, 0.1 % formic acid to 35 % (v/v)) ACN, 0.1 % formic acid for 90 min and from 35% (v/v) ACN, 0.1 % formic acid to 85 % (v/v)) ACN, 0.1 % formic acid for 10 min. The column was re-equilibrated at initial conditions after washing 30 min at 85% (v/v)) ACN, 0.1 % formic acid at a flow rate of 300 nL/min. For online LC-MS analysis, the nanoUPLC was coupled to the mass spectrometer through a nano-electrospray ionization (nanoESI) source emitter.

LC-QTOF-MS/MS Analysis (DDA)

DDA (Data Dependent Analysis) analysis were performed on an SYNAPT G2-Si high definition mass spectrometer (Waters) equipped with a NanoLockSpray dual electrospray ion source (Waters).Precut fused silica PicoTipR Emitters for nanoelectrospray, outer diameters : 360 µm; inner diameter: 20 µm; 10 µm tip; 2.5" length (Waters) were used for samples and Precut fused silica TicoTipR Emitters for nanoelectrospray, outer diameters : 360 nm; inner diameter: 20 µm; 2.5" length (Waters) were used for the lock mass.solution. The eluent was sprayed at a spray voltage of 2.8 kV with a sampling cone voltage of 25 V and a source offset of 30 V. The source temperature was set to 80°C. The cone gas flow was 20 liters/h with a nano flow gas pressure of 0.4 bar and the purge gas was turned off. The SYNAPT G2Si instrument was operated in DDA (data-dependent mode), automatically switching between MS and MS2. Full scan MS and MS2 spectra (m/z 400 - 2000) were acquired from 2 min after injection to 130 min in resolution mode (20,000 resolution FWHM at m/z 400) with a scan time of 0.1 sec. Tandem mass spectra of up to 10 precursors were generated in the trapping region of the ion mobility cell by using a collision energy ramp from 17/19 V (low mass, start/end) to up to 65/75 V (high mass, start/end). Charged ions (+2, +3, +4) are selected to be submitted to the MSMS fragmentation over the m/z range from 50 to 2000 with a scan time of 0.25 sec. For the post-acquisition lock mass correction of the data in the MS method, the doubly charged monoisotopic ion of [Glu1]-fibrinopeptide B was used at 100 fmol/µl using the reference sprayer of the nanoESI source with a frequency of 30 s at 0.5µl/min into the mass spectrometer. ESI-QTOF were processed with MASCOT search engine (Matrix Sciences) using the protein sequences introduced in the Bacteria_Uniprot database.

Relative catalytic efficiencies calculation

The relative catalytic efficiencies of a LarAH acting simultaneously on two substrates, S_X and S_Y, at rates v_x and v_y, were calculated using Eq. (1),

$$\frac{\mathrm{v_x}}{\mathrm{v_y}} = \frac{(k^{\mathrm{x}}_{\mathrm{cat}}/K^{\mathrm{x}}_{\mathrm{M}})\,[\mathrm{S_x}]}{(k^{\mathrm{y}}_{\mathrm{cat}}/K^{\mathrm{y}}_{\mathrm{M}})\,[\mathrm{S_y}]} \quad (1)$$

where if $[S_X] = [S_Y]$ the [S] terms cancel, and the ratio of the k_{cat}/K_M values for each substrate is equal to the relative rates at which the LarAH catalyzes the transformation of each substrate when both are present at equal concentrations with the enzyme in the same mixture [226]. v_x and v_y were determined by quantifying the products P_X and P_Y either spectrophotometrically or by capillary electrophoresis. For a LarAH active on more than two substrates, we determined its catalytic efficiency for each of its substrates by testing combinations of substrate pairs with the LarAH.

Phylogenetic analysis

The sequences of 12441 LarAHs from the LarA superfamily (DUF2088) were retrieved from the Interpro entry IPR048068 on EMBL-EBI (accessed February 26, 2024) [217]. This dataset of sequences was reduced by filtering all sequences by length with USEARCH v11.0.667 (command -sortbylength -minseqlength 300 -maxseqlength 600) and then by clustering all sequences using the UCLUST method implemented in the USEARCH package (command –cluster_fast –id 0.5 -centroids) [227], resulting in a list of 1212 representative LarAHs sequences. The 1212 LarAHs sequences were aligned with MAFFT v7.271 using FFT-NS-2 parameters [228,229]. The LarA superfamily phylogenetic tree was constructed from the alignment in maximum likelihood framework using IQ-TREE v2.0.6 [230]. 10 archaeal sequences from the DUF362 (Pfam entry PF04015) were used as outgroup since DUF362 and DUF2088 are part of the same clan (Pfam clan CL0471). The sequence evolution model, Q.pfam+R10 replacement matrix [231], was determined by ModelFinder as implemented in IQ-TREE2.0 [232]. Branch supports were measured by ultrafast bootstrap approximation 2.0 with 1000 replicates (option –bb 1000) [233] . The tree was rooted with the outgroup and visualized using iTOL v5 [234].

III.2.2 Supplementary data

Domains	# of species	% of all organisms with at least one LarAH
Bacteria	3279	85.2
Archaea	493	12.8
Eukaryota	75	1.9

Bacterial phylums	# of species	% of all bacteria with at least one LarAH
Bacillota	1091	33.3
Actinomycetota	609	18.6
Pseudomonadota	232	7.1
Planctomycetota	176	5.4
Thermodesulfobacteriota	174	5.3
Chloroflexota	136	4.1
Bacteroidota	91	2.8
Acidobacteriota	79	2.4
Myxococcota	74	2.3
Cyanobacteriota	61	1.9
Spirochaetota	56	1.7
Thermotogota	42	1.3
Other	458	13.8

Figure 2.S1 | Taxonomic distribution of LarAHs sequences. (**A**) Taxonomic distribution of LarAHs sequences across domains. (**B**) Taxonomic distribution of LarAHs sequences within bacteria. The number of species represent the number of microorganisms in each domain/phylum that contain at least one LarAH. Data assembled from the Interpro entry IPR048068 on the European Molecular Biology Laboratory - European Bioinformatics Institute (EMBL-EBI) obtained on February 26, 2024.

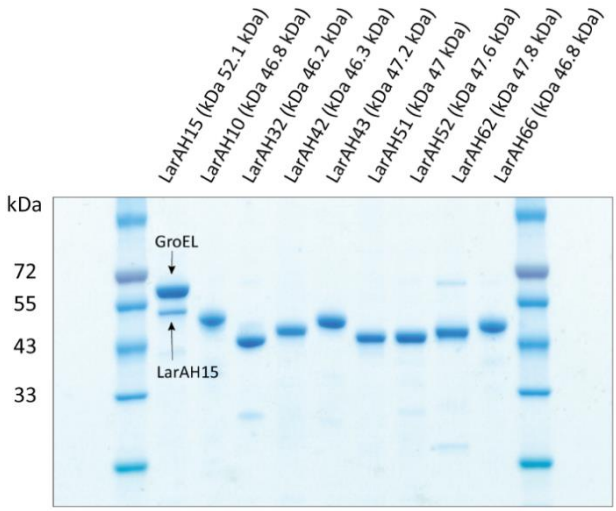

Figure 2.S2 | **Analysis of purified LarAHs from *E. coli* by SDS-PAGE.** The protein co-purified with LarAH15 was identified as the 60 kDa chaperonin protein Cpn60 (GroEL) by mass spectrometry analysis. LarA1 and LarAH5/MAR1 are not included, as their purification has been previously shown [95,210]. Sequences of the proteins are provided in Table 2.S2.

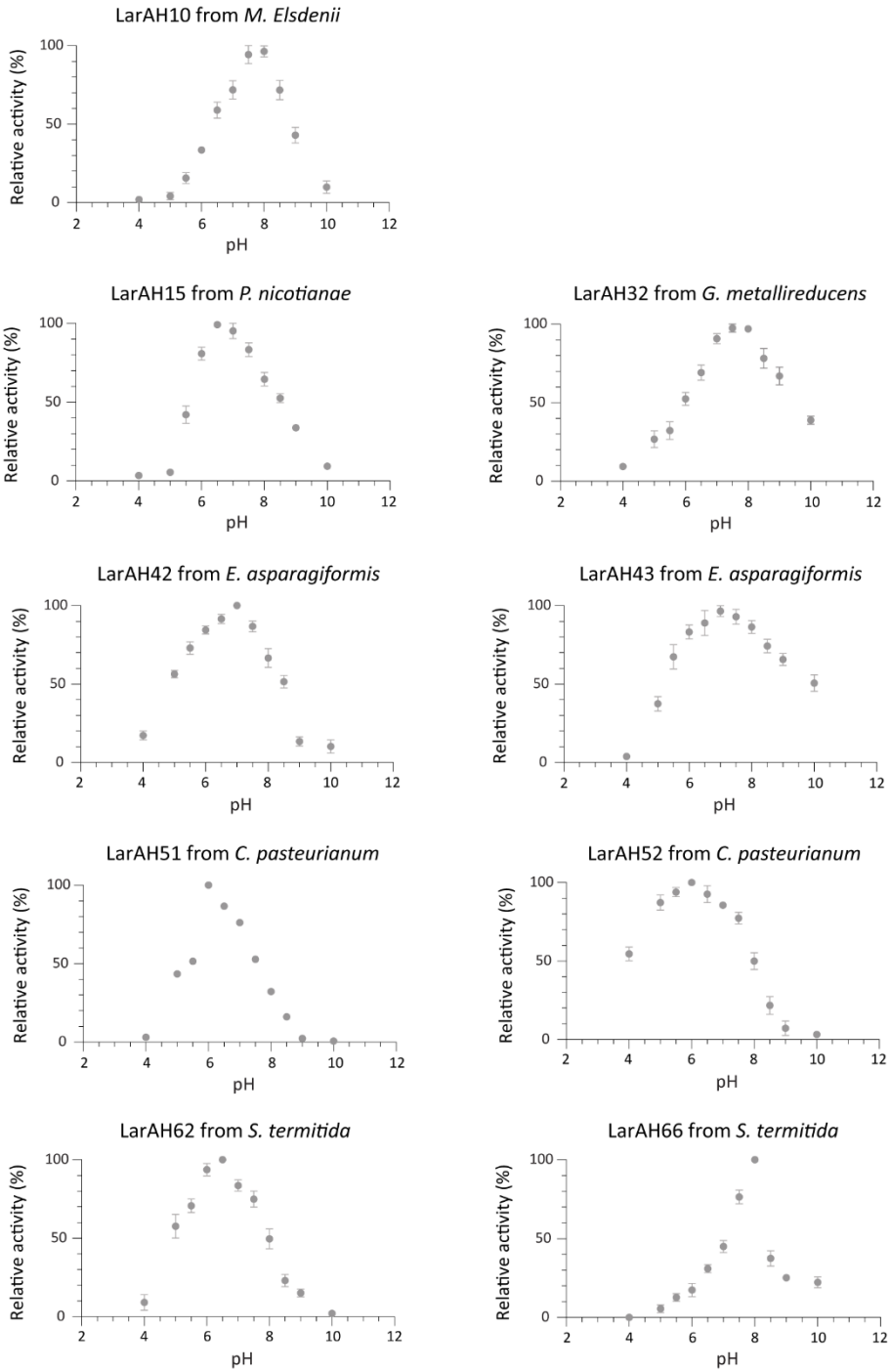

Figure 2.S3 | **Relative activity of the 9 investigated LarAHs as a function of pH.** The error bars represent the standard error (n=3)

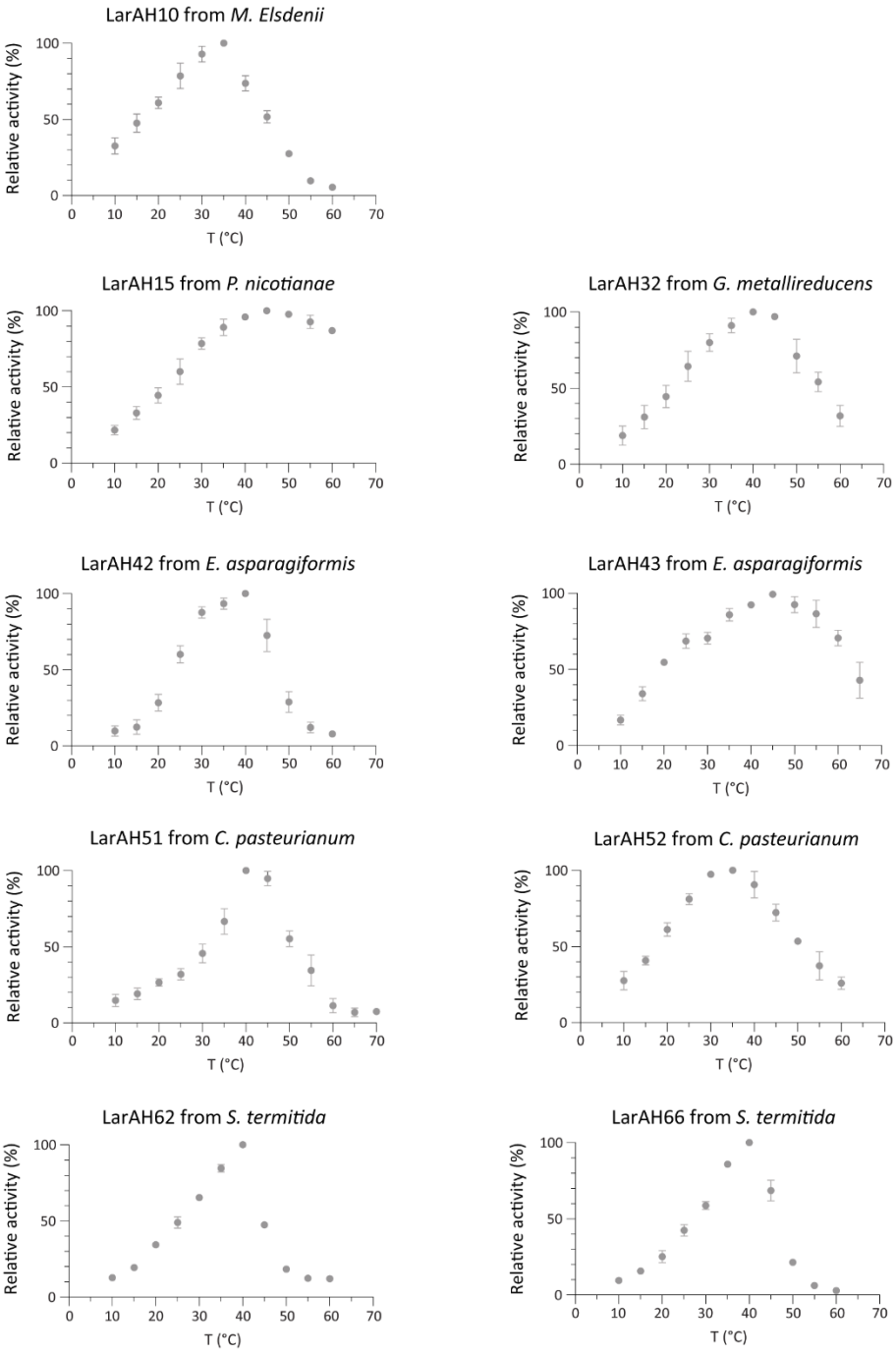

Figure 2.S4 | Relative activity of the 9 investigated LarAHs as a function of temperature. The error bars represent the standard error (n=3).

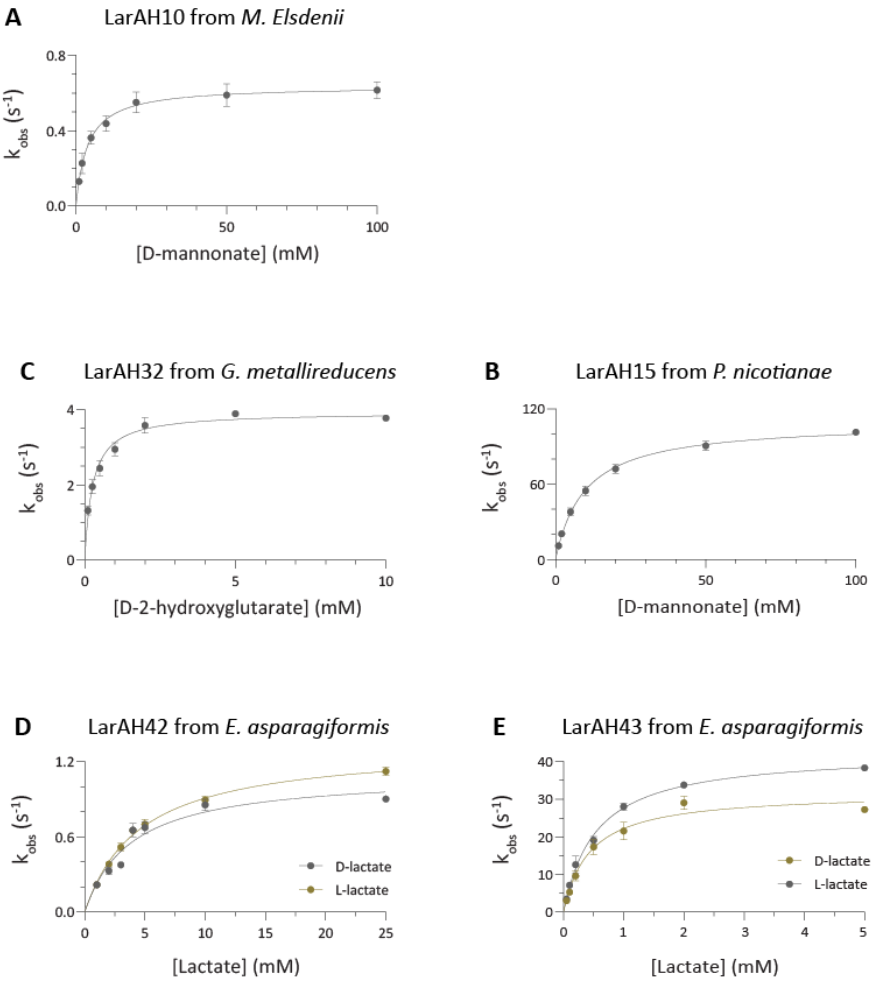
A
LarAH10 from M. Elsdenii
k_obs (s^-1)
[D-mannonate] (mM)
C
LarAH32 from G. metallireducens
k_obs (s^-1)
[D-2-hydroxyglutarate] (mM)
B
LarAH15 from P. nicotianae
k_obs (s^-1)
[D-mannonate] (mM)
D
LarAH42 from E. asparagiformis
k_obs (s^-1)
D-lactate
L-lactate
[Lactate] (mM)
E
LarAH43 from E. asparagiformis
k_obs (s^-1)
D-lactate
L-lactate
[Lactate] (mM)

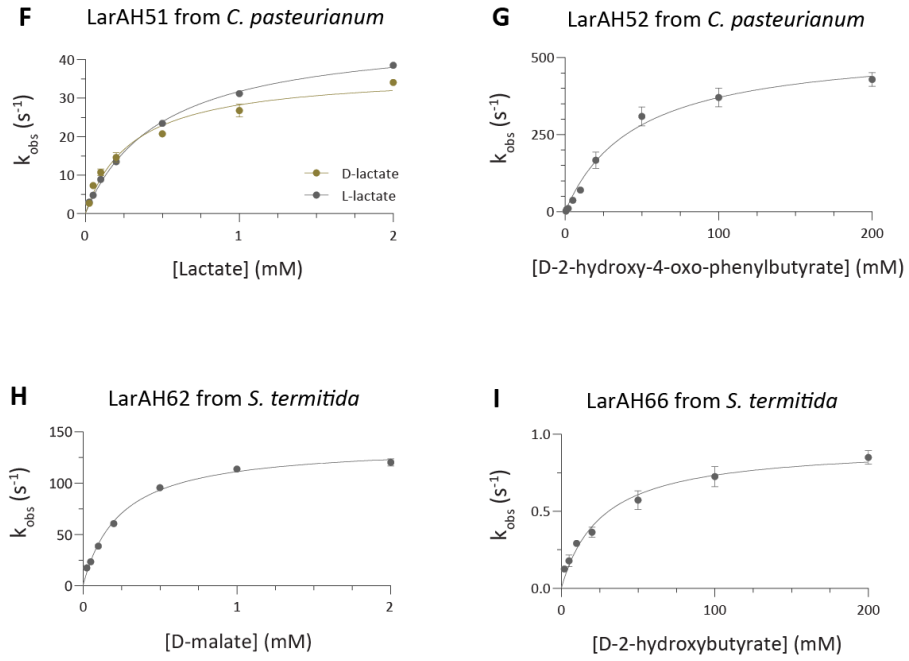

Figure 2.S5 | **Kinetic analysis of the 9 investigated LarAHs.** (**A**) D-gluconate/D-mannonate C2-epimerization by LarAH10 from *M. Elsdenii*, (**B**) D-gluconate/D-mannonate C2-epimerization by LarAH15 from *P. nicotianae*, (**C**) L-2-hydroxyglutarate racemization by LarAH32 from *G. metallireducens,* (**D**) D- and L-lactate racemization by LarAH42 from *E. asparagiformis,* (**E**) D- and L-lactate racemization by LarAH43 from *E. asparagiformis*, (**F**) D- and L-lactate racemization by LarAH51 from *C. pasteurianum,* (**G**) D-2-hydroxy-4-oxo-phenylbutyrate racemization by LarAH21 from *C. pasteurianum*, (**H**) D-malate racemization by LarAH62 from *S. termitida*, (**I**) D-2-hydroxybutyrate racemization by LarAH66 from *S. termitida*. The activities of the enzymes at the indicated substrate concentrations are shown as $k_{obs} = v_0/(E)_0$. The curves are the fitted curves using non-linear regression.

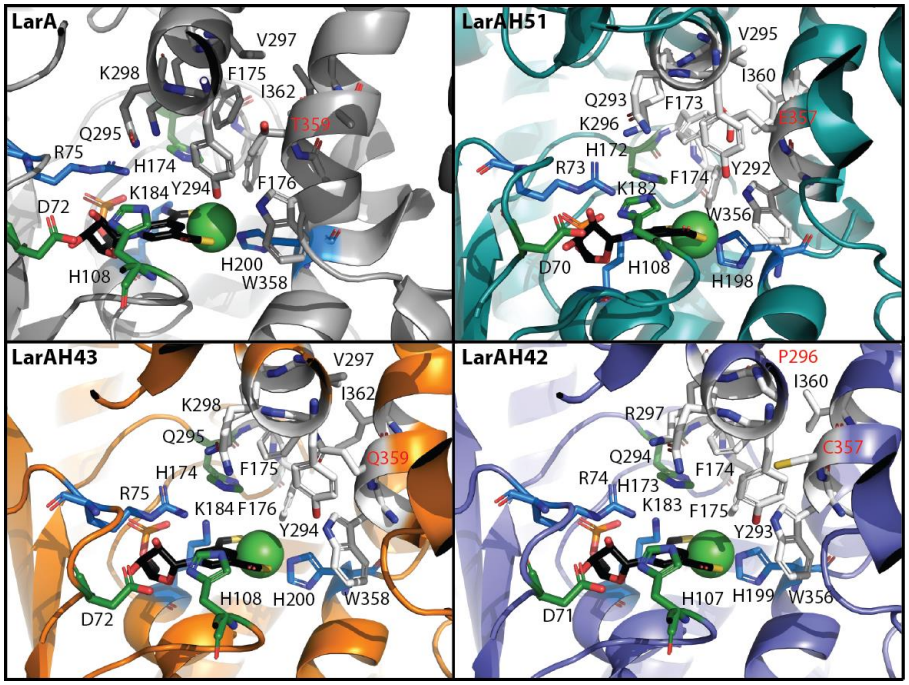

Figure 2.S6 | **Structural model of 4 lactate racemases.** The catalytic residues are shown with their carbons in green, the residues important for NPN binding are shown with their carbon in blue, other residues probably important for substrate specificity are shown with their carbons in white. NPN carbons are in black. Oxygen atoms are in red, nitrogen atoms are in blue, sulfur atoms are in yellow, phosphate atoms are in orange, and nickel ion is shown as a green ball. The residues corresponding to T359 of LarA1 are labelled in red.

Table 2.S1 | **Prevalence of LarAHs sequences among archaea and bacteria taxa.** Data assembled from the database of Clusters of Orthologous Genes (COGs) entry COG3875 on the National Center for Biotechnology Information (NCBI) obtained on September 22, 2024.

Taxa	COG3875 data	% of organisms with LarAHs	Mean of LarAHs per organisms
Archaea	[57/193 organisms 73 genes]	29.5	1.3
Asgardarchaeota	[7/8 organisms 20 genes]	87.5	2.8
Crenarchaeota	[0/29 organisms 0 genes]	0	0
Euryarchaeota	[36/103 organisms 38 genes]	34.9	1.1
Nitrososphaerota	[3/13 organisms 3 genes]	23.1	1
Thermoplasmatota	[7/17 organisms 7 genes]	41.2	1
Other Archaea	[4/23 organisms 5 genes]	17.4	1.2
Bacteria	[344/2103 organisms 550 genes]	16.4	1.6
Acidobacteriota	[11/16 organisms 14 genes]	68.7	1.3
Actinomycetota	[54/253 organisms 69 genes]	21.3	1.3
Aquificota	[0/9 organisms 0 genes]	0	0
Bacillota	[102/355 organisms 208 genes]	28.7	2
Bacilli	[11/152 organisms 11 genes]	7.2	1
Clostridia	[76/159 organisms 161 genes]	47.8	2.1
Erysipelotrichia	[1/14 organisms 1 genes]	7.1	1
Negativicutes	[10/12 organisms 29 genes]	83.3	2.9
Tissierella	[3/16 organisms 5 genes]	18.7	1.7
Other Bacillota	[1/2 organisms 1 genes]	50	1
Bacteroidota	[9/192 organisms 9 genes]	4.7	1
Bdellovibrionota	[0/7 organisms 0 genes]	0	0
Campylobacterota	[2/20 organisms 2 genes]	10	1
Chlamydiota	[0/12 organisms 0 genes]	0	0
Chlorobiota	[0/5 organisms 0 genes]	0	0
Chloroflexota	[8/19 organisms 14 genes]	42.1	1.7
Cyanobacteriota	[5/75 organisms 5 genes]	6.6	1
Defferibacterota	[7/7 organisms 7 genes]	100	1
Deinococcota	[1/7 organisms 1 genes]	14.3	1
Fusobacteriota	[1/9 organisms 1 genes]	11.1	1
Mycoplasmota	[2/24 organisms 2 genes]	8.3	1
Myxococcota	[15/17 organisms 21 genes]	88.2	1.4
Planctomycetota	[38/44 organisms 76 genes]	86.4	2
Pseudomonadota	[20/808 organisms 22 genes]	2.5	1.1
Alphaproteobacteria	[10/300 organisms 11 genes]	3.3	1.1
Betaproteobacteria	[3/166 organisms 3 genes]	1.8	1
Gammaproteobacteria	[6/338 organisms 7 genes]	1.8	1.2
Other Proteobacteria	[1/4 organisms 1 genes]	25	1
Spirochaetes	[7/22 organisms 14 genes]	31.8	2
Synergistetes	[6/10 organisms 13 genes]	60	2.2
Thermodesulfobacteriota	[27/56 organisms 45 genes]	48.2	1.7
Thermotogota	[6/12 organisms 6 genes]	50	1
Verrucomicrobiota	[3/24 organisms 7 genes]	12.5	2.3
Other bacteria	[17/100 organisms 20 genes]	17	1.2

Table 2.S2 | LC-ESI-QTOF-MS analysis of the 9 investigated LarAHs.

Match to*	Score	Sequence coverage (%)
LarAH10	658	96
LarAH15	326	77
LarAH32	588	67
LarAH42	251	48
LarAH43	3723	74
LarAH51	3084	56
LarAH52	4951	56
LarAH62	15319	58
LarAH66	3034	62

Table 2.S3 | Sequences of LarA and the 9 investigated LarAHs.

Name	Sequence
LarA	MVAIDLPYDKRTITAQIDDENYAGKLVSQAATYHNKLSEQETVEKSLDNPIGSDKLEELARGKHNIVIISSDHTRPVPSHIITPIL LRRLRSVAPDARIRILVATGFHRPSTHEELVNKYGEDIVNNEEIVMHVSTDDSSMVKIGQLPSGGDCIINKVAAEADLLISEGFI ESHFFAGFSGGRKSVLPGIASYKTIMANHSGEFINSPKARTGNLMHNSIHKDMVYAARTAKLAFIINVVLDEDKKIIGSFAGD MEAAHKVGCDFVKELSSVPAIDCDIAISTNGGYPLDQNIYQAVKGMTAAEATNKEGGTIIMVAGARDGHGGEGFYHNLAD VDDPKEFLDQAINTPRLKTIPDQWTAQIFARILVHHHVIFVSDLVDPDLITNMHMELAKTLDEAMEKAYAREGQAAKVTVIP DGLGVIVK
LarAH10	MMKTFSLPFGKSTQTVSLDEAHVLYDLHGNHVDAVADEQAAIRQALRHPIGSAPLKDVVQAGDTVAIVVSDITRLVHTAQ MLPIIVDELNQAGVKDDQITVVTAQGTHRAHTPEEDAIVCGADMVKRVKIVSHDCRDASQLTKIGTTTYGNDVYLNSHVV QADKVILTGAVSFHPMAGFGGGRKAVLPGVASYETIMRNHAMALTETFGGGCNPKCETSLLEDNPLHDDMKQAAALLNP CFLVNTVFSADGDLYEVVGGHWYEAWKKGCDDLLHIASVPIQDLADITIASAGGYPKDMNLYQSMKAPMNAVFATKPGG TMILTLDCPDIKEPAIFTDWFFRSDMDAFEKDLRADFSIPAFVAFKSHCIFRSLKEAYVVTRPENFDIIRHSGLIPAATLEEAWE KAQKNLPENYKVTIMGHAAATFPVRK
LarAH15	MTLLFAEGSKTTELSDERLREIVRETLQKLETQRGTKFEKAVIVPPDFTRFHSKSGVLSQYAYEYLQDKVTDVLPALGTHDAM TDEEISKMFGDIPKNLFRVHDWRNDVVTIGQVPAELIQKASDGKVNEPWPAQINRLLWEGGHDLVLSIGQVVPHEVMGM ANFNKNIFVGTGGSEGINFSHFIGAVYGMERMMGRADNPLRRILNYASTNFLQKLPLIYIQTVIGRGESGNLVTRGVFIGDD EECFMKAAELSLEVNFELLAAPIDKVVVYLDPEEFKSTWLGNKSIYRTRMAIADDGELIVLAPGVARFGEDKRIDELIRKYGYR TTPEVLAHLNANRDLMKNLSAAAHLIHGSSEGRFRITYCPGHLTKEEVEGVGFGYGNLQEMSAKYPVDKLQDGWNVDAD GERFFYISNPALGLWAYRGRFEGTPTDATSTSASATSTHLSAAADTTEACLDAGVGGGPFKHS
LarAH32	MDLHYGDTSFTLTLPPERLLGVIRPEIGVPVDRPETIIAAALDRCAETIGTFRPGERVVIVTSDITRYTGSELYLPLLVERLVATGI RERDMEILVALGIHRKQTEHEHQKIAGPLHGRIRIVDHDCDDPGQLAFIGRTSNGIEVTVNRRVVEADRVILTGTIGFHYFAG FGGGRKSILPGVASRATCMASHFAVLNPGEGTGKNPLAVTGNLEGNPVHGAMVEACAMVEPDFILNTVLSPDKRIMAAF AGPWREAHEEGCRFYAERFAWPLREKADLVVVSCGGFPKDINVIQSHKAMEYGSQALKEGGVMVLLAQCRDGYGNATFF DWFRFRDLGAFETRLRSHYEINGQTAYSLLQKAQKFRVILVSELPPEEVRTMGMTPARSLDEAMAQAAEFLPADYTAYVIPE GGTVLPVIKP
LarAH42	MRIDLPYDTKTVPLTIGEQNLEKIVISHISEASGEGTQEEMVRRALEQPVGTPRLRELARGKKRVVLVTSDHTRAVPSKITLPIL LGEIRAGNPGAEITILIATGLHRETTREEQICMFGAEIVERERIVVNRAFEKDEFVSMGELPSGAGFYVNRLAVDCDLLVTEGFI EPHFFAGFSGGRKSILPGICSAETVNENHSYKAIASPFAAAGVLEGNPIHEDMICAARRVNVQFILNVALNARKEIIAAFAGDV EAAHLEGCRYIRSISEEPAVTGDIVVTSNGGYPLDQNLYQSPKAVATAEACAGEDGVIIMVCACREGIGGSHFEELIMGGNP QEIDRKLSAVPPRETIPEQWCAQIYARILQAHPVILVTTYLDPEVVRRANMIPASTPDEALAMAFEMRGKDARVVVIPDGVS VMITKPVS
LarAH43	MKRFDLPYGRGTISLSLPERRVKAVLESHLHTYRPDLGEEELVNAALESPEGSPRLSQLAKGKHNVVMIASDHTRPVPSRHIIP AMLREIREGNPEADITILIATGCHRAPTREELIQKFGEEIAGREKIVIHSCEDSEDFVSLGTLPSGGELILNRMAVEADLLCAEGF IEPHFFAGFSGGRKSVLPGVAARKTVLANHCSAFIDSPYARTGIIEGNPIHRDMIYAAKKAGLAFIVNVVINQKKEIIHAVAGD CDLAHKKGVSFLNDWCRTPAVPADIVVSTNGGYPLDQNIYQAVKGMTAAEATVNEGGVIIMAAKSEDGHGGQVFYETFR DEPDVDRMMERFLATPAEGTIPDQWQSQIFARVLKRARVIYVSSAPPEMVRALHMIPADSMEEALRMADRLLGRPDGSV TVIPDGVSVMVTAPENGNAEI
LarAH51	MIKIPYSTKTLKINIDNKNLKGILISKAHNYKVNESQEYIVNRALDNPIGSERLEDLVKNKNNMVIITSDHTRPVPSNITMPILLN RIRKVNPSIDITILIATGFHRPTTREEMINKFGREIVEKEKIINHVSTDKNDLTNVGVLPSGGQLILNKLAINTELLISEGFIEPHFF AGFSGGRKSILPGIASAETIMANHCSEFINSNQARTGIIEDNPIHRDMLYAAEKAKLAFILNVVIDADKKIINAFAGDRRLAHEE GCKFVMELSSVKKIEADIAITSNGGYPLDQNIYQAVKGMTAAETTCRKGGVIIMIAACNDGHGGKSFYDNVSNAKNPRELLE RILNVPRNKTIPDQWEIQILARILNDYTVIMVTDLCDPSMIENMHMKHAKTFEEALKMAYNIKGEKAEVVVIPDGVSVVVSD
LarAH52	MKSIHMKYGNEKIEVSVDEDNLIQIIESNPFNLGKNENEVILDSLANPIGTPRLKDIVAKGEKICIVISDITRAWQRPYKFLPLIV EELNKSGISDKDITFLCAAGTHRNQTEKEHGLLLGPELSKRFKVIDHDCLDKNNLVYLGDTSYGTPVWINKIAMECDHIIITGAI VYHLLAGWAGGKKSILPGISGYESIMANHALSLGENIGDGSNPLVRSGYIENNPVHKDMLEAASFVKPSFMFNVIMGSDGN IAAAVSGNYIEAHKEGRELVNKIDGVKIHEKADLVIASAGGYPKDINLYQSSKTMINMNEAAKEGATLILISQCREGLGGDSDI KDIILNYDNILDREKSLRERYSISKFIGYYVCEMAEKYDFIMVSDIDQSLVKNANIKVVSTIDEALNIVYKKRGENLKTILMPKGA NTLPILQD
LarAH62	MQKKYTYKYGKGTVNFTVDESLVTDELYIRQCPVLSDPAESVREAIRNPIGCKPLRDIVKTGETVVFLVNDTTRIANSHIFMPI LLDELNSAGIPDQDMWIVFALGTHRLMTEEEMVGEVGSSVSQRVRLYNSDCRDAGQFRYFGTTSYGTPVYFNNKVVEAD HIICTGSVVHHFFAGFGGGRKAMLPGVAHYETVRKNHSLMLDANAVIGKLDGNPIYHDQVEGTEMCRPSFLLNVVLNEKK EFLKVFAGDYIQAHRECCEFVNGVYGVPVEKEADLVIASCGGYPKDINVYQLQKTMDNAWCAVREGGVVIILGECAEGSGS AIYEKTMQKYTTPEQVEAAVKADFQIGAHKAYAVTRLMKKAHFILVSSMLPELARLLLFTPARDMEEAMELAVNKFNLIQPR IILMPMGSITVPLINKSKCGNTGD
LarAH66	MAETVFEFGYGNSKLQVSLPAEKIINNVLGKPCPAIVDVPAAVRAALRNPIGTPPLKEVVKPGDKVAVVVSDITRAWVNFD QFLPVLLDELNDAGVPDQNIFIIAPGAHRLNTQAEFVVLCGEKVCHRVAVYNHDCHKQEELVYTGKTKGGVDCYINKRVAG ADKMILTGGIVHHLMAGFGGGRKAILPGISGFKTIQGNHLFCMNKEVGKGLNPNCIAGKLEENEMNEDMIEQAALARPDF LLNAVFTPENKFARFVAGHWYEAWLAGTKMVDEIYGIPITAQADLVVSSAGGFPKDINLYQGVKTIDNAYMAAKPGGVVIC CLELPDITEPAEFSDWFKYPTMLEHEMALRANFTIPGFLAYRLLDIARQLSLIIVTRQENAGFISKAGMIPATTVAEALALAKEK LGRDDYTITVMAAAANTVPVLK

Table 2.S4 | Bacterial strains and plasmids used in this study.

Strains	Characteristic(s)	Used for	Source or reference
Lc. Lactis NZ3900	MG1363 derivative		[233]
E. coli DH10B	F$^-$ *endA*1 *recA*1 *galE*15 *galK*16 *nupG rpsL* Δ*lacX*74 Φ80*lacZ*ΔM15 *araD*139 Δ(*ara*,*leu*)7697 *mcrA* Δ(*mrr-hsdRMS-mcrBC*) λ$^-$		Invitrogen
E. coli ArticExpress	Contains *Cpn60* and *Cpn10* from *Oleispira antarctica*		Agilent
Plasmids			
pGIR012	Cm^r; pNZ8048 with DNA encoding the StrepII-tag sequence translationally fused to *larA*	LarA purification	[36]
pGIR026	Em^r Amp^r; pGIR660 with DNA encoding the StrepII-tag sequence translationally fused at the 3'-end of the *larB* ORF	LarB purification	[36]
pGIR031	Cm^r; pNZ8048 with DNA encoding the StrepII-tag sequence translationally fused to *larC*	LarC purification	[36]
pGIR076	Amp^r; pBADHisA with DNA encoding *larE* translationally fused to the StrepII-tag sequence	LarE purification	[76]
pGIR313	Amp^r; pBADHisA with DNA encoding LarAH5/MAR1		[209]
pGIR315	Amp^r; pBADHisA with DNA encoding LarAH10		[209]
pGIR321	Amp^r; pBADHisA with DNA encoding LarAH15		This study
pGIR322	Amp^r; pBADHisA with DNA encoding LarAH32		This study
pGIR323	Amp^r; pBADHisA with DNA encoding LarAH42	LarAHs purification	This study
pGIR324	Amp^r; pBADHisA with DNA encoding LarAH43		This study
pGIR325	Amp^r; pBADHisA with DNA encoding LarAH51		This study
pGIR326	Amp^r; pBADHisA with DNA encoding LarAH52		This study
pGIR327	Amp^r; pBADHisA with DNA encoding LarAH62		This study
pGIR328	Amp^r; pBADHisA with DNA encoding LarAH66		This study

*Emr, Ampr, and Cmr indicate resistance to erythromycin, ampicillin, and chloramphenicol, respectively.

Table 2.S5 | List of primers used in this study.

Name	Sequence (5'-3')	Reference/source
LarAH15_A	TTTCCATGGCAACCTTATTATTTGCGGAGG	This study
LarAH15_B	AAAGCTAGCTGAGTGTTTGAAAGGTC	This study
LarAH32_A	TTTCCATGGACCTGCACTACGGTG	This study
LarAH32_B	TTTGCTAGCCGGCTTAATAACCGGCAGCAC	This study
LarAH42_A	TTTACATGTCCAGAATTGACCTTCCCTACGACAC	This study
LarAH42_B	TTTGCTAGCGGATACCGGTTTTGTGATCATC	This study
LarAH43_A	CCCACATGTCTAAACGATTTGATTTACCCTACGG	This study
LarAH43_B	TTTGCTAGCTATTTCCGCGTTCCCGTTC	This study
LarAH51_A	TTTTACATGTCCATTAAAATTCCCTATTCAACAAAAACCC	This study
LarAH51_B	TTTGCTAGCATCACTGACAACCACTGATAC	This study
LarAH52_A	TTTTACATGTCCAAAAGTATTCATATGAAATATGG	This study
LarAH52_B	TTTGCTAGCATCTTGTAAAATGGGAAGTG	This study
LarAH62_A	TTTTACATGTCCCAAAAAAAATATACCTACAAGTATG	This study
LarAH62_B	TTTGCTAGCATCGCCGGTGTTG	This study
LarAH66_A	AAAACCATGGCGGAAACAGTATTTGAGTTTG	This study
LarAH66_B	TTTGCTAGCTTTCAATACCGGCACAGTAT	This study
pBAD_up	GCAACTCTCTACTGTTTCTCCATAC	This study
pBAD_rev	CCGCCAGGCAAATTCTG	This study

† PciI, NcoI, NheI restriction sites introduced in the primers are underlined in primer sequences.

CHAPTER 3

Shedding light on a family of broad-spectrum 2-hydroxy acid and polyhydroxy acid (sugar acid) isomerases

Julian Urdiain-Arraiza and Benoît Desguin

In preparation for publication

Author's contributions

The study was conceived and designed by JUA and BD.
The laboratory work was performed by JUA (Figs 3.3, 3.S1, 3.S2, 3.S3, 3.S4 and Tables 3.1, 3.2, 3.S4, 3.S5).
The data were analyzed and interpreted by JUA (Fig. 3.1, 3.2, 3.3, 3.4, 3.S5 and Table 3.S3) and BD (Fig. 3.5, 3.6).
The manuscript was written by JUA and BD.
The manuscript was revised by JUA and BD.

The previous chapter explored various phylogenetic clusters in the LarA superfamily. Here, we investigated a previously unexplored and uncharacterized phylogenetic cluster of LarAHs within this superfamily. Initially, our focus was on a single LarAH from this group, which exhibited significant AHA racemization and PHA C2-epimerization activities, indicating promising biotechnological applications. To gain deeper insights, we purified a total four LarAHs from this cluster for further study.

Through substrate profiling of these LarAHs, we identified 15 racemization reactions across the 3 main classes of AHAs: aliphatic, aromatic, and polycarboxylic AHAs. In addition, we discovered 24 C2-epimerization reactions of PHAs spanning the 3 main classes of sugar acids: aldonic acids, uronic acids, and aldaric acids. Many of these LarAHs also catalyzed the C2-epimerization of aldonic acid derivatives, such as deoxy and keto aldonic acids. Given their wide range of activities, we classified these LarAHs as a family of broad-spectrum hydroxy acid isomerases (BSHIs). Notably, most of these C2-epimerization reactions were previously unreported, with no known enzymatic routes for synthesizing the corresponding sugar acid stereoisomers.

To facilitate a comprehensive understanding of each BSHI's potential for chemoenzymatic synthesis, we determined their temperature and pH-dependent activity profiles, kinetic parameters, and substrate specificities. We also demonstrated that BSHIs display distinct stereochemical preferences and hierarchical importance for different carbon positions, affecting their catalytic efficiencies. Finally, we analyzed the structural models of BSHIs and found that the structure of their C-terminal domain, which is responsible for the substrate binding, is completely different than the one of LarA1. This unique structure is particularly well-suited for accommodating bulky substrates and shows considerable flexibility, explaining the wide substrate range and adaptability of BSHIs.

Overall, we highlighted the remarkable biotechnological potential of BSHIs, a newly identified LarAH family within the LarA superfamily, for the stereoselective conversion of AHAs and PHAs.

III.3.1 Manuscript

Shedding light on a family of broad-spectrum 2-hydroxy acid and polyhydroxy acid (sugar acid) isomerases

Julian Urdiain-Arraiza[1] and Benoît Desguin[1]

[1] Louvain Institute of Biomolecular Science and Technology (LIBST), UCLouvain, 1348 Louvain-La-Neuve, Belgium.

Abstract

2-Hydroxy Acids (AHAs) and Polyhydroxy Acids (PHAs) find extensive applications across various industries including food, cosmetics, and organic synthesis. However, the synthesis of stereoisomers of these compounds, whether enzymatically or chemically, remains a significant challenge. In this work, we unveil a previously unexplored group of lactate racemase homologs (LarAHs) within the LarA superfamily. We investigated the biochemical properties, substrate specificities, stereoselective preferences and structural models of four LarAHs from this family. Our findings revealed that these LarAHs are broad-spectrum hydroxy acid isomerases (BSHIs), acting as racemases or C2-epimerases of a wide range of AHAs and PHAs. Specifically, we identified 15 racemization reactions spanning the 3 primary classes of AHAs: aliphatic, aromatic, and polycarboxylic AHAs. More importantly, we uncovered C2-epimerization reactions of PHAs encompassing the 3 main classes of sugar acids: aldonic acids, uronic acids, and aldaric acids. Moreover, most of these BSHIs also catalyze the C2-epimerization of derivatives of aldonic acid, such as deoxy aldonic acids and keto aldonic acids. In total, 24 C2-epimerization reactions of PHAs were identified, among which 20 were previously unreported. Structural models of these BSHIs revealed that the structure of their C-terminal domain, which is responsible for the substrate binding, is completely different than the one of LarA1, and can explain their broad substrate spectrum. In conclusion, BSHIs present promising avenues for the conversion of valuable stereoisomers of AHAs and PHAs, offering new possibilities for biotechnological applications.

Keywords

hydroxy acid, racemase, epimerase, aldonic acids, uronic acids, biotechnology, nickel-pincer nucleotide

INTRODUCTION

Hydroxy acids (HAs) are organic carboxylic acids ubiquitous in living organisms and serve as essential biological building blocks in industry [1]. The two main categories of HAs most prevalent in nature and in industry are α-hydroxy acids (AHAs), with one hydroxyl group on the second carbon, and polyhydroxy acids (PHAs), with multiple hydroxyl groups [235]. AHAs can be further subdivided into three main categories according to their chemical structure: (i) aliphatic AHAs, with straight or branched non-aromatic side chain; (ii) aromatic AHAs, with an aromatic ring-bearing side chain; (iii) polycarboxylic AHAs, with more than one carboxyl group [1,235]. Among PHAs, sugar acids are derived from saccharides through oxidation. The oxidation can occur at different positions on the sugar molecule, leading to 3 main categories of sugar acids with distinct properties and functions: (i) Aldonic acids, formed by oxidizing the aldehyde group of an aldose to a carboxylic acid; (ii) Uronic acids, formed by oxidizing the terminal hydroxyl group of an aldose or ketose to a carboxylic acid; (iii) Aldaric acids, formed by oxidizing both the aldehyde and the terminal hydroxyl groups of an aldose, generating a dicarboxylic acid [3,4].

In addition to being key metabolites of most metabolic pathways, the stereochemical diversity and variety of chemical structures that AHAs and PHAs offer opens a wide spectrum of potential biotechnological applications and therefore have considerable market potential [1,59]. (i) In cosmetics and skincare, these compounds are valued for their cleansing, conditioning, humectant and moisturing properties [36,37,235]. (ii) In medicine, they can serve as drug precursors for synthesizing various significant chiral compounds, including antimicrobial agents [39,44,45] antibiotics [40,41], and angiotensin-converting inhibitors [42,43]. (iii) In the food industry, they can function as food components and additives, e.g. as pH regulator, preservative, and flavoring agent [46–49]. (iv) In organic synthesis, they can serve as versatile platform chemicals to generate primary building blocks of industrially relevant products [50,164]. (v) In polymer synthesis, they can act as monomers for producing diverse biopolymers [51–53]. The significant growth in both quantity and variety of AHAs has driven the global market size to exceed USD$ 1.2 billion in 2021, projected to reach USD$ 2.3 billion by 2028 [54]. Similarly, the market for D-gluconic acid, a PHA among the most desirable biologically produced platform chemicals [236], is expected to grow from USD$ 0.18 billion in 2023 to USD$ 0.24 billion by 2032 [55].

Consequently, research focusing on the production of AHAs and PHAs has gained considerable attention from researchers [56–59]. However, few enzymatic production routes exist for AHAs and PHAs stereoisomers, especially for sugar acids, due to the high complexity of stereoselective synthesis [1,59].

A recently discovered superfamily of nickel-dependent hydroxy acid racemases and epimerases, the LarA superfamily, was shown to be able to racemize or C2-epimerize a wide range of AHAs and PHAs stereoisomers, with some LarAHs able to isomerize up to 16 different substrates [147,153]. The first identified enzyme of this superfamily was the lactate racemase of *Lactobacillus plantarum* (LarA1) [95], which was shown to use the (Nickel-Pincer Nucleotide) NPN cofactor through a proton-coupled hydride-transfer (PCHT) mechanism during which the NPN transiently accepts the substrate-derived hydride (Figure 1) [95,96,124,147,237]. The NPN cofactor, a substituted pyridinium mononucleotide that tricoordinates nickel, is sequentially synthesized by the LarB, LarE, and LarC biosynthetic enzymes from the precursor nicotinic acid adenine dinucleotide through consecutive carboxylation/hydrolysis, sulfur insertion, and nickel insertion reactions, respectively [120,131,132,215]. Interestingly, the genes encoding for the NPN-biosynthetic enzymes and LarA homologs (LarAHs) are widespread within eubacteria and archaea, and some are even found in unicellular eukaryotes [95,237]. Currently, the different families identified in the LarA superfamily are the lactate racemase (LAR) family, the short-chain aliphatic AHA racemases (SAR) family, the malate racemase (MAR) family, the hydroxyglutarate racemase (HGR) family, the hydrophobic AHA racemases (HHR) family, and the D-gluconate 2-epimerase (GntE) family. All these racemases and epimerases use the NPN cofactor for their activity, similarly to LarA1 [210] . However, half of the LarA superfamily remains unexplored and much remains to be discovered about the full range of reactions catalyzed by LarAHs.

In this study, we fill a significant part of this gap by identifying a previously unexplored large new family of broad-spectrum hydroxy acid isomerases (BSHIs) in the LarA superfamily. These LarAHs are able to isomerize up to 39 different AHAs and PHAs, of which many are sugar acids. These findings demonstrate the potential of the LarA superfamily for biotechnological and pharmaceutical applications in the conversion of HAs, especially for sugar acids.

RESULTS

Discovery of a family of broad-spectrum hydroxy acid isomerases (BSHIs)

To gain further insight into this novel family of LarAHs we selected four *larAH* genes from two distinct bacteria: *larAH26* from *Priesta megaterium* and *larAH41*, *larAH44* and *larAH49* from *Enterocloster asparagiformis*. Subsequently, we engineered vectors to generate the respective C-terminal Strep-Tag fusion proteins for overexpression and purification in *Escherichia coli* cells. After purification, the four LarAHs were obtained in soluble form and their identity was confirmed by electrospray ionization quadrupole time-of-flight mass spectrometry (ESI-Q-TOF-MS) analysis (Figure 3.S1, Tables 3.S1 & 3.S2). The purified LarAHs were then supplemented with *in vitro* synthesized NPN and subjected to activity assays in the presence of all substrates showed in Fig. 3.1 & 3.2. These assays were conducted through either coupling to another enzymatic reaction for spectrophotometric measurement or via chiral capillary electrophoresis (CE) [218].

In this family of LarAHs, we identified 9 racemization reactions on aliphatic AHAs, 4 racemization reactions on aromatic AHAs, and 2 racemization reactions on polycarboxy AHAs. Among aliphatic AHAs, we identified racemization reactions on DL-lactate, DL-glycerate, DL-2-hydroxybutyrate, DL-2,4-dihydroxybutyrate, DL-2-hydroxycaproate, DL-2-hydroxyisocaproate, DL-2-hydroxyvalerate, DL-2-hydroxyisovalerate, DL-2,3-dihydroxyisovalerate, DL-2-hydroxy-3,3-dimethylbutyrate. Among aromatic AHAs, we identified reactions on DL-3-phenyllactate, DL-3-(4-hydroxyphenyl)lactate, DL-2-hydroxy-4-phenylbutyrate and DL-2-hydroxy-4-oxo-4-phenylbutyrate. Among polycarboxy AHAs we identified reactions on malate and 2-hydroxyglutarate. Strikingly, most LarAHs investigated could catalyze the majority of these racemization reactions (Fig. 3.1, Fig 3.3 & Table 3.2).

Since these LarAHs have a catalytic pocket capable of accommodating and catalyzing the racemization of a wide array of AHAs, we explored whether they could catalyze C2-epimerization of stereoisomers of sugar acids, too. We detected novel C-2 epimerization reactions of stereoisomers in the three main classes of sugar acids: aldonic acids, uronic acids and aldaric acids.

Among aldonic acids, we detected novel C2-epimerization reactions of 2,3-dihydroxybutanoic acids, 2,3-trihydroxybutanoic acids, 2,3,4,5-tetrahydroxypentanoic acids, 2,3,4,6-tetrahydroxyhexanoic acids and 2,3,4,5,6-pentahydroxyhexanoic acids. We detected C2-epimerization reactions between the following C2-epimers: (i) For 2,3-dihydroxybutanoic acids: 4-deoxy-D-threonate and 4-deoxy-D-erythronate, 4-deoxy-L-threonate and 4-deoxy-L-erythronate; (ii) For 2,3,4-trihydroxybutanoic acids: D-threonate and D-erythronate, D-threonate and D-erythronate; (iii) For 2,3,4,5-tetrahydroxypentanoic acids: D-ribonate and D-arabinonate, L-ribonate and L-arabinonate, D-xylonate and D-lyxonate, L-xylonate and L-lyxonate; (iv) For 2,3,4,5-tetrahydroxyhexanoic acids: 6-deoxy-L-gluconate and 6-deoxy-L-mannonate, 6-deoxy-D-galactonate and 6-deoxy-D-talonate, 6-deoxy-L-galactonate and 6-deoxy-L-talonate; (v) For 2,3,4,5,6-pentahydroxyhexanoic acids: D-gluconate and D-mannonate, L-gluconate and L-mannonate, D-galactonate and D-talonate, L-galactonate and L-talonate, D-altronate and D-allonate, L-altronate and L-allonate, D-gulonate and D-idonate, L-gulonate and L-idonate. Among uronic acids, we detected novel C2-epimerization reactions of 2,3,4,5-tetrahydroxy-6-oxohexanoic acid stereoisomers such as the interconversion between D-glucuronate and L-iduronate as well as D-galacturonate and L-alturonate. Among aldaric acids, we detected novel C-2 epimerization reactions of 2,3-dihydroxybutanedioic acid stereoisomers such as the interconversion between L-tartrate and meso-tartrate (Fig. 3.2, Fig 3.3 & Table 3.2).

These LarAHs thus constitute a family of broad-spectrum hydroxy acid isomerases (BSHIs) capable of catalyzing racemization reactions spanning the three primary classes of AHAs and C2-epimerization reactions spanning the three primary classes of sugar acids.

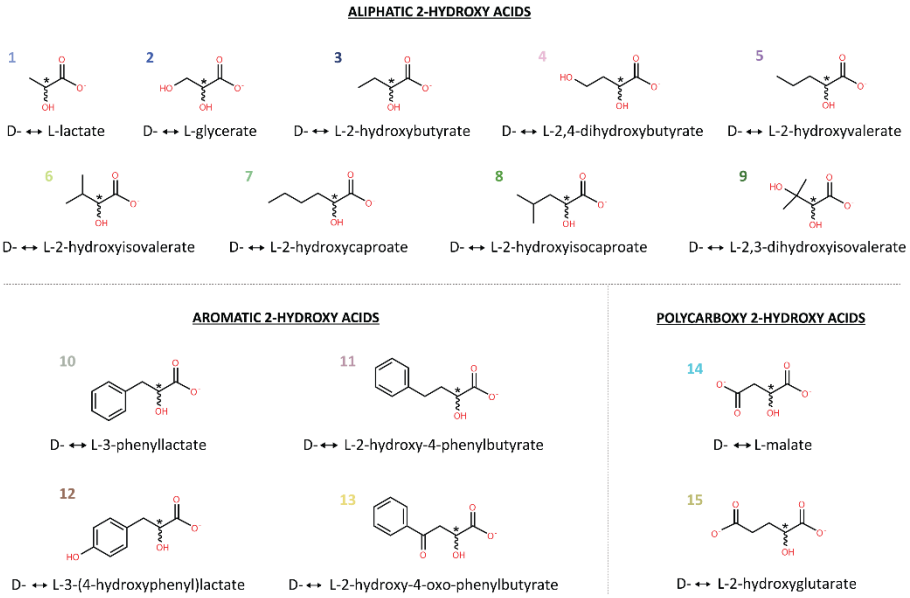

Figure 3.1 | Chemical structure of 2-hydroxy acids and polyhydroxy acids racemized by BSHIs. Each racemization reaction is labeled with a number and a color. The chiral carbons are depicted achiral for simplification. Black asterisks indicate stereoinversion sites, grey asterisks indicate other stereocenters in the molecule.

Table 3.1 | Kinetic parameters of the investigated BSHIs.

	Substrate	pH opt[a]	Temp opt[a] (°C)	K_M (mM)[b]	k_{cat} (s^{-1})[b]	k_{cat}/K_M (M^{-1} s^{-1})
LarAH26	D-mannonate	7-8	25-35	1.9 ± 0.2	37 ± 4	19 ± 4
LarAH41	D-mannonate	7	40	7.6 ± 1.6	1.1 ± 0.2	0.15 ± 0.03
LarAH44	L-lactate	8.5	35	2.2 ± 0.3	0.61 ± 0.05	0.27 ± 0.6
LarAH49	L-2-hydroxycaproate	7-7.5	30-35	3.2 ± 0.5	5.6 ± 0.7	1.8 ± 0.4

[a] : optimal pH range or temperature (temp), where activity was > 90% of the maximum activity.
[b] : ± 95% confidence interval based on non-linear regression using the Michaelis–Menten equation.

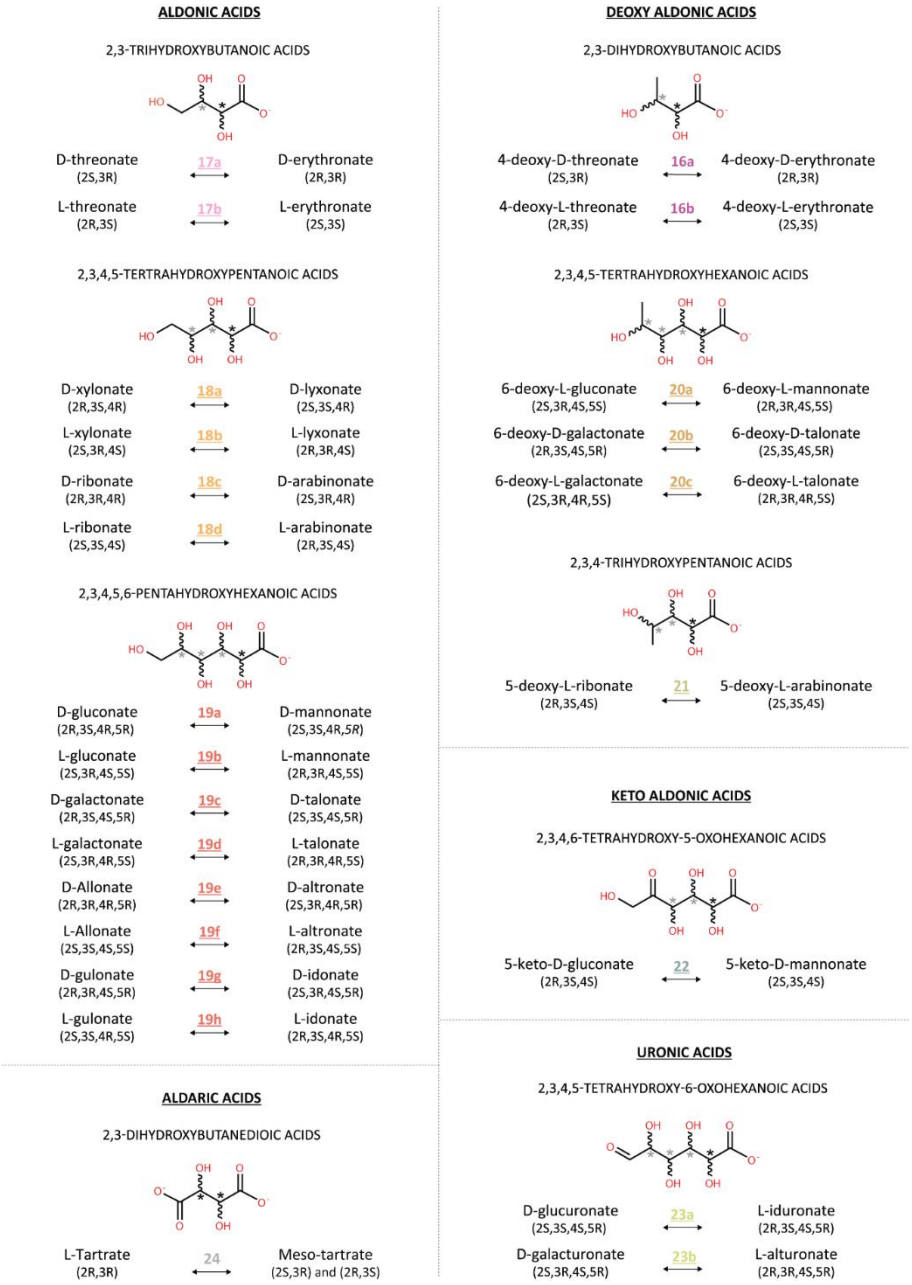

Figure 3.2 | Chemical structure and stereochemistry of the sugar acids C2-epimerized by BSHIs. Each C2-epimerization reaction is labelled with a number and a colour. The different C2-epimerization reactions of the same PHA are labeled with the same color and number, but a letter has been added to each number to differentiate the reactions. Labels of previously unreported reactions are underlined. The chiral carbons are depicted achiral for simplification. Black asterisks indicate stereoinversion sites, grey asterisks indicate other stereocenters in the molecule.

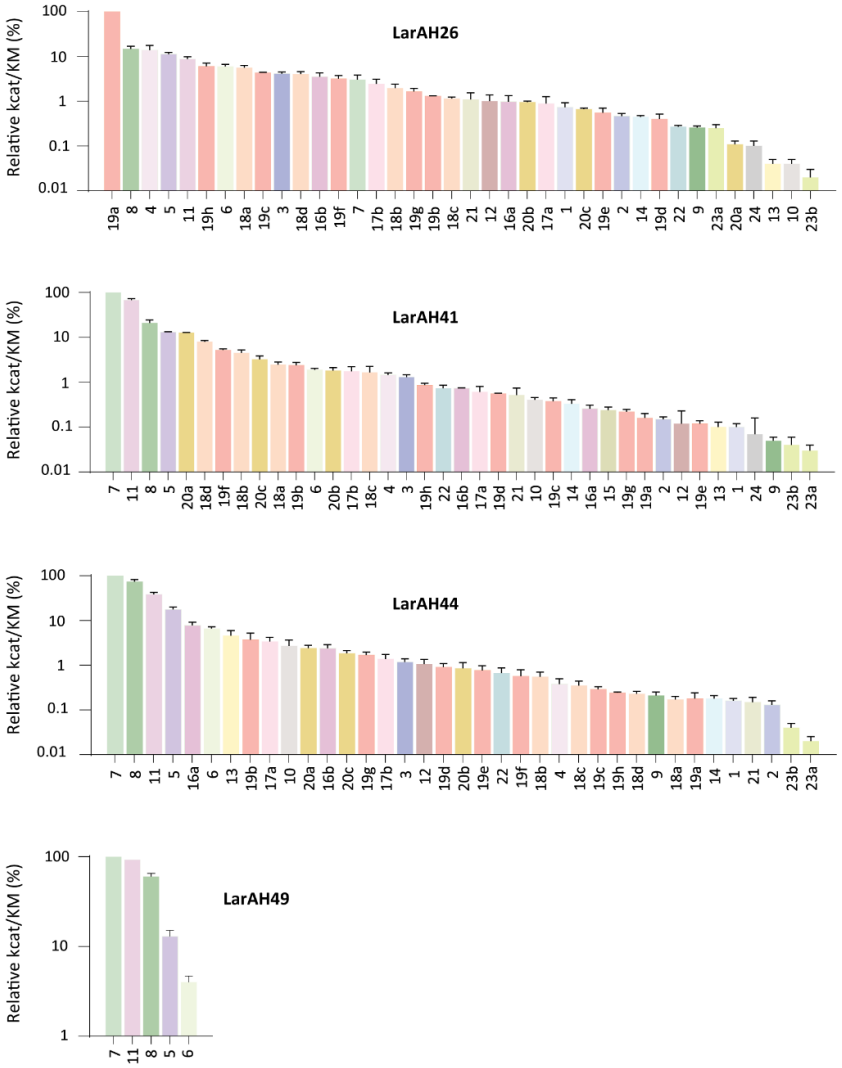

Figure 3.3 | **Relative catalytic efficiencies of the investigated BSHIs.** The catalytic efficiency for the preferred substrate was set to 100%. The color and label assigned to each reaction correspond to those used in Figs. 3.1 and 3.2. C2-epimerization reactions of the stereoisomers of the same PHA are indicated in the same color. The error bars represent the standard error (n=3).

Table 3.2 | **Catalytic efficiencies of the investigated BSHIs.** For each BSHI, the k_{cat}/K_M value of the substrate for which the kinetic parameters were obtained experimentally is in bold (Figure 3.S4 & Table 3.1). Additional k_{cat}/K_M values were calculated using the experimentally determined k_{cat}/K_M and the relative k_{cat}/K_M values. "-": no activity. Labels of previously unreported reactions are underlined.

	Reactions	k_{cat}/K_M (M^{-1} s^{-1})			
	Racemization of AHAs	LarAH26	LarAH41	LarAH44	LarAH49
1	L- ↔ D-lactate	(14 ± 4) x 10^1	93 ± 35	**(27 ± 5) x 10^1**	-
2	L- ↔ D-glycerate	90 ± 20	(13 ± 5) x 10^1	(21 ± 7) x 10^1	-
3	L- ↔ D-2-hydroxybutyrate	(80 ± 16) x 10^1	(12 ± 4) x 10^2	(19 ± 6) x 10^2	-
4	L- ↔ D-2,4-dihydroxybutyrate	(27 ± 9) x 10^2	(13 ± 5) x 10^2	(63 ± 23) x 10^1	-
5	L- ↔ D-2-hydroxyvalérate	(22 ± 4) x 10^2	(12 ± 4) x 10^3	(29 ± 7) x 10^3	(23 ± 7) x 10^1
6	L- ↔ D-2-hydroxyisovalérate	(12 ± 3) x 10^2	(17 ± 6) x 10^2	(11 ± 3) x 10^3	70 ± 22
7	L- ↔ D-2-hydroxycaproate	(59 ± 18) x 10^1	(90 ± 29) x 10^3	(16 ± 4) x 10^4	**(18 ± 4) x 10^2**
8	L- ↔ D-2-hydroxyisocaproate	(29 ± 6) x 10^2	(19 ± 7) x 10^3	(12 ± 3) x 10^4	(10 ± 3) x 10^2
9	L- ↔ D-2,3-dihydroxyisovalérate	50 ± 10	46 ± 17	(34 ± 10) x 10^1	-
10	L- ↔ D-3-phenyllactate	8 ± 2	(37 ± 13) x 10^1	(47 ± 16) x 10^2	-
11	L- ↔ D-2-hydroxy-4-phenylbutyrate	(17 ± 4) x 10^2	(61 ± 20) x 10^3	(63 ± 16) x 10^3	(16 ± 5) x 10^2
12	L- ↔ D-3-(4-hydroxyphenyl)lactate	(20 ± 8) x 10^1	(11 ± 6) x 10^1	(18 ± 6) x 10^2	-
13	L- ↔ D-2-hydroxy-4-oxo-4-phenylbutyrate	9 ± 3	93 ± 41	(76 ± 28) x 10^2	-
14	L- ↔ D-malate	87 ± 16	(30 ± 12) x 10^1	(28 ± 8) x 10^1	-
15	L- ↔ D-2-hydroxyglutarate	-	(22 ± 8) x 10^1	-	-
					-
	C2-epimerization of sugar acids				
16a	4-deoxy-D-threonate ↔ 4-deoxy-D-erythronate	(19 ± 8) x 10^1	(24 ± 9) x 10^1	(13 ± 4) x 10^3	-
16b	4-deoxy-L-threonate ↔ 4-deoxy-L-erythronate	(68 ± 20) x 10^1	(67 ± 22) x 10^1	(39 ± 11) x 10^2	-
17a	D-threonate ↔ D-erythronate	(17 ± 8) x 10^1	(56 ± 25) x 10^1	(56 ± 17) x 10^2	-
17b	L-threonate ↔ L-erythronate	(47 ± 15) x 10^1	(17 ± 7) x 10^2	(23 ± 7) x 10^2	-
18a	D-xylonate ↔ D-lyxonate	(11 ± 2) x 10^2	(22 ± 8) x 10^2	(29 ± 8) x 10^1	-
18b	L-xylonate ↔ L-lyxonate	(22 ± 6) x 10^1	(41 ± 15) x 10^2	(91 ± 31) x 10^1	-
18c	D-ribonate ↔ D-arabinonate	(38 ± 7) x 10^1	(15 ± 6) x 10^2	(59 ± 19) x 10^1	-
18d	L-ribonate ↔ L-arabinonate	(79 ± 17) x 10^1	(72 ± 24) x 10^2	(38 ± 10) x 10^1	-
19a	D-gluconate ↔ D-mannonate	**(19 ± 4) x 10^3**	**(15 ± 3) x 10^1**	(29 ± 11) x 10^1	-
19b	L-gluconate ↔ L-mannonate	78 ± 26	(21 ± 8) x 10^2	(61 ± 22) x 10^2	-
19c	D-galactonate ↔ D-talonate	(85 ± 14) x 10^1	(35 ± 13) x 10^1	(47 ± 12) x 10^1	-
19d	L-galactonate ↔ L-talonate	(25 ± 4) x 10^1	(51 ± 17) x 10^1	(15 ± 4) x 10^2	-
19e	D-allonate ↔ D-altronate	(32 ± 8) x 10^1	(11 ± 4) x 10^1	(13 ± 4) x 10^2	-
19f	L-allonate ↔ L-altronate	(62 ± 15) x 10^1	(47 ± 16) x 10^2	(94 ± 41) x 10^1	-
19g	D-idonate ↔ D-gulonate	(11 ± 3) x 10^1	(21 ± 7) x 10^1	(28 ± 8) x 10^2	-
19h	L-idonate ↔ L-gulonate	(12 ± 3) x 10^2	(78 ± 27) x 10^1	(40 ± 9) x 10^1	-
20a	6-deoxy-L-gluconate ↔ 6-deoxy-L-mannonate	21 ± 5	(11 ± 4) x 10^3	(40 ± 11) x 10^2	-
20b	6-deoxy-D-galactonate ↔ 6-deoxy-D-talonate	(19 ± 3) x 10^1	(17 ± 6) x 10^2	(14 ± 5) x 10^2	-
20c	6-deoxy-L-galactonate ↔ 6-deoxy-L-talonate	(13 ± 2) x 10^1	(30 ± 11) x 10^2	(30 ± 8) x 10^2	-
21	5-deoxy-L-ribonate ↔ 5-deoxy-L-arabinonate	(22 ± 8) x 10^1	(47 ± 22) x 10^1	(25 ± 8) x 10^1	-
22	5-keto-D-gluconate ↔ 5-keto-D-mannonate	52 ± 10	(67 ± 25) x 10^1	(11 ± 4) x 10^2	-
23a	D-galacturonate ↔ L-alturonate	4 ± 2	34 ± 18	61 ± 27	-
23b	L-iduronate ↔ D-glucuronate	48 ± 13	22 ± 9	40 ± 12	-
24	L- ↔ Meso-tartrate	20 ± 6	60 ± 27	-	-

Biochemical and substrate specificities of BSHIs

For a comprehensive biochemical characterization of each BSHI, we experimentally determined their temperature and pH-dependent activity profiles (Table 3.1 & Figs. 3.S2, 3.S3). LarAH26 shows an optimal pH range between pH 7 and pH 8, and an optimal temperature around 35°C. Notably, LarAH26 exhibit a relative activity above 85% between 20°C and 45°C, which correlates with the fact that *P. megaterium* is mesophilic and found in various environments, ranging from soil to plant roots. The optimal temperature of LarAH41, LarAH44 and LarAH49 is around 35°C, which correlates with the fact that *E. asparagiformis* comes from the human gut microbiota.

Further investigations aimed to identify the preferred substrates of the BSHIs. Elucidating the substrate specificities of these enzymes is crucial for future potential biotechnological applications. To achieve this, we determined the relative catalytic efficiencies of LarAH26, LarAH41, LarAH44 and LarAH49 for each of their substrates (Fig. 3.3). LarAH26 from *P. megaterium* exhibited the highest relative catalytic efficiency for D-gluconate whereas LarAH41, LarAH44 and LarAH49 from *E. asparagiformis* showed the highest relative catalytic efficiency for 2-hydroxycaproate (Fig. 3.2 & Table 3.2). Then, the k_{cat}/K_M values of each BSHI for all substrates were calculated (Table 3.2) using the kinetic parameters (k_{cat}, K_M and k_{cat}/K_M) experimentally determined for one substrate (Table 3.1 & Fig. 3.S4) and the relative catalytic efficiencies for all substrates (Fig. 3.3). We initially intended to experimentally determine the kinetic parameters of investigated BSHIs for their substrate with the highest relative catalytic efficiency. However, we were unable to experimentally determine the kinetic parameters of LarAH41 and LarAH44 for 2-hydroxycaproate due to their K_M values appearing to be in the µM range, which could not be precisely measured due to the limit of detection of the capillary electrophoresis (CE) method used [218]. Instead, we determined the kinetic parameters of LarAH41 for the conversion of D-mannonate to D-gluconate and LarAH44 for the conversion of L-lactate to D-lactate, using enzyme kits and spectrophotometry for precise measurements (Table 3.1 & Fig. 3.S4). Kinetic parameters of the NPN-supplemented LarAHs were determined by assuming 100% loading, given that an excess of NPN was added to the apoprotein; however, the extent of NPN loading could not be established. As a result, the values of k_{cat} and k_{cat}/K_M are probably underestimated.

BSHIs exhibit low activities on uronic acids. Uronic acids, like their aldose precursors, predominantly exist as cyclic hemiacetals (furanose or pyranose) and less than 1% of the molecules exist in the linear form ((carboxo-)aldohexose). Since the linear form is most probably the form used by BSHIs, as no proton abstraction of the hydroxyl is possible with the cyclic form, this could explain the very low k_{cat}/K_M observed, which is due to the very low availability of the linear form. BSHIs also show low catalytic efficiencies on substrates with 2 carboxylates such as polycarboxy AHAs (malate and 2-hydroxyglutarate) and aldaric acids (tartrate). Given that their preferred substrates seem to be hydrophobic AHA, this is not unexpected.

Stereoselective specificities of BSHIs

We elucidated the stereoselective preferences of LarAH26, LarAH41 and LarAH44 for C2-epimerization reactions across diverse PHAs for which we possessed all the stereoisomers, specifically 2,3-dihydroxybutanoic acids, 2,3,4-trihydroxybutanoic acids, 2,3,4,5-tetrahydroxypentanoic acids, and 2,3,4,5,6-pentahydroxyhexanoic acids (Figs. 3.4 & 3.S5). For each type of PHA, the focus was on comparing the k_{cat}/K_M values of all the possible C2-epimerization reactions to understand the stereoselective preferences of BSHIs for specific chiral configurations.

In the C2-epimerization of PHAs, LarAH26, LarAH41, and LarAH44 display distinct stereochemical preferences and hierarchical importance for different carbon positions affecting their catalytic efficiencies. LarAH26 prefers S configuration at C3, R configuration at C4, and R configuration at C5, with the importance order being C3 > C4 > C5. LarAH41 prefers S configuration at C3, C4, and C5, with the importance order being C5 > C4 > C3. LarAH44 prefers R configuration at C3 and S configuration at C4 and C5, with the importance order being C3 > C4 > C5 (Figs. 3.4 & 3.S5). These detailed findings demonstrate specific stereochemical requirements for optimal catalytic function for each BSHI investigated. Understanding these preferences is critical for potential strategic designs of chemoenzymatic synthesis processes.

		LarAH26	LarAH41	LarAH44
	2,3-DIHYDROXYBUTANOIC ACIDS	3S > 3R	3S > 3R	3R > 3S
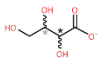	2,3-TRIHYDROXYBUTANOIC ACIDS	3S > 3R	3S > 3R	3R > 3S
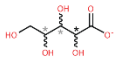	2,3,4,5-TERTRAHYDROXYPENTANOIC ACICS	3S > 3R 4R > 4S C3 > C4	3S > 3R 4S > 4R C4 > C3	3R > 3S 4S > 4R C3 > C4
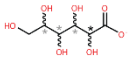	2,3,4,5,6-PENTAHYDROXYHEXANOIC ACIDS	3S > 3R 4R > 4S 5R > 5S C3 > C4 > C5	3S > 3R 4S > 4R 5S > 5R C5 > C4 > C3	3R > 3S 4S > 4R 5S > 5R C3 > C4 > C5
	Global stereochemical preference	**C3 (S) > C4 (R) > C5 (R)**	**C5 (S) > C4 (S) > C3 (S)**	**C3 (R) > C4 (S) > C5 (S)**

Figure 3.4 | Stereochemical preferences for poly-hydroxy acid C2-epimerization reactions of the investigated BSHIs. Summary of data from figures 3.3 and 3.S5. “>” shows the hierarchy of importance of the carbons and stereochemistry of the chiral centers of a PHA with regard to the catalytic efficiency of the enzyme.

Structural analysis of BSHIs

The structural models of the investigated BSHIs were retrieved from the AlphaFold 2 database [220,221]. The structural models were then aligned with the LarA1 structure using Pymol in order to deduce the position of the NPN cofactor. To compare the fold of BSHIs with the LarA1 fold, we first compared the structural model of LarAH41 with LarA1 structure (Figure 3.5). This comparison shows that the fold of the C-terminal domain of BSHIs is completely different from the fold of the C-terminal domain of LarA1. The C-terminal domain of LarA1 is composed of a central β-sheet composed of 6 parallel β-strands with two β-strands and one α-helix above, and two β-strands and five α-helices under this β-sheet. The C-terminal domain of LarAH41, on the other hand, is composed of a central β-sheet composed of 8 β-strands (6 parallel and 2 antiparallel) with three α-helices above and three α-helices under this β-sheet (Figure 3.5). The substrate binding pocket, which lies at the interface between both N-terminal and C-terminal domains, is mostly defined by the α-helices α11 and α14 in LarA1, whereas these two α-helices are absent from the substrate binding pocket of LarAH41 structural model. The substrate binding pocket of the LarAH41 structural model is defined by two long loops and by the α-helix α13, which is much closer to the N-terminal domain than in LarA1 structure (Figure 3.5 & 3.6).

A closer look of the catalytic sites of BSHIs shows that the residues involved in NPN binding and catalysis, which are part of their N-terminal domain, are conserved (Fig. 3.6, residues in blue and green) whereas the residues involved in substrate recognition are not (Fig. 3.6, residues in white). The catalytic site of BSHIs is much larger than the LarA1 catalytic site, and most of the residues are located on loops, rather than on α-helices (Fig. 3.6), which gives them more flexibility, probably allowing the binding pocket to adapt to many different substrates. The comparison between the different BSHIs shows that many residues are conserved between the different enzymes, e.g. the residues corresponding to T159, F191, K269, and N336 in LarAH26. Other residues vary from one BSHI to the other, explaining the small differences in substrate specificity observed (Fig. 3.3). The catalytic site of LarAH49 was not shown, as the residues forming the catalytic site are exactly the same as the residues of LarAH41.

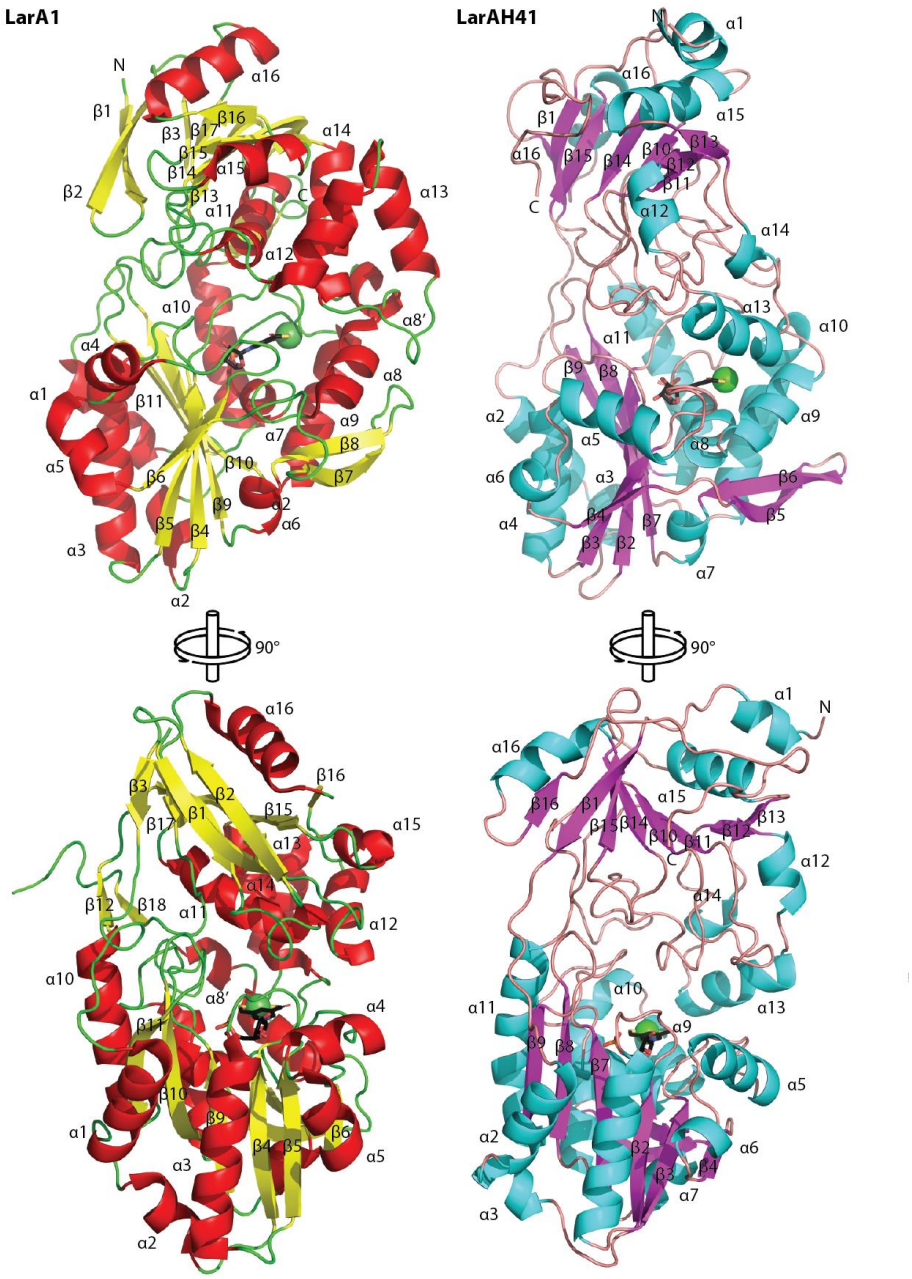

Figure 3.5 | **Structural comparison between LarA1 and LarAH41.** The LarA1 structure (PDB code: 5HUQ) is coloured with its loops in green, α-helices in red and β-sheets in yellow. The LarAH41 structural model retrieved from the Alphafold 2 database is coloured with its loops in pink, α-helices in cyan and β-sheets in magenta. The NPN is indicated in stick model with the nickel as a green ball.

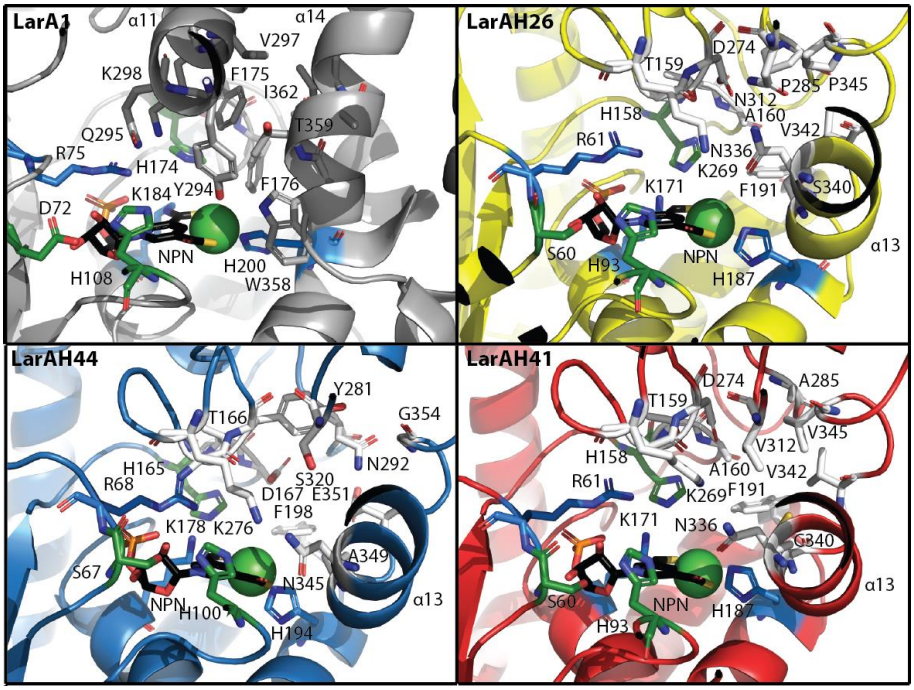

Figure 3.6 | Catalytic site comparison between LarA1, LarAH26, LarAH41, and LarAH44. The LarA1 structure was retrieved form the PDB database (PDB code: 5HUQ), and the LarAH26, LarAH41, and LarAH44 structure was retrieved from the Alphafold 2 database. The catalytic residues are shown with their carbons in green, the residues important for NPN binding are shown with their carbon in blue, other residues probably important for substrate specificity are shown with their carbons in white. NPN carbons are in black. Oxygen atoms are in red, nitrogen atoms are in blue, sulphur atoms are in yellow, phosphate atoms are in orange, and nickel ion is shown as a green ball.

DISCUSSION

AHAs and PHAs are ubiquitous in the living world and find extensive applications across various industries due to their stereochemical diversity and their variety of chemical structures. However, few enzymatic production routes exist for AHAs and PHAs stereoisomers, especially for sugar acids, due to the high complexity of stereoselective synthesis [1,59].

In this study, we discovered a novel family of LarAHs in the LarA superfamily, the BSHI family. Our findings demonstrated the ability of BSHIs to catalyze 15 distinct AHA racemization reactions and 24 distinct PHA (sugar acid) C2-epimerization reactions, 20 of which were previously unreported (Table 3.2). For aldonic acids, we observed C2-epimerization reactions of all stereoisomers of D-gluconate, D-xylonate, D-threonate and 4-deoxy-D-threonate. Additionally, we showed C2-epimerization reactions of aldonic acid derivatives such as keto and deoxy aldonic acids. For uronic acids, we showed C2-epimerization reactions of D-glucuronate/L-iduronate and D-galacturonate/L-alturonate. For aldaric acids, we showed C2-epimerization reactions of L-tartrate/Meso-tartrate. To date, no other enzymatic routes exist for synthesizing most of these acid sugar stereoisomers. Moreover, the structural model of these BSHIs suggests that their substrate binding site is particularly adapted for bulky substrates and shows considerable flexibility, allowing for such a broad substrate scope.

Overall, BSHIs exhibit high potential as biotechnological tools for the stereoselective conversion of a wide range of AHA and PHA stereoisomers. To fully realize this potential, three key aspects should be considered: (1) scaling up the production of HAs, (2) overcoming the average 50% yield limit of isomerases, and (3) enhancing the low k_{cat} values observed in some reactions. To address aspect (1), *Lactococcus lactis* could serve as a valuable microbial platform to scale up reaction volumes and increase the production of the desired stereoisomer. Indeed, the *in vivo* coexpression of *larAHs* and NPN biosynthetic genes (*larBCE)* allows for the production of active LarAH holoenzymes in *L. lactis* cultures, avoiding the need for *in vitro* NPN biosynthesis [141,210]. For instance, scaling up the conversion of D-glucuronate into L-iduronate and D-galacturonate into L-alturonate could be feasible. D-glucuronate and D-galacturonate are inexpensive and common compounds, whereas L-iduronate is a highly expensive compound used in the

production of heparinoid anticoagulants [238], and L-alturonate is not yet commercially available. To address aspect (2), coupling the reactions catalyzed by BSHIs with deracemization methods such as dynamic kinetic resolution (DKR) or multistep chiral separation with isomerizaton could potentially achieve theoretical yields of 100% of the desired stereoisomers [239–243]. Using BSHIs upstream and during these deracemization methods could theoretically convert a stereopure solution of the unwanted stereoisomer into a stereopure solution of the desired stereoisomer. To address aspect (3), one approach is directed evolution to increase the k_{cat} of BSHIs for specific reactions of interest [244]. Alternatively, purifying other LarAHs from the BSHI family may yield enzymes with higher k_{cat} values for the targeted reactions.

An important remaining question is the potential *in vivo* roles of the investigated BSHIs. The genomic context of genes encoding BSHIs may be indicative of their functions (Table 3.S3). LarAH26 likely acts as a D-gluconate/D-mannonate C2-epimerase in *P. megaterium*, as it shows a strong preference for the C2-epimerization of D-gluconate and D-mannonate over other reactions. This hypothesis is supported by the adjacent gene encoding a gluconate 5-dehydrogenase in the *P. megaterium* genome (Table 3.S3). Additionally, *P. megaterium* can utilize D-gluconic acid as a carbon source [245]. LarAH26 may enable D-mannonate to also serve as a carbon source by converting it into D-gluconate, allowing it to enter the gluconate pathway and the pentose phosphate pathway, thereby participating in carbohydrate metabolism in *P. megaterium* [246].

LarAH41, LarAH44 and LarAH49 from *E. asparagiformis* exhibited the highest relative catalytic efficiency for four substrates: 2-hydroxyvalerate, 2-hydroxycaproate, 2-hydroxyisocaproate, and 2-hydroxy-4-phenylbutyrate, with 2-hydroxycaproate being the preferred substrate for each enzyme (Fig. 3.2 & Table 3.2). LarAH49 appears to have the same substrate specificity as LarAH41, which is expected given their 57% identity and identical catalytic site residues. However, given the broad spectrum of reactions catalyzed by LarAH41, LarAH44, and LarAH49, it is possible that the native substrate has not been identified because it was not tested. For instance, the genetic context of LarAH41 and LarAH44 suggests that these enzymes play a role as C2-epimerases of sugar acids, rather than for the racemization of hydrophobic AHAs. The genomic neighborhood of *larAH41* and *larAH49*

includes several genes annotated as sugar transporters. Additionally, *larAH41* is in the same operon as several sugar epimerases. More importantly, *larAH41* and *larAH49* are near a 2-deoxy-D-gluconate 3-dehydrogenase and other genes annotated as related to 2-dehydro-3-deoxy-phosphogluconate metabolism and the Entner-Doudoroff pathway (Table 3.S3). This suggests that substrates such as 3-deoxy-D-mannonate could be C2-epimerized into 3-deoxy-D-gluconate by LarAH41 or LarAH49, for example. It is also possible that these enzymes isomerize multiple substrates and play multiple roles *in vivo*. *In vivo* deletion experiments will be necessary to evaluate these hypotheses.

CONCLUSION

The findings of this study reveal the remarkable potential of broad-spectrum hydroxy acid isomerases (BSHIs) within the LarA superfamily for the biotechnological conversion of stereoisomers of 2-hydroxy acids (AHAs) and polyhydroxy acids (PHAs). By investigating the biochemical properties, substrate specificities, and stereoselective preferences of four novel LarAHs, we identified extensive racemization and C2-epimerization capabilities spanning various AHAs and PHAs. Specifically, these enzymes demonstrated the ability to catalyze 15 racemization reactions across aliphatic, aromatic, and polycarboxylic AHAs, as well as 24 C2-epimerization reactions across aldonic, uronic, and aldaric acids, with 17 of these reactions being previously unreported. Structural analyses indicated that the broad substrate spectrum of these BSHIs is attributable to a unique C-terminal domain structure distinct from LarA1, providing flexibility in substrate binding and catalysis.

The ability of these BSHIs to catalyze a wide array of reactions, including previously unreported C2-epimerization of sugar acids, opens new avenues for the production of valuable HA stereoisomers. This can significantly impact various industries, including cosmetics, medicine, food, organic synthesis, and polymer production, by providing novel enzymatic routes for the conversion of important chiral compounds. Future research focusing on the characterization and optimization of novel BSHIs could further enhance their applicability, paving the way for innovative biotechnological processes.

MATERIAL & METHODS

Biological materials and growth conditions

Bacterial strains and plasmids used in the present study are listed in Table S3. All plasmid constructions were performed in *E. coli* DH10B. *E. coli* DH10B cells were grown with agitation at 37 °C in lysogeny broth supplemented with ampicillin (200 mg·L−1) or erythromycin (200 mg·L−1), when required. When expressing pBADHisA derivatives, induction was initiated by addition of L-arabinose (0.1%) and cells were grown at 30 °C for 4 h with agitation.

DNA techniques

DNA was introduced into *E. coli* cells by electrotransformation [224]. PCR amplifications used Q5 high-fidelity DNA polymerase (New England Biolabs). The primers used in this study were purchased from Eurogentec (Seraing, Belgium) and are listed in Table S4. Synthetic gene for LarAH26 sequence was purchased from Biomatik, digested with NcoI and NheI, and cloned into a similarly digested pGIR076 [16]. Genes encoding LarAH41 and LarAH44 and LarAH49 were amplified from the genomic DNA of *E. asparagiformis*, digested (PciI and NheI), and cloned into digested (NcoI and NheI) pGIR076. *E. asparagiformis* (DSM 15981) genome was purchased from DSMZ-German Collection of Microorganisms and Cell Cultures. In all cases, the sequence of the expression cassettes was verified by sequencing. Strains and primers used are listed in Tables S3 & S4, respectively.

Protein purification and in vitro NPN biosynthesis

In vitro biosynthesis of NPN was performed with purified LarB [119], LarE [132,215], and LarC [120] as previously described [141]. *E. coli* cells were induced to express LarAHs when the OD600 reached 0.4 with 0.1% L-arabinose. After 4 h, the culture was cooled to 4 °C and the cells were harvested by centrifugation at 6000×g for 10 min. The pellet was stored at −80 °C until further use. The cell pellet was thawed and resuspended in 20 ml of lysis buffer containing 100 mM Tris (pH 7.5), 300 mM NaCl and 1 mg/ml lysozyme. The cell suspension was incubated at 4°C for 30 min and sonicated 4 times for 1 min with one 1-minute rest on ice between each sonication. The supernatant was separated by centrifuging the lysate at 20000×g for 30 min

at 4°C. Clarified supernatant was loaded onto 2 ml of Strep-Tactin XT Superflow (IBA) resin equilibrated with 10 ml of wash buffer (W) composed of 100 mM Tris (pH 7.5), 300 mM NaCl. After loading, the resin was washed with 20 ml of W followed by elution with 15 ml of W containing 50 mM D-biotin (Sigma-Aldrich). The eluted proteins were ultracentrifuged using Amicon Ultra—15 mL MWCO 10 kDa centrifugal filter units to increase purified protein concentration. The identities of each purified LarAH protein were confirmed by electrospray ionization–time-of-flight mass spectrometry analysis. The protein concentrations were estimated with the Bradford assay [247].

Chemicals and reagents

All chemicals were either of analytical grade or reagent grade. D-lactic acid (sodium salt), L-lactic acid (sodium salt), D-glyceric acid (sodium salt), L-glyceric acid (sodium salt), D-malic acid, L-malic acid, D-2-hydroxybutyric acid, L-2-hydroxybutyric acid, DL-2-hydroxycaproic acid, DL-2-hydroxyisocaproic acid, L-2-hydroxyisocaproic acid, D-2-hydroxyisovaleric acid, L-2-hydroxyisovaleric acid, DL-2-hydroxyoctanoic acid, D-2,3-dihydroxyisovaleric acid (sodium salt), L-2,3-dihydroxyisovaleric acid (sodium salt), D-2-hydroxyglutaric acid (disodium salt), L-2-hydroxyglutaric acid (disodium salt), D-3-phenyllactic acid, L-3-phenyllactic acid, D-2-hydroxy-4-phenylbutyric acid, DL-mandelic acid, D-mandelic acid, D-Threonic acid (lithium salt), L-Threonic acid (hemicalcium salt), D-Erythronic acid (potassium salt), L-Erythronic acid (lithium salt), D-ribonic acid (lithium salt), L-ribonic acid (lithium salt), D-arabinonic acid (sodium salt), D-lyxonic acid (potassium salt), L-lyxonic acid (potassium salt), D-gluconic acid (sodium salt), D-altronic acid (lithium salt), L-gulonic acid (lactone), D-gulonic acid (lithium salt), 6-deoxy-L-galactonic acid (L-fuconic acid sodium salt), 6-deoxy-D-galactonic acid (D-fuconic acid lithium salt), 6-deoxy-L-mannonic acid (L-rhamnonic acid lithium salt), D-Glucuronic acid (sodium salt), D-Galacturonic acid (sodium salt), benzoic acid and L-histidine were purchased from Sigma-Aldrich. L-2-hydroxyvaleric acid, L-2-hydroxycaproic acid, L-2-hydroxy-4-phenylbutyric acid, DL-3-hydroxyoctanoic acid, L-arabinonic acid (lithium salt), D-xylonic acid (lithium salt), L-xylonic acid (lithium salt), L-gluconic acid (lactone), D-galactonic acid (lactone), L-galactonic acid (lactone), D-allonic acid (lactone), L-allonic acid (lactone), D-mannonic acid (lactone), L-mannonic acid (lactone), D-idonic acid (lactone), L-idonic acid (lactone), D-

talonic acid (lactone), 5-Deoxy-L-arabonic acid (lactone), 5-Keto-D-gluconic acid (potassium salt) and L-Iduronic acid (sodium salt) were purchased from Biosynth. L-talonic acid (potassium salt) was purchased from Omicro Biochemicals Inc. DL-2-hydroxyvaleric acid was purchased from Acros Organics. 4-Deoxy-D-erythronic acid (sodium salt hydrate), 4-Deoxy-L-erythronic acid (sodium salt hydrate), 4-Deoxy-D-threonic acid (sodium salt hydrate), 4-Deoxy-L-threonic acid (sodium salt hydrate), DL-3-hydroxybutyric acid, L-3-hydroxybutyric acid were purchased from Supelco. Vancomycin was purchased from Thermo Fisher Scientific.

Enzymatic assays

The following protocols were used for the biochemical characterization of each BSHI, unless otherwise specified. For LarAH26, reactions were performed with 0.1 µM of purified LarAH26, 0.5 µM NPN, 50 mM D-mannonate, and 100 mM Tris-HCl buffer (pH 8) in a final volume of 50 µl for 20 minutes at 30°C. For LarAH41, reactions were performed with 0.5 µM of purified LarAH41, 2.5 µM NPN, 100 mM D-mannonate, and 100 mM potassium phosphate buffer (pH 7) in a final volume of 50 µl for 45 minutes at 30°C. For LarAH44, reactions were performed with 1 µM of purified LarAH44, 5 µM NPN, 20 mM L-lactate, and 100 mM Tris-HCl buffer (pH 8) in a final volume of 50 µl for 45 minutes at 30°C. For LarAH49, reactions were performed with 0.2 µM of purified LarAH49, 1 µM NPN, 20 mM L-2-hydroxycaproate, and 100 mM potassium phosphate buffer (pH 7) in a final volume of 50 µl for 30 minutes at 30°C. To discover the activities of BSHIs, reactions were carried out with 5 µM of in vitro synthesized NPN and 2 µM of purified LarAH for 12 hours. The pH profiles of BSHIs were determined by incubating the enzymes with different buffers: acetic acid buffer (pH 4 to pH 5), potassium phosphate buffer (pH 6 to pH 8), and borate buffer (pH 9 to pH 10) (Fig. S2). The temperature profiles of BSHIs were determined by incubating the enzymes at temperatures ranging from 10°C to 60°C (Fig. S3). For K_M measurements, reactions were performed with varying concentrations of substrate (Fig. S4). For k_{cat} measurements, reactions were performed with substrate concentrations corresponding to the V_{max} of BSHIs for 5 min at the optimal pH and temperature of the respective BSHIs. All reactions were then stopped by incubation at 90 °C for 10 min and the products were assayed spectrophotometrically or by capillary electrophoresis. D-lactate, L-lactate, D-malate, D-2-hydroxyglutarate

racemization reactions and D-mannonate, L-iduronate C2-epimerization reactions were assayed spectrophotometrically at 340 nm with an Infinite 200 PRO plate reader (Tecan) using Megazyme kits. D-Lactate and L-lactate racemization reactions were assayed using the D-/L-Lactic Acid Assay Kit from Megazyme. D-malate racemization reactions were assayed using the L-Malic Acid Assay Kit from Megazyme. D-gluconate/D-mannonate C2-epimerization reactions were assayed using the D-Gluconic Acid Assay Kit from Megazyme. D-glucuronate/L-iduronate C2-epimerization reactions were assayed using the D-glucuronic Acid Assay Kit from Megazyme. L-2-hydroxyglutarate racemization reactions were assayed using *Acidaminococcus fermentans* D-hydroxyglutarate dehydrogenase (HGDH) [225], as previously described [210]. All other racemization and C2-epimerization reactions shown in Figure 3.1 and 3.2 were assayed by capillary electrophoresis [218].

Capillary electrophoresis

Enantiomers of AHAs and epimers of PHAs have been separated and detected using a versatile capillary electrophoresis method allowing the direct chiral separation of aliphatic and aromatic AHAs and PHAs [218]. All electrophoretic runs were run on a Capel 105 M from Lumex Instrument at 20 °C using -25 kV. Using a modified partial filling-counter current method with indirect UV detection, high resolution was achieved with vancomycin as a chiral selector added to the background electrolyte composed of 10 mM of benzoic acid/L-histidine at pH 5. Products were detected at 230 nm. For the separation and analysis of enantiomers, reaction mixtures were loaded onto a polyacrylamide-coated capillary of 54/46 cm total/effective length with an internal diameter of 50 µm from Agilent. For the separation and analysis of epimers, reaction mixtures were loaded onto a polyacrylamide-coated capillary of 122/112.5 cm total/effective length with an internal diameter of 50 µm from Agilent. The coating process of the fused-silica capillary inner surface by polyacrylamide starts by rinsing the capillary with 0.5 M HCl for 30 min and then with deionized water for 30 min. After rinsing, the capillary was silylated by flushing with a 3 % v/v solution of 3-(trimethoxysilyl)propylmethacrylate in 50 % aqueous acetone for 1 h. After the silylation process, the capillary was rinsed with deionized water for 25 min. The final polymerization step was performed by flushing of 3% w/v solution of acrylamide in deionized water with additions of 0.05% w/v

ammonium persulfate and 0.04 % v/V tetramethylethylenediamine for 45 min for the capillary with 50 µm i.d. x 122/112 cm total/effective length and 1 h for the capillary with 50 µm i.d. x 54/46 cm total/effective length. After the coating procedure, the capillary was rinsed with deionized water at 2000 mbar for 2 h.

Peptide separation using nanoUPLC

Proteolysis was performed with 1 µg of sequencing grade trypsin (Promega, USA) and allowed to continue overnight at 37°C. Each sample was dried under vacuum with Savant Speed Vac Concentrator. Digested proteins were dissolved in 20 µl of 0.1 % (v/v) formic acid and 2% (v/v) acetonitrile (ACN). Peptide mixture was separated by reverse phase chromatography on a NanoACQUITY UPLC MClass system (Waters) working with MassLynx V4.1 (Waters) software. 200ng of digested proteins were injected on a trap C18, 100Å 5 µm, 180 µm x 20 mm column (Waters) and desalted using isocratic conditions with at a flow rate of 15 µL/min using a 99% formic acid and 1% (v/v) ACN buffer for 3 min. Peptide mixture was subjected to reverse phase chromatography on a C18, 100Å 1.8 µm, 75 µm x 150 mm column (Waters) PepMap for 130 min at 35°C at a flow rate of 300 nL/min using a two part linear gradient from 1% (v/v) ACN, 0.1 % formic acid to 35 % (v/v)) ACN, 0.1 % formic acid for 90 min and from 35% (v/v) ACN, 0.1 % formic acid to 85 % (v/v)) ACN, 0.1 % formic acid for 10 min. The column was re-equilibrated at initial conditions after washing 30 min at 85% (v/v)) ACN, 0.1 % formic acid at a flow rate of 300 nL/min. For online LC-MS analysis, the nanoUPLC was coupled to the mass spectrometer through a nano-electrospray ionization (nanoESI) source emitter.

LC-QTOF-MS/MS Analysis (DDA)

DDA (Data Dependent Analysis) analysis were performed on an SYNAPT G2-Si high definition mass spectrometer (Waters) equipped with a NanoLockSpray dual electrospray ion source (Waters).Precut fused silica PicoTipR Emitters for nanoelectrospray, outer diameters : 360 µm; inner diameter: 20 µm; 10 µm tip; 2.5” length (Waters) were used for samples and Precut fused silica TicoTipR Emitters for nanoelectrospray, outer diameters : 360 m; inner diameter: 20 µm; 2.5” length (Waters) were used for the lock mass.solution. The eluent was sprayed at a spray voltage of 2.8 kV with a

sampling cone voltage of 25 V and a source offset of 30 V. The source temperature was set to 80°C. The cone gas flow was 20 liters/h with a nano flow gas pressure of 0.4 bar and the purge gas was turned off. The SYNAPT G2Si instrument was operated in DDA (data-dependent mode), automatically switching between MS and MS2. Full scan MS and MS2 spectra (m/z 400 - 2000) were acquired from 2 min after injection to 130 min in resolution mode (20,000 resolution FWHM at m/z 400) with a scan time of 0.1 sec. Tandem mass spectra of up to 10 precursors were generated in the trapping region of the ion mobility cell by using a collision energy ramp from 17/19 V (low mass, start/end) to up to 65/75 V (high mass,start/end). Charged ions (+2, +3, +4) are selected to be submitted to the MSMS fragmentation over the m/z range from 50 to 2000 with a scan time of 0.25 sec. For the post-acquisition lock mass correction of the data in the MS method, the doubly charged monoisotopic ion of [Glu1]-fibrinopeptide B was used at 100 fmol/µl using the reference sprayer of the nanoESI source with a frequency of 30 s at 0.5µl/min into the mass spectrometer. ESI-QTOF were processed with MASCOT search engine (Matrix Sciences) using the protein sequences introduced in the Bacteria_Uniprot database.

Relative catalytic efficiencies calculation

The relative catalytic efficiencies of a LarAH acting simultaneously on two substrates, SX and SY, at rates vx and vy, were calculated using Eq. (1),

$$\frac{\mathrm{v_x}}{\mathrm{v_y}} = \frac{(k^{\mathrm{x}}_{\mathrm{cat}}/K^{\mathrm{x}}_{\mathrm{M}})\,[\mathrm{S_x}]}{(k^{\mathrm{y}}_{\mathrm{cat}}/K^{\mathrm{y}}_{\mathrm{M}})\,[\mathrm{S_y}]} \qquad (1)$$

where if $[S_X] = [S_Y]$ the [S] terms cancel, and the ratio of the k_{cat}/K_M values for each substrate is equal to the relative rates at which the LarAH catalyzes the transformation of each substrate when both are present at equal concentrations with the enzyme in the same mixture [226]. vx and vy were determined by quantifying the products PX and PY either spectrophotometrically or by capillary electrophoresis. For a LarAH active on more than two substrates, we determined its catalytic efficiency for each of its substrates by testing combinations of substrate pairs with the LarAH.

III.3.2 Supplementary data

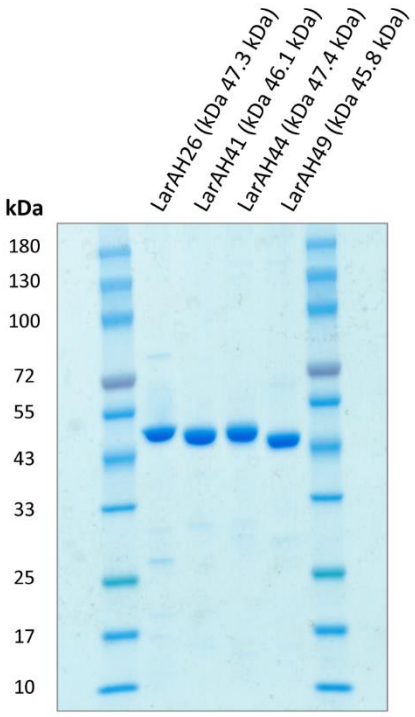

Figure 3.S1 | Analysis of the purified BSHIs from *E. coli* by SDS-PAGE. Sequences of the proteins are provided in Table S2.

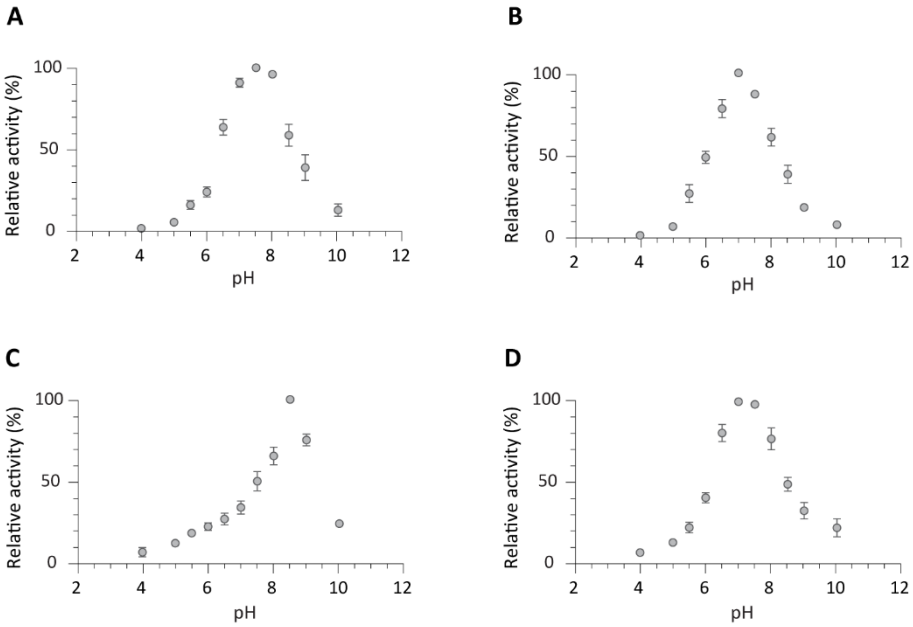

Figure 3.S2 | **pH-dependent activity of the investigated BSHIs. (A)** Relative activity of LarAH26 from *P. megaterium* as a function of pH, assessed for the C2-epimerization of D-mannonate. **(B)** Relative activity of LarAH41 from *E. asparagiformis* as a function of pH, assessed for the C2-epimerization of D-mannonate. **(C)** Relative activity of LarAH41 from *E. asparagiformis* as a function of pH, assessed for the racemization of L-lactate. **(D)** Relative activity of LarAH41 from *E. asparagiformis* as a function of pH, assessed for the racemization of L-2-hydroxycaproate. Error bars indicate standard error (n=3).

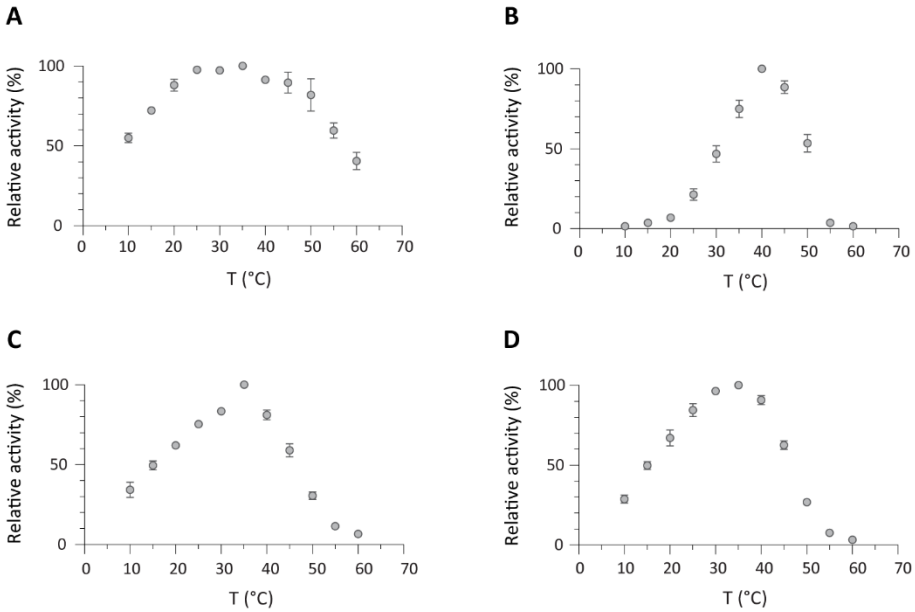

Figure 3.S3 | **Temperature-dependent activity of the investigated BSHIs. (A)** Relative activity of LarAH26 from *P. megaterium* as a function of temperature, assessed for the C2-epimerization of D-mannonate. **(B)** Relative activity of LarAH41 from *E. asparagiformis* as a function of temperature, assessed for the C2-epimerization of D-mannonate. **(C)** Relative activity of LarAH41 from *E. asparagiformis* as a function of temperature, assessed for the racemization of L-lactate. **(D)** Relative activity of LarAH41 from *E. asparagiformis* as a function of temperature, assessed for the racemization of L-2-hydroxycaproate. Error bars indicate standard error (n=3).

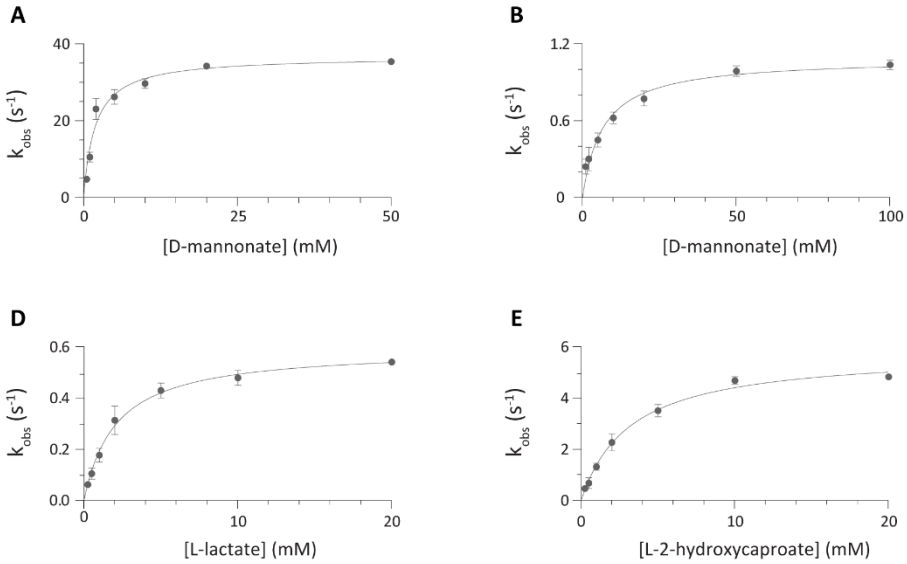

Figure 3.S4 | **Kinetic analysis of the investigated BSHIs. (A)** Kinetics of D-mannonate C2-epimerization by LarAH26 from *P. megaterium*, **(B)** Kinetics of D-mannonate C2-epimerization by LarAH41 from *E. asparagiformis*, **(C)** Kinetics of L-lactate racemization by LarAH44 from *E. asparagiformis,* **(D)** Kinetics of L-2-hydroxycaproate racemization by LarAH49 from *E. asparagiformis*. The activities of the enzymes at the indicated substrate concentrations are shown as $k_{obs} = v_0/(E)_0$. The curves are the fitted curves using non-linear regression. The error bars indicate SD (n = 3).

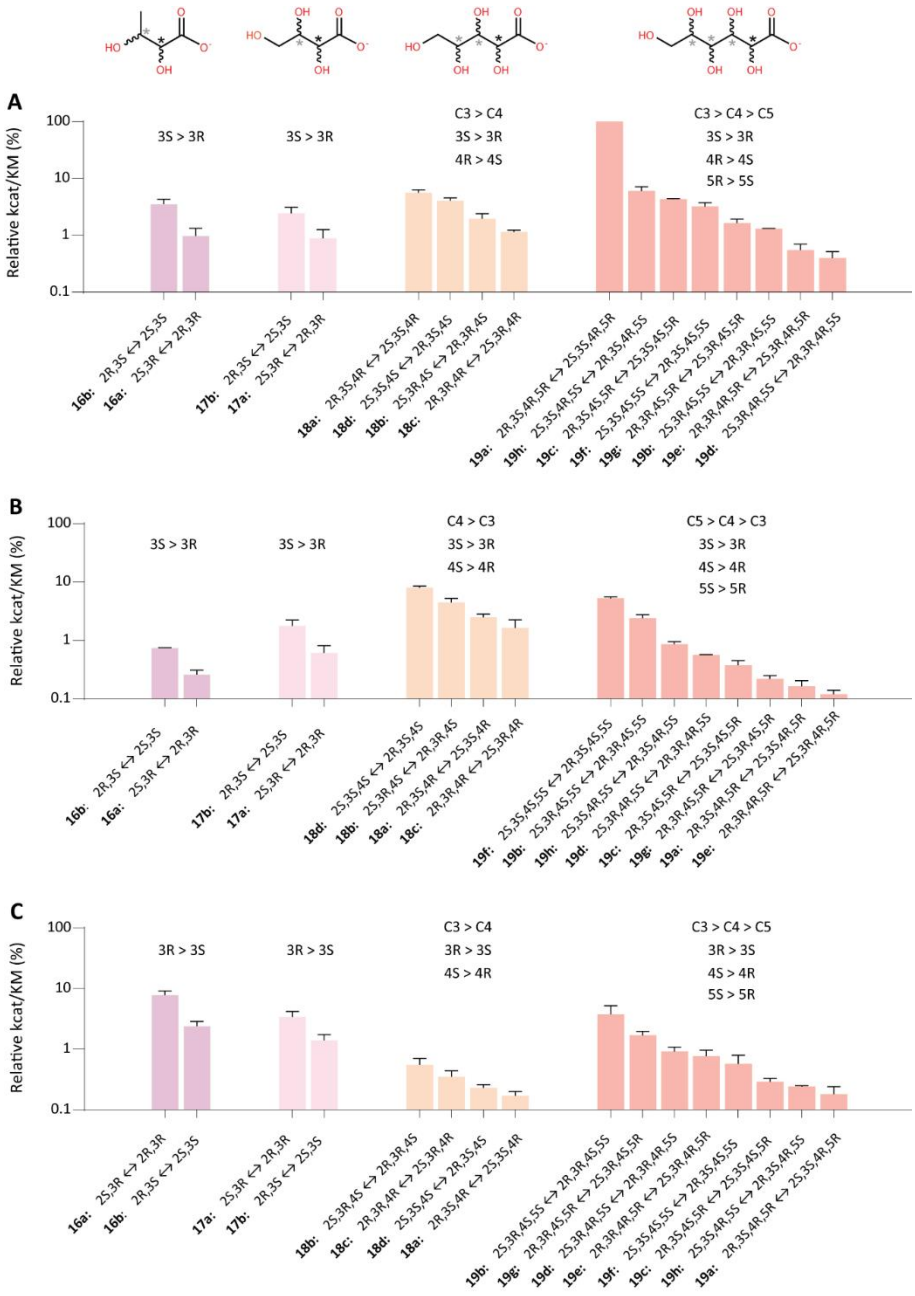

Figure 3.S5 | Stereochemical preferences for the C2-epimerization of poly-hydroxy acids of the investigated BSHIs. (A) Stereochemical preferences of LarAH26 from *P. megaterium*. **(B)** Stereochemical preferences of LarAH41 from *E. asparagiformis*. **(C)** Stereochemical preferences of LarAH44 from E. *asparagiformis*. The error bars represent the standard error (n=3).

Table 3.S1 | LC-ESI-QTOF-MS analysis of the investigated BSHIs.

Match to*	Score	Sequence coverage (%)
LarAH26	417	87
LarAH41	2207	53
LarAH44	220	40
LarAH49	214	42

Table 3.S2 | Sequences of the investigated BSHIs.

Name	Sequence
LarAH26	MGILQDLLKDVPIPKMAKVQVAFDDTKIHDVQHVLTEKLNQENIKRRITPGMEIAIAVGSRG LDQIVEMTATTVQFLKELGANPFIVPSMGSHGGATAEGQQEVLRHLGITEESVQCEIRSSME VVEIGQLSNGLPVFVDKHASKADGIIVVNRIKPHTAFRGPVESGLMKMISIGLGKQKGAEAC HQLGFKYMAENVPAMAKVIMQELPVLFGIASIENSFDKVAVIEVLPSEQIEDKETNLQIIAKQL LPKLYFDELDVLVIDEIGKNISGDGMDPNVTGRYPTPYAHGGPAVNKMVVLDLTPQTEGNA NGVGTADFTTQRLVDKANLEFMYANGLTSTVVAPTKIPTTLPNDRQAIQAAIKTSNILDFTQ VKMVRIKNTLELSEIEVSEALLNHIHSHPHMQQSSELYSISFNKEGNFLRVEDRNETII
LarAH41	MSAVSDILKQVTIPKMVRVKQSFPRPRIEDVKAAVLAELKRPEIAERLKPGKRIAVGVGSRGIT NYQLIVRTIVDELKRIGAKPFIVASMGSHGGATVEGQTEILAGYGITEEAMGCPLCIGTGTQVI GTTQDGLPVQIDAFAAQADGIIVVNRIKAHTAFMGDYESGLMKMLAIGLAKQAGADYCHA KGFGHMAETVPKFGRAIIQYSKLLFGLAIVENAYDDTYIVRAVPAESIAQEEPKLLLEAKANMS RILIPEADVLIVHEIGKNISGDGMDPNVSGTFATPYAHGGIKTQRVAVLNITQESHGNTVGW GMADVSTRKAFDSFDMDKTYPNSLTCRVTQVSKVPMIFKNDEECIKAAIKTCADVDVEHMR IVYIKNTLHMKEILVSEALADIARSIPQAEVCGECEPLSFDEQGNISGTYF
LarAH44	MFINFPEINDLMIQDREVTIPKMVTIRQHFDTYQIADIPLHIREQMEANAGAPERFKGKRIAI TAGSRGIPNIVVILRAICDILKEWGAKPFVVPAMGSHGGATAKGQEEVLASYGITEAGIGAPIR SSMDVVQYGTLPNGIPLFCDKLAFESDGIVICHKIKPHTDFRNEHESGLCKMIAIGLGKHKGA AAIHSQGFCGFGSFITEAARQFLQAAPVAFGVGMIQNAYDEIHTLEVIPGAQIMEADARLLK AAKQQLAGFKFDDIDVLIIDRIGKNISGYGFDPNVVGRSNSRCYGFEDPVRIKRLFIRGLTPES HHNGSGINEADITTRRCLNDIDWSETWTNLITATEIQGSKIPMYVNNDKEALTIALRCCNGA PRPHRVARIKDTLSMKELQVSEALYEAIRDQPDIEYVRGPEEILFDGEGFMS
LarAH49	MSVVNDIIKDIPLPNMVKVRQEFDRTRLENVAAEVRKCLERREILGNLRPGMTVAVAVGSR GISNHALIVRETVRFLRDHGARPFIVSSMGSHGGTTAEGQRAILEGYGIREEYCGCPVKAGTD CALIGYTGDGSPVYIDRYAAEAGGIVLVNRIKPHTAFRGPYESGLMKMMAIGLGKQKGAETC HAAGFENMAENIPRFAAAVLKNCNILAGIAILENAYDETREVIALAADEIPAKEPELLERAKRY MPRILVDHVDLLVVGQIGKNFSGDGMDPNIAGTFATKCASGGLNTKRVAVLDISDESHGNG VGFGMADVSTRRAYEKFDFEMSYPNALTCLVSQVVKVPMIFDSDQLCLKAGIKLCAGIEHRN ARVVYIHNTLKLGEIYISANLVPQAEAVEGVTVAGAERPMEFDGNGNLISI

Table 3.S3 | Genomic context of the investigated BSHIs. Operons of each LarAH are indicated in light grey. Genes neighboring operons are shown when informative. Genes of LarAHs are in bold.

	Gene	Function
Genomic context of LarAH26	>bmd-BMD_3418	Sugar transporter (Glycoside-Pentoside-Hexuronide)
	>bmd-BMD_3419	LarC
	>bmd-BMD_3420	LarC
	>bmd-BMD_3421	LarB
	>bmd-BMD_3422	LarE
	>bmd-BMD_3423	Gluconate 5-dehydrogenase
	>bmd-BMD_3424	**LarAH26**
	>bmd-BMD_3425	Glucuronate isomerase
	>bmd-BMD_3426	Sugar kinase of the NBD/HSP70 family (xylose repressor)
Genomic context of LarAH41	CLOSTASPAR_01113	HTH-type transcriptional regulator CueR, MerR family
	CLOSTASPAR_01114	**LarAH41**
	CLOSTASPAR_01115	2-deoxy-D-gluconate 3-dehydrogenase
	CLOSTASPAR_01116	
	CLOSTASPAR_01117	Ribulose-phosphate 3-epimerase
	CLOSTASPAR_01118	Ribose 5-phosphate isomerase
	CLOSTASPAR_01119	Transcriptional regulator, GntR family (Carbohydrates transport)
	CLOSTASPAR_01120	4-phosphoerythronate dehydrogenase; D-3-phosphoglycerate dehydrogenase
	CLOSTASPAR_01121	2-dehydro-3-deoxygalactonokinase
	CLOSTASPAR_01122	Ribose ABC transporter membrane protein
	CLOSTASPAR_01123	Ribose ABC transporter permease protein
Genomic context of LarAH44	CLOSTASPAR_02317	ROK family protein (CLLA : Glucokinase)
	CLOSTASPAR_02318	
	CLOSTASPAR_02319	Hydrolase, UxaA family, altronate hydratase
	CLOSTASPAR_02320	D-galactarate dehydratase/altronate hydrolase domain protein
	CLOSTASPAR_02321	3-ketoacyl-(acyl-carrier-protein) reductase, short chain dehydrogenase
	CLOSTASPAR_02322	demethylmenaquinone methyltransferase
	CLOSTASPAR_02323	mandelate racemase/muconate lactonizing enzyme
	CLOSTASPAR_02324	C4-dicarboxylate ABC transporter substrate-binding protein
	CLOSTASPAR_02325	TRAP transporter, DctQ-like membrane protein (small permease)
	CLOSTASPAR_02326	TRAP transporter, DctM subunit (large permease)
	CLOSTASPAR_02327	**LarAH_CLAS4**
	CLOSTASPAR_02328	Transcriptional regulator, LacI family
	CLOSTASPAR_02329	Putative chlorophyll synthesis pathway protein BchC, sorbitol dehydrogenase
Genomic context of LarAH49	CLOSTASPAR_06359	Sugar ABC transporter ATP-binding protein
	CLOSTASPAR_06358	sugar ABC transporter ATP-binding protein
	CLOSTASPAR_06357	Ribose transport system permease protein RbsC
	CLOSTASPAR_06356	Ribose transport system permease protein RbsC
	CLOSTASPAR_06355	D-ribose-binding periplasmic protein
	CLOSTASPAR_06354	Creatinine amidohydrolase
	CLOSTASPAR_06353	2-deoxy-D-gluconate 3-dehydrogenase (SDR family)
	CLOSTASPAR_06352	2-dehydro-3-deoxyphosphogluconate aldolase
	CLOSTASPAR_06351	**LarAH_CLAS9**
	CLOSTASPAR_06350	2-dehydro-3-deoxygalactonokinase
	CLOSTASPAR_06349	D-isomer specific 2-hydroxyacid/4-phosphoerythronate dehydrogenase
	CLOSTASPAR_06348	Uncharacterized membrane protein YczE

Table 3.S4 | Bacterial strains and plasmids used in this study.

Strains	Characteristic(s)	Use for	Source or reference
Lc. Lactis NZ3900	NZ3900		[233]
E. coli DH10B	F^- *endA*1 *recA*1 *galE*15 *galK*16 *nupG rpsL* Δ*lacX*74 Φ80*lacZ*ΔM15 *araD*139 Δ(*ara*,*leu*)7697 *mcrA* Δ(*mrr-hsdRMS-mcrBC*) λ^-		Invitrogen
E. coli ArticExpress	Contains *Cpn60* and *Cpn10* from *Oleispira antarctica*		Agilent
Plasmids			
pGIR026	Em^r Amp^r; pGIZ660 with DNA encoding the StrepII-tag translationally fused at the 3'-end of the *larB* ORF	LarB purification	[36]
pGIR031	Cm^r; pNZ8048 with DNA encoding the StrepII-tag sequence translationally fused to *larC*	LarC purification	[36]
pGIR076	Amp^r; pBADHisA with DNA encoding *larE* translationally fused to the StrepII-tag sequence	LarE purification	[76]
pGIR326	Amp^r; pBADHisA with DNA encoding LarAH26	LarAHs purification	This study
pGIR341	Amp^r; pBADHisA with DNA encoding LarAH41		This study
pGIR344	Amp^r; pBADHisA with DNA encoding LarAH44		This study
pGIR349	Amp^r; pBADHisA with DNA encoding LarAH49		This study

*Emr, Ampr, and Cmr indicate resistance to erythromycin, ampicillin, and chloramphenicol, respectively.

Table 3.S5 | List of primers used in this study.

Name	Sequence (5'-3')	Source
LarAH26_A	TTTCCATGGGTATTTTGCAAGATTTATTAAAAGATGTTC	This study
LarAH26_B	AAAGCTAGCAATAATTGTTTCATTTCTGTCCTCCACTC	This study
LarAH41_A	TTTACATGTCAAGCGCAGTGAGCGACATTTTAAAG	This study
LarAH41_B	TTTGCTAGCGAAGTACGTTCCGGAAATATTTC	This study
LarAH44_A	TTTACATGTTTATCAATTTTCCGG	This study
LarAH44_B	TTTGCTAGCACTCATAAAACCTTCCCCG	This study
LarAH49_A	CCCACATGTCCAGTGTTGTAAATGACATTATAAAAGAC	This study
LarAH49_B	CCCGCTAGCGATTGAAATCAGATTTCCGTTTC	This study
pBAD_up	GCAACTCTCTACTGTTTCTCCATAC	This study
pBAD_rev	CCGCCAGGCAAATTCTG	This study

† PciI, NcoI, NheI restriction sites introduced in the primers are underlined in primer sequences.

IV. GENERAL DISCUSSION & PERSPECTIVES

IV.1 Potential biotechnological applications of LarAHs

IV.1.1 LarAHs as tools for the production of valuable HAs

AHAs and PHAs have significant market potential and are widely used across various industries. However, the chemical or enzymatic synthesis of many stereoisomers of these compounds is highly complex [1,59]. Consequently, many HA stereoisomers are either rare or expensive. Some LarAHs show promise for biotechnological production of rare HA stereoisomers (see Chapter II & III). LarAHs have the potential to convert low-value HA stereoisomers into high-value ones, with a theoretical yield of 50% for racemases and depending of the equilibrium constant (K_{eq}) for epimerases. For racemization reactions, the theoretical yield is 50% since the equilibrium constant is around 1 [248,249]. For epimerization reactions, the theoretical yield depends on the K_{eq}, which may differ from 1 [250–252]. Notably, LarAHs could attract substantial interest for their ability to C2-epimerize sugar acids (see Chapter III), given the utility of these compounds as detergent components, pH regulators, corrosion inhibitors, additives in the food industry, monomers for polymeric materials, and biodegradable chelators for pharmaceuticals [59,253–255]. Table 3 shows a non-exhaustive list of valuable HAs with significant biotechnological applications for which LarAHs may offer a novel biosynthetic pathway.

One promising applications of LarAHs is the production of D-2,4-dihydroxybutyric acid (D-DHB) from L-2,4-dihydroxybutyric acid (L-DHB). DL-DHB is a molecule with considerable potential as a versatile chemical synthon, serving as a precursor for synthesis of the DL-methionine analogue DL-2-hydroxy-4-(methylthio)butyrate, which targets a substantial market in animal nutrition (Table 3). However, there is no natural pathway for the biosynthesis of D-DHB. DHB is a racemic molecule, chemically produced as DL-DHB but biologically produced only as L-DHB [50,256,257]. To address this, we are collaborating with Prof. Jean Marie François's team at the Toulouse Biotechnology Institute (TBI), who are interested in using D-DHB to produce a biopolymer. Indeed, the D-form is preferred for its ability to react with polyhydroxyalkanoate synthase [258,259]. We explored whether LarAHs could effectively convert L-DHB to D-DHB and identified nine different LarAHs capable of this conversion: LarA, LarAH24, LarAH26, LarAH2/SAR, LarAH41, LarAH42, LarAH43, LarAH44 and LarAH51 (see

Chapter II, Chapter III & Appendix Table A1). Among these enzymes, LarAH26 and LarAH2/SAR exhibited the highest activity and stability, continuing to produce D-DHB after six hours of incubation at 37°C (Appendix - Fig. A1). Based on these findings, the Toulouse team plans to develop an *in vivo* D-DHB production system in *E. coli* using either LarAH26 or LarAH2/SAR.

Table 3 | Valuable HAs isomerized by LarAHs and their applications.

HAs	Applications	Ref.
D- and L-3-phenyllactate	Broad-spectrum antimicrobial agents extensively used in food, feed, pharmaceutical, and cosmetic industries.	[39,260,261]
D-2-hydroxy-4-phenylbutyrate	Essential precursor for angiotensin-converting enzyme inhibitors (ACEI), vital in hypertension treatment.	[43,262,263]
D-2-hydroxybutyrate	Key building block for biodegradable poly(2-hydroxybutyric acid) and azinothricin family antitumour antibiotics.	[40,264]
L-iduronate	Critical precursor used in the production of heparinoid anticoagulants.	[238]
DL-2,4-dihydroxybutyrate	Precursor for synthesis of the methionine analogue 2-hydroxy-4-(methylthio)butyrate, targeting a substantial market in animal nutrition.	[50,256,257]

However, all reactions catalyzed by LarAHs result in stereoisomeric mixture, which limits the yield depending the equilibrium constant of the reaction. To obtain a pure sample of the desired stereoisomer, the unwanted stereoisomer must be removed or separated from the racemic mixture. Several chiral separation methods are available for this purpose [265,266]. Alternatively, an enzyme can be used to convert the unwanted stereoisomer into a removable compound. For example, in the production of L-iduronate from D-glucuronate by BSHIs, the residual D-glucuronate in the stereoisomeric mixture could be catabolized by microorganisms [267–269].

Overall, LarAHs show promise as biotechnological tools. To realize this potential, three key aspects require optimization: (1) scaling up the production of HAs, (2) overcoming the 50% yield limit, and (3) enhancing the low k_{cat} values observed in certain biotechnologically relevant reactions (e.g. the production of L-iduronate from D-glucuronate). To address the aspect

(3), one approach is directed evolution to increase the k_{cat} of LarAHs for specific reactions of interest [244]. Alternatively, purifying other LarAHs from the same phylogenetic group may yield LarAHs with higher k_{cat} values for these reactions. The strategies for addressing aspects (1) and (2) will be discussed in detail in the following sections.

IV.1.2 Large scale production of HA racemates with LarAHs

LarAHs and NPN offer a promising biosynthesis system for various valuable HA racemates. However, NPN remains the most challenging compound to synthesize within this system and limits the amount of HA that can be produced. To increase production, scaling up the biosynthesis of LarAHs bound to NPN is essential. Four strategies are possible for producing LarAH bound to NPN:

1. LarAH supplemented with in vitro biosynthesized NPN cofactor. This approach involves separately purifying LarB, LarE and the LarAH from *E. coli* cells, and LarC from *Lactococcus lactis* cells, followed by *in vitro* cofactor biosynthesis [141]. This approach yields highly concentrated NPN but is time-consuming and labor-intensive. Indeed, since single turnover enzymes are used [119,120], two molar equivalents of LarE and one molar equivalent of LarC are required, necessitating the overexpression and purification of large amounts of proteins (more than 250 times the mass of NPN obtained), which must be subsequently removed to obtain pure NPN. While ideal for *in vitro* LarAH characterization, this strategy is impractical for scaling up reactions and HA production.

2. LarAH supplemented with cell extract from a *L. lactis* strain expressing *larBCE*. In this strategy, the cell extract of a *L. lactis* strain with a plasmid expressing *larBCE* can be used to activate the purified LarAH apoprotein. Alternatively, if a cleaner reaction is desired, LarE loaded with NPN can be purified and then used to activate the LarAH apoprotein.

3. *L. lactis* strain with a plasmid coexpressing a *larAH* and *larBCE*. The in vivo coexpression of LarAH and *larBCE* in *L. lactis* allows for the production of the active LarAH holoenzyme in a single purification step. Currently, this is the most efficient strategy for obtaining large quantities of LarAH holoprotein.

4. *E. coli* strain with a plasmid coexpressing a *larAH* and *larBCE*. The *in vivo* coexpression of the *larAH* and *larBCE* in *E. coli* promises the best scalability for reaction volumes and HA production. However, the effectiveness of this strategy is significantly reduced in *E. coli* due to limited NPN synthesis. The exact reason for this inefficiency is unclear but could be related to issues with the solubility or toxicity of LarB, LarC, or LarE, or nickel availability in the *E. coli* cytoplasm. Despite this, optimizing NPN biosynthesis in *E. coli* should be possible, as closely related bacteria possess the *larBCE* genes [95,113], for example a strain of *Escherichia fergusonii*.

As mentioned, the *in vivo* coexpression of a *larAH* and *larBCE* in *Lactococcus lactis* is currently the most effective strategy for scaling up HA production. Thus, *L. lactis* could serve as a valuable microbial platform for producing HAs isomerized by LarAHs, such as the compounds listed in Table 3. To this end, a plasmid, pGIR210_LarAH26, which expresses both *larAH26* and *larBCE*, has been engineered and introduced into the *L. lactis* NZ3900 strain. LarAH26 belongs to the family of BSHIs, which is the group of LarAHs showing the greatest biotechnological potential. Specifically, LarAH26 was selected for its catalytic efficiency—its k_{cat} values are approximately tenfold higher than those of other members in this group, such as LarAH41, LarAH44, and LarAH49. This engineered strain has demonstrated increased production levels of most tested HAs, including D-DHB. Furthermore, it shows potential in scaling up the production of L-iduronate from D-glucuronate and L-alturonate from D-galacturonate. This is despite LarAH26's low catalytic efficiency for these reactions, which is attributed to the limited availability (< 1%) of the linear forms of these molecules in solution (see Section III.3.1). However, D-glucuronate and D-galacturonate may not enter *L. lactis* cells due to their bulky and highly polar nature, attributed to their four hydroxyl groups. Moreover, these substrates predominantly exist as negatively charged carboxylates at neutral pH, further hindering their entry into the cell. To facilitate their entry, the *L. lactis* strain could be engineered to co-express a specific transporter or permease that can actively transport D-galacturonate and D-galacturonate across the cell membrane [270–272]. Alternatively, lysate of the *L. lactis* strain could be used for the reaction to bypass the entry issue. Overall, future studies focused on the optimization and integration of the mentioned strategies could lead to breakthroughs in HA conversion, paving the way for more sustainable and cost-effective biotechnological processes.

IV.1.3 Production of optically pure HAs with LarAHs

The production of optically pure HAs represents a key objective in organic chemistry, given their significant importance in a number of industrial sectors, including pharmaceuticals, food, and cosmetics. One common methodology for producing optically pure compounds on a large scale involves the classical and kinetic resolution of racemic mixtures. However, these methods have a maximum theoretical yield of only 50%, with the remaining 50% of the starting material being discarded [241,273]. To address this limitation, deracemization strategies such as dynamic kinetic resolution (DKR) [242,243] and multistep chiral separation with racemization [241] have been developed (Fig. 11) These strategies have the potential to transform a racemic mixture into a single enantiomer with a 100% theoretical yield [239]. Our findings suggest that newly discovered C2-epimerization and racemization reactions catalyzed by LarAHs could have significant biotechnological applications in these methods for producing optically pure HAs. DKR involves treating a racemic mixture with a stereoselective catalyst that predominantly produces the desired stereoisomer, represented by the 2R-product in Figure 11A. Concurrently, an isomerase converts the remaining stereoisomer (the 2S-substrate) into the 2R-substrate, which can then be converted into the 2R-product by the stereoselective catalyst (Fig. 11A). Multistep chiral separation with racemization involves separating the stereoisomers by chiral chromatography or stereospecific crystallization, followed by progressive biocatalytic isomerization of the unwanted stereoisomer (Fig. 11B) [241]. Thus, these methods have the potential to achieve a 100% theoretical yield of the desired stereoisomer, provided an efficient isomerization enzyme is available [240]. LarAHs could fulfill this role and have important biotechnological uses in the stereospecific conversion of HA racemates for the production of optically pure HAs. Moreover, LarAHs could be utilized upstream to produce the racemate required for these methods. In this scenario, LarAHs could theoretically convert a stereopure solution of the unwanted stereoisomer into a stereopure solution of the desired stereoisomer. Therefore, the use of LarAHs for the chemo-selective interconversion of stereoisomers without side reactions holds great potential for the preparative-scale biotransformation of HAs.

A third and novel approach involves coupling LarAH-catalyzed racemization or C2-epimerization of HAs with a chiral resolution method based on preferential co-crystallization. Preferential co-crystallization separates stereoisomers by exploiting their ability to form different crystal structures with a chiral resolving agent [265,274]. To this end, we are collaborating with Prof. Tom Leyssens' laboratory at UCLouvain, which has recently developed a complete chiral resolution process for mandelic acid based on preferential co-crystallization, reaching 98-99% of enantiopurity [275]. The objective is to achieve an enzymatic reaction where induced co-crystallization with a chiral amine reduces the stereoisomer concentration in solution, shifting the reaction equilibrium towards product formation, theoretically achieving a 100% yield. We selected lactate and malate racemization as the initial test case for this approach for two reasons. First, numerous LarAHs are known to be active on lactate or malate. Second, numerous multicomponent crystals with lactate and malate exist in the Cambridge Crystallographic Data Centre (CCDC) [276], suggesting promising screening results with chiral amines. Given that ethanol promotes the co-crystallization of AHAs [275,277,278], we assessed the activity of a lactate racemase (LarAH2/SAR) and two malate racemases (LarAH9 and LarAH27) in varying ethanol concentrations. All selected LarAHs showed increased or maintained optimal activity at 5% and 10% ethanol, with reduced activity observed at higher concentrations (Appendix - Fig. A2). Further screening will be necessary to identify the crystal structures of co-crystals formed in 10% ethanol between chiral amines and lactate or malate using X-ray diffraction (XRD). Preliminary data indicated that (R)-(+)-1-phenylethylamine and (R)-(+)-1-(1-naphthyl)ethylamine are promising candidates for the formation of co-crystals with malate. Subsequently, solubility tests with the selected chiral amines will determine which has the lowest solubility, thereby ensuring the optimal final yield. Additionally, the activity of LarAHs in the presence of the selected chiral amines needs to be verified. Ongoing research and development may fully exploit the potential of LarAH-based systems for producing optically pure hydroxy acids, opening new avenues for biotechnological innovation.

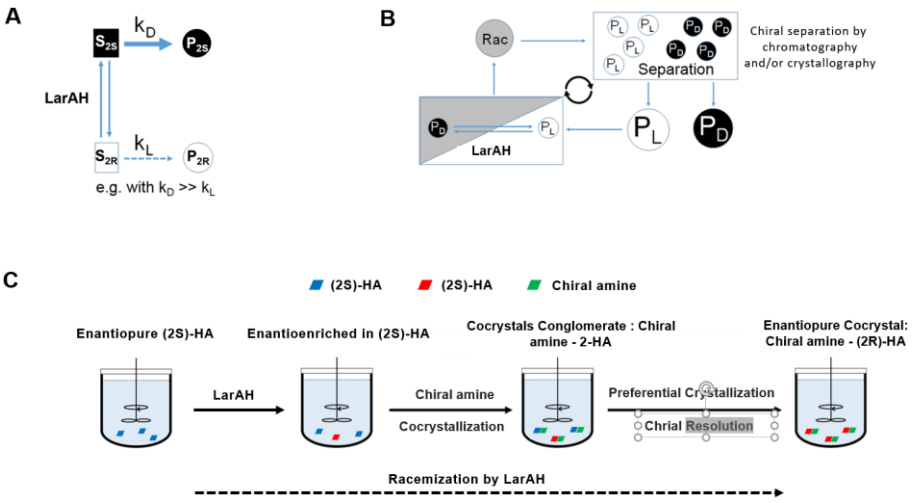

Figure 11 | **Methods for producing optically pure HAs involving LarAHs.** (**A**) Dynamic kinetic resolution using LarAHs. (**B**) Multistep chiral separation coupled with LarAH-catalyzed isomerization. Rac, racemate; S_{2S}, (2S)-substrate; S_{2R}, 2R-substrate; P_{2S}, (2S)-product; P_{2R}, 2R-product. (**C**) LarAH-catalyzed AHA isomerization coupled with a chiral resolution method based on preferential co-crystallization.

IV.2 LarAHs activation and inactivation kinetics

IV.2.1 Stability of LarAHs with NPN cofactor

The initial report of LarA purification revealed that purified LarA exhibits low stability, due to the rapid oxidation of its NPN cofactor and subsequent nickel loss [95]. Addition of L-ascorbic acid and nickel provides slight stabilization, while sulfite, a potent LarA inhibitor, stabilizes LarA activity for several days by protecting NPNylated LarA from oxidation and delaying nickel loss [95,96]. Further investigation into the properties of LarAHs with the NPN cofactor, especially their stability, would enhance our understanding of the complex interactions between NPN and NPN-dependent enzymes. This knowledge could prove invaluable for the prospective utilization of LarAHs in biotechnological applications. Moreover, knowledge of the respective stability of different LarAHs may facilitate the identification of optimal candidates for crystallographic studies with the substrate and NPN inside the enzyme. Previous attempts to crystallize LarA with lactate were unsuccessful due to its instability [95]. In contrast, LarAH2/SAR has demonstrated stability for up to five days in the presence of lactate (Appendix - Fig. A3).

Collaborators in the team of Prof. Hausinger at the Michigan State University (MSU) are currently attempting to obtain a three-dimensional structure of LarAH2/SAR with lactate and NPN through the co-expression of *larAH2/sar* and *larBCE* in *L. Lactis*.

The stability of several additional LarAHs has been evaluated during this thesis (Appendix - Fig. A3 & Table A2). Data showed that most LarAH stabilities assays have three common characteristics: (i) assays typically start with an increase in activity, which is due to the *in vitro* activation of the apoenzyme with NPN; (ii) the activity decreases over time; (iii) the presence of a substrate increases the stability of most LarAHs, likely because the reaction intermediate protects C4 of the NPN against solvent and thus prevents C4 from unwanted reactivity involving Ni loss [139]. Major differences are observed in activation-inactivation kinetics among LarAHs. While some remain stable for a few tens of minutes, akin to LarA1 [95], others remain stable for hours or days (Appendix - Fig. A3 & Table A2). Additionally, substrate presence strongly influences enzyme activation in some LarAHs but not in others.

IV.2.2 Binding of LarAHs to the NPN cofactor

To complete the stability analysis, it would be interesting to determine whether the binding of each LarAH to the NPN is covalent or non-covalent during enzyme activation. While LarA1 is known to be covalently attached to NPN through its Lys184, this interaction might not be universal among all LarA(H) proteins, even though they all possess a Lys residue analogous to Lys184 of LarA1. For example, LarA2 (the lactate racemase from *T. thermosaccharolyticum*) and the NPN cofactor dissociate during LarA2 purification, whereas an active holoenzyme was present prior to purification [95]. To determine the nature of LarAH binding to NPN, two types of mass spectrometry (MS) analysis may be employed following incubation of the LarAH with and without the NPN: intact protein analysis or post-trypsin digestion analysis. In both cases, the analysis will reveal a shift in mass ranging from 393 daltons (NPN without Ni^{2+}) to 449 daltons (NPN containing Ni^{2+}), depending on the modification of Lys184 [96]. Intact Protein Mass Spectrometry could distinguish covalent from non-covalent bonds by analyzing the mass of the enzyme-cofactor complex under denaturing conditions; a covalent bond is present if the cofactor remains attached after

denaturation. Post-trypsin digestion analysis is straightforward and involves comparing peptides from the LarAH apoprotein incubated with or without NPN. For LarAH without NPN, trypsin digestion will produce two peptides: peptide A (containing Lys184) and peptide B (formed just after Lys184). These can be determined by simulating trypsin digestion with the LarAH sequence. When LarAH is incubated with NPN, the NPN-binding modifies Lys184, preventing its cleavage and resulting in peptide C. Peptide C will have a cumulative weight equal to peptide A, peptide B, and NPN, indicating a covalent bond between LarAH and NPN. The analysis of LarA1 bound to the NPN cofactor can be employed as a positive control for both types of MS analysis to ascertain the efficacy of the experimental procedure, given LarA1 forms a covalent bond with NPN [96].

Additionally, to better understand these activation and inactivation processes, studying the interaction of the NPN cofactor with NPN-dependent enzymes, both with and without substrate, via isothermal titration calorimetry (ITC) and surface plasmon resonance (SPR) would be informative. Indeed, ITC could be used to measure the thermodynamics of the interaction between LarAHs and NPN [279], and SPR could be used to measure the binding kinetics and affinity between LarAHs and NPN [280]. Capillary electrophoresis-mass spectrometry (CE-MS) could also be utilized for the analysis of LarAHs under native conditions to observe alterations in the migration time of the enzyme upon activation by NPN [281,282].

IV.3 *In vivo* roles of LarAHs

IV.3.1 A few hypotheses

An important remaining question concerns the potential roles of the LarAHs *in vivo*. Given the metabolic significance of HAs in nature and the widespread distribution of LarAHs in microorganisms, it is expected that these enzymes play crucial metabolic roles. This is particularly relevant for MARs, LARs, GntEs, HHRs, HGRs, and BSHIs, given their prevalence within the LarA superfamily (Fig. 2.2). MARs are the most prevalent enzymes in the LarA superfamily and are found in both bacteria and archaea (Fig. 2.2). MARs may enable various bacterial and archaeal species to utilize both enantiomers of malate as carbon and electron sources. This is significant since malate is essential in the metabolism of several bacterial and archaea species,

especially in the glyoxylate cycle and the TCA cycle as an energy source [22–24,26–29]. Additionally, a malate racemase activity was previously observed in *Rhodobacter capsulatus*, allowing growth on D- and L-malate as carbon sources without the need for both D- and L-malate dehydrogenases [283,284]. However, this bacterium does not possess any LarAH in its genome. GntEs are primarily found in bacteria and some unicellular eukaryotes (Fig. 2.2), such as *Phytophthora* species. The C2-epimerization of D-gluconate and D-mannonate likely enables these metabolites to enter the pentose phosphate pathway [87], the Entner-Doudoroff pathway [285,286], glucose metabolism [287], or uronic acid metabolism [288,289]. These interconnected biochemical pathways are crucial for carbohydrate processing. HGRs are found exclusively in bacteria (Fig. 2.2) and may have multifaceted roles, as both enantiomers of 2-hydroxyglutarate are involved in numerous physiological metabolic processes. For instance, D-2-HG is involved in L-serine biosynthesis, while L-2-HG is an intermediate in the lysine degradation pathway of many bacteria [30–32]. However, the accumulation of each of the two enantiomers can be toxic to bacterial cells [290–292]. By allowing the interconversion of D- and L-2-HG, HGRs could help maintain metabolic balance, enabling flexibility in energy and carbon utilization for the TCA cycle, managing toxic metabolites, or facilitating amino acid metabolism. For SARs, HHRs, and BSHIs, hypothesizing their specific roles is more complex due to their wide range of catalytic activities. SARs and HHRs are found exclusively in bacteria (Fig 2.2) and may enable the use of various isomers of HAs as carbon and/or electron sources. These LarAHs could also enable the use of hydroxy acids as precursors for their corresponding amino acids. For instance, *Clostridium sporogenes*, which possess one LarAH from the HHR family and one LarAH from the LAR family, can grow in a medium where most of the amino acids necessary for its growth have been replaced by L-AHAs analogues [293].

Of particular interest is the presence of LarAHs in various species found in both animal and human microbiomes (e.g. *Enterorcloster asparagiformis*, *Coprococcus catus*, *Megasphaera elsdenii*, *Staphylococcus epidermidis*). This association might be linked to the fact that several racemic mixtures of AHAs, such as 2-hydroxyisocaproate and 2-hydroxyisovalerate, which are substrates racemized by many LarAHs, have been associated with healthier metabolic parameters in mice [5]. Additionally, a widespread expression of LarAHs in the healthy human gut microbiota has been observed [294],

suggesting a significant role in this environment. One hypothesis is that LarAHs play a crucial role in anaerobic environments, particularly within the human microbiome, by participating in the metabolism of AHAs. It is possible that some metabolites, such as D-AHAs, require LarAH activity for detoxification. For example, two D-AHAs—D-lactate [8] and D-2-hydroxyglutarate [13,291]—have been shown to have adverse effects in humans, and other D-AHAs likely exhibit toxicity since they are not typical metabolites in eukaryotic cells. Given the prevalence of LARs and HGRs in the LarA superfamily, it is plausible that some of these LarAHs play a role in detoxifying these metabolites.

IV.3.2 Methodology for the determination of the *in vivo* role of LarAHs

We have imagined a methodology to study the *in vivo* role of LarAHs. A useful starting point would be to induce and identify a phenotype through phenotypic and metabolomic screening by disrupting NPN synthesis, thereby reducing the activity of all LarAHs in the organism. One effective approach involves deleting one of the NPN biosynthesis genes (*larB*, *larC*, or *larE*). Alternatively, the organism could be grown in a chemically defined medium (CDM) lacking nicotinic acid, a precursor of NaAD, which is itself a precursor of NPN. Another potential method is to use an inhibitor of the NaAD synthesis pathway [295]; however, this approach may affect NAD production, which is crucial for the survival of all living cells [296]. It is important to note that disrupting NPN biosynthesis in an organism possessing multiple NPN-dependent enzymes could induce a phenotype that is difficult to analyze, particularly if one of these enzymes is essential for host survival.

Therefore, when multiple LarAHs are present in the same organism it is necessary to study the impact of individually disrupting or deleting each gene on the organism's phenotype to determine the specific *in vivo* role of each LarAH in the organism. This can be done by assessing growth on various carbon sources and analyzing metabolite production using capillary electrophoresis (CE). Studying individual gene deletions will confirm the involvement of each LarAH to the phenotype observed with the disruption of NPN biosynthesis. In addition, *in vitro* biochemical characterization of the LarAHs will guide the design of specific assays to be performed. Therefore,

combining *in vitro* and *in vivo* studies of LarAHs from the same organism will provide complementary insights. To investigate less obvious phenotypes, Biolog phenotype microarrays [297] and untargeted metabolomics analyses using capillary electrophoresis-mass spectrometry (CE-MS) could be performed [298]. Overall, *in vivo* studies can be completed by *in vitro* studies of the purified LarAHs performed during this thesis, in order to determine the role of these enzymes.

IV.3.3 Species of interest

Following the outlined methodology, we initially aimed to investigate the *in vivo* role of LarAHs in *E. asparagiformis*, an obligate anaerobic, Gram-positive, rod-shaped bacterium found in the human gut microbiota. The advantage of studying *E. asparagiformis in vivo* lies in the fact that this bacterium was isolated from the faeces of a healthy human donor, and nine distinct *larAHs* (*larAH41-49*) were identified in its genome [299]. Our original plan involved using the Clostron gene deletion system to study these nine LarAHs [300,301]. However, *E. asparagiformis* had never been shown to be genetically tractable, presenting a challenge for genetic studies. Therefore, one of our objectives was to develop a method to genetically modify this strain. To facilitate genetic manipulation, we aimed to establish an electrotransformation protocol for *E. asparagiformis*. A review article indicated that *E. asparagiformis* does not have genes encoding a restriction-modification (RM) system [302], which would otherwise hinder electrotransformation. We then purified a series of *E. coli-Clostridium* shuttle vectors and attempted to transform them into *E. asparagiformis*. Using protocols based on common electrotransformation parameters for *Clostridia* and an optimized protocol for *Clostridium pasteurianum* transformation [302,303], we conducted several transformation attempts. Despite our efforts, none of these attempts resulted in successful transformation. After multiple unsuccessful transformation attempts, we analyzed the genome of *E. asparagiformis* to confirm the absence of a RM system gene. Surprisingly, eight potential RM systems were identified (Appendix – Table A3), explaining the repeated transformation failures. To successfully transform or conjugate *E. asparagiformis*, it will be necessary to bypass the active restriction enzymes, either by inactivation or by prior methylation of the transformed DNA. However, this is highly challenging due to the number of RM systems present.

As an alternative, we selected *C. pasteurianum, which possesses* three LarAHs (LarAH51-53), for our study. *C. pasteurianum* is an anaerobic, nitrogen-fixing bacterium known for its ability to produce butanol and other solvents in industrial fermentation processes [304,305]. This bacterium has an RM system that can be bypassed by DNA methylation and for which a transformation protocol has already been established [303]. Specifically, *C. pasteurianum* can be transformed with DNA that has been methylated *in vivo* in *E. coli* by the methyltransferase M.FnuDII, which protects the restriction site (5'-CGCG-3'). We obtained the plasmid pFnuDIIMKn, which expresses the M.FnuDII methyltransferase gene, allowing us to prepare methylated DNA for transformation in *C. pasteurianum*. To investigate the *in vivo* role of the three LarAHs in *C. pasteurianum*, the plan is to disrupt each corresponding gene using the CRISPR Cas9D10A nickase-assisted system [306]. This will involve constructing pCBE plasmids designed to specifically inactivate the LarAHs by mutating a catalytic histidine essential to their activity. Alternatively, the ClosTron system could be used, as initially intended for *E. asparagiformis* [300]. In *E. coli*, the pCBE plasmids can be co-transformed with the pFnuDIIMKn plasmid to obtain methylated pCBE plasmids. Subsequently, these methylated plasmids can be used for transformation into *C. pasteurianum* to generate mutants which will allows us to study the *in vivo* functions of the LarAHs of *C. pasteurianum*. The biochemical characterization of LarAH51 and LarAH52 of *C. pasteurianum*, conducted as part of this thesis (see Section III.2.1), will help target the tests to be performed. To investigate the roles of LarAH51 and LarAH52 in *C. pasteurianum*, we can monitor the growth of the wild-type (WT) strain using lactate and 2-hydroxy-4-oxo-4-phenylbutyrate as the sole carbon sources. Substrate consumption and metabolite production will be measured using the capillary electrophoresis (CE) method developed in this thesis. Comparative growth analysis of *larAH51* and *larAH52* knockout strains with the WT strain will be conducted using each enantiomer of lactate for *ΔlarAH51* and 2-hydroxy-4-oxo-4-phenylbutyrate for *ΔlarAH52*. Additionally, RNA sequencing could identify differentially expressed genes in the *Δ*strains relative to the WT, providing insights into compensatory pathways or stress responses due to the loss of these LarAHs.

Several other species within the human microbiome, such as *Blautia hydrogenotrophica* and *Coprococcus catus* [307,308], possess LarAHs that differ from those in *E. asparagiformis and C. pasteurianum*. These species

could also be investigated. Understanding the role of these LarAHs in various species will enhance our comprehension of the human microbiome and the potential positive impact of LarAHs, as indicated by a proteomic study [294].

Exploring the roles of LarAHs in different contexts, e.g. in archaea and in eukaryotes, could also provide interesting insights. For instance, biochemical characterization performed during this thesis demonstrated that LarAH15 of *Phytophthora nicotianae* is a D-gluconate C2-epimerase (see Section III.2.1). *Phytophtora* species are devastating oomycete plant pathogen [309,310]. Moreover, all the LarAHs detected in eukaryotes belong the GntE family and most belong to *Phytophtora* species (see Section III.2.1). D-gluconate C2-epimerase activity catalyzed by LarAH15 could be crucial for *Phytophthora species* metabolism (see Section IV.3.1) and could be targeted by fungicides. Hence, *P. nicotianae* will be utilized to study the role of LarAHs in eukaryotes, specifically the C2-epimerization of D-gluconate, as an efficient CRISPR/Cas9 genome editing tool has been developed for this species [311]. For the study of LarAHs in archaeal species, *Methanosarcina mazei* is a suitable candidate because it possesses a LarAH and can be genetically modified [312].

IV.4 LarAHs could catalyze other types or reaction?

The question naturally arises whether all LarAHs catalyze the racemization of AHAs or the C2-epimerization of PHAs. As previously mentioned, two histidine residues in LarA1 (His108 and His174) function as bases for the racemization of lactate [96]. These two histidine residues are conserved throughout most of the LarA superfamily. However, several phylogenetic groups of the LarA superfamily contain LarAHs with only a single catalytic histidine [210], suggesting that these enzymes might catalyze other types of reaction. These particular LarAHs possess a residue corresponding to His108 of LarA1 but lack a residue equivalent to His174 of LarA1. This observation provides insight into the potential reactions catalyzed by these enzymes, given that His108 of LarA1 interacts with D-lactate, while His174 of LarA1 interacts with L-lactate [136]. If these LarAHs are also active on HAs, it is likely that they will primarily act on D-AHAs since only His108 is conserved in their catalytic site. Conversely, if only His174 were conserved, these LarAHs would be expected to act on L-AHAs. Furthermore, the presence of a single catalytic histidine implies that the chirality of the substrate and product will be preserved during the reaction. Considering the wide array of reactions

mediated by pincer complexes, such as the NPN [125,128], these LarAHs could potentially catalyze various other NPN-catalyzed reactions playing significant roles in some bacteria and archaea species. To date, four LarAHs from phylogenetic groups lacking His174 have been purified: LarAH13 from *Blautia wexlerea*, LarAH17 from *Frankia sp*., LarAH33 from *Myxococcus fulvus*, and LarAH36 from *Escherichia fergusonii*. We tested the activity of these LarAHs with a panel of HAs and detected no activity, supporting our hypothesis that they are neither racemases nor epimerases of AHAs.

IV.4.1 Deamination of D-amino acids to D-AHAs

The LarAH group lacking His174 may catalyze the conversion of amino acids into AHAs. In the proposed mechanism, a LarAH bound to NPN would remove a hydride from a D-amino acid, leading to the formation of an imine intermediate. A water molecule subsequently reacts with the imine intermediate, which releases ammonia (NH_3) and transforms the imine into a ketone intermediate. By reintroducing the hydride, the LarAH reduces the ketone to a hydroxyl group, producing the corresponding D-AHA from the D-amino acid. For example, these LarAHs could catalyze the deamination of D-alanine to D-lactate (Fig. 12A).

The significance of these potential reactions stems from the fact that D-Amino acids are associated with beneficial effects on bacterial metabolism and growth, but also with adverse effects [313,314]. For instance, high levels of D-serine are toxic in bacteria by inhibiting protein synthesis [315] and D-arginine is highly toxic to a wide variety of bacterial species [316]. Amino acid racemases would be an efficient way of detoxifying D-amino acids into L-amino acids [314]. However, these LarAHs could provide an alternative pathway for degrading D-amino acids into a nitrogen source (NH_3) and a carbon source (D-AHA), allowing detoxification and catabolic function at the same time [317]. Such a reaction catalyzed by a single enzyme has never been demonstrated. However, such a reaction is possible through the consecutive action of an L-amino acid deaminase (LAAD) and a AHA dehydrogenase [318–320].

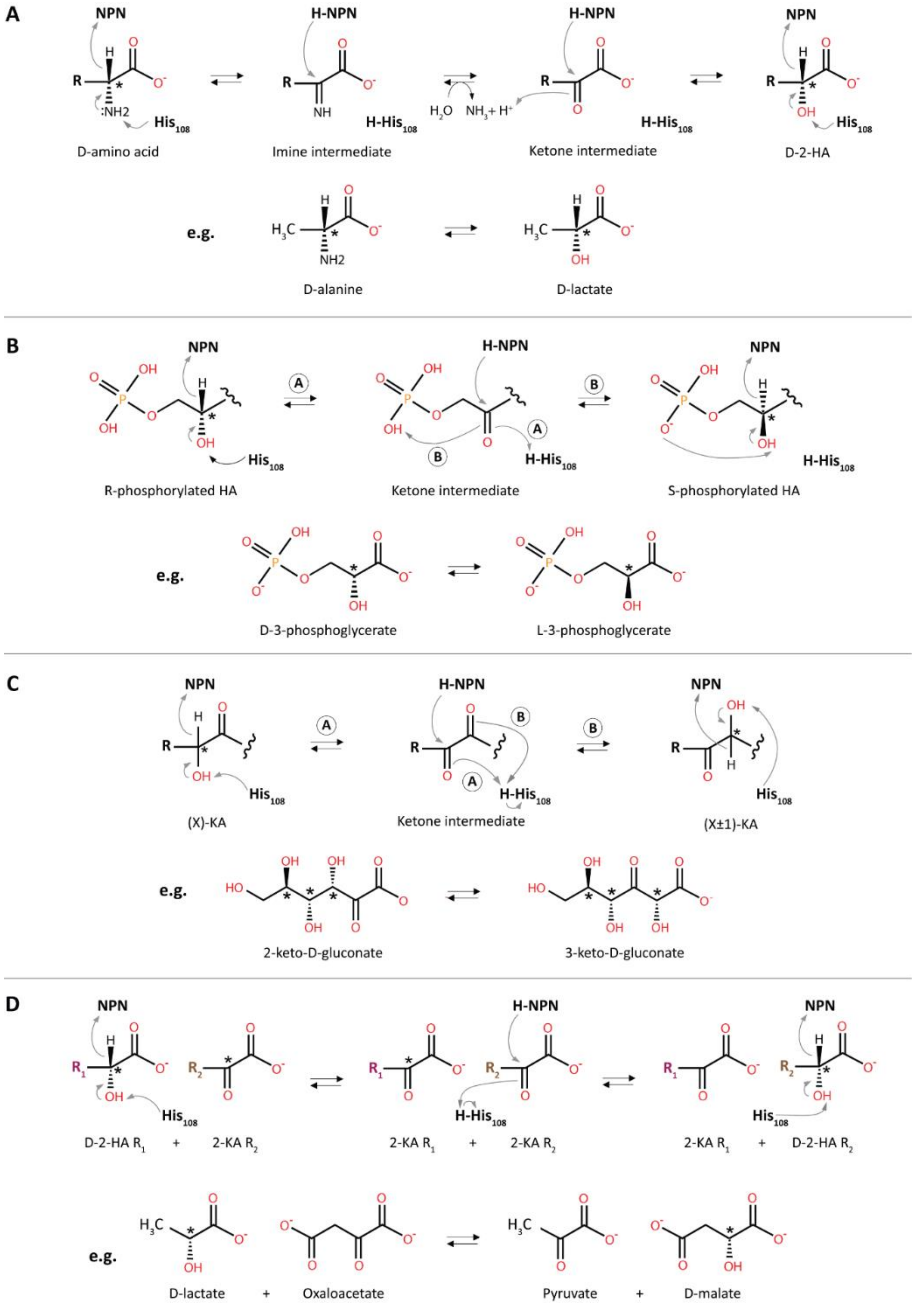

Figure 12 | Reactions potentially catalyzed by LarAHs with His108 as the sole catalytic histidine. (**A**) Deamination of amino acids to AHAs. (**B**) Racemization or C2-epimerization of phosphorylated HAs. (**C**) Intramolecular oxidoreductions of HAs. (**D**) Trans-hydroxylation of AHAs and their corresponding α-keto acids (AKAs)

IV.4.2 Racemization or C2-epimerization of phosphorylated AHAs

LarAHs with a single catalytic histidine could catalyze the racemization or C2-epimerization of phosphorylated AHAs. This could occur through substrate-assisted catalysis, where the substrate provides a catalytic element necessary for the reaction [320]. Given that the phosphate group of a phosphorylated AHA has a pKa_2 of around 7.2, the substrate can act as both an acid and a base, ideally placed to substitute for His174, which has a pKa of 6. Thus, His174 encumbering the active site may have disappeared to make room for the phosphate group. In this proposed mechanism, His108 would abstract the proton from the hydroxyl group of the phosphorylated R-AHA, while the phosphate group of the substrate would remove the proton from the hydroxyl group of the phosphorylated S-AHA (Fig. 12B). For example, these LarAHs could catalyze the racemization of molecules such as 3-phosphoglycerate or 6-phosphogluconate. Metabolically, this is relevant because phosphorylated AHAs such as D-3-phophoglycerate and D-6-phosphogluconate are crucial intermediates in the metabolism of bacteria and archaea [321–323]. However, L-3-phosphoglycerate and D-6-phosphomannonate have never been observed in nature [324], and no racemases or epimerases of phosphorylated AHAs have been identified to date. Furthermore, L-3-phosphoglycerate and D-6-phosphomannonate are not commercially available, making it difficult to assess a potential isomerization reaction.

IV.4.3 Intramolecular oxidoreduction of AHAs

Other types of isomerization reactions could be catalyzed by hydride transfer and should be considered. Instead of racemization or C2-epimerization, a LarAH lacking a residue corresponding to His174 of LarA1 may use a single isomer and transfer the hydride between two different carbons within the same AHA, achieving intramolecular oxidoreduction. For example, these LarAHs could catalyze the intramolecular oxidoreduction of 2-keto-D-gluconate to 3-keto-D-gluconate (Fig. 12C). Alternatively, these LarAH might actually possess a residue corresponding to His174 of LarA1 but positioned differently within the catalytic site. In this scenario, the residue must be situated near a carbon adjacent to the one from which the hydride is removed, rather than on the opposite side. This positioning would explain why the residue does not align with His174 of LarA1.

IV.4.4 Trans-hydroxylation of AHAs and α-keto acids (AKAs)

LarAHs with His108 as the sole catalytic histidine could potentially catalyze trans-hydroxylation reactions. The reactions involve the interconversion between two substrates, a D-AHA with side chain R_1 (D-AHA_{R1}) and a 2-keto acid with side chain R_2 (AKA_{R2}), and two products, a L-AHA with side chain R_2 (L-AHA_{R2}) and a 2-keto acid with side chain R_1 (AKA_{R1}) (Fig. 12D). For this reaction to occur, either both substrates must fit into the catalytic pocket simultaneously, which is highly unlikely as both substrates would have to be very close to the NPN, or one substrate must enter and exit the active site before the second substrate enters. This latter process is characteristic of a ping-pong (double-displacement) mechanism, commonly observed in enzymes [325], particularly in transaminases (aminotransferases) [326,327]. If these LarAHs operate via a ping-pong mechanism, the NPN would be in its reduced form when the D-AHA exits the catalytic site to let the 2-KA in. However, this type of reaction is also unlikely, given the instability of reduced NPN. Such a reaction would be completely new, as in the LarA1 mechanism, the pyruvate intermediate does not leave the catalytic site nor accumulate [124]. In this hypothetical reaction, His108 would abstract the proton from the hydroxyl of the D-AHA and transfer it to the ketone of the AKA. Concurrently, NPN would accept the hydride from the C2 of the D-AHA and transfer it to the C2 of the 2-KA. For instance, these LarAHs could catalyze the trans-hydroxylation of D-lactate and oxaloacetate to D-malate and pyruvate, and vice versa, through the following steps: (1) D-lactate enters the catalytic site and is oxidized to pyruvate; (2) pyruvate exits the catalytic site; (3) oxaloacetate enters the catalytic site and is reduced to D-malate.

IV.5 Prevalence and distribution of the NPN in Nature

The genes coding for the NPN-biosynthesis enzymes were identified without a *larA* gene in 15% of bacterial and archaeal genomes, suggesting that enzymes that are not homologous to LarA use NPN as well (see Section I.3.1) [95]. In microbial genomes, the NPN biosynthetic genes are found twice as frequently as those for *larAHs* [130]. This over-representation of *larBCE* relative to *larAHs* may indicate that NPN is used by enzymes catalyzing reactions other than HA racemization or C2-epimerization, not necessarily involving hydride transfer. Considering the diverse reactions mediated by pincer complexes [125], the range of their possible catalytic activities is vast, although nature has selected only a few [128]. It is likely that entire undiscovered enzyme superfamilies are catalyzing these reactions, offering significant potential for further biochemical research. Therefore, one of the main perspectives is to identify NPN-dependent enzymes that perform other chemical reactions.

IV.5.1 *In silico* identification of NPN-dependent non-LarAH enzymes

A bioinformatics analysis, based on genome-scale gene associations among COGs, identified several superfamilies of unknown proteins as probable NPN-dependent enzymes. By examining the COGs database [328,329], all COGs typically associated with *larB* genes (COG1691) in prokaryotic genomes were identified (data of Prof. Benoît Desguin). This analysis revealed that, in addition to the LarA superfamily (COG3875), several other enzyme superfamilies have a co-occurrence of more than 80% with *larB* genes. These include COG1453 (Predicted oxidoreductase of the aldo/keto reductase family), COG1625 (Fe-S oxidoreductase, related to NifB/MoaA family), COG1915 (Uncharacterized conserved protein), COG2006 (Uncharacterized conserved protein). All identified COGs are prevalent in prokaryotes, especially among cyanobacteria and archaea, coding for protein superfamilies of unknown function (Table 4).

Table 4 | **The LarA superfamily (COG3875) and other potential NPN-dependent superfamilies.** The occurrence represents the percentage of organisms possessing at least one enzyme from the indicated COGs. Data assembled from the COGs database on the NCBI obtained on June, 2024.

	COG3875	COG1453	COG1915	COG1625	COG2006
Occurence in bacteria (%)	14	16	7	11	15
Occurrence in cyanobacteria (%)	5	95	76	98	85
Occurence in archaea (%)	22	29	44	25	21

IV.5.2 *In vitro* identification of NPN-dependent non-LarAH enzymes

In organisms containing the *larBCE* genes but lacking *larAH* genes, a novel approach using affinity chromatography could identify new NPN-dependent enzymes without knowing their encoding genes. This strategy utilizes the covalent binding of the NPN to LarA1 at Lys184. It involves synthesizing an NPN-Strep-tag hybrid peptide, with the Strep-tag situated at one end and the NPN cofactor at the other, by generating a *larA1* construct with the Strep-tag near Lys184 (Fig. 13A). The construct is used to overexpress and purify LarA with the internal Strep-tag. The entire proteome is then digested with trypsin, producing the hybrid NPN-Strep-tag peptide. By passing the trypsin-digested proteome through a Strep-tactin column, the NPN-Strep-tag hybrid peptide can bind to it. Then, the cell lysate from an organism with NPN-dependent enzymes is passed through this column, capturing all NPN-dependent enzymes. The absence of competing NPN in the cell lysate can be ensured by genetic disruption of the NPN biosynthesis pathway. Captured NPN-dependent proteins are then eluted and identified using trypsin digestion followed by LC-MS analysis (Fig. 13A).

Alternatively, organisms could be grown in CDM with tetradeuterated or non-labelled nicotinic acid, followed by trypsin digestion and LC-MS analysis of the peptides (Fig. 13B). Comparing results could reveal NPNylated peptides with a two Dalton mass difference since the NPN cofactor is derived from nicotinic acid and retains two of its hydrogen atoms after biosynthesis [96]. This strategy requires cells that are auxotrophic for niacin or downregulate their de novo biosynthesis in the presence of exogenous niacin, as seen in many bacterial species [330]. Additionally, another approach involves using radiolabeled nickel (^{63}Ni) in the CDM, detecting

labeled NPN-dependent enzymes via 2D gel electrophoresis (Fig. 13C) [331,332]. This must be done in an anoxic environment to prevent NPN oxidation and nickel loss. However, this approach may also label other nickel enzymes.

IV.5.3 Prokaryotes with *larBCE* and without *larAH* worth investigating

NPN-dependent enzymes unrelated to LarA could be identified and studied in many bacteria and archaea. To investigate the reactions catalyzed by NPN-dependent enzymes identified through *in silico* or *in vitro* analysis, the same methodology as for the *in vitro* and *in vivo* study of LarAHs can be employed. This includes phylogenetic clustering, genome context examination, Biolog phenotype microarrays, and *in vitro* studies on the purified enzymes to test hypotheses regarding their catalytic activities (see. section IV.3.2).

Among bacteria, these enzymes could play significant role, particularly in cyanobacteria, where the identified COGs and *larBCE* genes are nearly universally present (Table 4), although not in a conserved cluster [95]. Unpublished results involving recombinantly expressed *larC* from *Synechocystis sp*. PCC 6803 demonstrated its ability to convert P2TMN into the NPN cofactor. This conversion was evidenced by the capacity of the product to activate LarA2 and racemize lactate [130]. Additionally, COG1625, COG1453, COG2006, and COG1915 are present in most cyanobacterial genomes from the COG database (Table 4). These findings suggest that cyanobacteria synthesize the NPN cofactor, which functions in several non-LarA-like proteins. Further supporting this hypothesis, the deletion of the LarB homolog-encoding gene, *cpmA*, in *Synechococcus elongatus* PCC 7942 resulted in a severe growth defect and an altered circadian phasing phenotype [333]. The methods described in IV.5.2 could be applied to cyanobacterial species such as *Synechocystis* sp. PCC 6803, *Synechococcus* PCC7942, as CDMs and DNA manipulation techniques have been developed for these species [334–336]. Another bacterium of particular interest is *Akkermansia muciniphila*, which possesses LarBCE and an enzyme from the COG2006. This interest stems from the fact that *A. muciniphila* is one of the most abundant single species in the human intestinal microbiota and is negatively correlated with obesity, diabetes, cardiometabolic diseases, and low-grade inflammation [337–339].

Among archaea, NPN-dependent enzymes unrelated to LarA are also prevalent, especially the COG1915, present in 44% of archaea in the COG database (Table 4). These enzymes may contribute to methanogenesis, as suggested by the omnipresence of *larBCE* genes, generally without the *larA* gene, in methanogenic archaea [95]. *Methanococcus maripaludis*, which is genetically modifiable [312], may serve as an excellent model organism for studying the role of NPN-dependent enzymes in methanogenesis. Other notable archaea to investigate include *Haloferax volcanii*, a halophilic archaeon for which a CDM and genetic tools have also been developed [340,341].

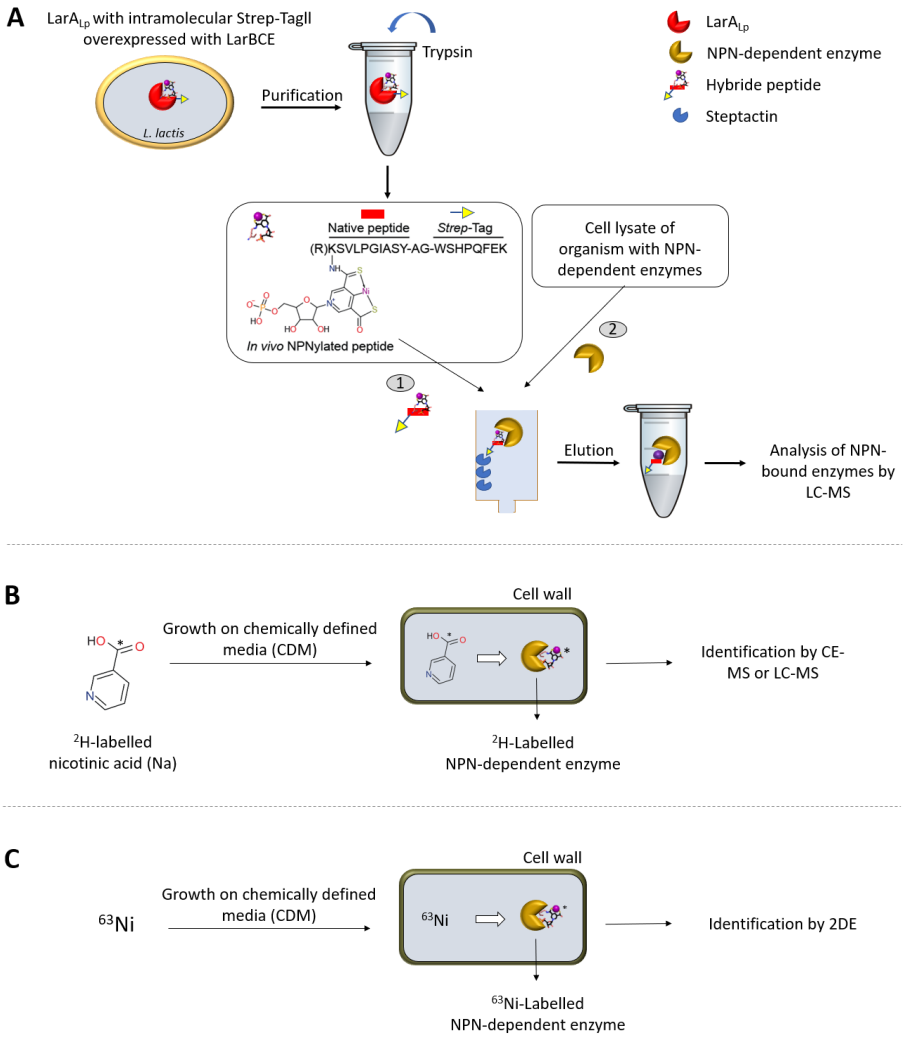

Figure 13 | *In vitro* identification of NPN-dependent enzymes unrelated to LarA. (**A**) Affinity chromatography for NPN-dependent enzyme with NPN-Strep-tag hybrid peptide. (**B**) ^{2}H-labeling of NPN-dependent enzyme. (**C**) ^{63}Ni-labeling of NPN-dependent enzyme.

IV.6 Conclusion

HAs are organic carboxylic acids that are ubiquitous in nature and play significant roles in various industrial and biological processes. The present work focused on the exploration, characterization and potential biotechnological applications of the LarA superfamily, a superfamily of hydroxy acid racemases and epimerases using the NPN cofactor.

More specifically, we first developed a versatile and efficient CE method for the chiral analysis of HA stereoisomers, providing a robust tool for studying the LarA superfamily. This method allows high-resolution separation and quantification of a wide range of underivatized stereoisomers in the three main HA categories: AHAs, BHAs and PHAs. Furthermore, the chiral analysis of underivatized PHAs, an area previously undocumented in the literature, opens new avenues for the study of sugar acids.

Using the developed CE method and a combination of biochemical, taxonomic and structural analysis, we showed the prevalence of seven LarAH families within the LarA superfamily, suggesting their metabolic importance across diverse organisms: LARs, SARs, MARs, HGRs, HHRs, GntEs and BSHIs. Among these LarAHs families, we identified and characterized the substrate specificities of three additional LARs, one additional MAR, one additional HGR, one additional GntE, three HHRs, and four BSHIs. Our results revealed that LarAHs are much more promiscuous than previously thought, with LARs also catalyzing the racemization of glycerate and hydroxybutyrate, HHRs catalyzing up to 16 distinct isomerization reactions, and BSHIs catalyzing up to 39 distinct isomerization reactions. These include 11 novel racemization reactions spanning the three major classes of AHAs (aliphatic, aromatic, and polycarboxylic AHAs) and 22 novel C2-epimerization reactions of PHAs spanning the three major classes of sugar acids (aldonic, uronic, and aldaric acids). Overall, our findings have significantly expanded the scope of NPN-dependent reactions catalyzed by members of the LarA superfamily.

More broadly, these investigations show the remarkable adaptability and importance of NPN-dependent enzymes for catalyzing isomerization reactions in bacteria and archaea. The wide range of reactions catalyzed by LarAHs present promising avenues for the biosynthesis of valuable stereoisomers of AHAs and PHAs, offering new possibilities for biotechnological applications.

V. APPENDIX

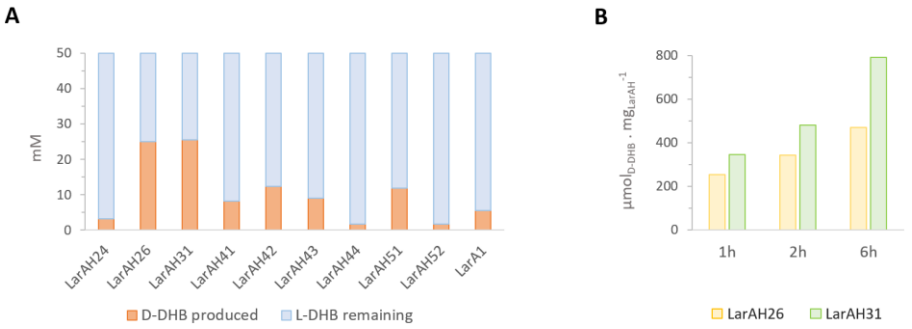

Figure A1 | Determination of the best LarAH candidate for D-DHB production from L-DHB. (**A**) Quantity of D-DHB produced by LarAHs at 37°C during 6h. Reaction conditions: 2 µM LarAH, 5 µM NPN, 50 mM L-DHB, 100 mM Tris-HCL pH 7.5. (**B**) Quantity of D-DHB produced per milligram of LarAH26 and LarAH31 at 37°C during 1h, 2h and 6h. Reaction conditions: 0.4 µM LarAH, 2 µM NPN, 100 mM L-DHB, 100 mM Tris-HCL pH 7.5.

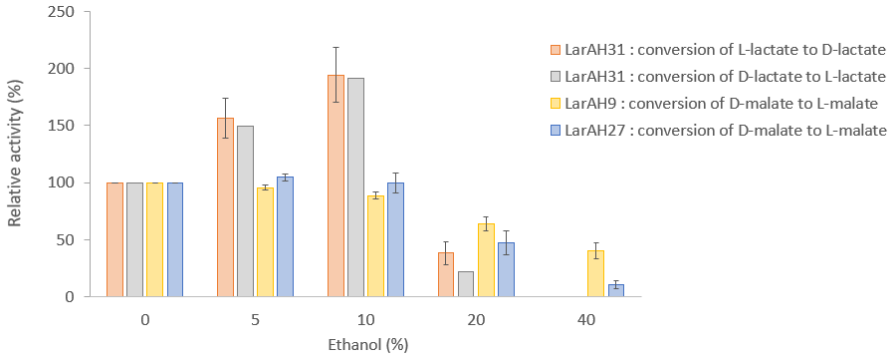

Figure A2 | Relative activity of LarAH9, LarAH27 and LarAH31 with various concentrations of ethanol. (A) LarAH31: conversion of L-lactate to D-lactate. (B) LarAH31 : conversion of D-lactate to L-lactate. (C) LarAH9: conversion of D-malate to L-malate. (D) LarAH27: conversion of D-malate to L-malate

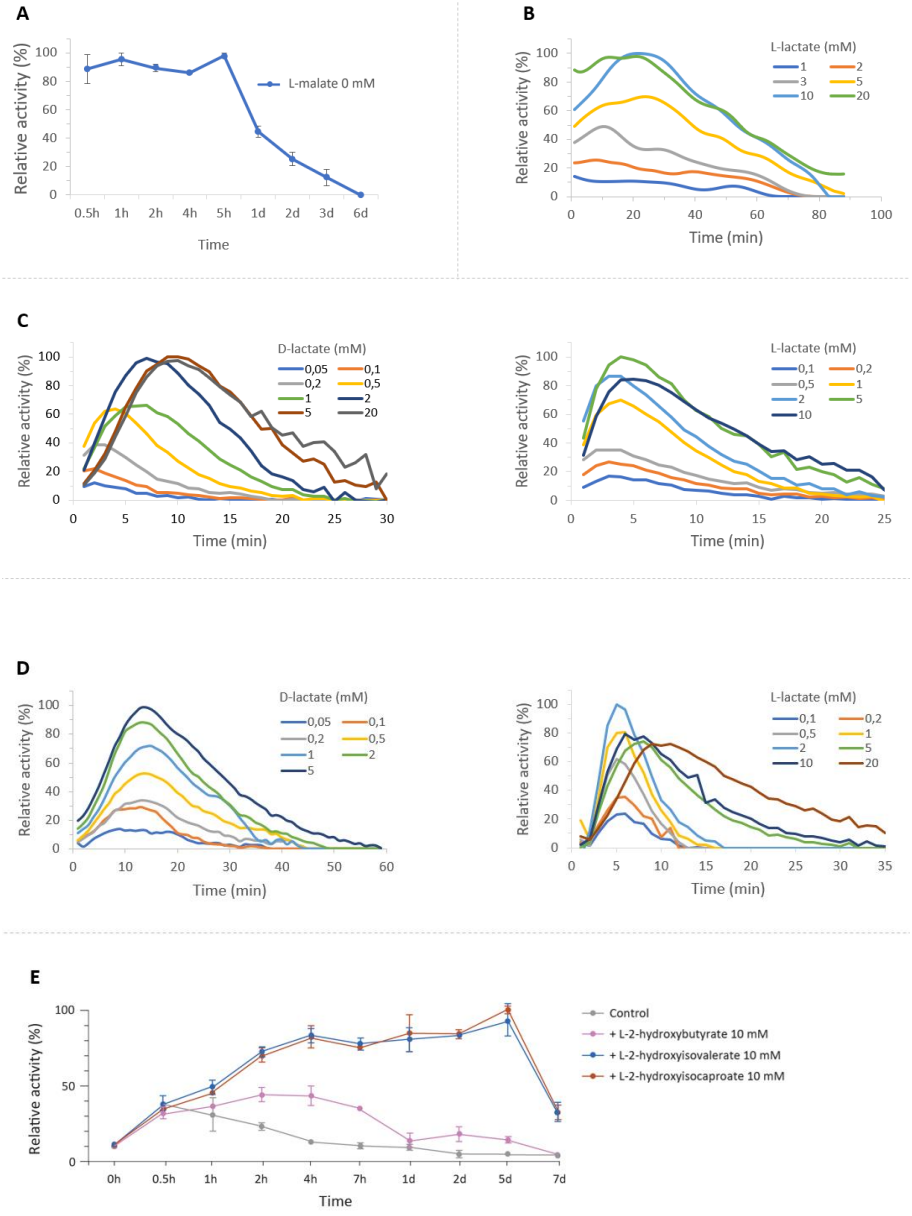

Figure A3 | Stability studies of (A) LarAH41 from *E. asparagiformis,* (B) LarAH42 from *E. asparagiformis,* (C) LarAH43 from *E. asparagiformis*, (D) LarAH51 from *C. pasteurianum*, (E) LarAH2/SAR from *I. pallida*. The curves for the short time (less than 100 min) stability studies are the data points (every min) of one representative experiment. The error bars in the long time (more than 1 day) stability studies represent the standard deviation (n=2). h : hour, d : day.

Table A1 | **Catalytic efficiencies of LarAH2/SAR.** The k_{cat}/K_M value of L-lactate was obtained experimentally [92]. Additional k_{cat}/K_M values were calculated using the experimentally determined k_{cat}/K_M and relative k_{cat}/K_M values.

Reactions	**Relative k_{cat}/K_M (%)**	**k_{cat}/K_M (M^{-1} s^{-1})**
Racemization of AHAs		
L- ↔ D-lactate	100 ± 0	(31 ± 9) x 10^3
L- ↔ D-2-hydroxybutyrate	95 ± 3	(30 ± 8) x 10^3
L- ↔ D-glycerate	26 ± 5	(82 ± 27) x 10^2
L- ↔ D-2,4-dihydroxybutyrate	16 ± 3	(51 ± 16) x 10^2
L- ↔ D-2-hydroxyvalerate	9.1 ± 0.9	(28 ± 8) x 10^2
L- ↔ D-2-hydroxyisovalerate	6.2 ± 1.5	(19 ± 7) x 10^2
L- ↔ D-2-hydroxyisocaproate	3.4 ± 0.4	(11 ± 3) x 10^2
L- ↔ D-3-phenyllactate	0.85 ± 0.09	(27 ± 8) x 10^1
L- ↔ D-2-hydroxy-4-phenylbutyrate	0.39 ± 0.08	(13 ± 4) x 10^1
L- ↔ D-2-hydroxy-3,3-dimethylbutyrate	0.17 ± 0.02	53 ± 16
L- ↔ D-2,3-dihydroxyisovalerate	0.13 ± 0.03	15 ± 15
C2-epimerization of sugar acids		
4-deoxy-L-threonate ↔ 4-deoxy-L-erythronate	4.8 ± 1.2	(15 ± 5) x 10^2
4-deoxy-D-threonate ↔ 4-deoxy-D-erythronate	2.8 ± 0.5	(89 ± 28) x 10^1
L-threonate ↔ L-erythronate	1.8 ± 0.4	(56 ± 20) x 10^1
D-threonate ↔ D-erythronate	1.3 ± 0.3	(42 ± 14) x 10^1

Table A2 | **Half life of LarAH41, LarAH42, LarAH43 from *E. asparagiformis* and LarAH51 from *C. pasteurianum.***

Enzyme	Substrate	$t_{1/2}$ at [S] [a]			
		0 mM	**0,5 mM**	**5 mM**	**20 mM**
LarAH41	L-malate	± 15h	NI	NI	NI
LarAH42	L-lactate	NI	30 min	31 min	34 min
LarAH43	D-lactate	NI	6 min	9 min	10
	L-lactate	NI	6 min	8 min	NI
LarAH51	D-lactate	NI	11 min	15 min	NI
	L-lactate	NI	4 min	6 min	11 min

[a]$t_{1/2}$: time after which the activity was around 50% of the maximum activity observed at room temperature and pH 8; analyzed for sample with the indicated concentration of substrate ([S])
NI: not investigated.

Table A3 | **Methyltransferases belonging to RM systems identified in *E. asparagiformis.***

Function	Accession N°
DNA adenine methylase	MBS5606717.1
DNA adenine methylase	EEG53573.1
Site-specific DNA-methyltransferase	WP_083790338.1
Site-specific DNA-methyltransferase	MBS6952417.1
Site-specific DNA-methyltransferase	RGX29093.1
DNA adenine methylase	MBS6955375.1
DNA adenine methylase	EEG52923.1
Cytosine methyltransferase	MBS6956682.1

VI. REFERENCES

[1] T.C. Bhalla, V. Kumar, S.K. Bhatia, Hydroxy Acids : Production and Applications, Adv. Ind. Biotechnol. (2014) 56–76.

[2] A. Kornhauser, S.G. Coelho, V.J. Hearing, Applications of hydroxy acids: classification, mechanisms, and photoactivity, Clin. Cosmet. Investig. Dermatol. 3 (2010) 135–142. https://doi.org/https://doi.org/10.2147/ccid.s9042.

[3] J.F. Robyt, Essentials of Carbohydrate Chemistry, 1st ed., Springer, 1998. https://doi.org/doi.org/10.1007/978-1-4612-1622-3.

[4] R.J. Ferrier, P.C. Collins, Monosaccharides: Their Chemistry and Their Roles in Natural Products, Wiley-VCH, 1995.

[5] N. Daniel, R.T. Nachbar, T.T.T. Tran, A. Ouellette, T.V. Varin, A. Cotillard, L. Quinquis, A. Gagné, P. St-Pierre, J. Trottier, B. Marcotte, M. Poirel, M. Saccareau, M.J. Dubois, P. Joubert, O. Barbier, H. Koutnikova, A. Marette, Gut microbiota and fermentation-derived branched chain hydroxy acids mediate health benefits of yogurt consumption in obese mice, Nat. Commun. 13 (2022). https://doi.org/10.1038/s41467-022-29005-0.

[6] S. Passarella, L. de Bari, D. Valenti, R. Pizzuto, G. Paventi, A. Atlante, Mitochondria and l-lactate metabolism, FEBS Lett. 582 (2008) 3569–3576. https://doi.org/10.1016/j.febslet.2008.09.042.

[7] M.L. Halperin, K.S. Kamel, D-lactic acidosis: Turning sugar into acids in the gastrointestinal tract, Kidney Int. 49 (1996) 1–8. https://doi.org/10.1038/ki.1996.1.

[8] D.G.A.M. Bianchetti, G.S. Amelio, S.A.G. Lava, M.G. Bianchetti, G.D. Simonetti, C. Agostoni, E.F. Fossali, G.P. Milani, D-lactic acidosis in humans: systematic literature review, Pediatr. Nephrol. 33 (2018) 673–681. https://doi.org/10.1007/s00467-017-3844-8.

[9] R. Rzem, M. Veiga-Da-Cunha, G. Noël, S. Goffette, M.C. Nassogne, B. Tabarki, C. Schöller, T. Marquardt, M. Vikkula, E. Van Schaftingen, A gene encoding a putative FAD-dependent L-2-hydroxyglutarate dehydrogenase is mutated in L-2-hydroxyglutaric aciduria, Proc. Natl. Acad. Sci. U. S. A. 101 (2004) 16849–16854. https://doi.org/10.1073/pnas.0404840101.

[10] M. Kranendijk, E.A. Struys, K.M. Gibson, W. V. Wickenhagen, J.E. Abdenur, J. Buechner, E. Christensen, R.D. De Kremer, A. Errami, P. Gissen, W. Gradowska, E. Hobson, L. Islam, S.H. Korman, T. Kurczynski, B. Maranda, C. Meli, C. Rizzo, C. Sansaricq, F.K. Trefz, R. Webster, C. Jakobs, G.S. Salomons, Evidence for genetic heterogeneity in D-2-hydroxyglutaric aciduria, Hum. Mutat. 31 (2010) 279–283. https://doi.org/10.1002/humu.21186.

[11] L. Dang, D.W. White, S. Gross, B.D. Bennett, M.A. Bittinger, E.M. Driggers, V.R. Fantin, H.G. Jang, S. Jin, M.C. Keenan, K.M. Marks, R.M. Prins, P.S. Ward, K.E. Yen, L.M. Liau, J.D. Rabinowitz, L.C. Cantley, C.B. Thompson, M.G. Vander Heiden, S.M. Su, M. Su, Cancer-associated IDH1 mutations produce 2-hydroxyglutarate, Nature. 462 (2009) 739. https://doi.org/10.1038/nature08617.

[12] M. Kranendijk, E.A. Struys, G.S. Salomons, M.S. Van Der Knaap, C. Jakobs, Progress in understanding 2-hydroxyglutaric acidurias, J. Inherit. Metab. Dis. 35 (2012) 571–587. https://doi.org/10.1007/s10545-012-9462-5.

[13] C. Reiter-Brennan, L. Semmler, A. Klein, The effects of 2-hydroxyglutarate on the tumorigenesis of gliomas, Contemp Oncol. 22 (2018) 215–222. https://doi.org/10.5114/wo.2018.82642.

[14] P. Ježek, 2-Hydroxyglutarate in Cancer Cells, Antioxidants Redox Signal. 33 (2020) 903–926. https://doi.org/10.1089/ars.2019.7902.

[15] V.G. Maurino, M.K.M. Engqvist, 2-Hydroxy Acids in Plant Metabolism, Arab. B. 13 (2015) e0182. https://doi.org/10.1199/tab.0182.

[16] K.M. Kean, P.A. Karplus, Structure and role for active site lid of lactate monooxygenase from Mycobacterium smegmatis, Protein Sci. 28 (2019) 135–149. https://doi.org/10.1002/pro.3506.

[17] D.W. Reed, P.L. Hartzell, The Archaeoglobus fulgidus D-lactate dehydrogenase is a Zn2+ flavoprotein, J. Bacteriol. 181 (1999) 7580–7587. https://doi.org/10.1128/jb.181.24.7580-7587.1999.

[18] A. Oren, P. Gurevich, Diversity of lactate metabolism in halophilic archaea, Can. J. Microbiol. 41 (1995) 302–307. https://doi.org/10.1139/m95-042.

[19] R.K. Thauer, K. Jungermann, K. Decker, Energy Conservation in Chemotrophic Anaerobic Bacteria, Manag. Res. News. 41 (1977) 100–180. https://doi.org/10.1108/eb027807.

[20] M. Falb, K. Müller, L. Königsmaier, T. Oberwinkler, P. Horn, S. Von Gronau, O. Gonzalez, F. Pfeiffer, E. Bornberg-Bauer, D. Oesterhelt, Metabolism of halophilic archaea, Extremophiles. 12 (2008) 177–196. https://doi.org/10.1007/s00792-008-0138-x.

[21] Y. Wang, J. Wu, M. Lv, Z. Shao, M. Hungwe, J. Wang, X. Bai, J. Xie, Y. Wang, W. Geng, Metabolism Characteristics of Lactic Acid Bacteria and the Expanding Applications in Food Industry, Front. Bioeng. Biotechnol. 9 (2021) 1–19. https://doi.org/10.3389/fbioe.2021.612285.

[22] W. Fukuda, Y.S. Ismail, T. Fukui, H. Atomi, T. Imanaka, Characterization of an archaeal malic enzyme from the hyperthermophilic archaeon Thermococcus kodakaraensis KOD1, Archaea. 1 (2005) 293–301. https://doi.org/10.1155/2005/250757.

[23] L.J. Yennaco, Y. Hu, J.F. Holden, Characterization of malate dehydrogenase from the hyperthermophilic archaeon Pyrobaculum islandicum, Extremophiles. 11 (2007) 741–746. https://doi.org/10.1007/s00792-007-0081-2.

[24] J. Roche, E. Girard, C. Mas, D. Madern, The archaeal LDH-like malate dehydrogenase from Ignicoccus islandicus displays dual substrate recognition, hidden allostery and a non-canonical tetrameric oligomeric organization, J. Struct. Biol. 208 (2019) 7–17. https://doi.org/10.1016/j.jsb.2019.07.006.

[25] J.A. Serrano, M. Camacho, M.J. Bonete, Operation of glyoxylate cycle in halophilic archaea: Presence of malate synthase and isocitrate lyase in Haloferax volcanii, FEBS Lett. 434 (1998) 13–16. https://doi.org/10.1016/S0014-5793(98)00911-9.

[26] F.M. Meyer, J. Stülke, Malate metabolism in Bacillus subtilis: Distinct roles for three classes of malate-oxidizing enzymes, FEMS Microbiol. Lett. 339 (2013) 17–22. https://doi.org/10.1111/1574-6968.12041.

[27] L. Xiong, E. Chan, J.L.L. Teng, S. Liu, S.K.P. Lau, P.C.Y. Woo, Malate-dependent carbon utilization enhances central metabolism and contributes to biological fitness of laribacter hongkongensis via CRP regulation, Front. Microbiol. 10 (2019). https://doi.org/10.3389/fmicb.2019.01991.

[28] J.P. Grossman, J.R. Postgate, The metabolism of malate and certain other compounds by Desulphovibrio desulphuricans, J. Gen. Microbiol. 12 (1955) 429–445. https://doi.org/10.1099/00221287-12-3-429.

[29] A.A. Vorobieva, M.S. Khan, P. Soumillion, Escherichia coli D-malate dehydrogenase, a generalist enzyme active in the leucine biosynthesis pathway, J. Biol. Chem. 289 (2014) 29086–29096. https://doi.org/10.1074/jbc.M114.595363.

[30] S. Knorr, M. Sinn, D. Galetskiy, R.M. Williams, C. Wang, N. Müller, O. Mayans, D. Schleheck, J.S. Hartig, Widespread bacterial lysine degradation proceeding via glutarate and L-2-hydroxyglutarate, Nat. Commun. 9 (2018) 2–11. https://doi.org/10.1038/s41467-018-07563-6.

[31] W. Zhang, M. Zhang, C. Gao, Y. Zhang, Y. Ge, S. Guo, X. Guo, Z. Zhou, Q. Liu, Y. Zhang, C. Ma, F. Tao, P. Xu, Coupling between D-3-phosphoglycerate

dehydrogenase and D-2-hydroxyglutarate dehydrogenase drives bacterial L-serine synthesis, Proc. Natl. Acad. Sci. U. S. A. 114 (2017) E7574–E7582. https://doi.org/10.1073/pnas.1619034114.

[32] X. Guo, M. Zhang, M. Cao, W. Zhang, Z. Kang, P. Xu, C. Ma, C. Gao, D-2-Hydroxyglutarate dehydrogenase plays a dual role in L-serine biosynthesis and D-malate utilization in the bacterium Pseudomonas stutzeri, J. Biol. Chem. 293 (2018) 15513–15523. https://doi.org/10.1074/jbc.RA118.003897.

[33] J.C. Páez-Franco, J. Torres-Ruiz, V.A. Sosa-Hernández, R. Cervantes-Díaz, S. Romero-Ramírez, A. Pérez-Fragoso, D.E. Meza-Sánchez, J.M. Germán-Acacio, J.L. Maravillas-Montero, N.R. Mejía-Domínguez, A. Ponce-de-León, A. Ulloa-Aguirre, D. Gómez-Martín, L. Llorente, Metabolomics analysis reveals a modified amino acid metabolism that correlates with altered oxygen homeostasis in COVID-19 patients, Sci. Rep. 11 (2021) 1–12. https://doi.org/10.1038/s41598-021-85788-0.

[34] P. Goffin, M. Deghorain, J.L. Mainardi, I. Tytgat, M.C. Champomier-Vergès, M. Kleerebezem, P. Hols, Lactate racemization as a rescue pathway for supplying D-lactate to the cell wall biosynthesis machinery in Lactobacillus plantarum, J. Bacteriol. 187 (2005) 6750–6761. https://doi.org/10.1128/JB.187.19.6750-6761.2005.

[35] A.P. Sousa, D.M. Cunha, C. Franco, C. Teixeira, F. Gojon, P. Baylina, R. Fernandes, Which role plays 2-hydroxybutyric acid on insulin resistance?, Metabolites. 11 (2021). https://doi.org/10.3390/metabo11120835.

[36] B.A. Green, R.J. Yu, E.J. Van Scott, Clinical and cosmeceutical uses of hydroxyacids, Clin. Dermatol. 27 (2009) 495–501. https://doi.org/https://doi.org/10.1016/j.clindermatol.2009.06.023.

[37] P. Babilas, U. Knie, C. Abels, Cosmetic and dermatologic use of alpha hydroxy acids, J. Ger. Soc. Dermatology. 10 (2012) 488–491. https://doi.org/https://doi.org/10.1111/j.1610-0387.2012.07939.x.

[38] C. Zhang, W. Song, J. Liu, X. Chen, L. Liu, Production of enantiopure (R)- or (S)-2-hydroxy-4-(methylthio)butanoic acid by multi-enzyme cascades, Bioresour. Bioprocess. 6 (2019). https://doi.org/10.1186/s40643-019-0244-x.

[39] Z. Zheng, C. Ma, C. Gao, F. Li, J. Qin, H. Zhang, K. Wang, P. Xu, Efficient conversion of phenylpyruvic acid to phenyllactic acid by using whole cells of bacillus coagulans SDM, PLoS One. 6 (2011) 23–26. https://doi.org/10.1371/journal.pone.0019030.

[40] C. Gao, W. Zhang, C. Ma, P. Liu, P. Xu, Kinetic resolution of 2-hydroxybutanoate racemic mixtures by NAD-independent l-lactate dehydrogenase, Bioresour. Technol. 102 (2011) 4595–4599. https://doi.org/10.1016/j.biortech.2011.01.003.

[41] K. Tang, J. Yi, K. Huang, G. Zang, Biphasic Recognition Chiral Extraction: A Novel Method for Separation of Mandelic Acid Enantiomers, Chirality. 21 (2009) 390–395. https://doi.org/10.1002/chir.20601.

[42] B. Chen, H.F. Yin, Z.S. Wang, J.Y. Liu, J.H. Xu, A new chemo-enzymatic route to chiral 2-hydroxy-4-phenylbutyrates by combining lactonase-mediated resolution with hydrogenation over Pd/C, Chem. Commun. 46 (2010) 2754–2756. https://doi.org/10.1039/b925402a.

[43] Y. Bai, S.T. Yang, Biotransformation of R-2-hydroxy-4-phenylbutyric acid by D lactate dehydrogenase and Candida boidinii cells containing formate dehydrogenase coimmobilized in a fibrous bed bioreactor, Biotechnol. Bioeng. 92 (2005) 137–146. https://doi.org/10.1002/bit.20582.

[44] M. Sakko, C. Moore, L. Novak-Frazer, V. Rautemaa, T. Sorsa, P. Hietala, A. Järvinen, P. Bowyer, L. Tjäderhane, R. Rautemaa, 2-hydroxyisocaproic acid is fungicidal for Candida and Aspergillus species, Mycoses. 57 (2014) 214–221. https://doi.org/10.1111/myc.12145.

[45] P. Lavermicocca, F. Valerio, A. Visconti, Antifungal activity of phenyllactic acid against molds isolated from bakery products, Appl. Environ. Microbiol. 69 (2003) 634–640. https://doi.org/10.1128/AEM.69.1.634-640.2003.

[46] E. Gracia-Moreno, R. Lopez, V. Ferreira, Quantitative determination of five hydroxy acids, precursors of relevant wine aroma compounds in wine and other alcoholic beverages, Anal. Bioanal. Chem. 407 (2015) 7925–7934. https://doi.org/https://doi.org/10.1007/s00216-015-8959-9.

[47] G. Zhao, G. Kuang, J. Li, H. Hadiatullah, Z. Chen, X. Wang, Y. Yao, Z.H. Pan, Y. Wang, Characterization of aldehydes and hydroxy acids as the main contribution to the traditional Chinese rose vinegar by flavor and taste analyses, Food Res. Int. 129 (2020). https://doi.org/https://doi.org/10.1016/j.foodres.2019.108879.

[48] R. Martín-Venegas, M. Teresa Brufau, A.M. Guerrero-Zamora, Y. Mercier, P.A. Geraert, R. Ferrer, The methionine precursor DL-2-hydroxy-(4-methylthio)butanoic acid protects intestinal epithelial barrier function, Food Chem. 141 (2013) 1702–1709. https://doi.org/10.1016/j.foodchem.2013.04.081.

[49] A. Zapaśnik, B. Sokołowska, M. Bryła, Role of Lactic Acid Bacteria in Food Preservation and Safety, Foods. 11 (2022) 1–17. https://doi.org/10.3390/foods11091283.

[50] T. Walther, C.M. Topham, R. Iragues, C. Auriol, A. Baylac, H. Cordier, C. Dressaire, L. Lozano-Huguet, N. Tarrat, N. Martineau, M. Stodel, Y. Malbert, M. Maestracci, R. Huet, I. André, M. Remaud-Siméon, J.M. François, Construction of a synthetic metabolic pathway for biosynthesis of the non-natural methionine precursor 2,4-dihydroxybutyric acid, Nat. Commun. 8 (2017). https://doi.org/10.1038/ncomms15828.

[51] A. Basu, K.R. Kunduru, J. Katzhendler, A.J. Domb, Poly(α-hydroxy acid)s and poly(α-hydroxy acid-co-α-amino acid)s derived from amino acid, Adv. Drug Deliv. Rev. 107 (2016) 82–96. https://doi.org/https://doi.org/10.1016/j.addr.2016.08.003.

[52] S. Il Moon, H. Urayama, Y. Kimura, Structural characterization and degradability of poly(L-lactic acid)s incorporating phenyl-substituted α-hydroxy acids as comonomers, Macromol. Biosci. 3 (2003) 301–309. https://doi.org/10.1002/mabi.200390038.

[53] N. Narayanan, P.K. Roychoudhury, A. Srivastava, L (+) lactic acid fermentation and its product polymerization, Electron. J. Biotechnol. 7 (2004). https://doi.org/10.2225/vol7-issue2-fulltext-7.

[54] K. Ahuja, M. Verma, Alpha Hydroxy Acid Market - By Product (Glycolic, Lactic, Citric), By Application (Cosmetics (Skincare, Hair Care, Makeup, Fragrances], Dermal) & Forecast, 2024-2032, 2024.

[55] S. Palwe, Gluconic Acid Market Research Report Information By Type (Glu Gluconic Acid, Glucono Delta Lactone, Sodium Salt of Gluconic Acid, Calcium Salt of Gluconic Acid, Others), By Application (Food & Beverage, Pharmaceuticals, Chemicals, Agriculture, Others), By, 2024.

[56] H. Groeger, Enzymatic Routes to Enantiomerically Pure Aromatic α-Hydroxy Carboxylic Acids: A Further Example for the Diversity of Biocatalysis, Adv. Synth. Catal. 343 (2001) 547–558. https://doi.org/10.1002/chin.200149278.

[57] C. Martin, M. Trajkovic, M.W. Fraaije, Production of Hydroxy Acids: Selective Double Oxidation of Diols by Flavoprotein Alcohol Oxidase, Angew. Chemie - Int. Ed. 59 (2020) 4869–4872. https://doi.org/10.1002/anie.201914877.

[58] M.H. Lee, H. Byeon, H.Y. Jang, Synthesis of α-Hydroxy Acids via Dehydrogenative Cross-Coupling of a Sustainable C2 Chemical (Ethylene Glycol) with Alcohols, J. Org. Chem. 87 (2022) 4631–4639. https://doi.org/10.1021/acs.joc.1c02981.

[59] T. Mehtiö, M. Toivari, M.G. Wiebe, A. Harlin, M. Penttilä, A. Koivula, Production and applications of carbohydrate-derived sugar acids as generic biobased chemicals, Crit. Rev. Biotechnol. 36 (2016) 904–916. https://doi.org/10.3109/07388551.2015.1060189.

[60] M.A. Keller, G. Piedrafita, M. Ralser, The widespread role of non-enzymatic reactions in cellular metabolism, Curr. Opin. Biotechnol. 34 (2015) 153–161. https://doi.org/10.1016/j.copbio.2014.12.020.

[61] D. Voet, J.G. Voet, Biochemistry, 4th ed., Wiley-VCH, 2010.

[62] R.A. Sheldon, D. Brady, M.L. Bode, The Hitchhiker's guide to biocatalysis: Recent advances in the use of enzymes in organic synthesis, Chem. Sci. 11 (2020) 2587–2605. https://doi.org/10.1039/c9sc05746c.

[63] O. Khersonsky, C. Roodveldt, D.S. Tawfik, Enzyme promiscuity: evolutionary and mechanistic aspects, Curr. Opin. Chem. Biol. 10 (2006) 498–508. https://doi.org/10.1016/j.cbpa.2006.08.011.

[64] G.A. Holdgate, T.D. Meek, R.L. Grimley, Mechanistic enzymology in drug discovery: A fresh perspective, Nat. Rev. Drug Discov. 17 (2018) 115–132. https://doi.org/10.1038/nrd.2017.219.

[65] E.L. Bell, W. Finnigan, S.P. France, A.P. Green, M.A. Hayes, L.J. Hepworth, S.L. Lovelock, H. Niikura, S. Osuna, E. Romero, K.S. Ryan, N.J. Turner, S.L. Flitsch, Biocatalysis, Nat. Rev. Methods Prim. 1 (2021). https://doi.org/10.1038/s43586-021-00044-z.

[66] J. Chapman, A.E. Ismail, C.Z. Dinu, Industrial applications of enzymes: Recent advances, techniques, and outlooks, Catalysts. 8 (2018). https://doi.org/10.3390/catal8060238.

[67] J.M. Choi, S.S. Han, H.S. Kim, Industrial applications of enzyme biocatalysis: Current status and future aspects, Biotechnol. Adv. 33 (2015) 1443–1454. https://doi.org/10.1016/j.biotechadv.2015.02.014.

[68] G.W. Huisman, S.J. Collier, On the development of new biocatalytic processes for practical pharmaceutical synthesis, Curr. Opin. Chem. Biol. 17 (2013) 284–292. https://doi.org/10.1016/j.cbpa.2013.01.017.

[69] S. Martínez Cuesta, S.A. Rahman, N. Furnham, J.M. Thornton, The Classification and Evolution of Enzyme Function, Biophys. J. 109 (2015) 1082–1086. https://doi.org/10.1016/j.bpj.2015.04.020.

[70] A.G. McDonald, K.F. Tipton, Enzyme nomenclature and classification: the state of the art, FEBS J. 290 (2023) 2214–2231. https://doi.org/10.1111/febs.16274.

[71] R.B. Silverman, The Organic Chemistry of Enzyme-Catalyzed Reactions, Second, Academic Press, 2002. https://doi.org/10.1016/C2009-0-22837-6.

[72] R.H. Petrucci, G.F. Herring, J.D. Madura, C. Bissonnette, General Chemistry: Principles and Modern Applications, 10th ed., Pearson Canada, Toronto, 2011.

[73] L.A. Nguyen, H. He, C. Pham-Huy, Chiral drugs: an overview, Int. J. Biomed. Sci. 2 (2006) 85–100. https://doi.org/10.59566/IJBS.2006.2085.

[74] K.M. Rentsch, The importance of stereoselective determination of drugs in the clinical laboratory, J. Biochem. Biophys. Methods. 54 (2002) 1–9. https://doi.org/10.1016/S0165-022X(02)00124-0.

[75] S.M. Cuesta, S.A. Rahman, J.M. Thornton, Exploring the chemistry and evolution of the isomerases, Proc. Natl. Acad. Sci. U. S. A. 113 (2016) 1796–1801. https://doi.org/10.1073/pnas.1509494113.

[76] S. Martinez Cuesta, N. Furnham, S.A. Rahman, I. Sillitoe, J.M. Thornton, The evolution of enzyme function in the isomerases, Curr. Opin. Struct. Biol. 26 (2014) 121–130. https://doi.org/10.1016/j.sbi.2014.06.002.

[77] M.E. Tanner, Understanding nature's strategies for enzyme-catalyzed racemization and epimerization, Acc. Chem. Res. 35 (2002) 237–246. https://doi.org/10.1021/ar000056y.

[78] K. Drauz, O. May, H. Groger, Enzyme Catalysis in Organic Synthesis, 3rd ed., Wiley-VCH, 2012. https://doi.org/10.1002/9783527639861.

[79] Z. Fang, W. Zhang, T. Zhang, C. Guang, W. Mu, Isomerases and epimerases for biotransformation of pentoses, Appl. Microbiol. Biotechnol. 102 (2018) 7283–7292. https://doi.org/10.1007/s00253-018-9150-y.

[80] S.H. Bhosale, M.B. Rao, V. V. Deshpande, Molecular and industrial aspects of glucose isomerase, Microbiol. Rev. 60 (1996) 280–300. https://doi.org/10.1128/mmbr.60.2.280-300.1996.

[81] S.H. Wilen, E.L. Eliel, L.N. Mander, Stereochemistry of Organic Compounds, Wiley-VCH, New York, 1994.

[82] B. Schnell, K. Faber, W. Kroutil, Enzymatic Racemisation and its Application to Synthetic Biotransformations, Adv. Synth. Catal. 345 (2003) 653–666. https://doi.org/10.1002/adsc.200303009.

[83] A. Bairoch, The ENZYME database in 2000, Nucleic Acids Res. 28 (2000) 304–305. https://doi.org/10.1093/nar/28.1.304.

[84] A.G. McDonald, S. Boyce, K.F. Tipton, ExplorEnz: The primary source of the IUBMB enzyme list, Nucleic Acids Res. 37 (2009) D593–D597. https://doi.org/10.1093/nar/gkn582.

[85] C.F. Gunsalus, R.Y. Stanier, I.C. Gunsalus, The enzymatic conversion of mandelic acid to benzoic acid. III. Fractionation and properties of the soluble enzymes., J. Bacteriol. 66 (1953) 548–553. http://www.ncbi.nlm.nih.gov/pubmed/13108854%0Ahttp://www.pubmedcentral.nih.gov/articlerender.fcgi?artid=PMC317432.

[86] U. Felfer, M. Goriup, M.F. Koegl, U. Wagner, B. Larissegger-Schnell, K. Faber, W. Kroutil, The substrate spectrum of mandelate racemase: Minimum structural requirements for substrates and substrate model, Adv. Synth. Catal. 347 (2005) 951–961. https://doi.org/10.1002/adsc.200505012.

[87] I.A. Rodionova, D.A. Scoot, N. V. Grishin, A.L. Osterman, D.A. Rodionov, Tagaturonate–fructuronate epimerase UxaE, a novel enzyme in the hexuronate catabolic network in Thermotoga maritima, Env. Microbiol. 14 (2012) 2920–2934. https://doi.org/10.1111/j.1462-2920.2012.02856.x.

[88] J.R. Stern, A. Del Campillo, Enzymatic racemization of β-hydroxybutyryl-S-CoA and the stereospecificity of enzymes of the fatty acid cycle, J. Am. Chem. Soc. 77 (1955) 1073–1074. https://doi.org/10.1021/ja01609a105.

[89] M.B. Taylor, E. Juni, Stereoisomeric specificities of 2,3-butanediol dehydrogenases, Biochim. Biophys. Acta. 39 (1960) 448–457. https://doi.org/10.1016/0006-3002(60)90197-9.

[90] S. Ranjan, K.K. Patnaik, M.M. Laloraya, Enzymic conversion of meso-tartarate to dextro-tartarate in tamarind, Naturwissenschaften. 48 (1961) 406. https://doi.org/10.1007/BF00609104.

[91] S. Hoshiko, Y. Kunimoto, K. Arima, T. Beppu, Mechanism of l-alloisocitric acid fermentation: Isocitrate epimerase activity in the cell-free extract of penicillium purpurogenum, Agric. Biol. Chem. 46 (1982) 143–151. https://doi.org/10.1080/00021369.1982.10865025.

[92] D.J. Neidhart, G.L. Kenyon, J.A. Gerlt, G.A. Petsko, Mandelate racemase and muconate lactonizing enzyme are mechanistically distinct and structurally homologous, Nature. 347 (1990) 692–694. https://doi.org/10.1038/347692a0.

[93] M.S. Hasson, I. Schlichting, J. Moulai, K. Taylor, W. Barrett, G.L. Kenyon, P.C. Babbitt, J.A. Gerlt, G.A. Petsko, D. Ringe, Evolution of an enzyme active site: The structure of a new crystal form of muconate lactonizing enzyme compared with mandelate racemase and enolase, Proc. Natl. Acad. Sci. U. S. A. 95 (1998) 10396–10401. https://doi.org/10.1073/pnas.95.18.10396.

[94] J.A. Fee, G.D. Hegeman, G.L. Kenyon, Mandelate Racemase from Pseudomonas putida. Subunit Composition and Absolute Divalent Metal Ion Requirement, Biochemistry. 13 (1974) 2528–2532. https://doi.org/10.1021/bi00709a008.

[95] B. Desguin, P. Goffin, E. Viaene, M. Kleerebezem, V. Martin-Diaconescu, M.J. Maroney, J.P. Declercq, P. Soumillion, P. Hols, Lactate racemase is a nickel-dependent enzyme activated by a widespread maturation system, Nat. Commun. 5 (2014) 3615. https://doi.org/10.1038/ncomms4615.

[96] B. Desguin, T. Zhang, P. Soumillion, P. Hols, J. Hu, R.P. Hausinger, A tethered niacin-derived pincer complex with a nickel-carbon bond in lactate racemase, Science (80-.). 349 (2015) 66–69. https://doi.org/10.1126/science.aab2272.

[97] F. George, C. Daniel, M. Thomas, E. Singer, A. Guilbaud, F.J. Tessier, A.M. Revol-Junelles, F. Borges, B. Foligné, Occurrence and dynamism of lactic acid bacteria in distinct ecological niches: A multifaceted functional health perspective, Front. Microbiol. 9 (2018) 1–15. https://doi.org/10.3389/fmicb.2018.02899.

[98] B. T, Lactic acid bacteria: their applications in foods, J. Bacteriol. Mycol. 5 (2018) 1065. https://doi.org/10.15406/jbmoa.2018.06.00182.

[99] F.J. Carr, D. Chill, N. Maida, The lactic acid bacteria: A literature survey, Crit. Rev. Microbiol. 28 (2002) 281–370. https://doi.org/10.1080/1040-840291046759.

[100] E.J. Quinto, P. Jiménez, I. Caro, J. Tejero, J. Mateo, T. Girbés, Probiotic Lactic Acid Bacteria: A Review, Food Nutr. Sci. 5 (2014) 1765–1775. https://doi.org/10.4236/fns.2014.518190.

[101] H.A. Seddik, F. Bendali, F. Gancel, I. Fliss, G. Spano, D. Drider, Lactobacillus plantarum and Its Probiotic and Food Potentialities, Probiotics Antimicrob. Proteins. 9 (2017) 111–122. https://doi.org/10.1007/s12602-017-9264-z.

[102] E.L. Tatum, W.H. Peterson, E.B. Fred, Enzymic racemization of optically active lactic acid, Biochem. J. 30 (1936) 1892–1897. https://doi.org/10.1042/bj0301892.

[103] H. Katagiri, K. Kitahara, Racemiase, an enzyme which catalyses racemization of lactic acids, Biochem. J. 31 (1937) 909–914. https://doi.org/10.1042/bj0310909.

[104] H. Katagiri, K. Kitahara, The lactic dehydrogenase of lactic acid bacteria, Biochem. J. 32 (1938) 1654–1657. https://doi.org/10.1042/bj0321654.

[105] K. Kitahara, A. Obayashi, S. Fukui, Racemiase. I. Cell-free racemiase, Enzymologia. 15 (1952) 259–266.

[106] K. Kitahara, A. Obayashi, DL-forming lactic acid bacteria, J. Gen. Appl. Microbiol. 1 (1955) 237–245. https://doi.org/10.2323/jgam.1.237.

[107] K. Kitahara, A. Obayashi, Studies on the enzymes of lactic acid bacteria . Part XI. Purification and identification of 'Coracemiase'., J. Agric. Chem. Soc. Japan. 33 (1959) 497–524.

[108] T. Hiyama, S. Mizushima, K. Kitahara, A racemizing enzyme system of Lactobacillus plantarum., J. Gen. Appl. Microbiol. 11 (1965) 51–60. https://doi.org/doi.org/10.2323/jgam.11.51.

[109] H. Katagiri, T. Sugimori, K. Imai, S. Komaki, M. Okuzumi, H. Anyoji, On the metabolism of organic acids by clostridium acetobutylicum, Agric. Biol. Chem. 25 (1961) 281–313. https://doi.org/10.1080/00021369.1961.10857808.

[110] S.S. Shapiro, D. Don, Lactic Acid Racemization in Clostridium butylicum. Evidence for a Direct Internal Hydride Shift, Biochemistry. 4 (1965) 2283–2288. https://doi.org/doi.org/10.1021/bi00887a004.

[111] T. Hiyama, S. Fukui, K. Kitahara, Purification and Properties of Lactate Racemase from Lactobacillus sake, J. Biochem. 64 (1968). https://doi.org/10.1093/oxfordjournals.jbchem.a128870.

[112] K.O. Stetter, O. Kandler, Formation of DL-lactic acid by lactobacilli and characterization of a lactic acid racemase from several streptobacteria, Arch. Mikrobiol. 94 (1973) 221–247. https://doi.org/10.1007/BF00417453.

[113] B. Desguin, P. Soumillion, R.P. Hausinger, P. Hols, Unexpected complexity in the lactate racemization system of lactic acid bacteria, FEMS Microbiol. Rev. 41 (2017) S71–S83. https://doi.org/10.1093/FEMSRE/FUX021.

[114] E.I. Garvie, Bacterial lactate dehydrogenases, Microbiol. Rev. 44 (1980) 106–139. https://doi.org/10.1128/mmbr.44.1.106-139.1980.

[115] T. Ferain, J.N. Hobbs, J. Richardson, N. Bernard, D. Garmyn, P. Hols, N.E. Allen, J. Delcour, Knockout of the two ldh genes has a major impact on peptidoglycan precursor synthesis in Lactobacillus plantarum, J. Bacteriol. 178 (1996) 5431–5437. https://doi.org/10.1128/jb.178.18.5431-5437.1996.

[116] C. Barna, D.H. Williams, The structure and mode of action of glycopeptide antibiotics of the vancomycin group, Ann. Rev. Microbiol. 38 (1984) 339–357. https://doi.org/10.1146/annurev.mi.38.100184.002011.

[117] B.J. Miller, C.M.A.P. Franz, G.S. Cho, M. Du Toit, Expression of the malolactic enzyme gene (mle) from Lactobacillus plantarum under winemaking conditions, Curr. Microbiol. 62 (2011) 1682–1688. https://doi.org/10.1007/s00284-011-9914-4.

[118] A. Lonvaud-Funel, Microbiology of the malolactic fermentation: Molecular aspects, FEMS Microbiol. Lett. 126 (1995) 209–214. https://doi.org/10.1016/0378-1097(95)00020-6.

[119] B. Desguin, P. Soumillion, P. Hols, R.P. Hausinger, Nickel-pincer cofactor biosynthesis involves LarB-catalyzed pyridinium carboxylation and LarE-dependent sacrificial sulfur insertion, Proc. Natl. Acad. Sci. U. S. A. 113 (2016) 5598–5603. https://doi.org/10.1073/pnas.1600486113.

[120] B. Desguin, M. Fellner, O. Riant, J. Hu, R.P. Hausinger, P. Hols, P. Soumillion, Biosynthesis of the nickel-pincer nucleotide cofactor of lactate racemase requires a CTP-dependent cyclometallase, J. Biol. Chem. 293 (2018) 12303–12317. https://doi.org/10.1074/jbc.RA118.003741.

[121] G.P. Bienert, B. Desguin, F. Chaumont, P. Hols, Channel-mediated lactic acid transport: A novel function for aquaglyceroporins in bacteria, Biochem. J. 454 (2013) 559–570. https://doi.org/10.1042/BJ20130388.

[122] B. Desguin, P. Goffin, N. Bakouche, A. Diman, E. Viaene, D. Dandoy, L. Fontaine, B. Hallet, P. Hols, Enantioselective regulation of lactate racemization by LarR in Lactobacillus plantarum, J. Bacteriol. 197 (2015) 219–230. https://doi.org/10.1128/JB.02192-14.

[123] B. Desguin, Lactate Racemization and Beyond, J. Bacteriol. Parasitol. 9 (2018) 2–5. https://doi.org/10.4172/2155-9597.1000335.

[124] J.A. Rankin, R.C. Mauban, M. Fellner, B. Desguin, J. McCracken, J. Hu, S.A. Varganov, R.P. Hausinger, Lactate Racemase Nickel-Pincer Cofactor Operates by a Proton-Coupled Hydride Transfer Mechanism, Biochemistry. 57 (2018) 3244–3251. https://doi.org/10.1021/acs.biochem.8b00100.

[125] J.T. Singleton, The Uses of Pincer Complexes in Organic Synthesis, ChemInform. 34 (2003) 1837–1857. https://doi.org/10.1002/chin.200324233.

[126] K.J. Szabo, W.O. F., Pincer and Pincer-Type Complexes: Applications in Organic Synthesis and Catalysis, John Wiley & Sons, 2015. https://doi.org/10.1002/anie.201501805.

[127] G. Van Koten, D. Milstein, Organometallic Pincer Chemistry, Springer, 2013. https://doi.org/10.1007/978-3-642-31081-2.

[128] J.L. Nevarez, A. Turmo, J. Hu, R.P. Hausinger, Biological Pincer Complexes, ChemCatChem. 12 (2020) 4242–4254. https://doi.org/10.1002/cctc.202000575.

[129] T. Xu, G. Bauer, X. Hu, A Novel Nickel Pincer Complex in the Active Site of Lactate Racemase, ChemBioChem. 17 (2016) 31–32. https://doi.org/10.1002/cbic.201500498.

[130] S. Chatterjee, S. Gatreddi, S. Gupta, J.L. Nevarez, J.A. Rankin, A. Turmo, J. Hu, R.P. Hausinger, Unveiling the mechanisms and biosynthesis of a novel nickel-pincer enzyme, Biochem. Soc. Trans. 50 (2022) 1187–1196. https://doi.org/10.1042/BST20220490.

[131] J.A. Rankin, S. Chatterjee, Z. Tariq, S. Lagishetty, B. Desguin, J. Hu, R.P. Hausinger, The LarB carboxylase/hydrolase forms a transient cysteinyl-pyridine intermediate during nickel-pincer nucleotide cofactor biosynthesis, Proc. Natl. Acad. Sci. U. S. A. 118 (2021) e2106202118. https://doi.org/10.1073/pnas.2106202118.

[132] M. Fellner, B. Desguin, R.P. Hausinger, J. Hu, Structural insights into the catalytic mechanism of a sacrificial sulfur insertase of the N-type ATP pyrophosphatase family, LarE, Proc. Natl. Acad. Sci. U. S. A. 114 (2017) 9074–9079. https://doi.org/10.1073/pnas.1704967114.

[133] M. Albrecht, Cyclometalation using d-block transition metals: Fundamental aspects and recent trends, Chem. Rev. 110 (2010) 576–623. https://doi.org/10.1021/cr900279a.

[134] T. Xu, M.D. Wodrich, R. Scopelliti, C. Corminboeuf, X. Hu, Nickel pincer model of the active site of lactate racemase involves ligand participation in hydride transfer, Proc. Natl. Acad. Sci. U. S. A. 114 (2017) 1242–1245. https://doi.org/10.1073/pnas.1616038114.

[135] R. Shi, M.D. Wodrich, H. Pan, F.F. Tirani, X. Hu, Functional Models of the Nickel Pincer Nucleotide Cofactor of Lactate Racemase, Angew. Chemie. 131 (2019) 17025–17028. https://doi.org/10.1002/ange.201910490.

[136] X. Zhang, L.W. Chung, Alternative mechanistic strategy for enzyme catalysis in a Ni-dependent lactate racemase (LarA): Intermediate destabilization by the cofactor, Chem. - A Eur. J. 23 (2017) 3623–3630. https://doi.org/10.1002/chem.201604893.

[137] M.J. Yu, S.L. Chen, From NAD+ to Nickel Pincer Complex: A Significant Cofactor Evolution Presented by Lactate Racemase, Chem. - A Eur. J. 23 (2017) 7545–7557. https://doi.org/10.1002/chem.201700405.

[138] B. Qiu, X. Yang, A bio-inspired design and computational prediction of scorpion-like SCS nickel pincer complexes for lactate racemization, Chem. Commun. 53 (2017) 11410–11413. https://doi.org/10.1039/c7cc06416k.

[139] S. Gatreddi, S. Dexin, R.P. Hausinger, J. Hu, Irreversible Inactivation of Lactate Racemase by Sodium Borohydride Reveals Reactivity of the Nickel–Pincer Nucleotide Cofactor, ACS Catal. 13 (2023) 1441–1448. https://doi.org/10.1021/acscatal.2c05461.

[140] B. Desguin, P. Soumillion, P. Hols, J. Hu, R.P. Hausinger, Lactate racemase and its niacin-derived, covalently-tethered, nickel cofactor, in: Biol. Chem. Nickel, 2017: pp. 220–236. https://doi.org/10.1039/9781788010580-00220.

[141] R.P. Hausinger, J. Hu, B. Desguin, The nickel-pincer coenzyme of lactate racemase: A case study of uncovering cofactor structure and biosynthesis, Methods Enzymol. 685 (2023) 341–371. https://doi.org/10.1016/bs.mie.2023.03.006.

[142] A. Turmo, J. Hu, R.P. Hausinger, Characterization of the nickel-inserting cyclometallase LarC from Moorella thermoacetica and identification of a cytidinylylated reaction intermediate, Metallomics. 14 (2022). https://doi.org/10.1093/mtomcs/mfac014.

[143] M.D. Ermolaeva, O. White, S.L. Salzberg, Prediction of operons in microbial genomes, Nucleic Acids Res. 29 (2001) 1216–1221. https://doi.org/10.1093/nar/29.5.1216.

[144] J. Tamames, G. Casari, C. Ouzounis, A. Valencia, Conserved clusters of functionally related genes in two bacterial genomes, J. Mol. Evol. 44 (1997) 66–73. https://doi.org/10.1007/PL00006122.

[145] M.Y. Galperin, E. V. Koonin, Who's your neighbor? New computational approaches for functional genomics, Nat. Biotechnol. 18 (2000) 609–613. https://doi.org/10.1038/76443.

[146] C.E. Martinez-Guerrero, R. Ciria, C. Abreu-Goodger, G. Moreno-Hagelsieb, E. Merino, GeConT 2: gene context analysis for orthologous proteins, conserved domains and metabolic pathways., Nucleic Acids Res. 36 (2008) 176–180. https://doi.org/10.1093/nar/gkn330.

[147] B. Desguin, J. Urdiain-Arraiza, M. Da Costa, M. Fellner, J. Hu, R.P. Hausinger, T. Desmet, P. Hols, P. Soumillion, Uncovering a superfamily of nickel-dependent hydroxyacid racemases and epimerases, Sci. Rep. 10 (2020). https://doi.org/10.1038/s41598-020-74802-6.

[148] S.J. Giovannoni, E. Schabtach, R.W. Castenholz, Isosphaera pallida, gen. and comb. nov., a gliding, budding eubacterium from hot springs, Arch. Microbiol. 147 (1987) 276–284. https://doi.org/10.1007/BF00463488.

[149] M. Göker, D. Cleland, E. Saunders, A. Lapidus, M. Nolan, S. Lucas, N. Hammon, S. Deshpande, J.F. Cheng, R. Tapia, C. Han, L. Goodwin, S. Pitluck, K. Liolios, I. Pagani, N. Ivanova, K. Mavromatis, A. Pati, A. Chen, K. Palaniappan, M. Land, L. Hauser, Y.J. Chang, C.D. Jeffries, J.C. Detter, B. Beck, T. Woyke, J. Bristow, J.A. Eisen, V. Markowitz, P. Hugenholtz, N.C. Kyrpides, H.P. Klenk, Complete genome sequence of Isosphaera pallida type strain (IS1BT), Stand. Genomic Sci. 4 (2011) 63–71. https://doi.org/10.4056/sigs.1533840.

[150] N. Christiansen, B.K. Ahring, Desulfitobacterium hafniense sp. nov., an anaerobic, reductively dechlorinating bacterium, Int. J. Syst. Bacteriol. 46 (1996) 442–448. https://doi.org/10.1099/00207713-46-2-442.

[151] R. Villemur, M. Lanthier, R. Beaudet, F. Lépine, The Desulfitobacterium genus, FEMS Microbiol. Rev. 30 (2006) 706–733. https://doi.org/10.1111/j.1574-6976.2006.00029.x.

[152] D.H. Currie, A.M. Guss, C.D. Herring, R.J. Giannone, C.M. Johnson, P.K. Lankford, S.D. Brown, R.L. Hettich, L.R. Lynd, Profile of secreted hydrolases, associated proteins, and SlpA in Thermoanaerobacterium saccharolyticum during the degradation of hemicellulose, Appl. Environ. Microbiol. 80 (2014) 5001–5011. https://doi.org/10.1128/AEM.00998-14.

[153] S. Gatreddi, J. Urdiain-Arraiza, B. Desguin, R.P. Hausinger, J. Hu, Structural and mutational characterization of a malate racemase from the LarA superfamily, BioMetals. (2022). https://doi.org/10.1007/s10534-022-00372-x.

[154] K. Takai, H. Kobayashi, K.H. Nealson, K. Horikoshi, Deferribacter desulfuricans sp. nov., a novel sulfur-, nitrate- and arsenate-reducing thermophile isolated from a deep-sea hydrothermal vent, Int. J. Syst. Evol. Microbiol. 53 (2003) 839–846. https://doi.org/10.1099/ijs.0.02479-0.

[155] M. Marounek, K. Fliegrova, S. Bartos, Metabolism and some characteristics of ruminal strains of Megasphaera elsdenii, Appl. Environ. Microbiol. 55 (1989) 1570–1573. https://doi.org/10.1128/aem.55.6.1570-1573.1989.

[156] S.A. Shetty, N.P. Marathe, V. Lanjekar, D. Ranade, Y.S. Shouche, Comparative genome analysis of Megasphaera sp. reveals niche specialization and its potential role in the human gut, PLoS One. 8 (2013) e79353. https://doi.org/10.1371/journal.pone.0079353.

[157] S. Wolf, J. Becker, Y. Tsuge, H. Kawaguchi, A. Kondo, J. Marienhagen, M. Bott, V.F. Wendisch, C. Wittmann, Advances in metabolic engineering of Corynebacterium glutamicum to produce high-value active ingredients for food, feed, human health, and well-being, Essays Biochem. 65 (2021) 197–212. https://doi.org/10.1042/EBC20200134.

[158] R. Huber, T.A. Langworthy, H. König, M. Thomm, C.R. Woese, U.B. Sleytr, K.O. Stetter, Thermotoga maritima sp. nov. represents a new genus of unique extremely thermophilic eubacteria growing up to 90°C, Arch. Microbiol. 144 (1986) 324–333. https://doi.org/10.1007/BF00409880.

[159] A.D. Frock, J.S. Notey, R.M. Kelly, The genus Thermotoga: Recent developments, Environ. Technol. 31 (2010) 1169–1181. https://doi.org/10.1080/09593330.2010.484076.

[160] R.P. Hausinger, B. Desguin, M. Fellner, J.A. Rankin, J. Hu, Nickel–pincer nucleotide cofactor, Curr. Opin. Chem. Biol. 47 (2018) 18–23. https://doi.org/10.1016/j.cbpa.2018.06.019.

[161] G. Crooks, G. Hon, J. Chandonia, S. Brenner, WebLogo: a sequence logo generator, Genome Res. 14 (2004) 1188–1190. https://doi.org/10.1101/gr.849004.1.

[162] A. Przybylska, M. Gackowski, M. Koba, Application of capillary electrophoresis to the analysis of bioactive compounds in herbal raw materials, Molecules. 26 (2021) 1–24. https://doi.org/10.3390/molecules26082135.

[163] M.S. Van Dyk, J.L.F. Kock, A. Botha, Hydroxy long-chain fatty acids in fungi, World J. Microbiol. Biotechnol. 10 (1994) 495–504. https://doi.org/https://doi.org/10.1007/BF00367653.

[164] G.M. Coppola, H.F. Schuster, alpha-Hydroxy Acids in Enantioselective Syntheses, Wiley-VCH, Weinheim, 1997.

[165] J. McConathy, M.J. Owens, Stereochemistry in Drug Action, J Clin Psychiatry. 5 (2003). https://doi.org/https://doi.org/10.4088/pcc.v05n0202.

[166] D. Matelska, I.G. Shabalin, J. Jabłońska, M.J. Domagalski, J. Kutner, K. Ginalski, W. Minor, Classification, substrate specificity and structural features of D-2-hydroxyacid dehydrogenases: 2HADH knowledgebase, BMC Evol. Biol. 18 (2018) 1–23. https://doi.org/https://doi.org/10.1186/s12862-018-1309-8.

[167] C. Calderón, M. Lämmerhofer, Chiral separation of short chain aliphatic hydroxycarboxylic acids on cinchonan carbamate-based weak chiral anion exchangers and zwitterionic chiral ion exchangers, J. Chromatogr. A. 1487 (2017) 194–200. https://doi.org/https://doi.org/10.1016/j.chroma.2017.01.060.

[168] L.-G. Bogos, I.-E. Pralea, R.-C. Moldovan, C.A. Iuga, Indirect Enantioseparations: Recent Advances in Chiral Metabolomics for Biomedical Research, Int. J. Mol. Sci. 23 (2022). https://doi.org/https://doi.org/10.3390/ijms23137428.

[169] A. Van Eeckhaut, Y. Michotte, Chiral separations by capillary electrophoresis: Recent developments and applications, Electrophoresis. 27 (2006) 2880–2895. https://doi.org/https://doi.org/10.1002/elps.200500375.

[170] S. Kodama, A. Yamamoto, A. Matsunaga, Direct chiral resolution of aliphatic α-hydroxy acids using 2-hydroxypropyl-β-cyclodextrin in capillary electrophoresis, Analyst. 124 (1999) 55–59. https://doi.org/https://doi.org/10.1039/a807351a.

[171] L. Saavedra, C. Barbas, Optimization of the separation lactic acid enantiomers in body fluids by capillary electrophoresis, J. Chromatogr. B. 766 (2002) 235–242. https://doi.org/https://doi.org/10.1016/S0378-4347(01)00473-X.

[172] C. Calderón, J. Horak, M. Lämmerhofer, Chiral separation of 2-hydroxyglutaric acid on cinchonan carbamate based weak chiral anion exchangers by high-performance liquid chromatography, J. Chromatogr. A. 1467 (2016) 239–245. https://doi.org/https://doi.org/10.1016/j.chroma.2016.05.042.

[173] S. Okubo, F. Mashige, M. Omori, Y. Hashimoto, K. Nakahara, H. Kanazawa, Y. Matsushima, Enantiomeric determination of L- and D-lactic acid in human cerebrospinal fluid by chiral ligand exchange high-performance liquid

chromatography, Biomed. Chromatogr. 14 (2000) 474–477. https://doi.org/https://doi.org/10.1002/1099-0801(200011)14:7<474::AID-BMC995>3.0.CO;2-3.

[174] E.J. Franco, H. Hofstetter, O. Hofstetter, Determination of lactic acid enantiomers in human urine by high-performance immunoaffinity LC-MS, J. Pharm. Biomed. Anal. 49 (2009) 1088–1091. https://doi.org/https://doi.org/10.1016/j.jpba.2009.01.033.

[175] M.S. Rashed, M. Alamoudi, H.Y. Aboul-Enein, Chiral liquid chromatography tandem mass spectrometry in the determination of the configuration of 2-hydroxyglutaric acid in urine, Biomed. Chromatogr. 14 (2000) 317–320. https://doi.org/https://doi.org/10.1002/1099-0801(200008)14:5<317::AID-BMC989>3.0.CO;2-V.

[176] S. Kodama, A. Taga, A. Yamamoto, Y. Ito, Y. Honda, K. Suzuki, T. Yamashita, T. Kemmei, S.I. Aizawa, Enantioseparation of DL-isocitric acid by a chiral ligand exchange CE with Ni(II)-D-quinic acid system, Electrophoresis. 31 (2010) 3586–3591. https://doi.org/https://doi.org/10.1002/elps.201000320.

[177] C. Desiderio, Z. Aturki, S. Fanali, Separation of α-hydroxy acid enantiomers by high performance capillary electrophoresis using copper(II)-L-amino acid and copper(II)-aspartame complexes as chiral selectors in the background electrolyte, Electrophoresis. 15 (1994) 864–869. https://doi.org/https://doi.org/10.1002/elps.11501501122.

[178] A. Nardi, A. Eliseev, P. Bocek, S. Fanali, Use of charged and neutral cyclodextrins in capillary zone electrophoresis : enantiomeric resolution of some 2-hydroxy acids, J. Chromatogr. 638 (1993) 247–253. https://doi.org/https://doi.org/10.1016/0021-9673(93)83435-U.

[179] M.G. Schmid, O. Lecnik, U. Sitte, G. Gubitz, Application of ligand-exchange capillary electrophorersis to the chiral separation of α-hydroxy acids and β-blockers, J. Chromatogr. A. 875 (2000) 307–314. https://doi.org/https://doi.org/10.1016/S0021-9673(99)01333-3.

[180] E. Pittler, N. Grawatsch, D. Paul, G. Gübitz, M.G. Schmid, Enantioseparation of amino acids, α-hydroxy acids, and dipeptides by ligand-exchange CEC using silica-based chiral stationary phases, Electrophoresis. 30 (2009) 2897–2904. https://doi.org/https://doi.org/10.1002/elps.200900092.

[181] S. Tong, M. Shen, D. Cheng, Y. Zhang, Y. Ito, J. Yan, Chiral ligand exchange high-speed countercurrent chromatography: mechanism and application in enantioseparation of aromatic α-hydroxyl acids, J. Chromatogr. A. 1360 (2014) 110–118.

https://doi.org/https://doi.org/10.1016/j.chroma.2014.07.057.

[182] I. Varfaj, M. Protti, A. Di Michele, A. Macchioni, W. Lindner, A. Carotti, R. Sardella, L. Mercolini, Efficient enantioresolution of aromatic α-hydroxy acids with Cinchona alkaloid-based zwitterionic stationary phases and volatile polar-ionic eluents, Anal. Chim. Acta. 1180 (2021). https://doi.org/https://doi.org/10.1016/j.aca.2021.338928.

[183] S. Tong, H. Zhang, M. Shen, Y. Ito, J. Yan, Enantioseparation of mandelic acid derivatives by high performance liquid chromatography with substituted β-cyclodextrin as chiral mobile phase additive and evaluation of inclusion complex formation, J. Chromatogr. B. 962 (2014) 44–51. https://doi.org/https://doi.org/10.1016/j.jchromb.2014.05.026.

[184] F. Ianni, Z. Pataj, H. Gross, R. Sardella, B. Natalini, W. Lindner, M. Lämmerhofer, Direct enantioseparation of underivatized aliphatic 3-hydroxyalkanoic acids with a quinine-based zwitterionic chiral stationary phase, J. Chromatogr. A. 1363 (2014) 101–108. https://doi.org/https://doi.org/10.1016/j.chroma.2014.03.060.

[185] R. Karongo, J. Jiao, H. Gross, M. Lämmerhofer, Direct enantioselective gradient reversed-phase ultra-high performance liquid chromatography tandem mass spectrometry method for 3-hydroxy alkanoic acids in lipopeptides on an immobilized 1.6 µm amylose-based chiral stationary phase, J. Sep. Sci. 44 (2021) 1875–1883. https://doi.org/https://doi.org/10.1002/jssc.202100104.

[186] X. Fu, Z. Xu, M. Gawaz, M. Lämmerhofer, UHPLC-MS/MS method for chiral separation of 3-hydroxy fatty acids on amylose-based chiral stationary phase and its application for the enantioselective analysis in plasma and platelets, J. Pharm. Biomed. Anal. 223 (2023). https://doi.org/https://doi.org/10.1016/j.jpba.2022.115151.

[187] S. Kodama, A. Yamamoto, A. Matsunaga, K. Hayakawa, Direct chiral resolution of tartaric acid in food products by ligand exchange capillary electrophoresis using copper(II)-D-quinic acid as a chiral selector, J. Chromatogr. A. 932 (2001) 139–143. https://doi.org/https://doi.org/10.1016/S0021-9673(01)01228-6.

[188] R. Knob, J. Petr, J. Ševčík, V. Maier, Enantioseparation of tartaric acid by ligand-exchange capillary electrophoresis using contactless conductivity detection, J. Sep. Sci. 36 (2013) 3426–3431. https://doi.org/https://doi.org/10.1002/jssc.201300507.

[189] G. Hancu, L.A. Papp, B. Szekely-Szentmiklosi, H. Kelemen, The Use of Antibiotics as Chiral Selectors in Capillary Electrophoresis: A Review, Molecules. 27 (2022). https://doi.org/https://doi.org/10.3390/molecules27113601.

[190] S. Fanali, B. Chankvetadze, Some thoughts about enantioseparations in capillary electrophoresis, Electrophoresis. 0 (2019) 2420–2437. https://doi.org/https://doi.org/10.1002/elps.201900144.

[191] A. Ewing, R. Wallingford, T. Olefirowicz, Capillary electrophoresis, Anal. Chem. 61 (1989) 292A-303A. https://doi.org/https://doi.org/10.1021/ac00179a002.

[192] C. Desiderio, S. Fanali, Chiral analysis by capillary electrophoresis using antibiotics as chiral selector, J. Chromatogr. A. 807 (1998) 37–56. https://doi.org/https://doi.org/10.1016/S0021-9673(98)00061-2.

[193] H.Y. Aboul-Enein, I. Ali, Macrocyclic antibiotics as effective chiral selectors for enantiomeric resolution by liquid chromatography and capillary electrophoresis, Chromatographia. 52 (2000) 679–691. https://doi.org/https://doi.org/10.1007/BF02490991.

[194] T.J. Ward, A.B. Farris, Chiral separations using the macrocyclic antibiotics: A review, J. Chromatogr. A. 906 (2001) 73–89. https://doi.org/https://doi.org/10.1016/S0021-9673(00)00941-9.

[195] T.J. Ward, C. Dann, A.P. Brown, Separation of enantiomers using vancomycin in a countercurrent process by suppression of electroosmosis, Chirality. 8 (1996) 77–83. https://doi.org/https://doi.org/10.1002/(SICI)1520-636X(1996)8:1<77::AID-CHIR13>3.0.CO;2-P.

[196] A. Amini, U. Paulsen-Sörman, D. Westerlund, Principle and Applications of The Partial Filling Technique in Capillary Electrophoresis, Chromatographia. 50 (1999) 497–506. https://doi.org/https://doi.org/10.1007/BF02490748.

[197] A. Amini, Recent developments in chiral capillary electrophoresis and applications of this technique to pharmaceutical and biomedical analysis, Electrophoresis. 22 (2001) 3107–3130. https://doi.org/https://doi.org/10.1002/1522-2683(200109)22:15<3107::AID-ELPS3107>3.0.CO;2-Z.

[198] L. Valtcheva, J. Mohammad, G. Pettersson, S. Hjertén, Chiral separation of β-blockers by high-performance capillary electrophoresis based on non-immobilized cellulase as enantioselective protein, J. Chromatogr. 638 (1993) 263–267. https://doi.org/https://doi.org/10.1016/0021-9673(93)83437-W.

[199] P. Bednar, Z. Aturki, Z. Stransky, S. Fanali, Chiral analysis of UV nonabsorbing compounds by capillary electrophoresis using macrocyclic antibiotics: 1. Separation of aspartic and glutamic acid enantiomers, Electrophoresis. 22 (2001) 2129–2135. https://doi.org/https://doi.org/10.1002/1522-2683(20017)22:11<2129::AID-ELPS2129>3.0.CO;2-J.

[200] L. Tan, Y. Wang, X. Liu, H. Ju, J. Li, Simultaneous determination of L- and D-lactic acid in plasma by capillary electrophoresis, J. Chromatogr. B. 814 (2005) 393–398. https://doi.org/https://doi.org/10.1016/j.jchromb.2004.10.059.

[201] W. Pormsila, X.Y. Gong, P.C. Hauser, Determination of the enantiomers of α-hydroxy- and α-amino acids in capillary electrophoresis with contactless conductivity detection, Electrophoresis. 31 (2010) 2044–2048. https://doi.org/https://doi.org/10.1002/elps.201000127.

[202] V. Maier, J. Petr, R. Knob, J. Horáková, J. Ševčík, Electrokinetic partial filling technique as a powerful tool for enantiomeric separation of DL-lactic acid by CE with contactless conductivity detection, Electrophoresis. 28 (2007) 1815–1822. https://doi.org/https://doi.org/10.1002/elps.200600578.

[203] S. Kodama, A. Yamamoto, A. Matsunaga, T. Soga, K. Minoura, Direct chiral resolution of lactic acid in food products by capillary electrophoresis, J. Chromatogr. A. 875 (2000) 371–377. https://doi.org/https://doi.org/10.1016/S0021-9673(99)01005-5.

[204] Q. Ren, K. Ruth, L. Thöny-Meyer, M. Zinn, Enatiomerically pure hydroxycarboxylic acids: current approaches and future perspectives, Appl. Microbiol. Biotechnol. 87 (2010) 41–52. https://doi.org/https://doi.org/10.1007/s00253-010-2530-6.

[205] J. Sjögren, J. Magnusson, A. Broberg, J. Schnürer, L. Kenne, Antifungal 3-Hydroxy Fatty Acids from Lactobacillus plantarum MiLAB 14, Appl. Environ. Microbiol. 69 (2003) 7554–7557. https://doi.org/https://doi.org/10.1128/AEM.69.12.7554-7557.2003.

[206] J. Mierziak, M. Burgberger, W. Wojtasik, 3-hydroxybutyrate as a metabolite and a signal molecule regulating processes of living organisms, Biomolecules. 11 (2021) 1–21. https://doi.org/10.3390/biom11030402.

[207] N.H. Youssef, K.E. Duncan, M.J. McInerney, Importance of 3-hydroxy fatty acid composition of lipopeptides for biosurfactant activity, Appl. Environ. Microbiol. 71 (2005) 7690–7695. https://doi.org/https://doi.org/10.1128/AEM.71.12.7690-7695.2005.

[208] M. Hilvo, I. De Santiago, P. Gopalacharyulu, W.D. Schmitt, J. Budczies, M. Kuhberg, M. Dietel, T. Aittokallio, F. Markowetz, C. Denkert, J. Sehouli, C. Frezza, S. Darb-Esfahani, E.I. Braicu, Accumulated metabolites of hydroxybutyric acid serve as diagnostic and prognostic biomarkers of ovarian high-grade serous carcinomas, Cancer Res. 76 (2016) 796–804. https://doi.org/https://doi.org/10.1158/0008-5472.CAN-15-2298.

[209] S. Gatreddi, J. Urdiain-Arraiza, B. Desguin, R.P. Hausinger, J. Hu, Structural and mutational characterization of a malate racemase from the LarA superfamily, BioMetals. 36 (2022) 303–313. https://doi.org/10.1007/s10534-022-00372-x.

[210] B. Desguin, J. Urdiain-Arraiza, M. Da Costa, M. Fellner, J. Hu, R.P. Hausinger, T. Desmet, P. Hols, P. Soumillion, Uncovering a superfamily of nickel-dependent hydroxyacid racemases and epimerases, Sci. Rep. 10 (2020) 18123. https://doi.org/10.1038/s41598-020-74802-6.

[211] W. Schtitzner, G. Caponecchi, S. Fanali, A. Rizzi, E. Kenndler, Improved separation of diastereomeric derivatives of enantiomers by a physical network of linear polyvinylpyrrolidone applied as pseudophase in capillary zone electrophoresis, Electrophoresis. 15 (1994) 769–773. https://doi.org/https://doi.org/10.1002/elps.11501501107.

[212] F. Kilár, S. Hjertén, Fast and high resolution analysis of human serum transferrin by high performance isoelectric focusing in capillaries, Electrophoresis. 10 (1989) 23–29. https://doi.org/https://doi.org/10.1002/elps.1150100107.

[213] W. Wang, F. Zhou, L. Zhao, J.R. Zhang, J.J. Zhu, Measurement of electroosmotic flow in capillary and microchip electrophoresis, J. Chromatogr. A. 1170 (2007) 1–8. https://doi.org/10.1016/j.chroma.2007.08.083.

[214] S. Tabata, Y. Kojima, T. Sakamoto, K. Igarashi, K. Umetsu, T. Ishikawa, A. Hirayama, R. Kajino-Sakamoto, N. Sakamoto, K. ichi Yasumoto, K. Okano, Y. Suzuki, S. Yachida, M. Aoki, T. Soga, L-2hydroxyglutaric acid rewires amino acid metabolism in colorectal cancer via the mTOR-ATF4 axis, Oncogene. 42 (2023) 1294–1307. https://doi.org/10.1038/s41388-023-02632-7.

[215] M. Fellner, J.A. Rankin, B. Desguin, J. Hu, R.P. Hausinger, Analysis of the Active Site Cysteine Residue of the Sacrificial Sulfur Insertase LarE from Lactobacillus plantarum, Biochemistry. 57 (2018) 5513–5523. https://doi.org/10.1021/acs.biochem.8b00601.

[216] R.D. Finn, P. Coggill, R.Y. Eberhardt, S.R. Eddy, J. Mistry, A.L. Mitchell, S.C. Potter, M. Punta, M. Qureshi, A. Sangrador-Vegas, G.A. Salazar, J. Tate, A. Bateman, The Pfam protein families database: Towards a more sustainable future, Nucleic Acids Res. 44 (2016) D279–D285. https://doi.org/10.1093/nar/gkv1344.

[217] T. Paysan-Lafosse, M. Blum, S. Chuguransky, T. Grego, B.L. Pinto, G.A. Salazar, M.L. Bileschi, P. Bork, A. Bridge, L. Colwell, J. Gough, D.H. Haft, I. Letunić, A. Marchler-Bauer, H. Mi, D.A. Natale, C.A. Orengo, A.P. Pandurangan, C. Rivoire, C.J.A. Sigrist, I. Sillitoe, N. Thanki, P.D. Thomas, S.C.E. Tosatto, C.H. Wu, A. Bateman, InterPro in 2022, Nucleic Acids Res. 51 (2023) D418–D427. https://doi.org/10.1093/nar/gkac993.

[218] J. Urdiain-Arraiza, B. Desguin, Versatile capillary electrophoresis method for the direct chiral separation of aliphatic and aromatic α-hydroxy acids, β-hydroxy acids and polyhydroxy acids using vancomycin as chiral selector, J. Chromatogr. A. 1715 (2024) 464611. https://doi.org/10.1016/j.chroma.2023.464611.

[219] A. Bar-Even, E. Noor, Y. Savir, W. Liebermeister, D. Davidi, D.S. Tawfik, R. Milo, The moderately efficient enzyme: Evolutionary and physicochemical trends shaping enzyme parameters, Biochemistry. 50 (2011) 4402–4410. https://doi.org/10.1021/bi2002289.

[220] J. Jumper, R. Evans, A. Pritzel, T. Green, M. Figurnov, O. Ronneberger, K. Tunyasuvunakool, R. Bates, A. Žídek, A. Potapenko, A. Bridgland, C. Meyer, S.A.A. Kohl, A.J. Ballard, A. Cowie, B. Romera-Paredes, S. Nikolov, R. Jain, J. Adler, T. Back, S. Petersen, D. Reiman, E. Clancy, M. Zielinski, M. Steinegger, M. Pacholska, T. Berghammer, S. Bodenstein, D. Silver, O. Vinyals, A.W. Senior, K. Kavukcuoglu, P. Kohli, D. Hassabis, Highly accurate protein structure prediction with AlphaFold, Nature. 596 (2021) 583–589. https://doi.org/10.1038/s41586-021-03819-2.

[221] M. Varadi, D. Bertoni, P. Magana, U. Paramval, I. Pidruchna, M. Radhakrishnan, M. Tsenkov, S. Nair, M. Mirdita, J. Yeo, O. Kovalevskiy, K. Tuny, A. Žídek, H. Tomlinson, D. Hariharan, J. Abrahamson, T. Green, J. Jumper, D. Hassabis, S. Velankar, AlphaFold Protein Structure Database in 2024: providing structure coverage for over 214 million protein sequences, Nucleic Acids Res. 52 (2024) D368–D375. https://doi.org/10.1093/nar/gkad1011.

[222] K. Yu, Q. Li, X. Sun, X. Peng, Q. Tang, H. Chu, L. Zhou, B. Wang, Z. Zhou, X. Deng, J. Yang, J. Lv, R. Liu, C. Miao, W. Zhao, Z. Yao, Q. Wang, Bacterial indole-3-lactic acid affects epithelium–macrophage crosstalk to regulate intestinal homeostasis, Proc. Natl. Acad. Sci. 120 (2023) e2309032120.

[223] F. Panabières, G.S. Ali, M.B. Allagui, R. J.D. Dalio, N. C. Gudmestad, M.-L. Kuhn, S. Guha Roy, L. Schena, A. Zampounis, Phytophthora nicotianae diseases worldwide: new knowledge of a long-recognised pathogen, Phytopathol. Mediterr. 55 (2016) 20–40. https://doi.org/10.14601/Phytopathol.

[224] J. Sambrook, E. Fritsch, T. Maniatis, Molecular cloning: a laboratory manual, 2nd ed., Cold Spring Harbor Laboratory Press, New York, 1989.

[225] B.M. Martins, S. Macedo-Ribeiro, J. Bresser, W. Buckel, A. Messerschmidt, Structural basis for stereo-specific catalysis in NAD+-dependent (R)-2-hydroxyglutarate dehydrogenase from Acidaminococcus fermentans, FEBS J. 272 (2005) 269–281. https://doi.org/10.1111/j.1432-1033.2004.04417.x.

[226] R. Eisenthal, M.J. Danson, D.W. Hough, Catalytic efficiency and kcat/KM: a useful comparator?, Trends Biotechnol. 25 (2007) 247–249. https://doi.org/10.1016/j.tibtech.2007.03.010.

[227] R.C. Edgar, Search and clustering orders of magnitude faster than BLAST, Bioinformatics. 26 (2010) 2460–2461. https://doi.org/10.1093/bioinformatics/btq461.

[228] K. Katoh, J. Rozewicki, K.D. Yamada, MAFFT online service: Multiple sequence alignment, interactive sequence choice and visualization, Brief. Bioinform. 20 (2018) 1160–1166. https://doi.org/10.1093/bib/bbx108.

[229] K. Katoh, K. Misawa, K.I. Kuma, T. Miyata, MAFFT: A novel method for rapid multiple sequence alignment based on fast Fourier transform, Nucleic Acids Res. 30 (2002) 3059–3066. https://doi.org/10.1093/nar/gkf436.

[230] B.Q. Minh, H.A. Schmidt, O. Chernomor, D. Schrempf, M.D. Woodhams, A. Von Haeseler, R. Lanfear, E. Teeling, IQ-TREE 2: New Models and Efficient Methods for Phylogenetic Inference in the Genomic Era, Mol. Biol. Evol. 37 (2020) 1530–1534. https://doi.org/10.1093/molbev/msaa015.

[231] B.Q. Minh, C.C. Dang, L.S. Vinh, R. Lanfear, QMaker: Fast and Accurate Method to Estimate Empirical Models of Protein Evolution, Syst. Biol. 70 (2021) 1046–1060. https://doi.org/10.1093/sysbio/syab010.

[232] S. Kalyaanamoorthy, B.Q. Minh, T.K.F. Wong, A. Von Haeseler, L.S. Jermiin, ModelFinder: Fast model selection for accurate phylogenetic estimates, Nat. Methods. 14 (2017) 587–589. https://doi.org/10.1038/nmeth.4285.

[233] D.T. Hoang, O. Chernomor, A. Von Haeseler, B.Q. Minh, L.S. Vinh, UFBoot2: Improving the ultrafast bootstrap approximation, Mol. Biol. Evol. 35 (2018) 518–522. https://doi.org/10.1093/molbev/msx281.

[234] I. Letunic, P. Bork, Interactive tree of life (iTOL) v5: An online tool for phylogenetic tree display and annotation, Nucleic Acids Res. 49 (2021) W293–W296. https://doi.org/10.1093/nar/gkab301.

[235] A. Kornhauser, Applications of hydroxy acids: classification, mechanisms, and photoactivity, Clin. Cosmet. Investig. Dermatol. (2010) 135. https://doi.org/10.2147/ccid.s9042.

[236] T. Werpy, G. Petersen, Top Value Added Chemicals from Biomass: Volume I -- Results of Screening for Potential Candidates from Sugars and Synthesis Gas, United States, 2004. https://doi.org/10.2172/15008859.

[237] J. Urdiain-Arraiza, A. Vandenberghe, G. Dimitrova, B. Desguin, Unveiling 14 novel 2-hydroxy acid racemization and epimerization reactions in the lactate racemase superfamily, (2024).

[238] P.H. Hsieh, D.F. Thieker, M. Guerrini, R.J. Woods, J. Liu, Uncovering the Relationship between Sulphation Patterns and Conformation of Iduronic Acid in Heparan Sulphate, Sci. Rep. 6 (2016) 1–8. https://doi.org/10.1038/srep29602.

[239] C. Aranda, G. Oksdath-Mansilla, F.R. Bisogno, G. de Gonzalo, Deracemisation Processes Employing Organocatalysis and Enzyme Catalysis, Adv. Synth. Catal. 362 (2020) 1233–1257. https://doi.org/10.1002/adsc.201901112.

[240] Y. Li-Cheng, H. Deng, R. Hans, Recent Progress and Developments in Chemoenzymatic and Biocatalytic Dynamic Kinetic Resolution, Org. Process Res. Dev. 26 (2022) 1925–1943. https://doi.org/10.1021/acs.oprd.1c00463.

[241] C. Femmer, M. Bechtold, T.M. Roberts, S. Panke, Exploiting racemases, Appl. Microbiol. Biotechnol. 100 (2016) 7423–7436. https://doi.org/10.1007/s00253-016-7729-8.

[242] F.F. Huerta, A.B.E. Minidis, J.E. Bäckvall, Racemisation in asymmetric synthesis. Dynamic kinetic resolution and related processes in enzyme and metal catalysis, Chem. Soc. Rev. 30 (2001) 321–331. https://doi.org/10.1039/b105464n.

[243] M.T. El Gihani, J.M.J. Williams, Dynamic kinetic resolution, Curr. Opin. Chem. Biol. 3 (1999) 11–15. https://doi.org/10.1016/S1367-5931(99)80003-9.

[244] A. Currin, N. Swainston, P.J. Day, D.B. Kell, Synthetic biology for the directed evolution of protein biocatalysts: Navigating sequence space intelligently, Chem. Soc. Rev. 44 (2015) 1172–1239. https://doi.org/10.1039/c4cs00351a.

[245] H.H. Hwang, P.R. Chien, F.C. Huang, P.H. Yeh, S.H.W. Hung, W.L. Deng, C.C. Huang, A Plant Endophytic Bacterium Priestia megaterium StrainBP-R2 Isolated from the Halophyte Bolboschoenus planiculmis Enhances Plant Growth under Salt and Drought Stresses, Microorganisms. 10 (2022). https://doi.org/10.3390/microorganisms10102047.

[246] J.A. Wushensky, T. Youngster, C.M. Mendonca, L. Aristilde, Flux connections between gluconate pathway, glycolysis, and pentose-phosphate pathway during carbohydrate metabolism in Bacillus megaterium QM B1551, Front. Microbiol. 9 (2018) 1–13. https://doi.org/10.3389/fmicb.2018.02789.

[247] M.M. Bradford, A rapid and sensitive method for the quantitation of microgram quantities of protein utilizing the principle of protein-dye binding., Anal. Biochem. 72 (1976) 248–254. https://doi.org/10.1006/abio.1976.9999.

[248] M.P. Lambert, F.C. Neuhaus, Mechanism of D-cycloserine action: alanine racemase from Escherichia coli W., J. Bacteriol. 110 (1972) 978–987. https://doi.org/10.1128/jb.110.3.978-987.1972.

[249] F. Breveglieri, M. Mazzotti, Role of Racemization Kinetics in the Deracemization Process via Temperature Cycles, Cryst. Growth Des. 19 (2019) 3551–3558. https://doi.org/10.1021/acs.cgd.9b00410.

[250] A.J.E. Borg, A. Dennig, H. Weber, B. Nidetzky, Mechanistic characterization of UDP-glucuronic acid 4-epimerase, FEBS J. 288 (2021) 1163–1178. https://doi.org/10.1111/febs.15478.

[251] H. Itoh, H. Okaya, A.R. Khan, S. Tajima, S. Hayakawa, K. Izumori, Purification and Characterization of D -Tagatose 3-Epimerase from Pseudomonas sp. ST-24, Biosci. Biotechnol. Biochem. 58 (1994) 2168–2171. https://doi.org/10.1271/bbb.58.2168.

[252] H.J. Kim, E.K. Hyun, Y.S. Kim, Y.J. Lee, D.K. Oh, Characterization of an Agrobacterium tumefaciens D-psicose 3-epimerase that converts D-fructose to D-psicose, Appl. Environ. Microbiol. 72 (2006) 981–985. https://doi.org/10.1128/AEM.72.2.981-985.2006.

[253] E. Gabirondo, A. Sangroniz, A. Etxeberria, S. Torres-Giner, H. Sardon, Poly(hydroxy acids) derived from the self-condensation of hydroxy acids: From polymerization to end-of-life options, Polym. Chem. 11 (2020) 4861–4874. https://doi.org/10.1039/d0py00088d.

[254] F. Pezzotti, M. Therisod, Enzymatic synthesis of aldonic acids, Carbohydr. Res. 341 (2006) 2290–2292. https://doi.org/10.1016/j.carres.2006.05.023.

[255] T. Gajda, B. Gyurcsik, T. Jakusch, K. Burger, B. Henry, J.J. Delpuech, Coordination chemistry of polyhydroxy acids: Role of the hydroxy groups, Inorganica Chim. Acta. 275–276 (1998) 130–140. https://doi.org/10.1016/s0020-1693(97)06108-2.

[256] T. Walther, F. Calvayrac, Y. Malbert, C. Alkim, C. Dressaire, H. Cordier, J.M. François, Construction of a synthetic metabolic pathway for the production of 2,4-dihydroxybutyric acid from homoserine, Metab. Eng. 45 (2018) 237–245. https://doi.org/10.1016/j.ymben.2017.12.005.

[257] C.J.R. Frazão, N. Wagner, K. Rabe, T. Walther, Construction of a synthetic metabolic pathway for biosynthesis of 2,4-dihydroxybutyric acid from ethylene glycol, Nat. Commun. 14 (2023). https://doi.org/10.1038/s41467-023-37558-x.

[258] M. Winnacker, Polyhydroxyalkanoates: Recent Advances in Their Synthesis and Applications, Eur. J. Lipid Sci. Technol. 121 (2019) 1–9. https://doi.org/10.1002/ejlt.201900101.

[259] K. Sudesh, H. Abe, Y. Doi, Synthesis, structure and properties of polyhydroxyalkanoates: Biological polyesters, Prog. Polym. Sci. 25 (2000) 1503–1555. https://doi.org/10.1016/S0079-6700(00)00035-6.

[260] Z. Zheng, B. Sheng, C. Gao, H. Zhang, T. Qin, C. Ma, P. Xu, Highly stereoselective biosynthesis of (R)-2-hydroxy carboxylic acids through rationally re-designed mutation of d-lactate dehydrogenase, Sci. Rep. 3 (2013) 6–11. https://doi.org/10.1038/srep03401.

[261] W. Hao, C. Guang, W. Zhang, W. Mu, Recent development of phenyllactic acid: physicochemical properties, biotechnological production strategies and applications, Crit Rev Biotechnol. 43 (2023) 293–308. https://doi.org/10.1080/07388551.2021.2010645.

[262] N.K. Sweitzer, What Is an Angiotensin Converting Enzyme Inhibitor?, Circulation. 108 (2003) 1–3. https://doi.org/10.1161/01.cir.0000075957.16003.07.

[263] E. Schmidt, O. Ghisalba, D. Gygax, G. Sedelmeier, Optimization of a process for the production of (R)-2-hydroxy-phenylbutyric acid - an intermediate for inhibitors of angiotensin converting enzyme, J. Biotechnol. 24 (1992) 315–327. https://doi.org/10.1016/0168-1656(92)90040-g.

[264] C. Gao, W. Zhang, Y. Huang, C. Ma, P. Xu, Efficient conversion of 1,2-butanediol to (R)-2-hydroxybutyric acid using whole cells of Gluconobacter oxydans, Bioresour. Technol. 115 (2012) 75–78. https://doi.org/10.1016/j.biortech.2011.11.009.

[265] J. Sui, N. Wang, J. Wang, X. Huang, T. Wang, L. Zhou, H. Hao, Strategies for chiral separation: from racemate to enantiomer, Chem. Sci. 14 (2023) 11955–12003. https://doi.org/10.1039/d3sc01630g.

[266] M. Ciriani, R. Oliveira, C.A.M. Afonso, Semi-continuous and continuous processes for enantiomeric separation, Green Chem. 24 (2022) 4328–4362. https://doi.org/10.1039/d1gc03668h.

[267] J. Kuivanen, M. Arvas, P. Richard, Clustered genes encoding 2-keto-l-gulonate reductase and l-idonate 5-dehydrogenase in the novel fungal d-glucuronic acid pathway, Front. Microbiol. 8 (2017) 1–10. https://doi.org/10.3389/fmicb.2017.00225.

[268] G. Ashwell, Enzymes of glucuronic and galacturonic acid metabolism in bacteria, Methods Enzymol. 5 (1962) 190–208. https://doi.org/10.1016/S0076-6879(62)05205-2.

[269] S. Dagley, P.W. Trudgill, the Metabolism of Galactarate, D-Glucarate and Various Pentoses By Species of Pseudomonas, Biochem. J. 95 (1965) 48–58. https://doi.org/10.1042/bj0950048.

[270] J. Sloothaak, M. Schilders, P.J. Schaap, L.H. de Graaff, Overexpression of the Aspergillus niger GatA transporter leads to preferential use of D-galacturonic acid over D-xylose, AMB Express. 4 (2014) 1–9. https://doi.org/10.1186/s13568-014-0066-3.

[271] K.R. Mekjian, E.M. Bryan, B.W. Beall, C.P. Moran, Regulation of Hexuronate Utilization in Bacillus subtilis, J. Bacteriol. 181 (1999) 426–433.

[272] G. Nemoz, J. Robert-Baudouy, F. Stoeber, Physiological and Genetic Regulation of the Aldohexuronate Transport System in Escherichia coli, J. Bacteriol. 127 (1976) 706–718.

[273] E. Garcia-Urdiales, I. Alfonso, V. Gotor, Enantioselective Enzymatic Desymmetrizations in Organic Synthesis, Chem. Rev. 105 (2005) 313–354. https://doi.org/10.1021/cr040640a.

[274] C. Rougeot, J.E. Hein, Application of Continuous Preferential Crystallization to Efficiently Access Enantiopure Chemicals, Org. Process Res. Dev. 19 (2015) 1809–1819. https://doi.org/10.1021/acs.oprd.5b00141.

[275] X. Buol, C. Caro Garrido, K. Robeyns, N. Tumanov, L. Collard, J. Wouters, T. Leyssens, Chiral Resolution of Mandelic Acid through Preferential Cocrystallization with Nefiracetam, Cryst. Growth Des. 20 (2020) 7979–7988. https://doi.org/10.1021/acs.cgd.0c01236.

[276] C.R. Groom, I.J. Bruno, M.P. Lightfoot, S.C. Ward, The Cambridge structural database, Acta Crystallogr. Sect. B Struct. Sci. Cryst. Eng. Mater. 72 (2016) 171–179. https://doi.org/10.1107/S2052520616003954.

[277] V. Sládková, O. Dammer, G. Sedmak, E. Skořepová, B. Kratochvíl, Ivabradine hydrochloride (S)-mandelic acid co-crystal: In situ preparation during formulation, Crystals. 7 (2017). https://doi.org/10.3390/cryst7010013.

[278] M. Karimi-Jafari, L. Padrela, G.M. Walker, D.M. Croker, Creating cocrystals: A review of pharmaceutical cocrystal preparation routes and applications, Cryst. Growth Des. 18 (2018) 6370–6387. https://doi.org/10.1021/acs.cgd.8b00933.

[279] M. Bastos, O. Abian, C.M. Johnson, F. Ferreira-da-Silva, S. Vega, A. Jimenez-Alesanco, D. Ortega-Alarcon, A. Velazquez-Campoy, Isothermal titration calorimetry, Nat. Rev. Methods Prim. 3 (2023) 17. https://doi.org/10.1038/s43586-023-00199-x.

[280] O.A. Raitman, V.I. Chegel, A.B. Kharitonov, M. Zayats, E. Katz, I. Willner, Analysis of NAD(P)+ and NAD(P)H cofactors by means of imprinted polymers associated with Au surfaces: A surface plasmon resonance study, Anal. Chim. Acta. 504 (2004) 101–111. https://doi.org/10.1016/S0003-2670(03)00511-7.

[281] K. Maráková, M. Opetová, R. Tomašovský, Capillary electrophoresis-mass spectrometry for intact protein analysis: Pharmaceutical and biomedical applications (2018–March 2023), J. Sep. Sci. 46 (2023). https://doi.org/10.1002/jssc.202300244.

[282] A.K. Schwenzer, L. Kruse, K. Jooß, C. Neusüß, Capillary electrophoresis-mass spectrometry for protein analyses under native conditions: Current progress and perspectives, Proteomics. 24 (2024) 2300135. https://doi.org/10.1002/pmic.202300135.

[283] J.R. Stern, C.S. Hegre, Inducible D-Malic Enzyme in Escherischia Coli, Nature. 212 (1966) 1611–1612. https://doi.org/10.1038/2121611a0.

[284] M. Martínez-Luque, F. Castillo, R. Blasco, Assimilation of D-malate by Rhodobacter capsulatus E1F1, Curr. Microbiol. 43 (2001) 154–157. https://doi.org/10.1007/s002840010279.

[285] N. Peekhaus, T. Conway, What's for dinner?: Entner-Doudoroff metabolism in Escherichia coli, J. Bacteriol. 180 (1998) 3495–3502. https://doi.org/10.1128/jb.180.14.3495-3502.1998.

[286] X. Qiu, Y. Tao, Y. Zhu, Y. Yuan, Y. Zhang, H. Liu, Y. Gao, M. Teng, L. Niu, Structural insights into decreased enzymatic activity induced by an insert sequence in mannonate dehydratase from Gram negative bacterium, J. Struct. Biol. 180 (2012) 327–334. https://doi.org/10.1016/j.jsb.2012.06.013.

[287] R.C. Eisenberg, W.J. Dobrogosz, Gluconate metabolism in Escherichia coli., J. Bacteriol. 93 (1967) 941–949. https://doi.org/10.1128/jb.93.3.941-949.1967.

[288] J.D. Smiley, G. Ashwell, Uronic Acid Metabolism in Bacteria, J. Biol. Chem. 235 (1960) 1571–1575. https://doi.org/10.1016/s0021-9258(19)76842-2.

[289] D.J. Wichelecki, D.C. Gra, N. Al-obaidi, S.C. Almo, J.A. Gerlt, Identification of the in Vivo Function of the High-Efficiency D-Mannonate Dehydratase in Caulobacter crescentus NA1000 from the Enolase Superfamily, Biochemistry. 53 (2014) 4087–4089. https://doi.org/doi.org/10.1021/bi500683x.

[290] A.M. Intlekofer, B. Wang, H. Liu, H. Shah, C. Carmona-Fontaine, A.S. Rustenburg, S. Salah, M.R. Gunner, J.D. Chodera, J.R. Cross, C.B. Thompson, L-2-Hydroxyglutarate production arises from noncanonical enzyme function at acidic pH, Nat. Chem. Biol. 13 (2017) 494–500. https://doi.org/10.1038/nchembio.2307.

[291] A. Karlstaedt, X. Zhang, H. Vitrac, R. Harmancey, H. Vasquez, J.H. Wang, M.A. Goodell, H. Taegtmeyer, Oncometabolite D-2-hydroxyglutarate impairs α-ketoglutarate dehydrogenase and contractile function in rodent heart, Proc. Natl. Acad. Sci. U. S. A. 113 (2016) 10436–10441. https://doi.org/10.1073/pnas.1601650113.

[292] X. Du, H. Hu, The Roles of 2-Hydroxyglutarate, Front. Cell Dev. Biol. 9 (2021). https://doi.org/10.3389/fcell.2021.651317.

[293] N.M. Dixon, R.W. Lovitt, D.B. Kell, J.G. Morris, The growth and nutrition of Clostridium sporogenes NCIB 8053 in defined media, J. Appl. Bacteriol. 62 (1987) 71–80. https://doi.org/10.1111/j.1365-2672.1987.tb02700.x.

[294] S. Chatterjee, G.S. Stupp, S.K.R. Park, J.C. Ducom, J.R. Yates, A.I. Su, D.W. Wolan, A comprehensive and scalable database search system for metaproteomics, BMC Genomics. 17 (2016) 642. https://doi.org/10.1186/s12864-016-2855-3.

[295] L. Sorci, Y. Pan, Y. Eyobo, I. Rodionova, N. Huang, S. Zhong, A.D.M. Jr, H. Zhang, L. Andrei, Targeting NAD biosynthesis in bacterial pathogens. Structure- based development of inhibitors of nicotinate mononucleotide adenylyltransferase NadD, Chem Biol. 16 (2009) 849–861.

[296] S. Amjad, S. Nisar, A.A. Bhat, A.R. Shah, M.P. Frenneaux, K. Fakhro, M. Haris, R. Reddy, Z. Patay, J. Baur, P. Bagga, Role of NAD+ in regulating cellular and metabolic signaling pathways, Mol. Metab. 49 (2021). https://doi.org/10.1016/j.molmet.2021.101195.

[297] A.M. Mackie, K.A. Hassan, I.T. Paulsen, S.G. Tetu, Biolog phenotype microarrays for phenotypic characterization of microbial cells, Methods Mol. Biol. 1096 (2014) 123–130. https://doi.org/10.1007/978-1-62703-712-9_10.

[298] Á. López-gonzálvez, J. Godzien, A. García, C. Barbas, Capillary Electrophoresis Mass Spectrometry as a Tool for Untargeted Metabolomics, Methods Mol Biol. 1978 (2019) 55–77. https://doi.org/10.1007/978-1-4939-9236-2_5.

[299] R. Mohan, P. Namsolleck, P.A. Lawson, M. Osterhoff, M.D. Collins, C.A. Alpert, M. Blaut, Clostridium asparagiforme sp. nov., isolated from a human faecal sample, Syst. Appl. Microbiol. 29 (2006) 292–299. https://doi.org/10.1016/j.syapm.2005.11.001.

[300] S.A. Kuehne, N.P. Minton, ClosTron-mediated engineering of Clostridium, Bioengineered. 3 (2012) 247–254. https://doi.org/10.4161/bioe.21004.

[301] J.T. Heap, O.J. Pennington, S.T. Cartman, G.P. Carter, N.P. Minton, The ClosTron: A universal gene knock-out system for the genus Clostridium, J. Microbiol. Methods. 70 (2007) 452–464. https://doi.org/10.1016/j.mimet.2007.05.021.

[302] M.E. Pyne, M. Bruder, M. Moo-Young, D.A. Chung, C.P. Chou, Technical guide for genetic advancement of underdeveloped and intractable Clostridium, Biotechnol. Adv. 32 (2014) 623–641. https://doi.org/10.1016/j.biotechadv.2014.04.003.

[303] M.E. Pyne, M. Moo-Young, D.A. Chung, C.P. Chou, Development of an electrotransformation protocol for genetic manipulation of Clostridium pasteurianum, Biotechnol. Biofuels. 6 (2013). https://doi.org/10.1186/1754-6834-6-50.

[304] B. Dabrock, H. Bahl, G. Gottschalk, Parameters Affecting Solvent Production by Clostridium pasteurianum, Microbiology. 58 (1992) 1233–1239. https://doi.org/10.1128/aem.58.4.1233-1239.1992.

[305] K.A. Taconi, K.P. Venkataramanan, D.T. Johnson, Growth and Solvent Production by Clostridium pasteurianum ATCCVR 6013TM Utilizing Biodiesel-Derived Crude Glycerol as the Sole Carbon Source, Environ. Prog. Sustain. Energy. 28 (2009) 676–680. https://doi.org/10.1002/ep.

[306] Q. Li, F.M. Seys, N.P. Minton, J. Yang, Y. Jiang, W. Jiang, S. Yang, CRISPR–Cas9 D10A nickase-assisted base editing in the solvent producer Clostridium beijerinckii, 2019. https://doi.org/10.1002/bit.26949.

[307] N. Reichardt, S.H. Duncan, P. Young, A. Belenguer, C. McWilliam Leitch, K.P. Scott, H.J. Flint, P. Louis, Phylogenetic distribution of three pathways for propionate production within the human gut microbiota, ISME J. 8 (2014) 1323–1335. https://doi.org/10.1038/ismej.2014.14.

[308] X. Liu, B. Mao, J. Gu, J. Wu, S. Cui, G. Wang, J. Zhao, H. Zhang, W. Chen, Blautia—a new functional genus with potential probiotic properties?, Gut Microbes. 13 (2021) 1–21. https://doi.org/10.1080/19490976.2021.1875796.

[309] E.M. Hansen, Phytophthora species emerging as pathogens of forest trees, Curr. For. Reports. 1 (2015) 16–24. https://doi.org/10.1007/s40725-015-0007-7.

[310] P. Scott, M.K.F. Bader, T. Burgess, G. Hardy, N. Williams, Global biogeography and invasion risk of the plant pathogen genus Phytophthora, Environ. Sci. Policy. 101 (2019) 175–182. https://doi.org/10.1016/j.envsci.2019.08.020.

[311] Y. Fang, L. Cui, B. Gu, F. Arredondo, B.M. Tyler, Efficient genome editing in the oomycete phytophthora sojae using CRISPR/Cas9, Curr. Protoc. Microbiol. (2017) 21A.1.1-21A.1.26. https://doi.org/10.1002/cpmc.25.

[312] H. Atomi, T. Imanaka, T. Fukui, Overview of the genetic tools in the Archaea, Front. Microbiol. 3 (2012). https://doi.org/10.3389/fmicb.2012.00337.

[313] T. Miyamoto, H. Homma, D-Amino acid metabolism in bacteria, J. Biochem. 170 (2021) 5–13. https://doi.org/10.1093/jb/mvab043.

[314] G. Zhang, H.J. Sun, Racemization in reverse: Evidence that D-amino acid toxicity on Earth is controlled by bacteria with racemases, PLoS One. 9 (2014) 1–6. https://doi.org/10.1371/journal.pone.0092101.

[315] J. Soutourina, P. Plateau, S. Blanquet, Metabolism of D-aminoacyl-tRNAs in Escherichia coli and Saccharomyces cerevisiae cells, J. Biol. Chem. 275 (2000) 32535–32542. https://doi.org/10.1074/jbc.M005166200.

[316] L. Alvarez, A. Aliashkevich, M.A. De Pedro, F. Cava, Bacterial secretion of D-arginine controls environmental microbial biodiversity, ISME J. 12 (2018) 438–450. https://doi.org/10.1038/ismej.2017.176.

[317] W. Qin, S.P. Wei, Y. Zheng, E. Choi, X. Li, J. Johnston, X. Wan, B. Abrahamson, Z. Flinkstrom, B. Wang, H. Li, L. Hou, Q. Tao, W.W. Chlouber, X. Sun, M. Wells, L. Ngo, K.A. Hunt, H. Urakawa, X. Tao, D. Wang, X. Yan, D. Wang, C. Pan, P.K. Weber, J. Jiang, J. Zhou, Y. Zhang, D.A. Stahl, B.B. Ward, X. Mayali, W. Martens-Habbena, M.-K.H. Winkler, Ammonia-oxidizing bacteria and archaea exhibit differential nitrogen source preferences, Nat. Microbiol. 9 (2024) 524–536. https://doi.org/10.1038/s41564-023-01593-7.

[318] G. Gourinchas, E. Busto, M. Killinger, N. Richter, B. Wiltschi, W. Kroutil, A synthetic biology approach for the transformation of l-α-amino acids to the corresponding enantiopure (R)- or (S)-α-hydroxy acids, Chem. Commun. 51 (2015) 2828–2831. https://doi.org/10.1039/c4cc08286a.

[319] E. Busto, N. Richter, B. Grischek, W. Kroutil, Biocontrolled formal inversion or retention of L -α-amino acids to enantiopure (R)- or (S)-hydroxyacids, Chem. - A Eur. J. 20 (2014) 11225–11228. https://doi.org/10.1002/chem.201403195.

[320] G. Molla, R. Melis, L. Pollegioni, Breaking the mirror: L-Amino acid deaminase, a novel stereoselective biocatalyst, Biotechnol. Adv. 35 (2017) 657–668. https://doi.org/10.1016/j.biotechadv.2017.07.011.

[321] D.C. Volke, K. Olavarría, P.I. Nikel, Cofactor Specificity of Glucose-6-Phosphate Dehydrogenase Isozymes in Pseudomonas putida Reveals a General Principle Underlying Glycolytic Strategies in Bacteria, MSystems. 6 (2021) 1–21. https://doi.org/10.1128/msystems.00014-21.

[322] G.A. Grant, D-3-phosphoglycerate dehydrogenase, Front. Mol. Biosci. 5 (2018). https://doi.org/10.3389/fmolb.2018.00110.

[323] S.K. Spaans, R.A. Weusthuis, J. van der Oost, S.W.M. Kengen, NADPH-generating systems in bacteria and archaea, Front. Microbiol. 6 (2015). https://doi.org/10.3389/fmicb.2015.00742.

[324] A.R. Portis, M.A.J. Parry, Discoveries in Rubisco (Ribulose 1,5-bisphosphate carboxylase/oxygenase): A historical perspective, Photosynth. Res. 94 (2007) 121–143. https://doi.org/10.1007/s11120-007-9225-6.

[325] N.N. Ulusu, Evolution of Enzyme Kinetic Mechanisms, J. Mol. Evol. 80 (2015) 251–257. https://doi.org/10.1007/s00239-015-9681-0.

[326] S.F. Velick, J. Vavra, A kinetic and equilibrium analysis of the glutamic oxaloacetate transaminase mechanism., J. Biol. Chem. 237 (1962) 2109–2122. https://doi.org/10.1016/s0021-9258(19)63406-x.

[327] Toney MD, Aspartate aminotransferase: an old dog teaches new tricks, Arch. Biochem. Biophys. 544 (2014) 119–127. https://doi.org/10.1016/j.abb.2013.10.002.Aspartate.

[328] M.Y. Galperin, K.S. Makarova, Y.I. Wolf, E. V. Koonin, Expanded Microbial genome coverage and improved protein family annotation in the COG database, Nucleic Acids Res. 43 (2015) D261–D269. https://doi.org/10.1093/nar/gku1223.

[329] R.L. Tatusov, M.Y. Galperin, D.A. Natale, E. V. Koonin, The COG database: A tool for genome-scale analysis of protein functions and evolution, Nucleic Acids Res. 28 (2000) 33–36. https://doi.org/10.1093/nar/28.1.33.

[330] D.A. Rodionov, X. Li, I.A. Rodionova, C. Yang, L. Sorci, E. Dervyn, D. Martynowski, H. Zhang, M.S. Gelfand, A.L. Osterman, Transcriptional regulation of NAD metabolism in bacteria: Genomic reconstruction of NiaR (YrxA) regulon, Nucleic Acids Res. 36 (2008) 2032–2046. https://doi.org/10.1093/nar/gkn046.

[331] T. Rabilloud, C. Lelong, Two-dimensional gel electrophoresis in proteomics: A tutorial, J. Proteomics. 74 (2011) 1829–1841. https://doi.org/10.1016/j.jprot.2011.05.040.

[332] M. Berth, F.M. Moser, M. Kolbe, J. Bernhardt, The state of the art in the analysis of two-dimensional gel electrophoresis images, Appl. Microbiol. Biotechnol. 76 (2007) 1223–1243. https://doi.org/10.1007/s00253-007-1128-0.

[333] M. Katayama, N.F. Tsinoremas, T. Kondo, S.S. Golden, cpmA, a gene involved in an output pathway of the cyanobacterial circadian system, J. Bacteriol. 181 (1999) 3516–3524. https://doi.org/10.1128/jb.181.11.3516-3524.1999.

[334] C.H. Huang, C.R. Shen, H. Li, L.Y. Sung, M.Y. Wu, Y.C. Hu, CRISPR interference (CRISPRi) for gene regulation and succinate production in cyanobacterium S. elongatus PCC 7942, Microb. Cell Fact. 15 (2016) 1–11. https://doi.org/10.1186/s12934-016-0595-3.

[335] R. Rippka, J. Deruelles, J.B. Waterbury, Generic assignments, strain histories and properties of pure cultures of cyanobacteria, J. Gen. Microbiol. 111 (1979) 1–61. https://doi.org/10.1099/00221287-111-1-1.

[336] G.I. Kufryk, M. Sachet, G. Schmetterer, W.F.J. Vermaas, Transformation of the cyanobacterium Synechocystis sp. PCC 6803 as a tool for genetic mapping: Optimization of efficiency, FEMS Microbiol. Lett. 206 (2002) 215–219. https://doi.org/10.1016/S0378-1097(01)00540-7.

[337] P.D. Cani, C. Depommier, M. Derrien, A. Everard, W.M. de Vos, Akkermansia muciniphila: paradigm for next-generation beneficial microorganisms, Nat. Rev. Gastroenterol. Hepatol. 19 (2022) 625–637. https://doi.org/10.1038/s41575-022-00631-9.

[338] C. Depommier, A. Everard, C. Druart, H. Plovier, M. Van Hul, S. Vieira-Silva, G. Falony, J. Raes, D. Maiter, N.M. Delzenne, M. de Barsy, A. Loumaye, M.P. Hermans, J.P. Thissen, W.M. de Vos, P.D. Cani, Supplementation with Akkermansia muciniphila in overweight and obese human volunteers: a proof-of-concept exploratory study, Nat. Med. 25 (2019) 1096–1103. https://doi.org/10.1038/s41591-019-0495-2.

[339] P.D. Cani, W.M. de Vos, Next-generation beneficial microbes: The case of Akkermansia muciniphila, Front. Microbiol. 8 (2017). https://doi.org/10.3389/fmicb.2017.01765.

[340] R.U. Haque, F. Paradisi, T. Allers, Haloferax volcanii for biotechnology applications: challenges, current state and perspectives, Appl. Microbiol. Biotechnol. 104 (2020) 1371–1382. https://doi.org/10.1007/s00253-019-10314-2.

[341] T. Kauri, R. Wallace, D.J. Kushner, Nutrition of the Halophilic Archaebacterium, Haloferax volcanii, Syst. Appl. Microbiol. 13 (1990) 14–18. https://doi.org/10.1016/S0723-2020(11)80174-8.